Experiments with a two-dimensional model of the general circulation

J.D. Haigh

St. Cross College

A thesis submitted for the degree of Doctor of Philosophy in the University of Oxford.

Department of Atmospheric Physics,

Clarendon Laboratory, Oxford.

July 1980

Abstract

Experiments have been conducted with a two-dimensional time-dependent, numerical model of the general circulation of the atmosphere up to the mesopause. A scheme for the calculation of cooling rates due to the 15μm band of carbon dioxide is developed. It uses the Curtis matrix approach which incorporates cooling-to-space, transfer of radiation between atmospheric layers and non-equilibrium effects in the upper mesosphere. The sensitivity of the cooling rate calculations to the choice of collisional relaxation time is investigated. An 'almost exact' scheme to calculate heating rates due to the absorption of solar radiation by ozone and molecular oxygen is presented. Use of both new radiation schemes enables the diabatic heating rate to be calculated to the upper boundary of the model. Other heat sources in the region of the mesopause are discussed. Incorporation of the new schemes considerably improves the modelled temperature structure of the stratosphere and lower mesosphere. The upper mesosphere is not well reproduced with no indication of the observed cold summer mesopause. The heat and momentum budgets of the mesosphere are studied. Eddy momentum fluxes derived from satellite observations of planetary waves are found to be significant for the circulation and transport properties of the stratosphere but incapable of producing the required distribution of angular momentum in the mesosphere. A Rayleigh friction parameterisation is included in the mesosphere to reproduce the observed zonal wind and temperature structure. Momentum deposition by tides and gravity waves is discussed. Curtis matrices are calculated with higher mixing ratios of carbon dioxide and the effects of increased atmospheric CO_2 on stratospheric temperatures and ozone is investigated. Temperature decreases of up to about 10K are predicted with increases in ozone concentration

in the upper stratosphere. In the lower stratosphere the ozone increases are restricted to high latitudes and a decrease shown in equatorial regions. The latitudinal variations are reflected in the ozone column density. An experiment is conducted in which chlorofluorocarbons are released into the model atmosphere and the effects on stratospheric ozone are in exactly the opposite sense to those predicted for the CO_2 case. A run in which CO_2 and CFCs are introduced simultaneously shows that the two effects are not linearly additive. A simple photochemical theory is used to investigate the temperature dependence of ozone and to explain the non-linearity of the coupled experiment.

Acknowledgements

I would like to thank Dr. C.D. Walshaw for accepting me as his research student and for his support throughout my research.

I am indebted to Dr. J.A. Pyle for advice and encouragement without which this thesis would never have been completed.

The program for calculating the basic Curtis matrix, described in Chapter 3, was provided by Dr. A.P. Williams. The work described in Chapter 4 was suggested by Prof. J.T. Houghton. Chapter 8 was the subject of lively debate with Prof. S. Venkateswaran of the University of California. Members of Oxford University Atmospheric Physics Department, especially Dr. C.F.Rogers, Dr. A.J. Crane, Dr. J.J. Barnett and Mr. J.T. Schofield, have made helpful and interesting comments on many aspects of the work.

I am grateful to Mr. R.J. Wells for his advice and assistance with computing problems and to Mrs J. Whitney for typing the manuscript.

The Natural Environment Research Council provided financial support for the first two years of this research. Paul Fouracre provided moral support during the third.

Contents

CHAPTER 1

Introduction

1.1 Numerical modelling of the atmosphere

The use of numerical models has become established as an important part of the overall effort to understand and explain the structure, composition and behaviour of the atmosphere. A wide variety of models have been employed to test theories of atmospheric physics and chemistry, to try to reprɒduce the observed features of the atmosphere and to predict possible changes in its state. The specifications of a particular model will depend on the aims of the modeller; for example, it may be of global scale and simulate climatic change over centuries, it might attempt to reproduce the development of a localised thunderstorm over a few hours or it may be a steady state representation of the mean concentration of a particular minor constituent. Obviously there are many possibilities.

To study the general circulation of the atmosphere a model would, ideally, have three-dimensional global coverage with high resolution in each dimension, include all possible dynamical effects, detailed and diurnally varying radiation calculations and a photochemical scheme which contained all known atmospheric constituents and the reactions between them. Such a model is far from being constructed; the computing effort it would require is prohibitive for even the largest and fastest computers currently in existence. Thus a choice of approximations must be made depending upon which atmospheric features are to be investigated.

Three-dimensional models include, in general, fairly good representations of dynamical processes but only rudimentary schemes for radiation and photochemistry. One-dimensional models (including only variation with altitude) have been used to study radiative transfer and atmospheric chemistry in detail

but in neither case is there any interaction with the dynamics and furthermore the transport of chemical species is treated in a very empirical manner. Two-dimensional (latitude - height) models provide a compromise between the heavy computing requirements of the three-dimensional models and the simplistic dynamics of one-dimensional models. On a rotating planet with a homogeneous underlying surface the values of meteorological quantities averaged over a sufficiently long period of time may be expected to show no variation with longitude so a model in which the variables are averaged round latitude circles should provide a reasonably accurate representation.

The work described in this thesis involves experiments with a two-dimensional model of the general circulation already established at Oxford University (Harwood and Pyle, 1975). The basic framework of the Model is given in Chapter 2. A major part of the work has been the replacement of the schemes to calculate solar and thermal heating rates by more accurate methods which, moreover, extend up to the top of the model domain. The thermal radiation scheme is described in Chapter 3, the solar heating scheme in Chapter 5 and the effects on model behaviour of introducing the new methods in Chapter 6. Chapter 4 deals with the dependence of infrared radiative cooling calculations on the values of collisional relaxation time used.

The new scheme for calculating cooling rates due to the carbon dioxide 15μm band allows for a choice of CO_2 mixing ratio. Atmospheric CO_2 amount are increasing and in Chapter 7 the possible consequences for stratospheric ozone are assessed using the Model. The results are compared with predictions of the effects of the release of chlorofluorocarbons (CFCs) and an experiment with the Model in which CO_2 and CFCs are simultaneously increased is discussed.

In Chapter 8 the heat and momentum budgets of the mesosphere are reviewed with particular reference to the role played by planetary waves and the driving forces of the mean meridional circulation.

In the next section the observed structure of the atmosphere is briefly described as a basis for later comparisons.

1.2 The observed structure of the atmosphere

1.2.1 Temperatures

The different regions of the atmosphere are classified according to temperature lapse late and may be identified in Fig. 1.1 which shows a representative zonal mean temperature cross-section for the northern hemisphere solstices compiled by Murgatroyd (1969a). The lowest region is the troposphere in which the temperature decreases with altitude at the wet adiabatic lapse rate ($dT/dz \sim -7$ K km^{-1}) up to about 16 km in the tropics and about 10 km in middle and high latitudes. Thus the tropopause, i.e. the division between the troposphere and the stratosphere, is at a higher temperature in polar than in equatorial regions and has breaks in all seasons at about 40°N. Extending between the tropopause and 50 km is the stratosphere in which the temperature increases with height due to the absorption of solar radiation by ozone. The gradient is steepest near the summer pole and here the temperatures exceed 290 K at the stratopause, defining the upper boundary of the stratosphere; in winter high latitudes the lower stratosphere is almost isothermal and there is only a slight increase in the upper stratosphere to around 240 K at 50 km. Above the stratopause is the mesosphere; here the temperatures decrease sharply in the summer hemisphere, dropping to below 160 K at the polar mesopause which exists at around 85 km. In winter high latitudes the mesosphere is almost isothermal so that the temperature, of around 240 K, at the winter polar mesopause is higher than that at the same altitude in summer. Above the mesopause is the thermosphere in which strong absorption of solar ultraviolet radiation, particularly by O_2, leads to a steep increase of temperature with altitude.

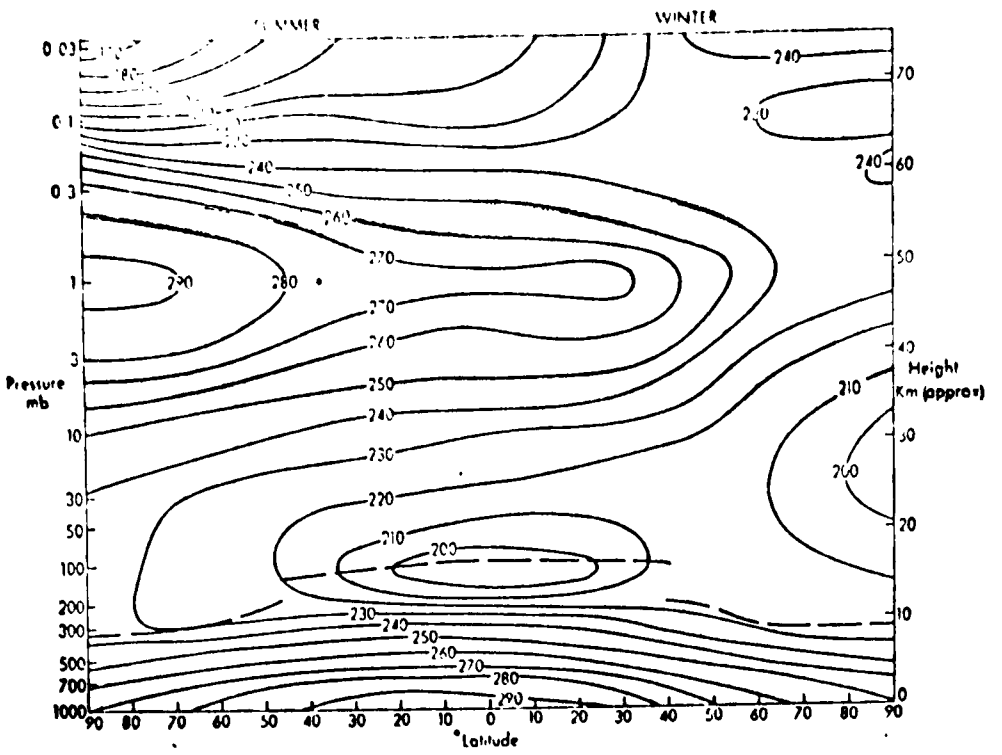

Fig.1.1 Representative zonal mean temperatures.

From Murgatroyd(1969a).

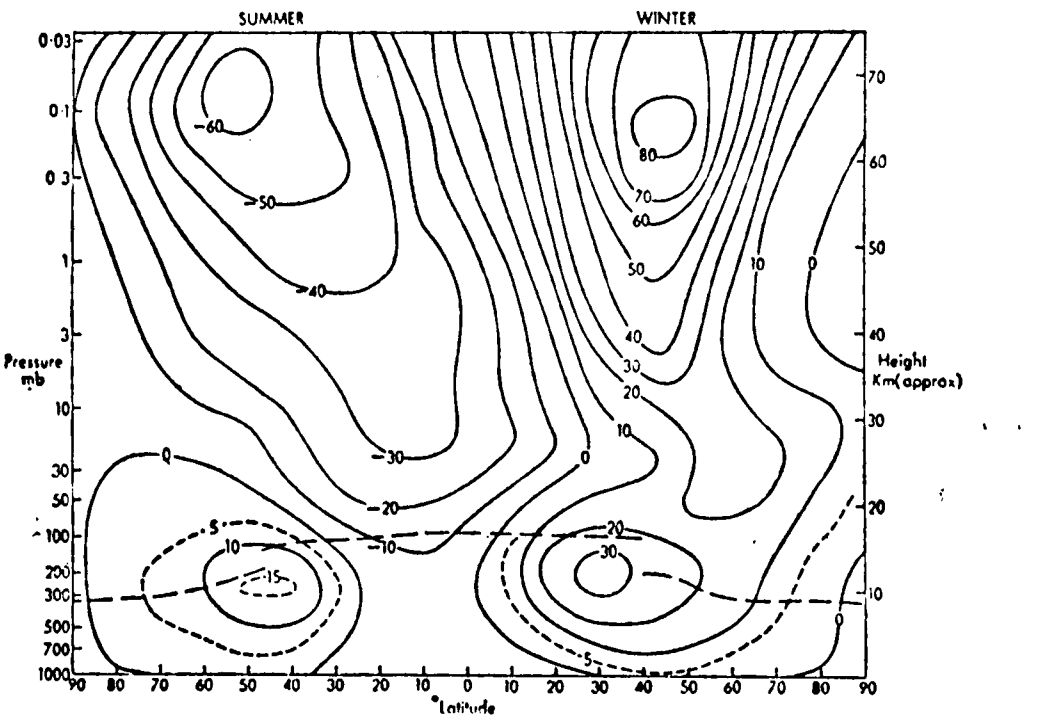

Fig.1.2 Representative zonal mean zonal winds.

From Murgatroyd(1969a).

1.2.2 Zonal winds

Fig. 1.2 shows the zonal wind field corresponding to the temperatures of Fig. 1.1. In the troposphere and lower stratosphere mid-latitudes there are westerly jets with maxima, of about 30 m s^{-1} in winter and 15 m s^{-1} in summer, near the tropopause breaks. There are easterlies in low latitudes and near the poles in the troposphere. In the upper stratosphere and mesosphere there is a strong westerly jet in winter, maximum 80 m s^{-1} at 65 km, and an easterly jet in summer reaching -60 ms^{-1}. The summer easterlies encroach into the winter hemisphere.

The winds of Fig. 1.2 represent average conditions and indicate the magnitude of the annual oscillation above the tropopause. The zonal wind varies on the scales longer and shorter than one year, however, and an instantaneous value may be quite different from the mean. In the tropics there is a strong (amplitude ~ 20 m s^{-1}) quasi-biennial oscillation in the stratosphere which is increasingly modulated by a semi-annual cycle (amplitude reaching ~30 m s^{-1}) above about 32 km.

In addition to these cyclic variations there are irregular short-term fluctuations associated with vertically propagating waves which occur over a wide range of spatial and time scales from small-scale turbulence (on the scale of a few metres) through internal gravity waves (horizontal scale ~100 km) and synoptic scale waves ($\lambda \sim 1000$ km) to planetary scale waves ($\lambda \sim 10000$ km). These waves are of varying significance for the transport of heat and momentum at different altitudes. In particular planetary waves are important for the meridional circulation of the stratosphere although they may not be significant to the mean zonal wind or temperature fields (see Chapter 8). One striking effect of planetary waves is the sudden stratospheric warming (Scherhag, 1952) that occurs during some winters and in which the high latitude polar night jet may actually reverse for several days.

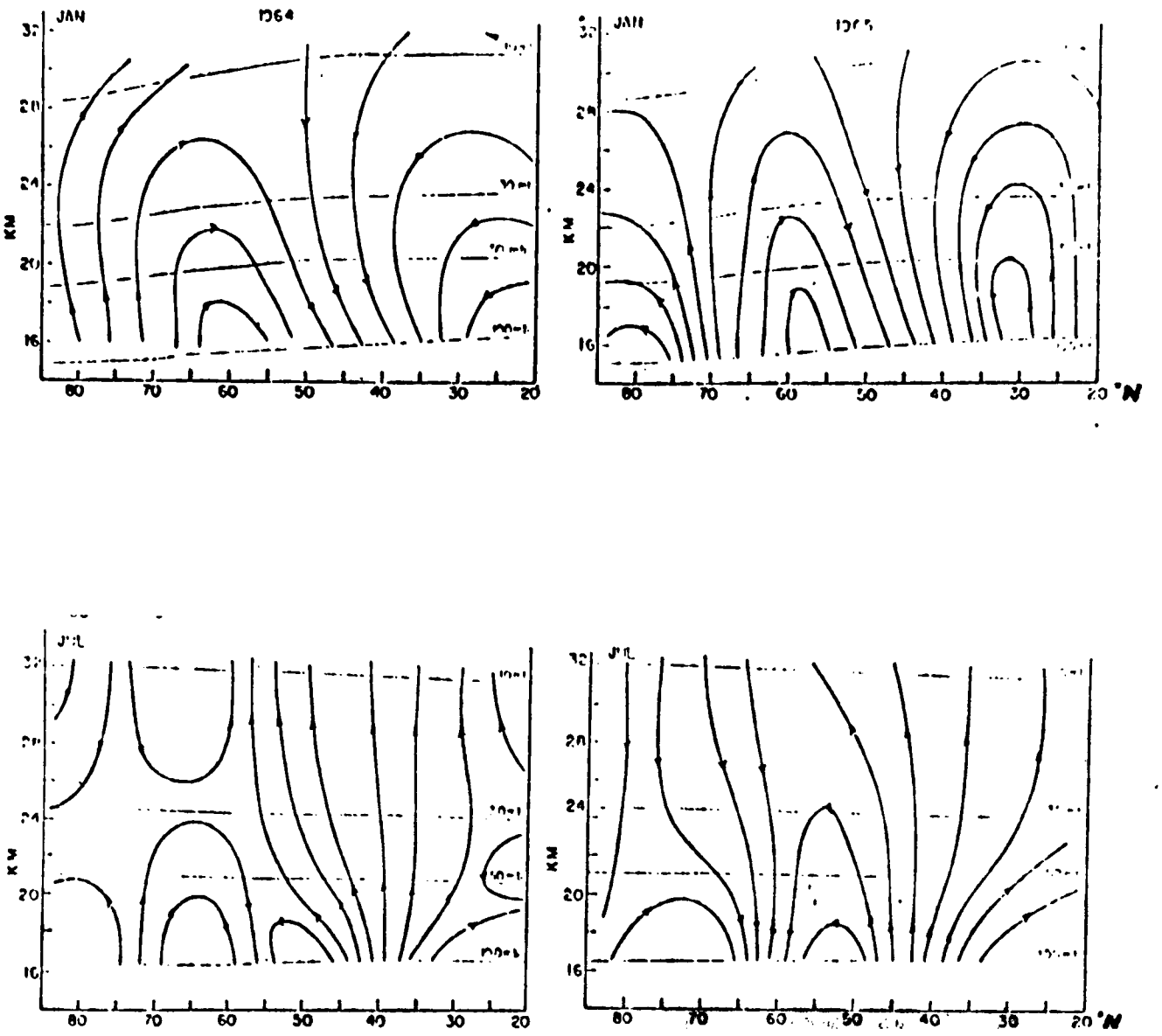

Fig.1.3 Mean meridional circulations for January and July, 1964 and 1965. From Vincent(1968).

1.2.3 The mean meridional circulation

The vertical and meridional velocities are smaller and more variable than the zonal velocity and more difficult to measure. Thus they are usually deduced indirectly from the momentum and thermodynamic equations using observed zonal velocities and temperatures. Meridional ciculations so derived by, among others, Murgatroyd (1969b) show in the troposphere a three-cell structure in each hemisphere: a direct Hadley cell in low latitudes, an indirect Ferrel cell in mid-latitudes and a weaker direct cell in polar regions. Similar calculations were made by Vincent (1968) for the lower stratosphere of the northern hemisphere and Adler (1975) for the southern hemisphere. Vincent's results for the solstices are shown in Fig. 1.3. The tropospheric structure is replaced by a two-cell system with ascent throughout the summer hemisphere and in winter high latitudes and descent in winter mid-latitudes. In the upper stratosphere and mesosphere, in order to maintain the observed zonal flow against frictional effects, it appears that the mean meridional circulation consists of one large cell with rising motion near the summer pole and sinking near the winter pole (see Chapter 8).

1.2.4 Ozone

Although ozone is only a minor constituent of the atmosphere (maximum mixing ratio of the order of 10 ppm) it plays an important role in the heat balance through its absorption of solar radiation and emission of thermal radiation. It also protects the earth's surface from ultra-violet rays which would be harmful to living tissue. In most of the experiments described in this thesis, as in the atmosphere, the ozone concentration depends on the radiative flux, temperature, mean circulations, eddy motions and the concentration of other minor constituents. In turn, these quantities depend on each other and on the ozone distribution. The system is thus highly coupled and it is

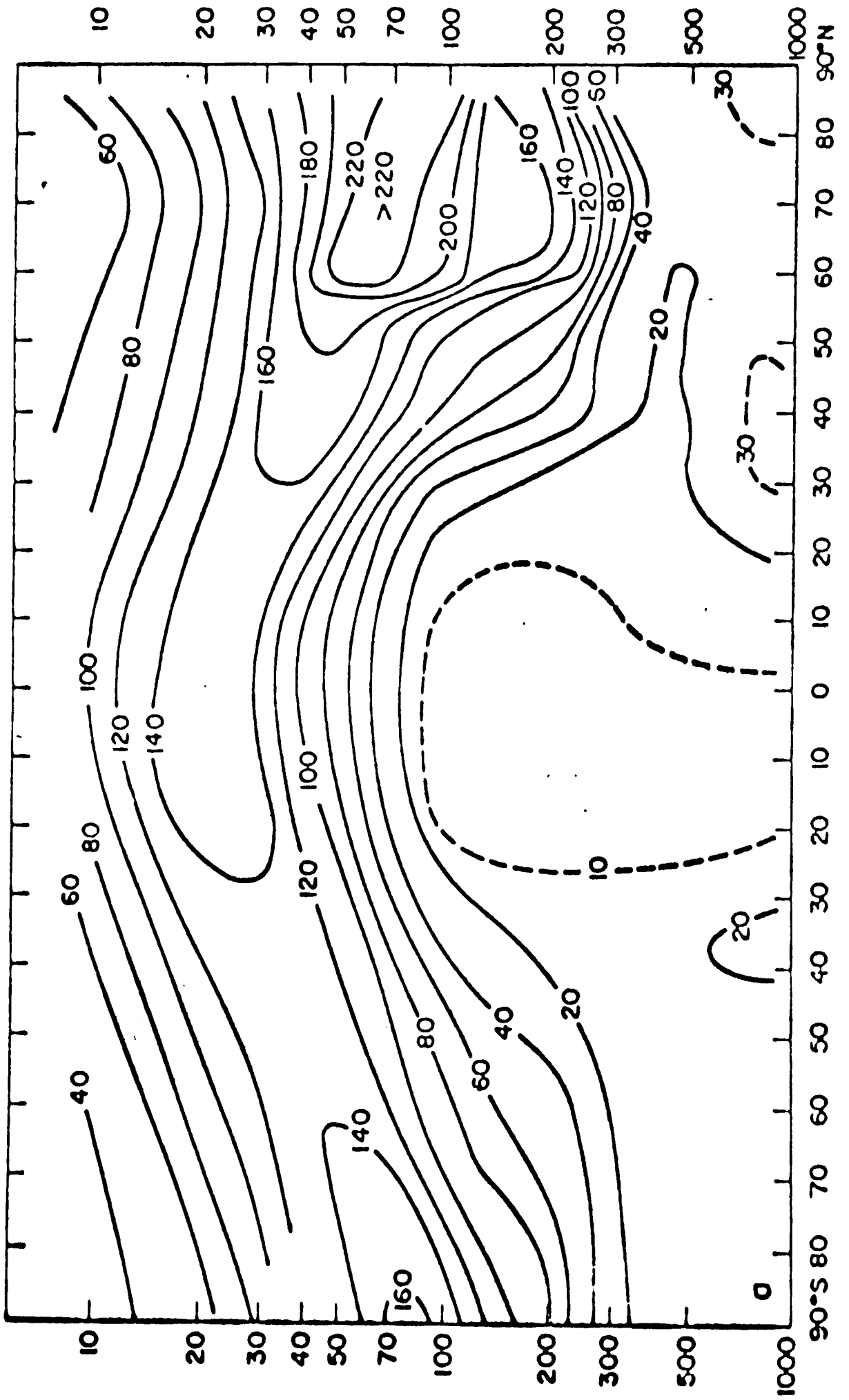

Figure 1.4 OZONE CROSS-SECTION (nb) FOR MARCH/APRIL. FROM "DÜTSCH(1971).

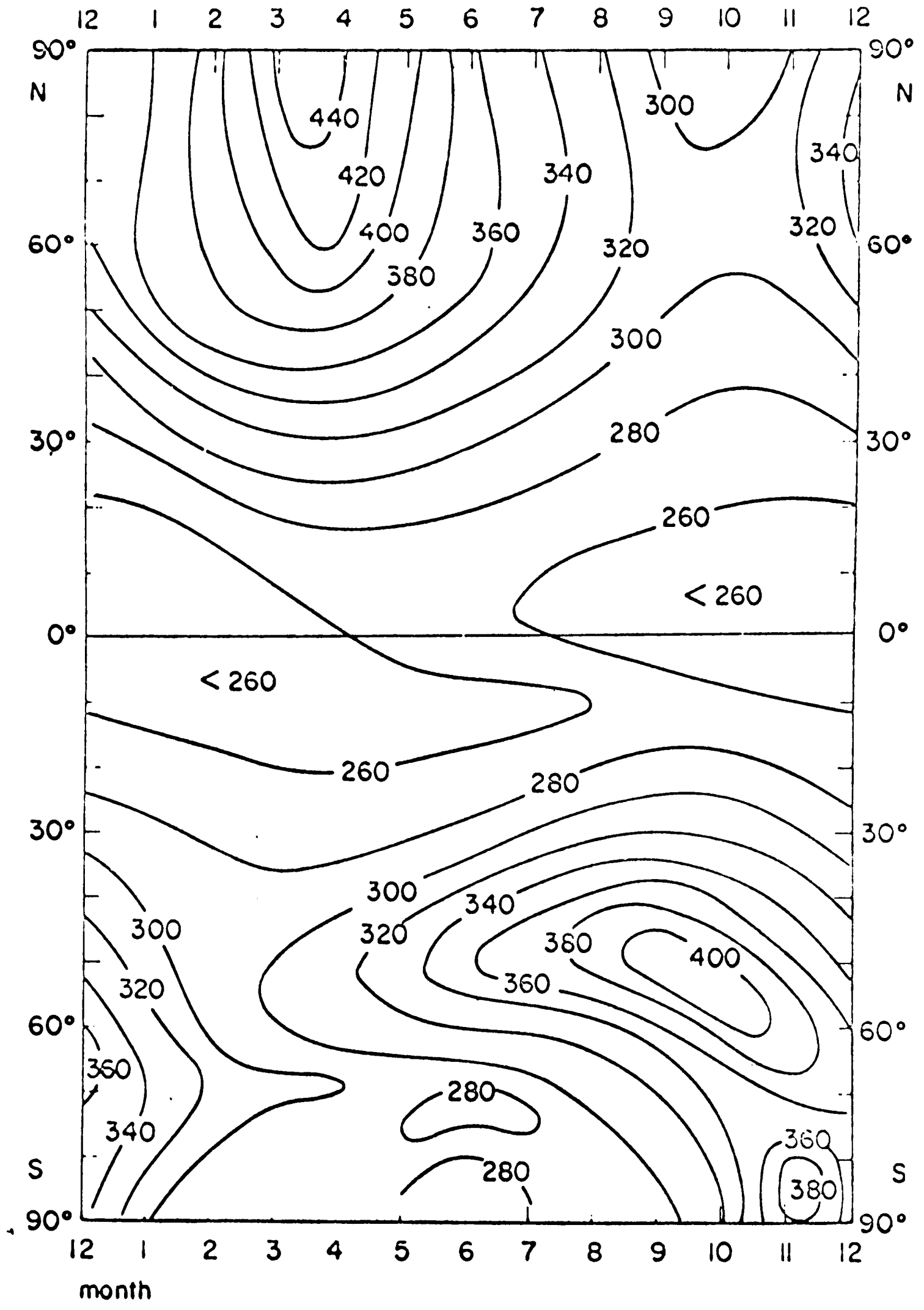

Figure 1.5 LATITUDE-TIME SECTION OF TOTAL OZONE (DOBSON UNITS). FROM DÜTSCH (1971).

important for a successful model to reproduce the observed ozone fields.

Fig. 1.4 shows a cross-section of ozone partial pressure in March/April from Dütsch (1971). Maximum amounts in the middle stratosphere occur in low latitudes, as would be expected from a photochemical source. In the lower stratosphere, however, there are large values in polar regions and low values near the equator; this is due to dynamical effects which dominate the slow photochemistry at these altitudes. The maximum partial pressure occurs at around 70mb in spring high latitudes. Fig. 1.5 shows a latitude-time section of ozone column density. Maxima occur in spring and minima in autumn in both hemispheres but the behaviour differs between the hemispheres in other respects. In the north the maximum occurs at the pole whereas in the south it is located around 50^{o}. This may be explained by different planetary wave activity in the two hemispheres (Pyle, 1976). The absolute values are generally larger in the north.

It is the task of the modeller to reproduce the fields of wind, temperature and ozone described above. To do this, as shall be demonstrated in Chapter 2, the effects of planetary waves, radiation and photochemistry must be included and schemes for calculating these are described in succeeding chapters. Radiation schemes, in particular, are discussed in some detail. The treatment of radiation is important because the solar radiation absorbed and its redistribution at longer wavelengths is crucial to the heat balance, and thus the circulation, of the atmosphere.

In Chapter 2 the framework of the Oxford University two-dimensional model will be described.

CHAPTER 2

Description of the Model

2.1 Introduction

The Oxford University Model was established to provide a framework for inquiring into the sensitivity of the atmosphere to changes imposed upon it, into the inter-relationships between dynamics, radiation and chemistry and for studying the budgets of heat, momentum and minor atmospheric constituents. To achieve these aims without using the vast computing requirements of a three-dimensional treatment a two-dimensional (zonal mean) time-dependent approach was adopted. Detailed formulations of the model have been given by Harwood and Pyle (1975) and Pyle (1976) but an outline will be given here as a background for the experiments described later.

2.2 The Dynamical Basis

2.2.1 The dynamical equations

The Navier-Stokes equations for a fluid on a rotating sphere are :

$$\frac{D\underline{v}}{Dt} = -2\underline{\Omega}\wedge\underline{v} + \underline{\Omega}\wedge(\underline{\Omega}\wedge\underline{r}) + \underline{g}' + \underline{F} - \frac{1}{\rho}\nabla p \qquad (2.1)$$

$$\frac{D\rho}{Dt} + \rho\,\nabla.\underline{v} = 0 \qquad (2.2)$$

where $$\frac{D}{Dt} \equiv \frac{\partial}{\partial t} + u\frac{\partial}{\partial x} + v\frac{\partial}{\partial y} + w\frac{\partial}{\partial \xi}$$

$\underline{r}$ is the position vector with coordinates x, y, ξ

$\underline{v}$ is the velocity vector with components u, v, w

$\underline{\Omega}$ is the angular velocity of the earth's rotation

$\underline{F}$ is the total frictional force per unit mass

$\underline{g}'$ is the acceleration due to gravity

ρ is the density

p is the pressure

$\frac{1}{\rho}\nabla p$ is the pressure gradients force and $2\,\underline{\Omega}\wedge\underline{v}$ the Coriolis force. The centrifugal force may be combined with the gravity term to give an effective gravity

$$\underline{g} = \underline{g}' + \underline{\Omega}\wedge(\underline{\Omega}\wedge\underline{r}) \quad .$$

The coordinate system is chosen with respect to a spherical earth radius a with x as distance eastwards y distance northwards and $\xi = -\ln(p/p_o)$ where p_o = 1000 *mb*. For application in a general circulation model a good approximation to the vertical component of the momentum equation is the hydrostatic equation :

$$dp = -\rho dZ \qquad (2.3)$$

where Z is the geopotential.

The x- component of the momentum equation is :

$$\frac{\partial u}{\partial t} + u\frac{\partial u}{\partial x} + v\frac{\partial u}{\partial y} + w\frac{\partial u}{\partial \xi} - \frac{uv}{a}\tan(\phi) - 2\Omega v\sin(\phi) + \frac{\partial Z}{\partial x} = 0 \qquad (2.4)$$

neglecting friction. ϕ is latitude. The equation of continuity (2.2) becomes :

$$\frac{\partial u}{\partial x} + \frac{\partial v}{\partial y} - \frac{v}{a}\tan(\phi) + \frac{\partial w}{\partial \xi} - w = 0 \qquad (2.5)$$

Also needed is the thermodynamic equation :

$$\frac{\partial \theta}{\partial t} + u\frac{\partial \theta}{\partial x} + v\frac{\partial \theta}{\partial y} + w\frac{\partial \theta}{\partial \xi} = q \qquad (2.6)$$

where the potential temperature $\theta = T\,(p/p_o)^{-\kappa}$, q is the diabatic heating rate and $\kappa = R/C_p$.

For a two-dimensional model dealing in zonal means all quantities must be averaged with respect to longitude λ. For example the zonal mean

of a quantity is given by :

$$\bar{s} = \frac{1}{2\pi} \int_0^{2\pi} s \, d\lambda$$

Deviation from the zonal mean is represented by $s' = s - \bar{s}$. Zonally averaging equations (2.4), (2.5) and (2.6) yields :

$$\frac{\partial}{\partial t}\left(\bar{\tau}\cos(\phi)e^{-\xi}\right) + \frac{\partial}{\partial y}\left(\bar{V}\bar{\tau}\right) + \frac{\partial}{\partial \xi}\left(\bar{W}\bar{\tau}\right) = H \qquad (2.7)$$

$$\frac{\partial}{\partial y}\bar{V} + \frac{\partial}{\partial \xi}\bar{W} = 0 \qquad (2.8)$$

$$\frac{\partial}{\partial t}\left(\bar{\theta}\cos(\phi)\, e^{-\xi}\right) + \frac{\partial}{\partial y}\left(\bar{V}\bar{\theta}\right) + \frac{\partial}{\partial \xi}\left(\bar{W}\bar{\theta}\right) = \bar{q}\cos(\phi)e^{-\xi} + Q \qquad (2.9)$$

where $\tau = (\Omega a \cos\phi + u)\, a \cos(\phi)$ is the absolute zonal angular momentum per unit mass.

$$V = ve^{-\xi}\cos(\phi) \qquad (2.10)$$

$$W = we^{-\xi}\cos(\phi) \qquad (2.11)$$

$$H = -\frac{\partial}{\partial y}\left(\overline{V'\tau'}\right) - \frac{\partial}{\partial \xi}\left(\overline{W'\tau'}\right) \qquad (2.12)$$

$$Q = -\frac{\partial}{\partial y}\left(\overline{V'\theta'}\right) - \frac{\partial}{\partial \xi}\left(\overline{W'\theta'}\right) \qquad (2.13)$$

H arises from the divergence of the eddy momentum flux and Q from the divergence of the eddy heat flux. The representation of eddy fluxes in a zonal mean model is one of the most difficult problems and will be discussed in section 2.4.3.

To complete the equations the geostrophic approximation is used in the y component of the momentum equation and combined with the hydrostatic equation and the equation of state $p = \rho RT$ to give a thermal wind relationship :

$$\frac{\partial \bar{\tau}}{\partial \xi} = -\frac{R\, e^{-\kappa\xi}}{2\Omega \tan(\phi)} \frac{\partial \bar{\theta}}{\partial \phi} \qquad (2.14)$$

Use of these approximations filters out acoustic and gravity waves which would lead to computational instability without rather short timesteps. White (1979) has pointed out that the inclusion of the term $\frac{uv}{a}\tan(\phi)$ in the x momentum equation without the corresponding term, $\frac{u^2}{a}\tan(\phi)$, in the y momentum equation leads to inconsistency in the energy budget. However experiments in which the extra term is included in the thermal wind equation have shown that this is only a small effect (Harwood, private communication).

Equations (2.7), (2.8), (2.9) and (2.14) form a closed set for the dependent variables $\bar{\tau}, \bar{V}, \bar{W}, \bar{\theta}$.

For convenience the equations are made dimensionless using a consistent set of scaling factors. Solutions are then obtained as follows. From Equation (2.8) a stream function ψ may be defined such that

$$\bar{V} = -\frac{\partial \psi}{\partial \xi} \qquad W = \frac{\partial \psi}{\partial \phi} \qquad (2.15)$$

The time derivatives in Equations (2.7.) and (2.9) are removed by differentiating with respect to ξ and ϕ respectively and using Equation (2.14). Substituting for $\bar{V}$ and $\bar{W}$ from Equation (2.15) an equation for ψ is obtained :

$$\begin{aligned} &-\bar{\tau}\psi_{\xi\xi} + 2\bar{\tau}\psi_{\xi\phi} + \left(e^{-\kappa\xi\xi_s}\frac{1}{\tan(\phi)}\bar{\theta}_\xi\right)\psi_{\phi\phi} \\ &-\left(\xi_s\bar{\tau}_\phi + e^{-\kappa\xi\xi_s}\left(1+\sin^2(\phi)\right)\frac{1}{\sin^2(\phi)}\bar{\theta}_\phi\right)\psi_\xi \\ &+\left(\xi_s\bar{\tau}_\xi + e^{-\kappa\xi\xi_s}\bar{\theta}_\xi + \kappa\xi_s e^{-\kappa\xi\xi_s}\frac{1}{\tan(\phi)}\bar{\theta}_\phi\right)\psi_\phi \qquad (2.16) \\ &= RHS \end{aligned}$$

where RHS is a function of H, Q and q but not ψ. Subscripts ξ and ϕ indicate differentiation with respect to these quantities. ξ_s is the scaling factor for the vertical coordinate. Given sufficient boundary conditions Equation (2.16) can be solved for ψ yielding the meridional circulation

which maintains the thermal wind balance between the zonal mean westerly wind and the zonal mean north-south temperature gradient against the perturbing effects of diabatic heating and eddy fluxes. $\bar{V}$ and $\bar{W}$, calculated from Ψ, are used in equations (2.7) and (2.9) to give values of $d\bar{\tau}/dt$ and $d\bar{\theta}/dt$ which yield $\bar{\tau}$ and $\bar{\theta}$ at the next timestep (see section 2.3.2 on time integration). The equation for Ψ is solved again at the new timestep with the new values of $\bar{\tau}$ and $\bar{\theta}$ and the process repeated. The boundary conditions on Ψ are $\Psi=0$ at $\phi=\pm\pi/2$, implying zero flux through the pole and $\Psi=0$ at $\xi=0$ and at the top boundary. The upper boundary condition is necessarily artificial but it has been shown (Harwood and Pyle, 1973) that the effects of the upper boundary are confined to within six vertical gridpoints of the lid. Thus by setting the upper boundary at about 100km the main region of interest (0-80km) will not be affected.

2.2.2 The treatment of matter

The equation for the time rate of change of a substance with mixing ratio X is :

$$\frac{\partial X}{\partial t} + u\frac{\partial X}{\partial x} + v\frac{\partial X}{\partial y} + w\frac{\partial X}{\partial \xi} = P$$

where P is the rate at which the substance is produced per unit mass of air. Using scaling factors and zonally averaging this becomes :

$$\frac{\partial}{\partial t}\left(\bar{X}e^{-3\xi_s}\cos(\phi)\right) + \frac{\partial}{\partial \phi}\left(\bar{V}\bar{X}\right) + \frac{\partial}{\partial \xi}\left(\bar{W}\bar{X}\right) = Pe^{-3\xi_s}\cos(\phi) + E \qquad (2.17)$$

where $$E = -\frac{\partial}{\partial \phi}\left(\overline{V'X'}\right) - \frac{\partial}{\partial \xi}\left(\overline{W'X'}\right)$$

The eddy flux divergence E is written in terms of mean quantities as described in section 2.4.3. Equation (2.17) is used to step forward in time

using the mean motion field obatined from equation (2.16).

2.3 Computational Details

2.3.1 Space representation

A portion of the finite difference grid used is shown in Fig. 2.1. The ϕ-ξ plane is divided into 19 x 29 equal rectangles of width $h = \pi/19$ and height $k = \frac{1}{2}$(pressure scale height). τ, θ, q, Q and H are held at the centre of each rectangle ; W at the midpoint of the horizontal sides ; V at the midpoint of the vertical sides and ψ at the corners. If the notation s(L,M) is used to denote the value of a variable s at the point $\phi = -\pi/2 + (L-1)h/2$, $\xi = (M-1)k/2$ then equation (2.15) may be written :

$$V(L,M) = \left[\psi(L,M-1) - \psi(L,M+1)\right]/k \quad \text{at} \begin{Bmatrix}\text{even M}\\ \text{odd L}\end{Bmatrix} \text{only}$$

$$W(L,M) = \left[\psi(L+1,M) - \psi(L-1,M)\right]/h \quad \text{at} \begin{Bmatrix}\text{odd M}\\ \text{even L}\end{Bmatrix} \text{only} \qquad (2.18)$$

Equation (2.18) ensures that the total mass of the system is conserved. Similarly the finite difference forms of equations (2.7) and (2.9) are constructed so that the total absolute angular momentum is conserved and the mass averaged potential temperature is constant for adiabatic motion. The finite difference analog of equation (2.16) is :

$$\begin{aligned}
&\psi(L+2,M+2)\, D_2(L,M) + \psi(L,M+2)\, D_1(L,M) + \psi(L-2,M+2)\, D_8(L,M)\\
&+ \psi(L+2,M)\, D_3(L,M) + \psi(L,M) + \psi(L-2,M)\, D_7(L,M)\\
&+ \psi(L+2,M-2)\, D_4(L,M) + \psi(L,M-2)\, D_5(L,M) + \psi(L-2,M-2)\, D_6(L,M)\\
&= RHS(L,M)
\end{aligned} \qquad (2.19)$$

in which D_i (L,M) are functions of $\bar{\tau}$ and $\bar{\theta}$ and RHS is a function of H, Q and q. These are given in Appendix A.

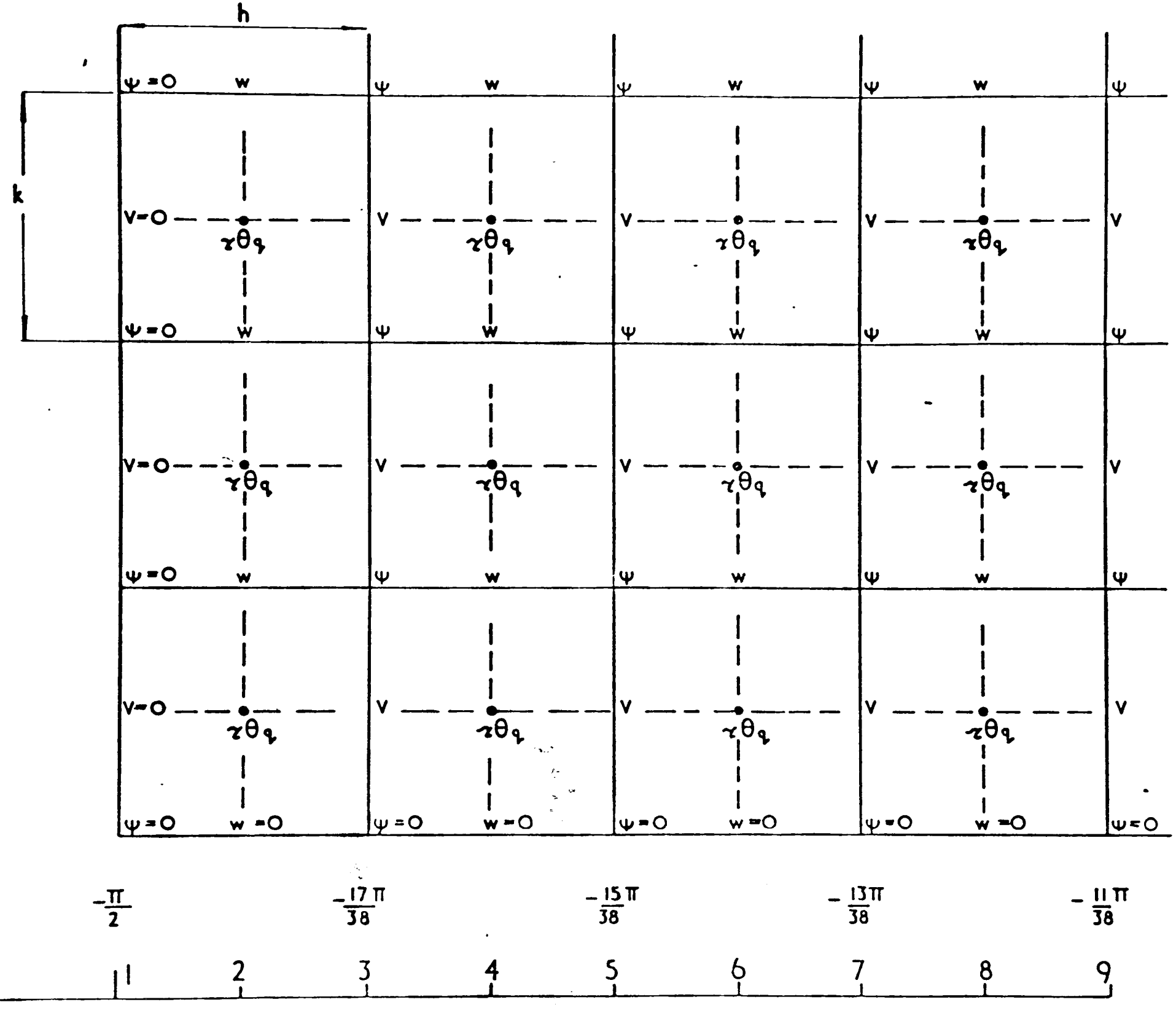

$\zeta^* = \log \frac{p_0}{p}$	M
1·5	7
	6
1	5
	4
0·5	3
	2
0	1

Fig.2.1 Section of the model grid.

The integration procedure is to solve (2.19) for ψ by Liebman relaxation using the values of $\bar{\tau}$, $\bar{\theta}$, H, Q and q at time t. $\bar{V}$ and $\bar{W}$ are calculated from and used in the finite difference forms of equations (2.7) and (2.9) to give $\partial\bar{\tau}/dt$ and $\partial\bar{\theta}/dt$ which are then used with the time integration scheme (see next section) to give the values of $\bar{\tau}$ and $\bar{\theta}$ at time $t + \Delta t$. The process is repeated for as many steps as required. The over-relaxation parameter for the Liebman relaxation was determined by a numerical experiment.

2.3.3 Time Integration

The Adams-Bashforth scheme is used for integration over time (see e.g. Haltiner, 1971). In this method the value α_n of a quantity α at time $t_o + n\Delta t$ (t_o is initial time, Δt is the timestep and n is an integer) is given by

$$\alpha_n = \alpha_{n-1} + \frac{\Delta t}{2}(3 f_{n-1} - f_{n-2}) \qquad (2.20)$$

where $$f_n = \left(\frac{\partial \alpha}{\partial t}\right)_{t = t_o + n\Delta t}$$

The next term in the expression (which indicates the order of the truncation error involved) is $$\frac{5}{12}(\Delta t)^3 \left(\frac{d^3\alpha}{dt^3}\right)_{t = t_o + (n-1)\Delta t}$$

Since this is an implicit scheme (i.e. it involves more than one time step) a spurious computational mode is generated but this decays exponentially if Δt is less than some value determined by the equation for the time rate - of - change. For example the photochemistry scheme, in the absence of advection, requires the solution of an equation like $\frac{\partial \alpha}{\partial t} = \frac{\alpha_e - \alpha}{T_r}$ where α is a concentration, α_e the equilibrium concentration and T_r the relaxation time constant.

It can be shown that the computational mode generated in the Adams-Bashforth scheme will decay if $\Delta t < T_r$. The physical mode represents an exponential approach to the equilibrium value with relaxation time T_c given by

$$T_c = T_r \left(1 + \frac{5}{12}\left(\frac{\Delta t}{T_r}\right)^2 + O\left(\frac{\Delta t}{T_r}\right)^3\right)$$

So a choice of $\Delta t = \frac{1}{2}T_r$ will give 90% accuracy for the relaxation time and ensure that the computational mode is damped. In all the runs described in this work Δt = 4 hours.

2.3.3. Conditions for solution of the equations

There is a singularity in equation (2.14) at $\phi=0$ due to the term $(\tan(\phi))^{-1}$; however this problem is circumvented by the grid chosen which does not require this expression to be evaluated at $\phi=0$.

Solutions to equation (2.16) can only be found if it is elliptic everywhere. This condition reduces to

$$-\frac{\partial\bar{\theta}}{\partial\xi}\frac{\partial\bar{\tau}}{\partial\phi} + \frac{\partial\bar{\theta}}{\partial\phi}\frac{\partial\bar{\tau}}{\partial\xi} \begin{cases} > 0 & ; \quad \phi > 0 \\ < 0 & ; \quad \phi < 0 \end{cases}$$

which expressed in physical terms means that the gradient of the absolute angular momentum on an isentropic surface must be directed towards the equator. This is achieved in the Model by introducing an equatorwards momentum flux whenever the equatorward $\bar{\tau}$ gradient is less than a certain value.

2.4 Eddy Fluxes

2.4.1 Boundary Fluxes

The momentum flux across the earth's surface is an important component of the angular momentum budget and is calculated as a function of the model state. The sensible heat flux is also calculated explicitly to

balance the tropospheric heat budget. The flux of latent heat through the lower boundary is specified (see section 2.5).

The fluxes of heat and momentum are calculated as functions of wind and temperature, using the method of Clarke (1970), at the lowest level. The underlying surface is assumed to be an infinite heat-capacity ocean with temperatures obtained by zonally averaging the monthly mean sea-surface temperatures of Washington and Theile (1970).

2.4.2 Convective adjustment

Above the tropopause the atmosphere can remain statically stable under the action of radiation alone. In the troposphere itself, however, static stability is maintained by vertical fluxes of heat associated with both cyclone and cumulus scale motion. To simulate this effect in the model an upward heat flux is introduced whenever the lapse rate exceeds 6.5 K km^{-1}.

2.4.3 Large scale eddy transport

Eddies play an essential part in maintaining the general circulation (Green, 1972). To include these deviations from the zonal mean is a major problem in a two-dimensional model. The approach usually adopted is that of Reed and German (1965) in which eddy fluxes are expressed in terms of the zonal mean variables using K-theory. Thus the northward eddy flux of a substance s is written :

$$\overline{v's'} = -K_{yy}\frac{\partial \bar{s}}{\partial y} - K_{y\zeta}\frac{\partial \bar{s}}{\partial \zeta}$$

and the upward flux :

$$\overline{w's'} = -K_{\zeta y}\frac{\partial \bar{s}}{\partial y} - K_{\zeta\zeta}\frac{\partial \bar{s}}{\partial \zeta}$$

The K factors are supposedly related to the slope of the mixing surface $\alpha = d\zeta/dy$ and are inter-related :

$$K_{y\zeta} = K_{\zeta y} = \frac{g}{RT}\,\bar{\alpha}\,K_{yy} \qquad K_{\zeta\zeta} = \left(\frac{g}{RT}\right)^2 \left(\bar{\alpha}^2 + \overline{\alpha'^2}\right) K_{yy}$$

The K factors are assumed to be functions of the basic state and independent of the property being diffused. Several sets of these coefficients have been calculated ; in the Oxford Model those of Luther (1973) are used. These are specified monthly from 0 to 60 km and from equator to north pole with a 1km resolution in height and 10^{o} in latitude.

K-theory is not entirely satisfactory. The justification for its use has been that it produces realistic distributions in tests. Recently work by Pyle and Rogers (1980) has suggested that a firmer physical base may exist, though unrelated to the mixing-length theory of Reed and German.

K-theory may only be employed for quantities that are conserved by the fluid motion. Thus it can be used for heat and matter but not for momentum which may be transferred to and from fluid particles by pressure forces. In the Model eddy fluxes of angular momentum are specified monthly in the stratosphere from values calculated by Dr. A.J. Crane from Nimbus IV and V spacecraft data. In more recent experiments with the model both eddy heat and momentum fluxes have been specified climatologically up to the mesopause level. The results of these experiments, together with a further discussion of the limitations of K-theory, are given in Chapter 8.

2.5 Radiation Schemes

The diabatic heating function q, required by the thermodynamic equation (2.6), may be divided into three parts : the heating due to the absorption of solar radiation (section 2.5.1), the cooling due to the transfer of thermal radiation (section 2.5.2) and heating due to latent heat

release. The last of these is specified climatologically from the values of Newell et al (1969).

A major part of the work described in this thesis has been the extension of the radiation calculations into the mesosphere, this is detailed in Chapters 3 and 5. Here a description of the schemes used previously will be given for the sake of comparison.

2.5.1 Solar heating

In the stratosphere the overwhelming contribution to the heating comes from the absorption of solar radiation by ozone. A method constructed by Mr. D Rendel calculates this heating as a function of height, latitude, date and ozone mixing ratio profile. The amount of ozone in the path of the solar beam, as a function of height for each latitude, is calculated and then tabulations of absorption versus absorber amount (Kennedy, 1964) used to compute the energy depletion of the solar beam crossing each rectangle and hence the rate of heating. An empirical formula was fitted to Kennedy's values :

$$S = 385.28 - 2.24764 \exp(-400A) - 12.953 \exp(-75A) - 12.9645 \exp(-4.5A) - 357.144 \exp(-0.1A)$$

where S is the power removed per unit area (in Wm^{-2}) and A is the path length of ozone traversed (in atmo-cm).

The heating rates are calculated for each latitude 5 times per day and a Gaussian integration performed to obtain the average heating rate for the day as a function of height above 25km. At first ozone mixing ratios were specified from Edwards (1970), more recently model-generated values have been employed. Heating is calculated between 25 and 80km.

2.5.2 Thermal radiation

The radiative cooling of the troposphere is fixed at 1.5 K day^{-1} below 8km and 0.75 K day^{-1} in the region 8 to 12 km. Between 12 and 24 km the cooling is set to zero as is the solar heating. Rodgers (1967) has shown that the lower stratosphere is in approximate radiative equilibrium.

The main contributions to the long-wave cooling in the stratosphere and mesosphere come from the 15μm band of carbon dioxide and the 9.6μm band of ozone. Following Houghton (1968) this cooling is treated as a function of height and temperature only :

$$\frac{\partial T}{\partial t} = K_1(\xi)\, B(T) + K_2(\xi) \qquad (2.21)$$

where B(T) is the Planck function at temperature T. The factors K_1 and K_2 were calculated for CO_2 and O_3 by Pyle (1976). The TELLUS program (based mainly on the work described by Rodgers and Walshaw, 1966) was used to calculate the heating rates appropriate to nine different temperature profiles and then dT/dt was plotted against B(T) at several different heights to find $K_1(\xi)$ and $K_2(\xi)$ by a least squares fit. The 9.6μm O_3 cooling is calculated between 25 and 60 km. The 15μm CO_2 cooling is calculated from 25 to 80 km.; however above 60 km the regressions for K_1 and K_2 are not very good. This is because heat transfer between different layers of the atmosphere becomes important (i.e. the cooling to space approximation is no longer valid) and at higher altitudes Local Thermodynamic Equilibrium breaks down so that Equation (2.21) is no longer applicable. For these reasons the net heating rate, q, at 55 km is reduced smoothly to zero at 80 km.

2.6 Photochemical Schemes

The radiative balance of the atmosphere depends critically on the ozone distribution. This is determined by the solar flux and by the concentrations of other minor constituents which react chemically with ozone. For a model to be able to simulate the feedback that occurs between radiation, temperature and ozone distribution it needs an interactive photochemical scheme. In most of the runs described in this thesis a simple linearised photochemical scheme has been used but in some, particularly those described in Chapter 7, a more complete non-linear scheme has been introduced. Both will mow be briefly described.

2.6.1 Linear photochemical scheme

The classical oxygen only photochemical scheme (Chapman, 1930) consists of the reactions :

$$
\begin{aligned}
O_2 + h\nu &\rightarrow O + O && J_2 \\
O_2 + O + M &\rightarrow O_3 + M && k_2 \\
O_3 + h\nu &\rightarrow O_2 + O && J_3 \\
O_3 + O &\rightarrow 2O_2 && k_3 \\
O + O + M &\rightarrow O_2 + M && k_1
\end{aligned}
\qquad (2.22)
$$

where k_i and J_i are the reaction rate constants and dissociation rates. The last reaction is not important below about 55 km and is neglected. Assuming a rapid equilibrium is established between O and O_3 the production rate of ozone is given by (Dütsch, 1968) :

$$
\frac{d[O_3]}{dt} = 2J_2[O_2] - \frac{2k_3 J_3 [O_3]^2}{k_2 [O_2][M]} \qquad (2.23)
$$

In equilibrium $$[O_3]_e = \left(\frac{J_2 k_2 [M]}{J_3 k_3}\right)^{1/2} [O_2] \quad .$$

Considering small perturbations from the equilibrium state Equation (2.23) may be written :

$$\frac{d[O_3]}{dt} = \frac{[O_3]_e - [O_3]}{t_r} \qquad (2.24)$$

to first order in perturbation quantities.

The relaxation time t_r is given by :

$$t_r = \frac{k_2 [O_2] [M]}{4 k_3 J_3 [O_3]_e}$$

Dissociation coefficients and values of $[O_3]_e$ and t_r were calculated for the solstices and equinoxes at all gridpoints (Pyle, 1976). In the Model the rate of change of ozone concentration is determined by Equation (2.24), using the appropriate $[O_3]_e$ and t_r, unless t_r is less than 6 hours in which case $[O_3]$ is set to its equilibrium value $[O_3]_e$.

2.6.2 More complete non-linear scheme

The Chapman scheme tends to predict too high values for $[O_3]$ because it neglects other ozone destruction mechanisms. A scheme involving all the reactions in the stratosphere would need prohibitive amounts of computing time but a scheme incorporating only the most important reactions gives satisfactory results. The reactions used in a more complete photochemical scheme for the Model are given in Table 2.1 ; those involving chlorine compounds are only included in perturbation studies (see Chapter 7). The computational method (Pyle, 1980) is to write continuity equations (including photochemical sources and eddy fluxes) for the following families of species :

$O(^1D)$, O and O_3; N, NO, NO_2 and $ClONO_2$; HNO_3; H_2O_2; H, OH and HO_2; Cl, ClO, $ClONO_2$ and HCl; $CFCl_3$; CF_2Cl_2. Photochemical equilibrium is assumed among the species in each group. The other species : H_2O, CH_4, H_2, N_2O and CO are assumed to be invariant and are specified, independent of latitude.

The results of the Model as specified in this Chapter (with the linear photochemical scheme) are discussed in section 6.1.

Table 2.1

The photochemical scheme.

$O_2 + h\nu \rightarrow O + O$	
$O + O_2 + M \rightarrow O_3 + M$	1.05E(−34) exp (510/T)
$O_3 + h\nu \rightarrow O + O_2$	$\lambda > 3077$ Å
$O_3 + h\nu \rightarrow O(^1D) + O_2$	$\lambda \leq 3077$ Å
$O + O_3 \rightarrow 2O_2$	1.9E(−11) exp (−2300/T)
$O(^1D) + N_2 \rightarrow O + N_2$	2.0E(−11) exp (108/T)
$O(^1D) + O_2 \rightarrow O + O_2$	2.9E(−11) exp (67/T)
$O(^1D) + H_2O \rightarrow 2OH$	2.3E(−10)
$O(^1D) + CH_4 \rightarrow CH_3^* + OH$	1.3E(−10)
$O(^1D) + H_2 \rightarrow H + OH$	1.3E(−10)
$OH + O \rightarrow H + O_2$	4.2E(−11)
$H + O_2 + M \rightarrow HO_2 + M$	2.1E(−32) exp (290/T)
$HO_2 + O \rightarrow OH + O_2$	3.5E(−11)
$H + O_3 \rightarrow OH + O_2$	2.6E(−11)
$OH + O_3 \rightarrow HO_2 + O_2$	1.5E(−12) exp (−1000/T)
$HO_2 + O_3 \rightarrow OH + 2O_2$	3.7E(−14) exp (−1025/T)
$CO + OH \rightarrow CO_2 + H$	(1 + 4.18E(−20)·[M])·2.1E(−13) exp (−115/T)
$HO_2 + HO_2 \rightarrow H_2O_2 + O_2$	6.4E(−13) exp (500/T)
$H_2O_2 + OH \rightarrow H_2O + HO_2$	1.0E(−11) exp (−750/T)
$H_2O_2 + h\nu \rightarrow 2OH$	
$OH + HO_2 \rightarrow H_2O + O_2$	5.1E(−11)
$OH + CH_4 \rightarrow H_2O + CH_3$	2.36E(−12) exp (−1710/T)
$OH + OH \rightarrow H_2O + O$	1.0E(−11) exp (−550/T)
$O(^1D) + N_2O \rightarrow 2NO$	7.0E(−11)
$O(^1D) + N_2O \rightarrow N_2 + O_2$	7.0E(−11)
$NO + O_3 \rightarrow NO_2 + O_2$	9.0E(−13) exp (−1200/T)
$NO_2 + O \rightarrow NO + O_2$	9.1E(−12)
$NO_2 + h\nu \rightarrow NO + O$	
$NO_2 + O_3 \rightarrow NO_3\dagger + O_2$	1.2E(−13) exp (−2450/T)
$HO_2 + NO \rightarrow NO_2 + OH$	1.2E(−12)
$NO_2 + OH + M \rightarrow HNO_3 + M$	Anastasi *et al.* (1976)
$HNO_3 + h\nu \rightarrow NO_2 + OH$	
$HNO_3 + OH \rightarrow H_2O + NO_3$	8.0E(−14)
$NO + h\nu \rightarrow N + O$	Based on Cieslik and Nicolet (1973)
$N + NO \rightarrow N_2 + O$	8.2E(−11) exp (−410/T)
$N + O_2 \rightarrow NO + O$	5.5E(−12) exp (−3220/T)
$N + O_3 \rightarrow NO + O_2$	5.0E(−12) exp (−650/T)
$CFCl_3 + h\nu \rightarrow 3Cl$	
$CF_2Cl_2 + h\nu \rightarrow 2Cl$	
$CFCl_3 + O(^1D) \rightarrow ClO + 2Cl$	2.3E(−10)
$CF_2Cl_2 + O(^1D) \rightarrow ClO + Cl$	2.0E(−10)
$Cl + O_3 \rightarrow ClO + O_2$	2.7E(−11) exp (−257/T)
$ClO + O \rightarrow Cl + O_2$	1.07(−10) exp (−224/T)
$ClO + NO \rightarrow Cl + NO_2$	8.0E(−12) exp (250/T)
$ClO + NO_2 + M \rightarrow ClONO_2 + M$	Based on Zellner (1977) and Zahniser *et al.* (1977)
$ClONO_2 + h\nu \rightarrow ClO + NO_2$	
$ClONO_2 + O \rightarrow ClO + NO_3$	4.5E(−12) exp (−840/T)
$CH_4 + Cl \rightarrow CH_3 + HCl$	7.3E(−12) exp (−1260/T)
$H_2 + Cl \rightarrow H + HCl$	3.5E(−11) exp (−2290/T)
$OH + HCl \rightarrow H_2O + Cl$	2.8E(−12) exp (−400/T)
$HO_2 + Cl \rightarrow O_2 + HCl$	2.5E(−11)

HNO_3, H_2O_2 and HCl are removed from the model troposphere with a time constant of 20 days.

*) $CH_3 \rightarrow 3HO_2$, instantaneous.

†) $NO_3 \rightarrow$ (a) $NO_2 + O$ and $\rightarrow$ (b) $NO + O_2$ with (a):(b) = 10:4, instantaneous.

N.B. 1.0E(−10) ≡ 1.0×10^{-10}.

References – see Pyle (1980)

CHAPTER 3

The calculation of infrared radiative cooling in the stratosphere and mesosphere

3.1 Introduction

The calculation of radiative heating and cooling forms an essential part of the specifications of a circulation model. In the stratosphere and mesosphere the major contribution to the thermal radiation budget comes from the 15μm band of carbon dioxide. The 9.6μm band of ozone is also significant in the stratosphere and this is discussed briefly in section 3.6. The main part of this Chapter is concerned with the use of a Curtis matrix in calculating atmospheric cooling due to the CO_2 15μm band.

Above about 60km the cooling - to - space approximation is not accurate and above approximately 75km the assumption of Local Thermodynamic Equilibrium (L.T.E.) is no longer valid for the CO_2 15μm band. In order to calculate the effects of thermal radiation at these altitudes a method which can incorporate transfer of radiation between levels and calculation of the source function is needed.

The Curtis matrix approach is such a method and as it needs to be calculated only once, for a standard atmosphere, and can then be used on any realistic temperature profile with only small error it provides an efficient method for use in numerical models. The calculation of the matrix, described below, is based on work by Williams (1971).

3.2 The solution of Schwarzchild's equation

The starting point of all radiative transfer theory is Schwarzchild's equation :

$$\frac{\partial I_\nu(\theta,z')}{\partial z'} = -k_\nu(z')\sec(\theta)\left[I_\nu(\theta,z') - J(z')\right] \qquad (3.1)$$

expressed here in a form applicable to the stratified atmosphere of Fig. 3.1. $I_\nu(\theta, z')$ is the monochromatic (wavenumber $\nu = 1/\lambda$) radiative intensity crossing, at angle θ to the vertical, an infinitessimal layer of atmosphere thickness dz' at height z'. $k_\nu(z')$ is the monochromatic volume absorption coefficient which is a rapidly varying function of frequency depending on the structure of the spectral band under consideration. $J_\nu(z')$ is the source function (equal to the local Planck function under the conditions of L.T.E.).

To solve equation (3.1) first an optical depth, τ, is defined :

$$\tau = \int_{z'}^{z} k_\nu(z'') \sec(\theta)\, dz''$$

where only the case $z > z'$ is considered at present.

so $$\frac{\partial \tau}{\partial z'} = -k_\nu(z') \sec(\theta)$$

and equation (3.1) may be written

$$\frac{\partial I_\nu(\theta, z')}{\partial \tau} = I_\nu(\theta, z') - J_\nu(z')$$

This equation may be integrated with the help of an integrating factor $e^{-\tau}$:

$$I_\nu(\theta, z')\, e^{-\tau} \Big|_b^z = \int_z^b -J_\nu(z')\, e^{-\tau} \frac{\partial \tau}{\partial z'}\, dz'$$

or

$$I_\nu(\theta, z) = I_\nu(\theta, b)\, e^{-\tau(z'=b)} + \int_b^z k_\nu(z') \sec(\theta) J_\nu(z') e^{-\tau} dz' \qquad (3.2)$$

where b is the bottom of the region under consideration. The first term on the right-hand side is the intensity at z due to the intensity $I_\nu(\theta, b)$ incident at the bottom boundary, the second term is the attenuated intensities originating from all layers of the atmosphere between b and z. The attenuating factor $e^{-\tau}$ is called the transmission of the atmospheric path with optical depth τ :

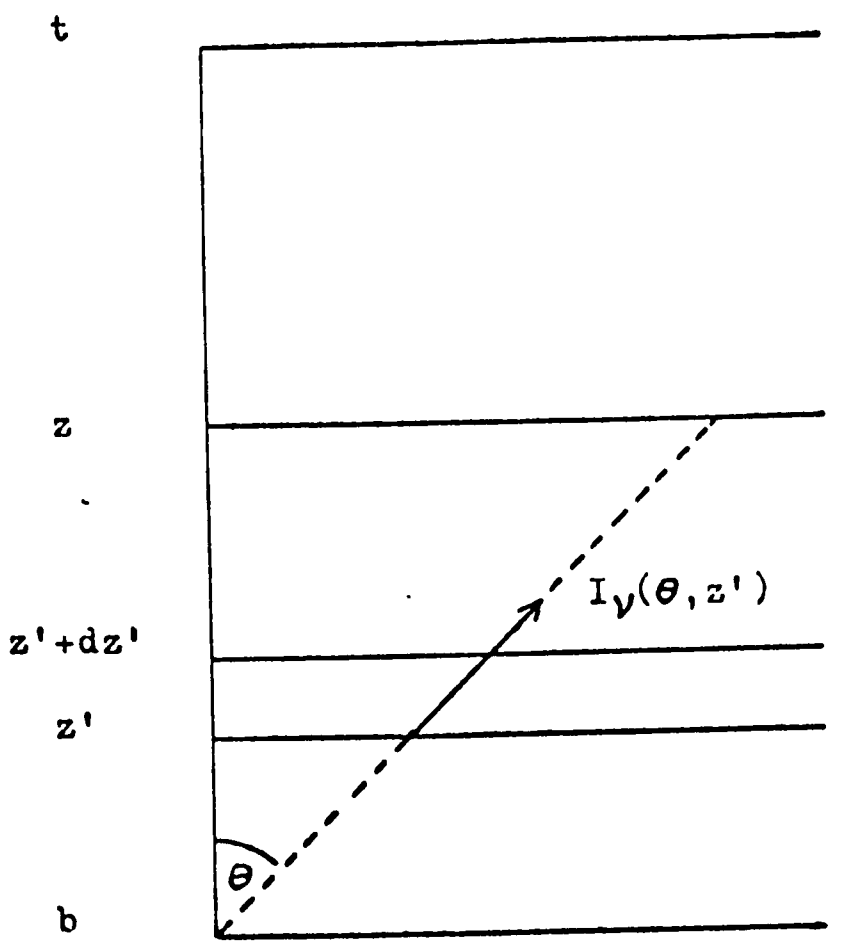

Figure 3.1 Stratified Atmosphere

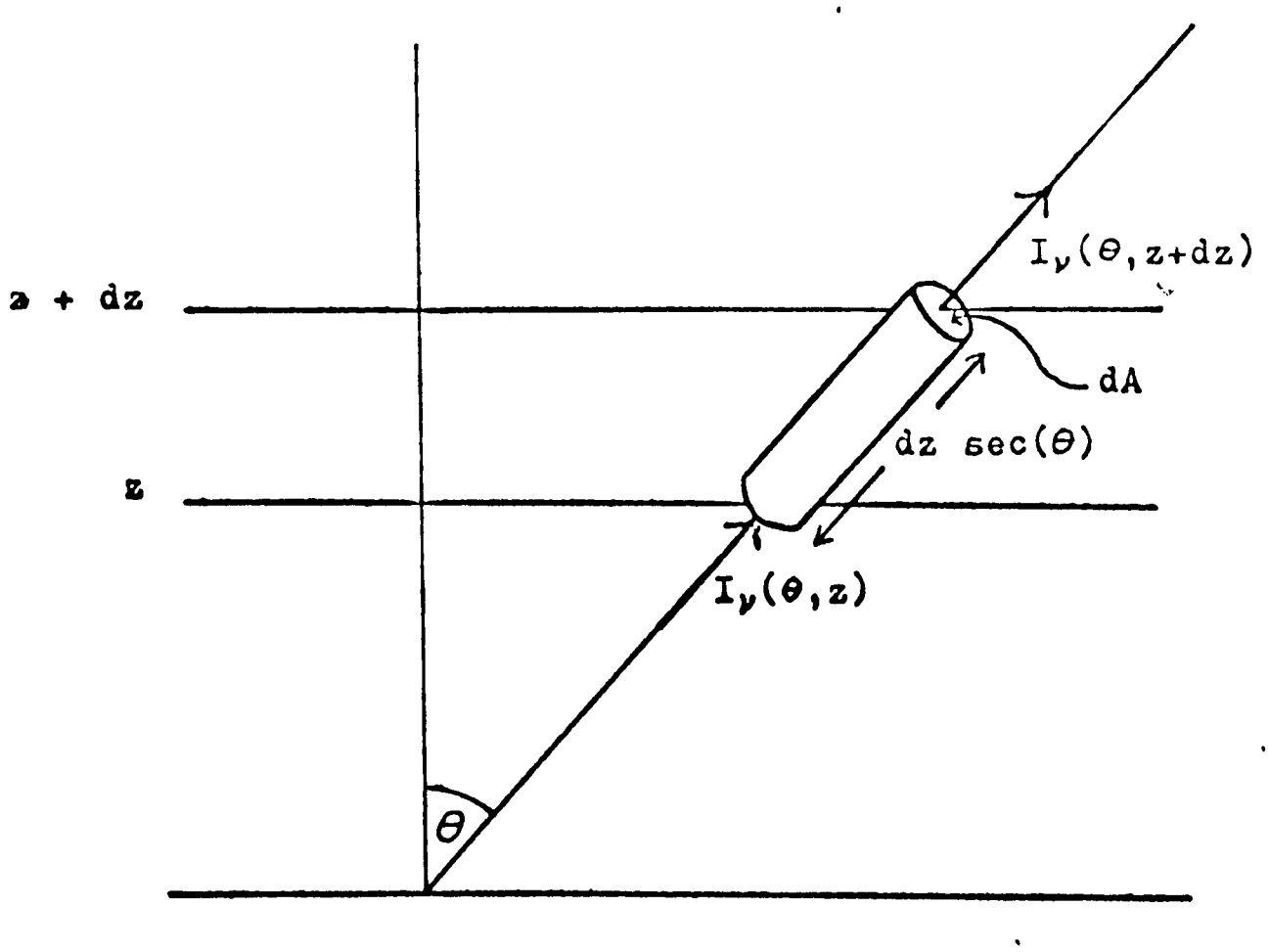

Figure 3.2 Cylindrical volume element along the direction of $I_\nu(\theta, z)$

$$T_\nu(\theta,z,z') = e^{-\tau} = \exp\left\{-\int_{z'}^{z} k_\nu(z'')\sec(\theta)\,dz''\right\}$$

so that $$\frac{\partial T_\nu(\theta,z,z')}{\partial z'} = T_\nu(\theta,z,z')\,k_\nu(z')\sec(\theta)$$

Equation (3.2.) may be written :

$$I_\nu(\theta,z) = I_\nu(\theta,b)\,T_\nu(\theta,z,b) + \int_b^z J_\nu(z')\,\frac{\partial T_\nu}{\partial z'}(\theta,z,z')\,dz'$$

The upward flux of energy at z, F↑(z), is obtained by integrating $I_\nu(\theta,z)\cos(\theta)$ with respect to solid angle over a hemisphere and with respect to frequency over the band width $\Delta\nu$. If the lower boundary is the ground or a layer of cloud $I_\nu(\theta,b)$ may be assumed independent of θ. Both $I_\nu(\theta,b)$ and $J_\nu(z')$ vary little with frequency compared with the transmission thus $I_\nu(\theta,b)$ may be replaced by I (b) and $J_\nu(z')$ by J(z'). The integration for upward flux gives :

$$\frac{F^{\uparrow}(z)}{\pi\Delta\nu} = I(b)\,T_F(z,b) + \int_b^z J(z')\,\frac{\partial T_F(z,z')}{\partial z'}\,dz'$$

where $$T_F(z,z') = \frac{1}{\pi\Delta\nu}\int_{\Delta\nu}\int_0^{\pi/2} T_\nu(\theta,z,z')\cos(\theta)\,2\pi\sin(\theta)\,d\theta\,d\nu$$

is the flux transmission of a slab of atmosphere between z and z' for the spectral interval $\Delta\nu$.

The procedure may be repeated for the case $z<z'$ and the downward flux at z, F↓(z), due to the atmosphere between z and the upper boundary t is given by :

$$\frac{F^{\downarrow}(z)}{\pi\Delta\nu} = I(t)\,T_F(t,z) - \int_z^t J(z')\,\frac{\partial T_F(z',z)}{\partial z'}\,dz'$$

To avoid the calculation of the flux transmission gradients the flux equations are integrated by parts :

$$\frac{F^{\uparrow}(z)}{\pi \Delta \nu} = J(z) + \left[I(b) - J(b)\right] T_F(z,b) - \int_b^z T_F(z,z') \frac{dJ(z')}{dz'} dz' \qquad (3.3)$$

$$\frac{F^{\downarrow}(z)}{\pi \Delta \nu} = J(z) + \left[I(t) - J(t)\right] T_F(t,z) + \int_z^t T_F(z',z) \frac{dJ(z')}{dz'} dz' \qquad (3.4)$$

If the lower boundary is taken as the ground (b=0) and assumed to be black then $I(0) = B(T_g)$. The lower levels of the atmosphere are in L.T.E. so $J(0) = B(0)$; making a further assumption that the temperature of the air near the surface is equal to the ground temperature, i.e. $J(0) = B(T_g)$, the second term in equation (3.3.) vanishes. The lower limit of the integration in (3.3) may be raised from 0 to z_1 if the contribution from this region is small. The lower stratosphere is almost isothermal so $dJ(z')/dz'$ is very small there. The contribution from the troposphere to a point in the stratosphere is negligible because of the low transmission. Thus the lower boundary may be raised from the ground to about 20km without seriously affecting the calculation of upward flux above 20km.

The contribution to downward flux at 15μm from space and in the solar spectrum is negligible thus $I(t) = 0$ is a valid assumption if $t = \infty$, i.e. outside the atmosphere. It is more practical to set the upper boundary at a level Z ; the terms involving contributions from atmospheric regions above Z will be negligible if $dJ(z')/dz'$ is a constant above Z. Above about 70km and the breakdown of L.T.E. the source function is almost independent of local temperature so that for $Z \geq 70$km $dJ(z')/dz' \simeq 0$ and the condition is

satisfied. The flux equations become :

$$\frac{F^{\uparrow}(z)}{\pi \Delta\nu} = J(z) - \int_{z_1}^{z} T_F(z,z') \frac{dJ(z')}{dz'} dz' \qquad (3.5)$$

$$\frac{F^{\downarrow}(z)}{\pi \Delta\nu} = J(z) - J(Z) T_F(\infty;z) + \int_{z}^{Z} T_F(z,z') \frac{dJ(z')}{dz'} dz' \qquad (3.6)$$

A method for the numerical solution of the height integration was suggested by Curtis (1956). The atmosphere between z_1 and Z is divided into N-1 layers of equal thickness $\mathcal{E}$:

$$z = z_1 + (n-1)\mathcal{E}$$
$$z' = z_1 + (r+\alpha-1)\mathcal{E} \qquad 0 \leq \alpha \leq 1$$

thus n is the label of the layer under consideration ($1 \leq n \leq N$) and r is a count over all layers above, or below, layer n. The integration is replaced by a sum over levels :

$$\frac{F_n\uparrow}{\pi \Delta\nu} = J_n - \sum_{r=1}^{n-1} \int_0^1 T_F(n, r+\alpha) \frac{dJ_{r+\alpha}}{d\alpha} d\alpha$$

$$\frac{F_n\downarrow}{\pi \Delta\nu} = J_n - J_N T_F(\infty, n) + \sum_{r=n}^{N-1} \int_0^1 T_F(r+\alpha, n) \frac{dJ_{r+\alpha}}{d\alpha} d\alpha$$

Defining

$$T_{n,r} = \int_0^1 T_F(n, r+\alpha)\, d\alpha \qquad n > r$$
$$\int_0^1 T_F(r+\alpha, n)\, d\alpha \qquad n \leq r$$

and assuming that the source function is a linear function of height between two levels the flux equations may be expressed :

$$\frac{F_n\uparrow}{\pi \Delta\nu} = J_1 T_{n,1} - \sum_{r=2}^{n-1} J_r \left(T_{n,r-1} - T_{n,r}\right) + J_n \left(1 - T_{n,n-1}\right) \qquad (3.7)$$

$$\frac{F_n\downarrow}{\pi \Delta\nu} = J_n \left(1 - T_{n,n}\right) + \sum_{r=n+1}^{N-1} J_r \left(T_{n,r-1} - T_{n,r}\right) + J_N \left(T_{n,N-1} - T_F(\infty, n)\right) \qquad (3.8)$$

The source function and transmission calculations may now be separated. Defining a function of transmission differences C_F equations (3.7) and (3.8) may be written :

$$F_n^{\uparrow} = \sum_{r=1}^{n} C_F^{\uparrow}{}_{n,r}\, J_r \qquad\qquad F_n^{\downarrow} = \sum_{r=n}^{N} C_F^{\downarrow}{}_{n,r}\, J_r$$

or in matrix notation :

$$\underset{\sim}{F}^{\uparrow} = \underset{\approx}{C_F}^{\uparrow}\, \underset{\sim}{J} \qquad\qquad \underset{\sim}{F}^{\downarrow} = \underset{\approx}{C_F}^{\downarrow}\, \underset{\sim}{J}$$

These may be combined into one matrix equation :

$$\underset{\sim}{F} = \underset{\approx}{C_F}\, \underset{\sim}{J} \qquad (3.9)$$

where $\underset{\sim}{F}$ is a column matrix of dimension 2N with elements $F_N^{\downarrow}$, $F_N^{\uparrow}$,....., $F_n^{\downarrow}$, $F_n^{\uparrow}$,.....$F_1^{\downarrow}$, $F_1^{\uparrow}$ and $\underset{\approx}{C_F}$ is a matrix of dimensions N x 2N with alternate rows from $\underset{\approx}{C_F}^{\downarrow}$ and $\underset{\approx}{C_F}^{\uparrow}$.

The heating rate is determined by the divergence of the fluxes :

$$\frac{\partial T}{\partial t} = -\frac{1}{\rho c_p}\frac{\partial \hat{F}(z)}{\partial z} \qquad \text{where} \quad \hat{F} = F^{\uparrow} - F^{\downarrow}$$

$$= -\frac{g}{p c_p}\frac{\partial \hat{F}(s)}{\partial s}$$

where s is the vertical coordinate in a logpressure scale :

$$\frac{\partial s}{\partial z} = \frac{\rho g}{p}$$

Taking ε as the spacing, in pressure scale heights, between levels a quantity h may be defined such that

$$h(s) = -\varepsilon \frac{\partial \hat{F}(s)}{\partial s} \qquad (3.10)$$

The mean heating rate of layer n is

$$\bar{h}_n = -\left(\hat{F}_{n+1} - \hat{F}_n\right)$$

and of layer n-1 :

$$\bar{h}_{n-1} = -\left(\hat{F}_n - \hat{F}_{n-1}\right)$$

The heating rate at level n is assumed to be the average of the values in its two neighbouring layers i.e.

$$\begin{aligned} h_n &= \tfrac{1}{2}\left(\bar{h}_n + \bar{h}_{n-1}\right) \\ &= -\tfrac{1}{2}\left(\hat{F}_{n+1} - \hat{F}_{n-1}\right) \\ &= \tfrac{1}{2}\left(F^{\downarrow}_{n+1} - F^{\uparrow}_{n+1} - F^{\downarrow}_{n-1} + F^{\uparrow}_{n-1}\right) \end{aligned} \qquad (3.11)$$

For layers 1 and N a linear extrapolation is used. This formulation may be written :

$$\begin{aligned} \underset{\sim}{h} &= \underset{\approx}{A}\ \underset{\sim}{F} \\ &= \underset{\approx}{A}\ \underset{\approx}{C_F}\ \underset{\sim}{J} \qquad \text{using Equation (3.9)} \end{aligned}$$

or

$$\underset{\sim}{h} = \underset{\approx}{C}\ \underset{\sim}{J} \qquad (3.12)$$

This defines the Curtis matrix $\underset{\approx}{C} = \underset{\approx}{A}\ \underset{\approx}{C_F}$. Matrix $\underset{\approx}{A}$ consists of the multiplying factors given by equation (3.11). $\underset{\approx}{C_F}$ depends on the transmission functions. The separation of transmission and source functions makes the calculation of heating rates possible in regions where L.T.E. does not apply.

3.3 The Source Function

The source function is the intensity of the radiation emitted by the gas in the frquency interval of interest. In its ν_2 band carbon dioxide emits radiation at wavelengths around 15μm. The transitions which take place involve changes in the vibrational energy of the molecule and often

also in the rotational energy as each vibrational energy level has a fine structure of rotational lines.

Consider a transition between a state (v,j) and a state (v',j'), where v and j and the vibrational and rotational quantum number respectively, with line centre at ν_t. Because each of the levels has a natural width there is a finite probability of absorption or emission at all frequencies close to ν_t. Apart from radiative processes transitions may also be induced by collisions between molecules. The collisional relaxation time τ is defined as the average time a molecule exists in a particular state before being knocked into a different state by a collision. τ is inversely proportional to the probability of relaxation by collisions and the collision rate is directly proportional to pressure so $\tau(p) = \frac{p_s}{p}\,\tau(p_s)$ where p_s is a standard pressure.

[It is unfortunate that conventionally the same symbol, τ, is used for optical depth and collisional relaxation time. It should not lead to confusion here, however, as the two quantities are never used in the same expression.]

If L.T.E. prevails the population of the energy levels is distributed according to the Boltzmann distribution and maintained by collisional processes. The equilibrium population of the levels is disturbed by radiative processes and an indication of the validity of L.T.E. is given by $\tau(p)/\theta$ where θ is the radiative relaxation time (related to the spontaneous emission rate, see below). If this ratio is much less than unity the dominant relaxation mechanism is by collisions ; as it increases radiative effects become more important and one can say that L.T.E. breaks down where $\tau(p)/\theta \simeq 1$. For the CO_2 15μm band this occurs at about 75-80km. Because changes in rotational state alone involve much smaller amounts of energy collisions are more efficient at maintaining a Boltzmann distribution

among the rotational levels in one particular vibration state. Thus for rotational lines $\tau(\rho)/\theta = 1$ at about 150km and at all heights of interest in this work equilibrium may be assumed.

The spontaneous emission rate per unit volume is :

$$n(\nu) = \sum_t L_t(\nu)\ n(v')\ f(v';j')\ a(j',j)\ A(v',v)$$

the induced emission rate per unit volume :

$$ne(\nu) = \sum_t L_t(\nu)\ n(v')\ f(v',j')\ be(j',j)\ Be(v',v)\ \rho(\nu)$$

and the absorption rate per unit volume :

$$na(\nu) = \sum_t L_t(\nu)\ n(v)\ f(v,j)\ ba(j,j')\ Ba(v,v')\ \rho(\nu) \qquad (3.13)$$

where the suffix t denotes a particular transition

$L_t(\nu)$ is the line shape function i.e. the relative probability that the transition involves a photon of wavenumber ν.

n(v) is the number density of molecules in vibrational state v.

f(v,j) is the fraction of n(v) molecules in rotational state j.

a(j',j) A(v',v) is the Einstein coefficient for spontaneous emission, factorised into two components assuming the vibrational and rotational wave functions are separable.

be(j',j) Be(v',v) is the Einstein coefficient for induced emission.

ba(j,j') Ba(v,v') is the Einstein coefficient for absorption.

$\rho(\nu)$ is the energy density per unit wavenumber interval.

In equilibrium n + ne = na

$$\therefore\ \bar{\rho}(\nu) = \frac{a(j',j)\ A(v',v)}{\frac{g(j)\,g(v)}{g(j')\,g(v')}\ ba(j,j')\ Ba(v,v')\ e^{hc\nu/kT} - be(j',j)\ Be(v',v)} \qquad (3.14)$$

where the overbar on ρ indicates the thermodynamic equilibrium value and where the Boltzmann equilibrium distribution has been used viz :

$$\frac{\bar{n}(v)\, f(v,j)}{\bar{n}(v')\, f(v',j')} = \frac{g(j)\, g(v)}{g(j')\, g(v')}\; e^{hcv/kT}$$

g(j) is the statistical weight of state j.

For a system in thermodynamic equilibrium the Planck function for radiative energy density is :

$$\bar{\rho}(v) = \frac{8\pi hc v^3}{e^{hcv/kT} - 1} \qquad (3.15)$$

Equations (3.14) and (3.15) are only consistent if

$$\left.\begin{aligned} &\frac{g(j)\, g(v)}{g(j')\, g(v')}\; ba(j,j')\, Ba(v,v') = be(j',j)\, Be(v',v) \\ \text{and} \quad &\frac{a(j',j)\, A(v',v)}{be(j',j)\, Be(v',v)} = 8\pi hc v^3 \end{aligned}\right\} \qquad (3.16)$$

In general the system will not be in equilibrium and the net number of quanta emitted $cm^{-3} s^{-1} (cm^{-1})^{-1}$ is

$$Ne(v)\, dv = \left(n(v) + ne(v) - na(v) \right) dv$$

Which may be rewritten, using equations (3.13) and (3.16) :

$$Ne(v)dv = \sum_t L_t(v)\, n(v)\, f(v,j)\, ba(j,j')\, Ba(v,v') \;\times$$

$$\left(8\pi hc v^3 \frac{g(j)g(v)}{g(j')g(v')} \frac{n(v')f(v',j')}{n(v)f(v,j)} + \left(\frac{g(j)g(v)n(v')f(v',j')}{g(j')g(v')n(v)f(v,j)} - 1 \right) \rho(v) \right) \qquad (3.17)$$

Consider photons travelling only within a solid angle Ω in a direction making an angle θ to the vertical axis. The energy density of this radiation at altitude z is

$$\rho_\nu(\theta,z) = \frac{1}{c} I_\nu(\theta,z)\, d\Omega$$

Where c is the velocity of the photons (i.e. the speed of light). In a cylindrical element whose cross-sectional area is dA and length is dzsec(θ) (see Fig. 3.2) the net increase in number of photons travelling in this direction due to processes within the elements is $Ne(\theta,\nu)d\Omega\, d\nu\, dz\, sec(\theta)dA$ where the number per unit volume $Ne(\theta,\nu)$ is given by equation (3.17) with $\rho(\nu)$ replaced by $\rho_\nu(\theta,z)$ and the spontaneous emission term multiplied by $d\Omega/4\pi$ to give the contribution within the solid angle $d\Omega$. The net energy emitted within the volume is

$$Ne(\theta,\nu)\, d\Omega\, d\nu\, dz\, sec(\theta)\, dA\, hc\nu = \frac{\partial I_\nu(\theta,z)}{\partial z} dz\, d\Omega\, d\nu\, dA$$

Thus the change in radiative intensity between the two ends of the cylinder may be expressed by :

$$\frac{\partial I_\nu(\theta,z)}{\partial z} = hc\nu\, sec(\theta) \sum_t L_t(\nu)\, n(\nu)\, f(\nu,j)\, ba(j,j')\, Ba(\nu,\nu') \quad X$$

$$\left\{ 2hc\nu^3 \frac{n(\nu')\bar{n}(\nu)}{n(\nu)\bar{n}(\nu')} e^{-hc\nu/kT} + \frac{1}{c} I_\nu(\theta,z) \left[\frac{n(\nu')\bar{n}(\nu)}{n(\nu)\bar{n}(\nu')} e^{-hc\nu/kT} - 1 \right] \right\}$$

This is the equation of radiative transfer, comparison with equation (3.1) yields :

$$k_\nu(z) = h\nu \sum_t L_t(\nu)\, n(\nu)\, f(\nu,j)\, ba(j,j')\, Ba(\nu,\nu') \left(1 - \frac{n(\nu')\bar{n}(\nu)}{n(\nu)\bar{n}(\nu')} e^{-hc\nu/kT} \right)$$

$$J_\nu(z) = \frac{h\nu}{k_\nu(z)} \sum_t L_t(\nu)\, n(\nu)\, f(\nu,j)\, ba(j,j')\, Ba(\nu,\nu')\, 2hc^2\nu^3 \frac{n(\nu')\bar{n}(\nu)}{n(\nu)\bar{n}(\nu')} e^{-hc\nu/kT} \qquad (3.18)$$

alternatively : $$k_\nu(z) = \bar{k}_\nu(z)\,\frac{n(v)}{\bar{n}(v)}\,\frac{\left[1-\frac{n(v')\,\bar{n}(v)}{n(v)\,\bar{n}(v')}\,e^{-hc\nu/kT}\right]}{\left[1-e^{-hc\nu/kT}\right]}$$

$$J_\nu(z) = B_\nu(z)\,\frac{\bar{k}_\nu(z)}{k_\nu(z)}\,\frac{n(v')}{\bar{n}(v')}$$

where the Planck function

$$B_\nu(z) = \frac{2hc^2\nu^3}{\left(e^{hc\nu/kT}-1\right)}$$

Consider a fundamental band - that between the ground state (v=0) and the first excited state (v'=1). The population density of the lower state n(0) will not deviate greatly from its equilibrium value $\bar{n}(0)$. The same cannot be assumed for n(1) but $\frac{n(1)}{\bar{n}(1)}\,e^{-hc\nu/kT} \ll 1$ thus for

a fundamental band $$k_\nu(z) \simeq \bar{k}_\nu(z)$$

$$J_\nu(z) \simeq B_\nu(z)\,\frac{n(1)}{\bar{n}(1)}$$

The rate of increase of population density n(1) due to excitation by collisions between CO_2 and air molecules is

$$\frac{dn(1)}{dt} = k_1'\,n(0)\,n_A - k_1\,n(1)\,n_A$$

where k_1' , k_1 are rate constants and n_A is the number density of air molecules. If Hl is the rate of increase of n(1) due to radiative processes (i.e. the net number of photons absorbed per unit volume per second) then the kinetic equation, an expression for the steady state balance of n(1), may be written :

$$k_1'\,n(0)\,n_A - k_1\,n(1)\,n_A + Hl = 0$$

where processes which could increase n(1) by transfer from higher energy states have been ignored (for justification of this see Shved, 1965 and Kuhn and London, 1969).

In thermodynamic equilibrium Hl=0 and $\frac{k_1'}{k_1} = \frac{\bar{n}(1)}{\bar{n}(0)}$

This relationship between rate constants must apply under all conditions so, assuming $n(0) \simeq \bar{n}(0)$ the rate of change equation and the kinetic equation may be written :

$$\frac{dn(1)}{dt} = -k_1 n_A \left(n(1) - \bar{n}(1)\right)$$

$$k_1 n_A \left(n(1) - \bar{n}(1) = Hl \right. \qquad (3.19)$$

The source function becomes

$$J_\nu(z) = B_\nu(z) \left[1 + \frac{Hl}{k_1 n_A \bar{n}(1)} \right] \qquad (3.20)$$

The collisional relaxation time τ may be defined by

$$\frac{dE_v}{dt} = -\frac{E_v - \overline{E_v}}{\tau}$$

where E_v is the total vibrational excitation energy of a system of molecules. Assume this system is those in the first excited state then $E_v = n(1)\, hc\nu$ and

$$\frac{dn(1)}{dt} = -\frac{n(1) - \bar{n}(1)}{\tau}$$

By comparison with equation (3.19) $\tau = (k_1 n_A)^{-1}$

From equation (3.20) $J_\nu(z) = B_\nu(z) \left[1 + \frac{\tau Hl}{n(1)} \right]$ (3.21)

n_A is proportional to pressure so $\tau \propto p^{-1}$, as has been assumed earlier in this section. τ (p_s) has been measured in the laboratory for CO_2 in N_2 and O_2 but until recently (Allen, 1979) not at atmospheric temperatures. The effect of using different values of τ in calculating cooling rates is discussed in Chapter 4.

For hot bands, i.e. transitions which do not involve the ground (v=0) state similar arguments can be applied. Consider, for example, the transition from the v =2 state to the v=1 state. Assuming that

$$\frac{n(2)\ \bar{n}(1)}{\bar{n}(2)\ n(1)}\, e^{-hc\nu/kT} \ll 1$$

ignoring higher energy terms and assuming further that $\frac{\bar{n}(1)}{n(1)} \simeq 1$ the expression for the source function is :

$$J_\nu(z) = B_\nu(z)\left[1 + \frac{H2}{k_{21}\, n_A\, \bar{n}(2)}\right]$$

$$= B_\nu(z)\left[1 + \frac{\tau\, H2}{\bar{n}(2)}\right]$$

assuming τ is the same for hot bands as the fundamental band. From equation (3.18) an expression for the volume absorption coefficient under conditions of L.T.E. is obtained :

$$\bar{k}_\nu(z) = \sum_t L_t(\nu)\, \bar{n}(v)\, f(v,j)\, ba(j,j')\, Ba(v,v')\, h\nu \left[1 - e^{-hc\nu/kT}\right]$$

The absorption coefficient per atmo.-cm. is defined :

$$\bar{k}_{s\nu}(z) = \frac{n_s}{n}\ \bar{k}_\nu(z)$$

where n_s is the number density of CO_2 molecules at S.T.P. (i.e. Loschsmidt's number).

Or $$\bar{k}_{s\nu}(z) = \sum_t L_t(\nu)\, s_t$$

s_t is the line-strength of transition t :

$$s_t = n_s\, \frac{\bar{n}(v)}{n}\, f(v,j)\, ba(j,j')\, Ba(v,v')\, h\nu \left[1 - e^{-hc\nu/kT}\right]$$

The band strength

$$S_s^{v-v'} = \sum s_t$$

$$= n_s\, \frac{\bar{n}(v)}{n}\, Ba(v,v')\, h\nu \left[1 - e^{-hc\nu/kT}\right] \qquad (3.23)$$

The radiative relaxation time, θ, of an excited vibrational state is given by the inverse of the v-dependent component of the probability, per unit time, of spontaneous emission.

$$\theta^{-1} = A(v,v') = 8\pi h\nu^3 c \frac{g(v)}{g(v')} Ba(v,v') \qquad (3.24)$$

from equation (3.14).

Making use of the relationship

$$\frac{\bar{n}(v')}{n(v)} = \frac{g(v')}{g(v)} e^{-hc\nu/kT}$$

Ba(v,v') can be eliminated between equations (3.23) and (3.24) yielding :

$$4\pi S^{v-v'} B_\nu \theta = \bar{n}(v') h c \nu \qquad \text{where } S^{v-v'} = \frac{n}{n_s} S_s^{v-v'}$$

This relationship can be used to substitute for n(1) in equation (3.21) and n(2) in (3.22) giving a general expression for the source function :

$$J_\nu = B_\nu + \frac{hc\nu H}{4\pi S^{v-v'}} \frac{\tau}{\theta}$$

The quantity H is given by $H = \frac{-1}{hc\nu} \frac{d\hat{F}}{dz}$ and is thus related to h, defined by equation (3.10) :

$$H = \frac{1}{hc\nu} \frac{\rho g}{p} \frac{1}{\varepsilon} h$$

giving the final expression for the source function :

$$J_\nu = B_\nu + \frac{\rho g \tau}{4\pi S^{v-v'} p \theta} h$$

which may be written in matrix form :

$$\underset{\sim}{J} = \underset{\sim}{B} + \underset{\approx}{E}\,\underset{\sim}{h}$$

where $\underset{\approx}{E}$ is a diagonal matrix with elements $\frac{\rho g \tau}{4\pi S^{r-r'} p \theta}$ appropriate to each level of the atmosphere. A simpler derivation of this relationship is given by Houghton (1977).

It is now clear that the magnitude of the elements of $\underset{\approx}{E}$ determine the deviation from L.T.E. at each level. This equation may be combined with equation (3.12) to yield $\underset{\sim}{h} = \underset{\approx}{C}\,\underset{\sim}{B} + \underset{\approx}{C}\,\underset{\approx}{E}\,\underset{\sim}{h}$ which may be inverted to give $\underset{\sim}{h} = (\underset{\approx}{I} - \underset{\approx}{C}\,\underset{\approx}{E})^{-1}\,\underset{\approx}{C}\,\underset{\sim}{B}$ where $\underset{\approx}{I}$ is the unit matrix. This expresses the heating rate at each level in terms of known atmospheric parameters and avoids the intermediate step of calculating the source function explicitly.

The difference between using the sum of the heating rates calculated for individual bands and treating all bands as one combined band is discussed by Williams and Rodgers (1972).

3.4 Calculation of transmission functions

To calculate the elements of the Curtis matrix the transmissions of the atmosphere between each level and all the other levels must be found, or in the notation of section 3.1, the value of $T_{n,r}$ for all n and r. The integration of T_F over α (see definition of $T_{n,r}$) is carried out by the method devised by Kubik (1965).

$$T_F(z,z') = \frac{1}{\Delta\nu}\int_{\Delta\nu} 2\int_0^{\pi/2} \exp\left\{-\int_{z'}^{z} k_\nu(z'')\sec(\theta)\,dz''\right\}\cos(\theta)\sin(\theta)\,d\theta\,d\nu$$

$$= 2\int_0^{\pi/2} T_{\Delta\nu}(\theta,z,z')\cos(\theta)\sin(\theta)\,d\theta$$

where

$$T_{\Delta\nu}(\theta,z,z') = \frac{1}{\Delta\nu}\int_{\Delta\nu} \exp\left\{-\int_{z'}^{z} k_\nu(z'')\sec(\theta)\,dz''\right\}d\nu$$

$$= \frac{1}{\Delta\nu}\int_{\Delta\nu} e^{-\tau_0 \sec(\theta)}\,d\nu \qquad (3.25)$$

where $\tau_0 = \int_{z'}^{z} k_\nu(z'')\,dz''$

For a particular value of $\theta=\theta', T_F(z,z') = T_{\Delta\nu}(\theta', z,z')$. This value is usually denoted by the diffusivity factor $\beta = \sec(\theta')$. Williams (1971) discusses in detail the choice of β, showing that for weak absorption by a single line the appropriate value is 2, for strong Lorentz absorption 1.78 and for strong Doppler absorption about 1.65. He concludes that for a whole band the value that can be used most accurately under all conditions is 1.7.

$$T_F(z,z') = \frac{1}{\Delta\nu}\int_{\Delta\nu} e^{-\beta\tau_\nu}\, d\nu$$

The optical depth

$$\tau_\nu = \int_z^{z'} k_\nu(z'')\, dz''$$

$$\simeq \int_z^{z'} \bar{k}_\nu(z'')\, dz''$$

$$= \int_z^{z'} \bar{k}_{s\nu}(z'')\,\frac{n}{n_s}\, dz'' \qquad = \int_m^{m'} \bar{k}_{s\nu}(m'')\, dm''$$

The path-length is atmo.-cm., m, is related to z by $dm'' = \frac{n}{n_s}\, dz'' = \frac{x}{\rho_s g}\, dp''$ where x is the volume mixing ratio of CO_2 and ρ_s is the density of air at S.T.P. This integral is much simpler if the integrand may be represented by a homogeneous path. In this case $\tau_\nu = \bar{k}_{s\nu}\int dm''$.

The Curtis-Godson approximation has been shown to be sufficiently accurate for the CO_2 15μm band (Walshaw and Rodgers, 1963) and enables a mean absorber amount and mean pressure $\bar{p}$ to be defined for a homogeneous path such that the transmission is approximately equal to the real path.

$$\bar{m} = \int dm'' = \frac{1}{\rho_0 g}\int x\, dp''$$

$$\bar{p} = \frac{\int p''\, dm''}{\int dm''} = \frac{\int x\, p''\, dp''}{\int x\, dp''}$$

This idea may be extended futher to define the mass-weighted mean temperature, $\overline{T}$, of a path.

$$\overline{T} = \frac{\int T \, dm''}{\int dm''} = \frac{\int x \, T \, dp''}{\int x \, dp''}$$

For carbon dioxide the mixing ratio is constant up to about 100km and the expressions for m, p and T simplify further :

$$\overline{m} = \frac{x}{\rho g} |p - p'|$$

$$\overline{p} = \frac{1}{2}(p + p')$$

$$\overline{T} = \frac{1}{|p - p'|} \int T \, dp''$$

$\overline{T}$ may be simply evaluated by assuming that the temperature depends linearly on log (pressure) between levels.

It remains to calculate $\overline{k}_{s\nu} = \sum_t L_t s_t$ where L_t is the shape and s_t the strength of the line corresponding to transition t. Line-strengths have been calculated by Williams (1971) and Drayson and Young (1967). Lineshapes depend on the mechanism(s) by which the lines are broadened. Spectral lines suffer natural broadening due to the uncertainty in the exact position of the energy levels, however this effect is small ($\sim 3 \times 10^{-11}$ cm^{-1}) and negligible compared with other mechanisms. Important in the lower atmosphere is pressure, or Lorentz, broadening which is due to the effect of other molecules on the molecule which is changing its energy state. Assuming a 'strong' interaction between the molecules (i.e. billiard ball type collisions) and basic kinetic theory it can be shown that the line shape will be of the form

$$L_t(\nu) = \frac{\alpha_L}{\pi \left\{ (\nu - \nu_t)^2 + \alpha_L^2 \right\}}$$

where the Lorentz half-width $\alpha_L = (2\pi c \, t_c)^{-1}$. Because of its dependence on t_c ,

the time between collisions, α_L is proportional to pressure and may be written $\alpha_L = \alpha_{LS}\, p/p_s$. The expression only strictly applies to molecules all travelling with the same speed but errors incurred by averaging over all t_c are small compared with, say, the use of a single value of α_{LS} for air which involves taking the mean of two broadening partners (N_2 and O_2). α_{LS} is also dependent on temperature but this effect is less important and is neglected here. An appropriate value for α_{LS} for N_2 - pressure broadening is 0.08 cm^{-1} .

The other important source of line broadening is the Doppler effect in which the apparent frequency of the radiation emitted by a molecule is dependent on its velocity. Assuming that the translational states are in thermodynamic equilibrium it can be shown that the lineshape due to Doppler broadening is

$$L_t(\nu) = \frac{1}{\alpha_D \pi^{1/2}} \exp\left\{-\left(\frac{\nu-\nu_t}{\alpha_D}\right)^2\right\}$$

where the Doppler width $\alpha_D = \frac{\nu_t}{c}\left(\frac{2RT}{M}\right)^{1/2}$.

The dependence of α_D on temperature is small over the range of atmospheric temperatures and may be neglected without serious error. The value of α_D for T = 200K is $6.1 \times 10^{-4}\, cm^{-1}$. It can be seen that at high pressure ($\gtrsim$10mb) the Lorentz broadening dominates however its effect decreases with increasing altitude until Doppler broadening becomes the more important mechanism. At intermediate heights both effects are significant and fora single line the Voigt profile (a convolution of the Lorentz and Doppler shapes) may be used.

To evaluate $\bar{k}_{s\nu}$ exactly a knowledge of the position, shape and strength of every line in the band would be necessary and the calculation would involve a large amount of computing time. A way round this is to assume a particular distribution of lines within the band such that the

transmission may be expressed as an algebraic function. Two such band models have been used extensively - the Elsasser regular model and the Goody random model - however neither of these is particularly suitable for describing the CO_2 15μm band in which the lines are quite regularly spaced but of widely ranging strengths. An alternative is to use an independent line model; this assumes no overlapping of lines (a valid assumption for the CO_2 15μm band above 50km and a good approximation for some way below). In this case $\bar{k}_{s\nu}$ receives a contribution from only one line at any particular frequency and the summation over transitions may be removed :

$$\bar{k}_{s\nu} = L_t(\nu)\, s_t$$

The intergral over the frequency interval $\Delta\nu$ may be replaced by a sum of integrals over subinterval $\delta\nu_t$ where each $\delta\nu_t$ contains a single line. Equation (3.25) may then be written

$$T_{\Delta\nu}(\theta, z, z') = \frac{1}{\Delta\nu} \sum_t \int_{\delta\nu_t} e^{-L_t(\nu)\, s_t\, \bar{m}\, \sec(\theta)}\, d\nu \qquad (3.26)$$

For a path of optical depth $\tau_\nu = L_t(\nu)\, s_t\, \bar{m}\, \sec(\theta)$ the equivalent width of a single line is

$$W_t = \int_0^\infty (1 - e^{-\tau_\nu})\, d\nu$$

Assuming that the contribution to τ_ν is negligible outside the frequency range $\delta\nu_t$ the range of integration may be reduced :

$$W_t = \delta\nu_t - \int_{\delta\nu_t} e^{-\tau_\nu}\, d\nu$$

and from equation (3.26)

$$T_{\Delta\nu}(\theta, z, z') = 1 - \frac{\sum W_t}{\Delta\nu} \qquad (3.27)$$

For large optical depths, specifically for paths low in the atmosphere, it is possible that $\sum W_t$, found in this way using the independent line model, might exceed $\Delta\nu$ thus giving a negative value for the transmission. To avoid this equation (3.27) is replaced by

$$T_{\Delta\nu}(\theta, z, z') = \exp\left(-\sum W_t / \Delta\nu\right)$$

which gives a better approximation to $T_{\Delta\nu}$ at low altitudes, where the overlapping of lines may not be ignored, and is virtually unchanged from (3.27) at higher altitudes.

To economise on computing effort line strengths are grouped according to magnitude so that an equivalent width needs to be calculated only once for each group. The number of lines in each group is specified at temperature intervals of 20K with a linear interpolation assumed for intermediate temperatures.

The equivalent width of a line with a Lorentz profile is given by

$$W_L = 2\pi\alpha_L \mathcal{L}(s_t \bar{m} \beta / 2\pi\alpha_L)$$

where the Landenberg-Reiche function is given, in terms of Bessel functions, by

$$\mathcal{L}(u) = u e^{-u} \left[I_0(u) + I_1(u)\right]$$

The equivalent width of a line with a Doppler profile is given by

$$W_D = \alpha_D D(s_t \bar{m} \beta / \pi^{1/2} \alpha_D)$$

where

$$D(w) = \int_{-\infty}^{\infty} \left[1 - \exp\left(-we^{-x^2}\right)\right] dx \qquad x = \frac{\nu - \nu_t}{\alpha_D}$$

Both $\mathcal{L}(u)$ and $D(w)$ may be given by numerical approximations (Rodgers and Williams, 1974). However the equivalent width of a Voigt profile may not be approximated easily by a numerical method (a fast method to compute the Voigt profile is given by Drayson, 1976). Rodgers and Williams show that an expression for the

equivalent width of a mixed-shape spectral line, which may be used with less than about 8% error, is

$$W = \left[W_L^2 + W_D^2 - \left(\frac{W_L W_D}{W_W} \right)^2 \right]^{1/2}$$

where W_W is the equivalent width of a weak line ($W_W = S_e \bar{m} \beta$).

Using the above approximations the transmission function may be calculated and hence the elements of the Curtis matrix.

3.5 Heating Rates

Using a Curtis matrix calculated using the U.S.A. 1962 Standard Atmosphere temperature profile with $\Delta\nu = 375$ cm^{-1}, collisional relaxation times from recent measurements (see Chapter 4), a volume mixing ratio of 320 ppm and other parameters as specified previously in the text heating rates were evaluated for the temperature structure of Fig. 3.3 appropriate to the December solstice. The results are given in Fig. 3.4. The greatest cooling occurs at the summer stratopause, where the temperature reaches 285K and cooling-to-space predominates, and in the winter lower thermosphere, where temperatures increase sharply above the isothermal mesopause region. The cold temperatures at the summer mesopause lead to a situation in which the absorption of radiation emitted from lower regions is greater than the emission of radiation at that level and a net heating, rather than cooling, results.

The general features of Fig. 3.4 are similar to those of previous heating rate calculations for solstice conditions (Murgatroyd and Goody, 1958; Kukn and London, 1969). A more detailed comparison is difficult due to the different temperature structures used.

Fig. 3.5 shows the U.S.A. 1962 Standard Atmosphere temperature profile and Fig. 3.6 the corresponding heating rates due to the CO_2 15μm band as

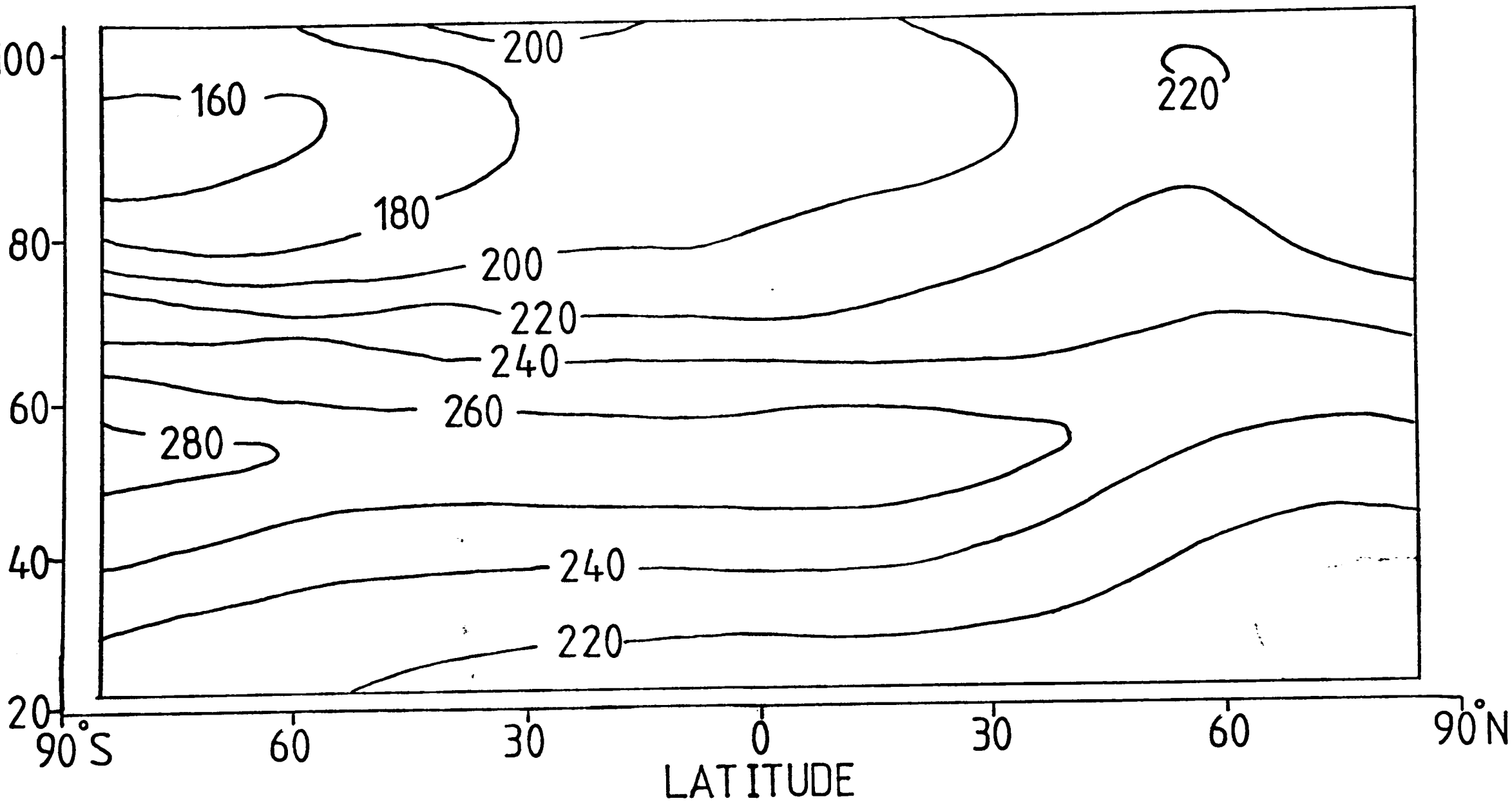

Fig. 3.3 December solstice temperatures from Groves (1970) (K)

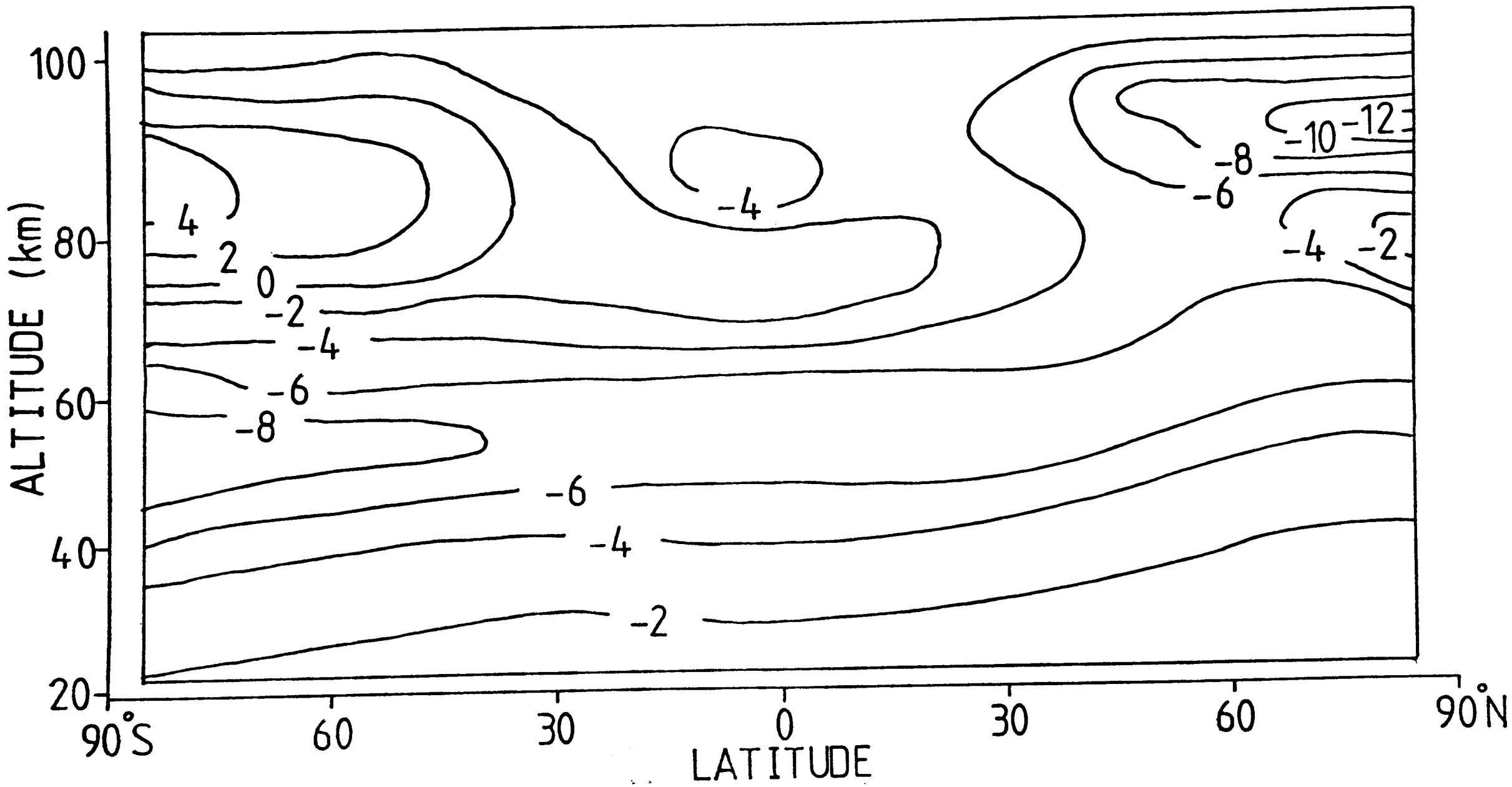

Fig. 3.4 Heating rates due to CO_2 15μm band (K/day)
for temperatures of Fig. 3.3

calculated by (a) the method described above, (b) Dickinson (1973) and (c) the method previously used in the Model. Dickinson used an exact line-by-line method for each CO_2 vibrational band with an approximate Voigt line shape, temperature dependent collisional relaxation time and a CO_2 volume mixing ratio of 330 ppm. The agreement between his results and those of the Curtis matrix approach is good as would be expected, within the bounds of the approximations used in each method, as the Curtis matrix was specifically calculated for the U.S.A. temperature profile. More interesting would be to compare Dickinson's parameterisation for calculating the cooling rates for other temperature profiles with cooling rates calculated using the Curtis matrix. However Dickinson was concerned with total infrared cooling and the parameters he provides are appropriate to the sum of cooling in the CO_2 15μm and the O_3 96μm bands. (The standard atmosphere cooling rate for the ozone was also calculated by a line-by-line method). Thus a direct comparison of the two methods for CO_2 cooling is not possible without repeating Dickinson's work.

Experiments in which the results of using the correct Curtis matrix for a given temperature profile were compared with the results of using the standard atmosphere matrix show a maximum error in the cooling rate of 1 K day^{-1} throughout the region. Dickinson's method is accurate to within 10% of the exact solution below 60km but deviates markedly above this altitude.

The third heating rate profile shown in Fig. 3.6 is that calculated for the standard atmosphere using the method described in section 2.5.2. Below 47km it corresponds well with the other calculations, above this however the cooling rate is too small with a difference of ~ 4 K day^{-1} above 55km. The difference is due to the use of the Lorentz profile for line broadening at all heights in the TELLUS program (which was designed for use at lower altitudes).

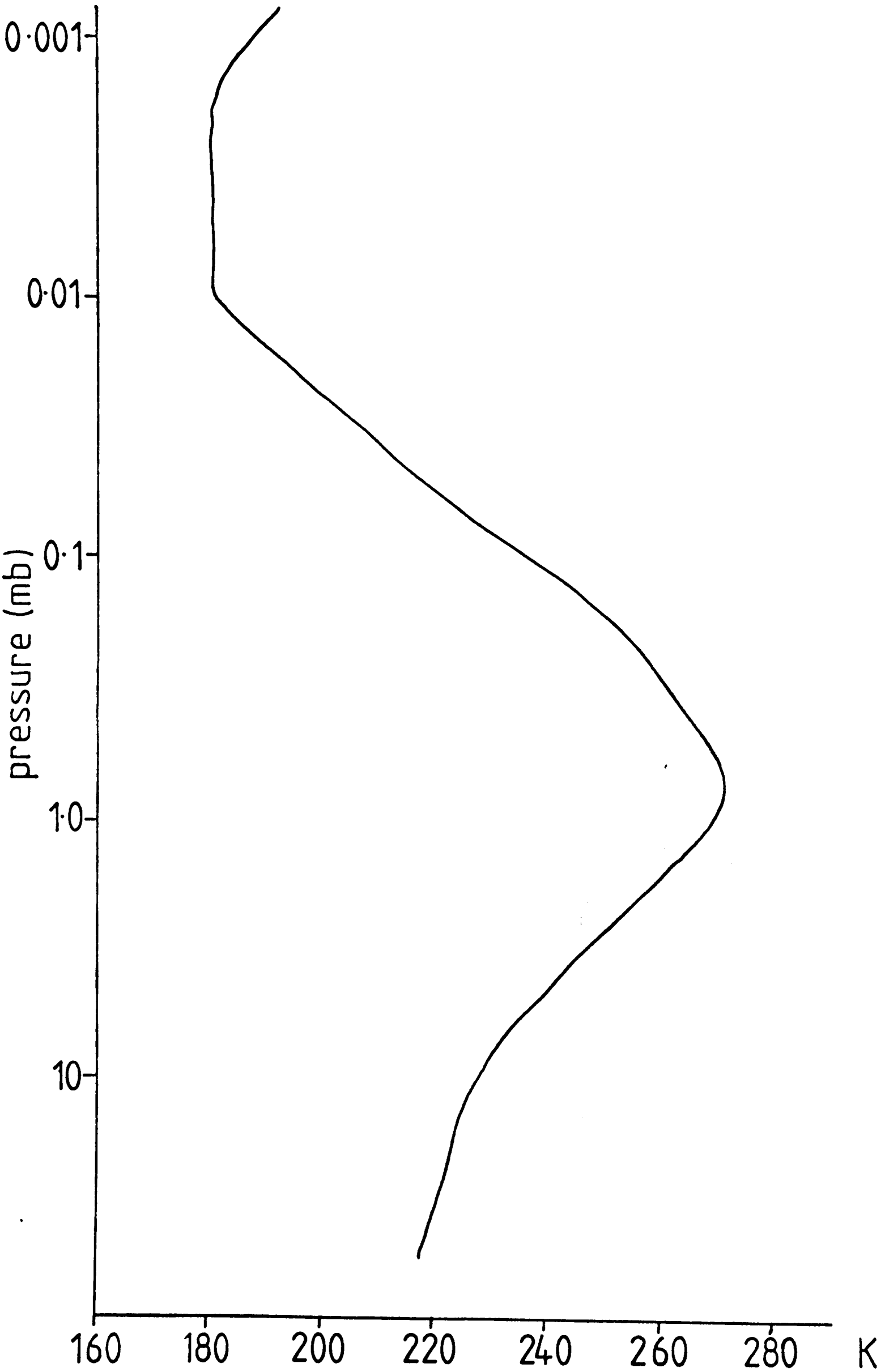

Fig. 3.5 U.S.A. 1962 Standard Atmosphere temperatures.

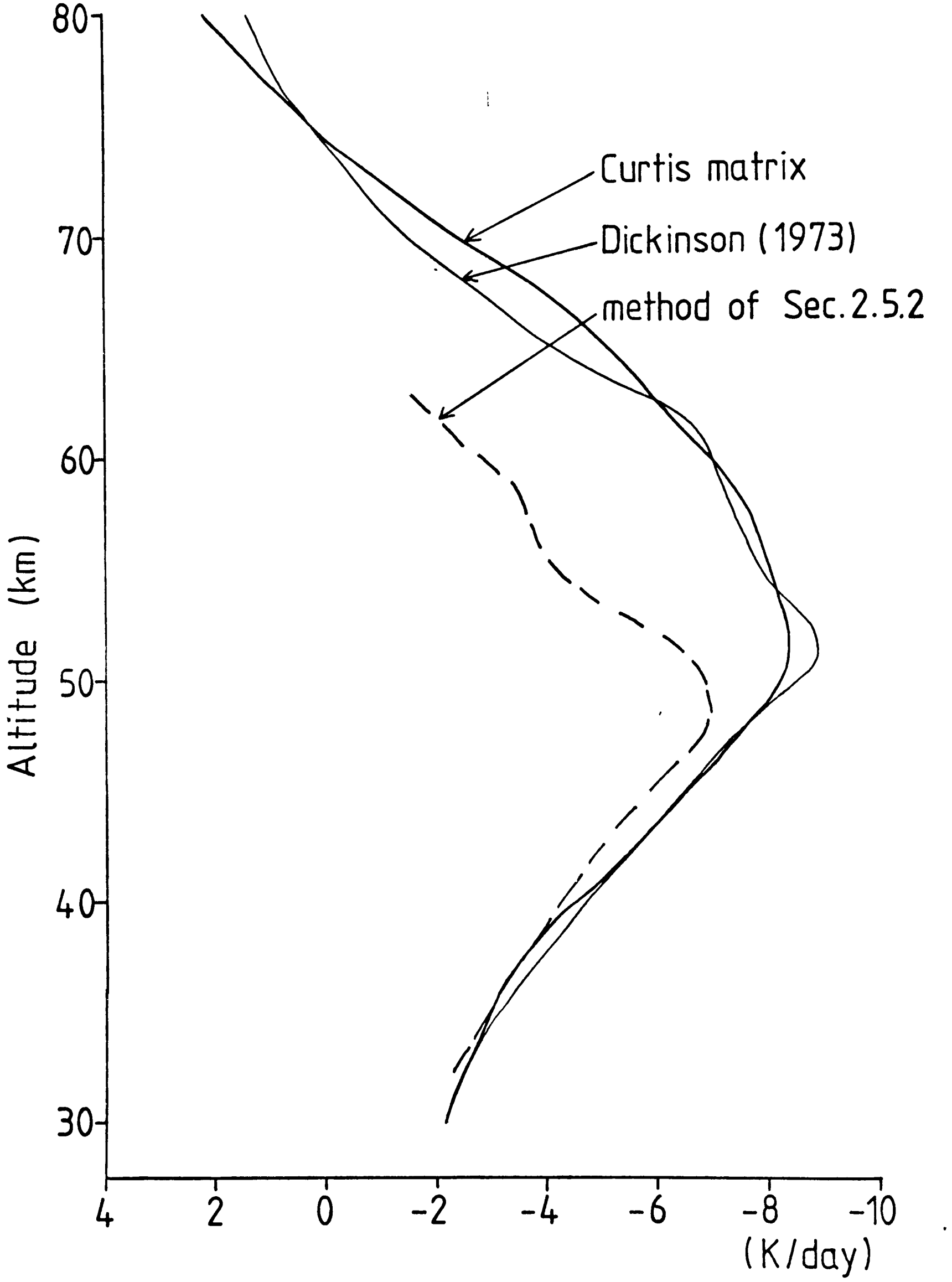

Fig. 3.6 Heating rates due to CO_2 15μm band for U.S.A. temps.

The results of using the Curtis matrix method in the Model and comparisons with the previous method are given in Chapter 6.

3.6 Radiative cooling in the 9.6μm band of ozone

The transfer of radiation in the 9.6μm band of ozone is only significant below about 60km and calculations of cooling rates due to this band need not be concerned with the breakdown of L.T.E. or transfer of radiation between atmospheric levels. Thus the scheme used in the Model was not replaced when the radiation calculations were extended to the mesopause. However it is interesting to compare the results of the method described in section 2.5.2 with those of Dickinson (1973). The cooling rates ealculated for the U.S.A. 1962 Standard Atmosphere temperature profile by the two schemes are shown in Fig. 3.7. There are large differences, especially in the middle stratosphere where variations may have a significant effect on temperature when the scheme is used in a Model. The discrepancies are almost certainly due to the different ozone profiles assumed in the derivation of the schemes. When used in models both methods calculate cooling rates in a manner dependent on temperature but independent of ozone concentrations. A scheme which is sensitive to both parameters would be more satisfactory particularly as in some of the experiments with the Model (see Chapter 7) the ozone amount deviates widely from its mean value.

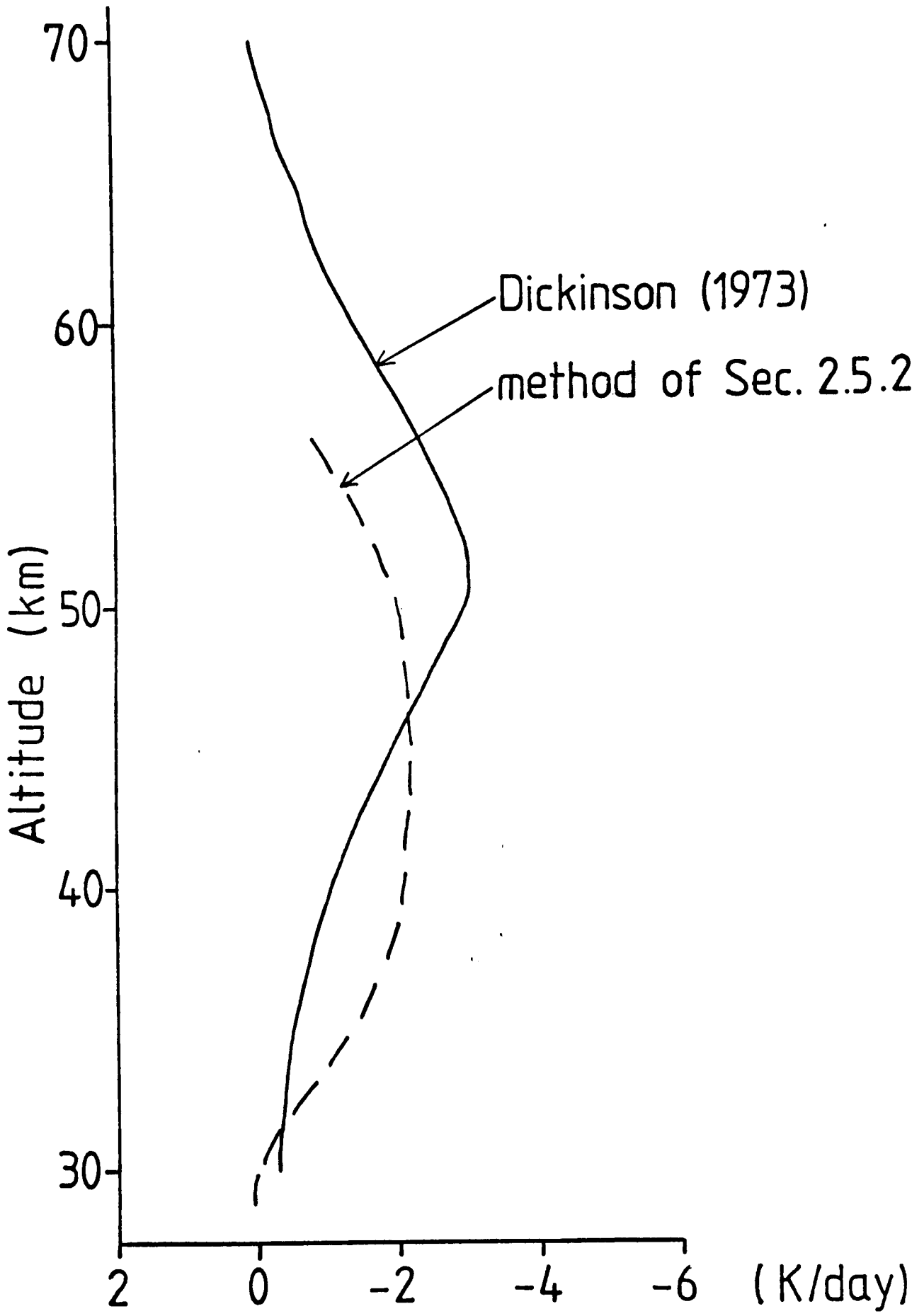

Fig. 3.7 Heating rates due to O_3 9·6μm band for U.S.A. temps.

CHAPTER 4

The collisional relaxation time for the $CO_2(\nu_2)$ vibration

4.1 A simple theory of molecular collisions

It was shown in section 3.3 that in order to calculate heating rates for regions of the atmosphere which cannot be assumed to be in Local Thermodynamic Equilibrium the collisional relaxation time, τ, must be known. τ is the inverse of the probability per unit time that a molecule in an excited state will release its excitation energy due to a collision. Thus it depends on the frequency of the collisions Z and the probability P_{10} that a collision will cause the given transition:

$$\tau^{-1} = Z\ P_{10}$$

The collision rate is given by kinetic theory as $Z = 4n\sigma^2(\pi KT/m)^{\frac{1}{2}}$ where n is the molecular number density, σ the collisional cross-section and m the molecular mass. However not all the molecules with which the excited molecule (v=1) collides will be in the ground state (v=0) and the expression for Z must be modified:

$$Z = 4n\sigma^2(\pi KT/m)^{\frac{1}{2}}\ (1 - n(1)/n(0))$$

where only the molecules in the ground and first excited state have been considered. The average probability per collision for a vibrational transition is given by various theoretical models. The Landau-Teller theory assumes a repulsive potential of the form $e^{-\alpha r}$ and results in an expression for P_{10} :

$$P_{10} = \exp\left\{-3(\pi^4 m \nu^2/\alpha^2 KT)^{1/3}\right\}$$

where ν is the frequency of the $v(1\rightarrow 0)$ transition. Many non-polar molecules show such a linear relationship between $\ln P_{10}$ and $T^{-1/3}$. The situation is more complicated with polar molecules because the intermolecular potential depends upon the orientation of the molecules before the collision.

Inclusion of this attractive potential in more involved theories gives a more complicated dependence of P_{10} on temperature but at temperatures for which the dipole (or quadrapole) interaction energy is much greater than RT the $T^{-1/3}$ law still holds.

For amixture of gases the mass of the molecule must be replaced by 2x the reduced mass, μ, of the collision:

$$\mu = \frac{m_A m_B}{m_A + m_B}$$

and the collision cross-section replaced by a hybrid value σ_{AB}:

$$\sigma_{AB}^2 = \frac{1}{2}\left(\sigma_A^2 + \sigma_B^2\right)$$

Thus the value of the collisional relaxation time of, for example, the CO_2 bending (ν_2) vibration measured in pure CO_2 will not apply to CO_2 in a mixture with other gases. For calculations involving atmospheric CO_2 we need to know the value of τ for a dilute mixture of CO_2 in predominantly N_2 and O_2.

The theory of molecular collisions and vibrational-translational energy transfer is dicussed more fully by, for example, Stevens (1967) and Lambert (1977).

4.2 The temperature dependence of τ

Until recently measurements of the collisional relaxation times for gases were confined to temperatures above about 290K. In reviews Cottrell and M^{c}Coubrey (1961) and Read (1965) found that for the CO_2 ν_2 vibration a value of 6-7 μs atm. in pure CO_2 at 290K corresponded to the majority of measurements. Taylor and Bitterman (1969) found a spread in results of at least 25% to each side of this value and in the absence of measurements at lower temperature it was not known whether the nearly linear plots of $\log_{10}\tau$ against $T^{-1/3}$ could be extrapolated down to 180K or the even lower temperatures appropriate to the summer polar mesopause.

Houghton (1969), using the Schwartz, Slawsky and Herzfeld (1952) theory of inelastic collisions and fitting the results to the measured value of 6 μs atm in pure CO_2 at 290K, predicted a range of values from 9 to 5 μs atm in an oxygen-nitrogen mixture over the temperature range 180 to 240K. Most calculations of the heating due to the transfer of thermal radiation in the atmosphere have neglected the temperature dependence of τ. Curtis and Goody (1956) used a value of 15 μs atm. Drayson (1967) and Kuhn and London (1969) performed calculations using values from 2 to 20 μs atm. Williams (1971) also showed the effects of using different values but for mostof his computations used 10 μs atm.

More recently the improvement of measuring techniques and the purity of the gases available have enabled experimenters to conduct more accurate estimations. The purity is particularly important for the CO_2 case because any trace of water vapour present can greatly decrease the measured value of τ. This rapid relaxation by water vapour is probably due to the formation of H_2CO_3.

Merrill and Amme (1969) measured τ by an acoustic dispersion method with CO_2 mixed in varying concentrations with O_2 and N_2. Their results at 300K were: for almost pure N_2, 10 μs atm; for almost pure O_2, 9 μs atm. These were larger than previous measurements but since then other workers using different methods have produced similar results. [Cannemeyer and de Vries (1974) using an optic-acoustic (spectrophone) method, Bass (1973) with an ultrasonic absorption method and Simpson et al (1977) using a laser-Schlieren technique are some]. These results consistently indicate that O_2 relaxes CO_2 (ν_2) faster than N_2; the theories of Landau and Teller (1936) and Schwartz, Slawsky and Herzfeld (1952) predict that O_2 should be slightly less efficient than N_2 in this respect due to its larger reduced mass. The disagreement must reflect some stronger interaction between the

oxygen molecule and the carbon dioxide molecule although the nature of this attraction is not clear.

The errors involved in assuming a linear extrapolation of the Landau-Teller plot to lower temperatures were demonstrated by Allen et al (1977) who measured the relaxation time in pure CO_2 and a CO_2 - Ar mixture down to 150K by a laser fluorescence technique. Below 300K the CO_2 - CO_2 relaxation time is almost independent of temperature at a value of about 7 μatm; the departure of the CO_2 - Ar values from the high temperature Landau-Teller behaviour is not so pronounced but still clear.

The results of Simpson et al (1977) for CO_2 - N_2 and CO_2 - O_2 mixtures did not show the same curvature as the CO_2 - CO_2 values of Allen et al at 295K and the authors extrapolated the data using a similar curvature to the Allen et al CO_2 - Ar results giving an estimated value at 210K of 22 μs atm for CO_2 - air (with no curvature the figure would have been about 20% higher).

Finally laser fluorescence measurements were carried out in CO_2 - N_2 mixtures down to a temperature of 170K (Allen, 1979). Their results are shown in Fig. 4.1 along with a linear extrapolation of higher temperature measurements. It can be seen that the value of $\tau_{CO_2-N_2}$ levels off below 300K to an almost constant value of 16 μs atm below about 185K. This is a more rapid fall-off than predicted by Simpson et al (1977). The value of 16 μs atm at 170K is just over half the value of 28 μs atm which is obtained from straight extrapolation of older, higher-temperature, measurements and which was used previously in heating rate calculations. From the work of Simpson et al (1977) we may assume that O_2 is about 20% more efficient than N_2 at relaxing CO_2 (ν_2) so for CO_2 - air at 180K we obtain a value for τ of about 15μs atm.

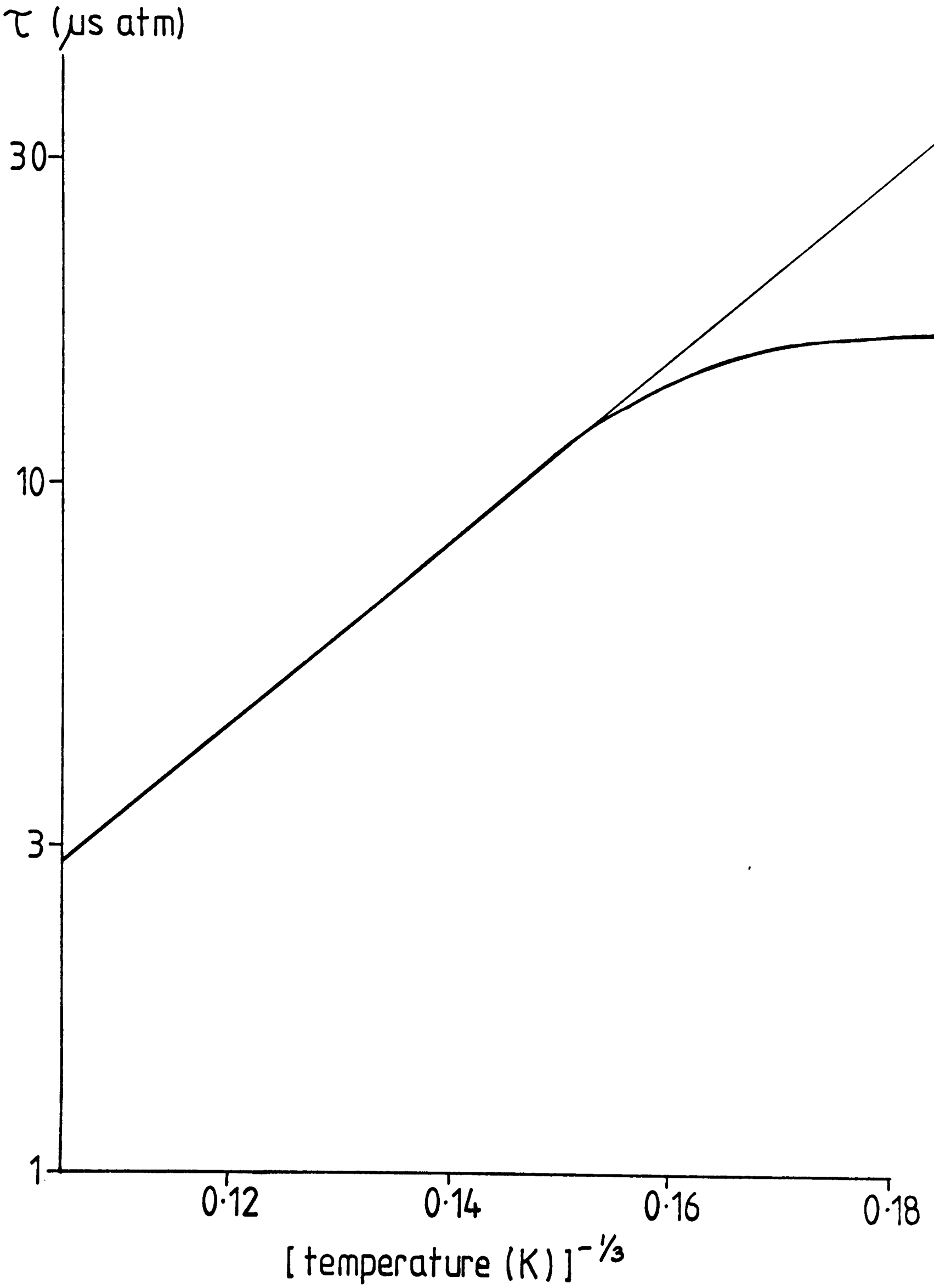

Fig. 4.1

4.3 The effect of using different τ values in calculating cooling rates

As was shown in section 3.2 the deviation of a gas from Local Thermodynamic Equilibrium may be expressed in terms of a diagonal matrix whose elements are directly proportional to τ. Thus the cooling rates calculated for regions of the atmosphere above about 75km depend critically on the values of τ used. In order to evaluate this effect three different temperature profiles were chosen and the corresponding cooling rates, due to thermal emission in the 15μm band of CO_2, were calculated, using the Curtis Matrix method of Chapter 3, for three cases:

(a) Assuming Local Thermodynamic Equilibrium,

(b) Using the latest measurements of τ (Allen, 1979),

(c) Using values of τ gained by extrapolating older measurements at higher temperatures (i.e. as were used previously).

A brief discussion of this work has been given by Allen et al (1979).

Fig. 4.2 shows the U.S.A. 1962 standard atmosphere temperature profile, the corresponding heating rates for cases (a), (b) and (c) and the heating rate due to the absorption of solar ultraviolet radiation by ozone and molecular oxygen assuming a solar declination and daylength appropriate to 1st July at 30°N. The solar heating is included so that the magnitude of the changes in the CO_2 cooling may be seen in the context of the other major component of the heat budget; it is calculated using the method described in Chapter 5. Figs. 4.3 and 4.4 show similar calculations for temperature profiles appropriate to January at 70°N and December at 70°S. In all three Figures it can be seen that the use of the new τ values, case (b), increases the magnitude of the cooling (or heating) relative to case (c). The largest change is in the polar winter lower thermosphere where the cooling increased by about 2.5 K day^{-1}, this is particularly significant at a time when the solar heating is small (<1 K day^{-1}).

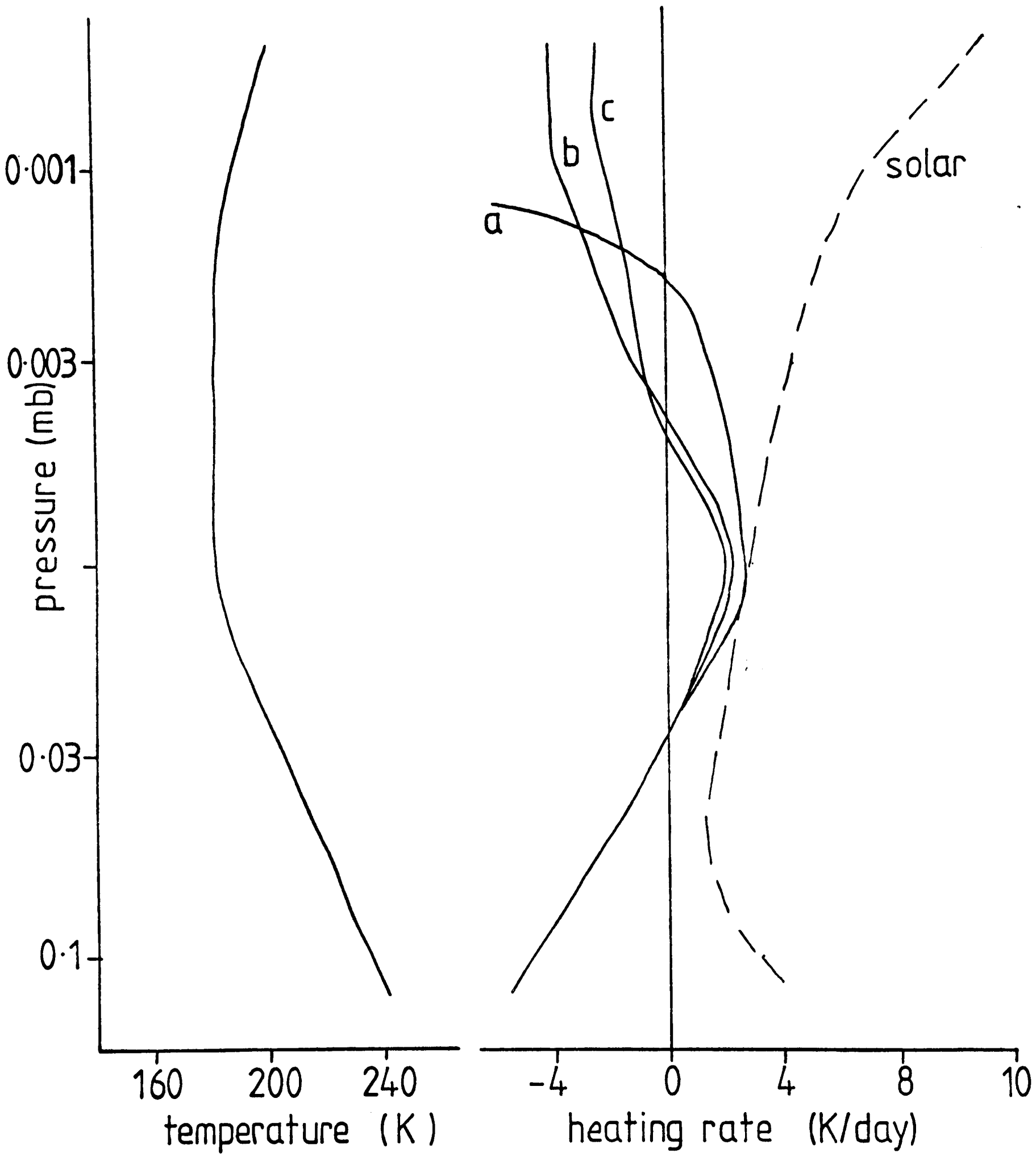

Fig.4.2 cooling rates for USA 1962 standard atmosl

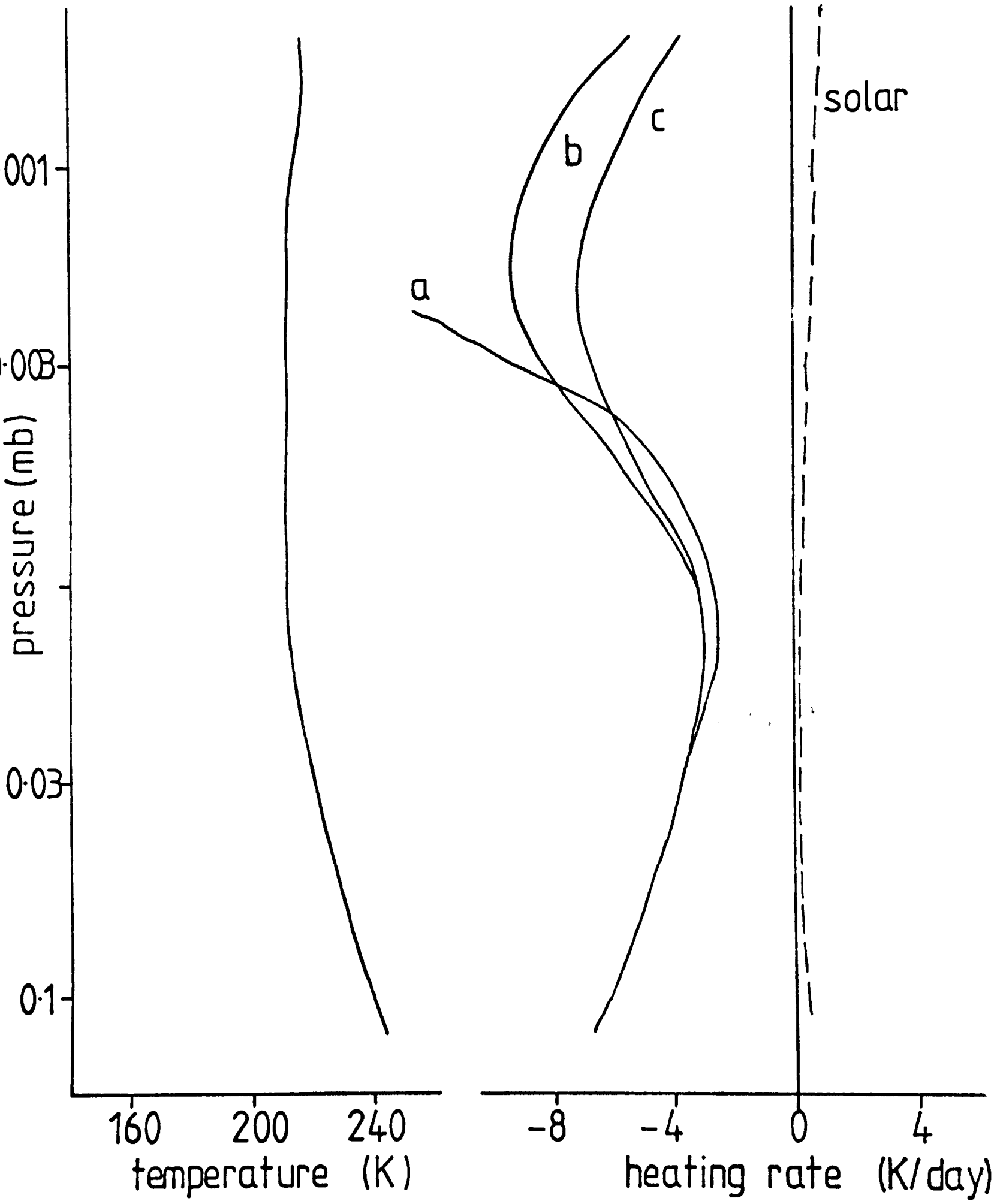

Fig. 4.3 cooling rates for Jan. 70°N

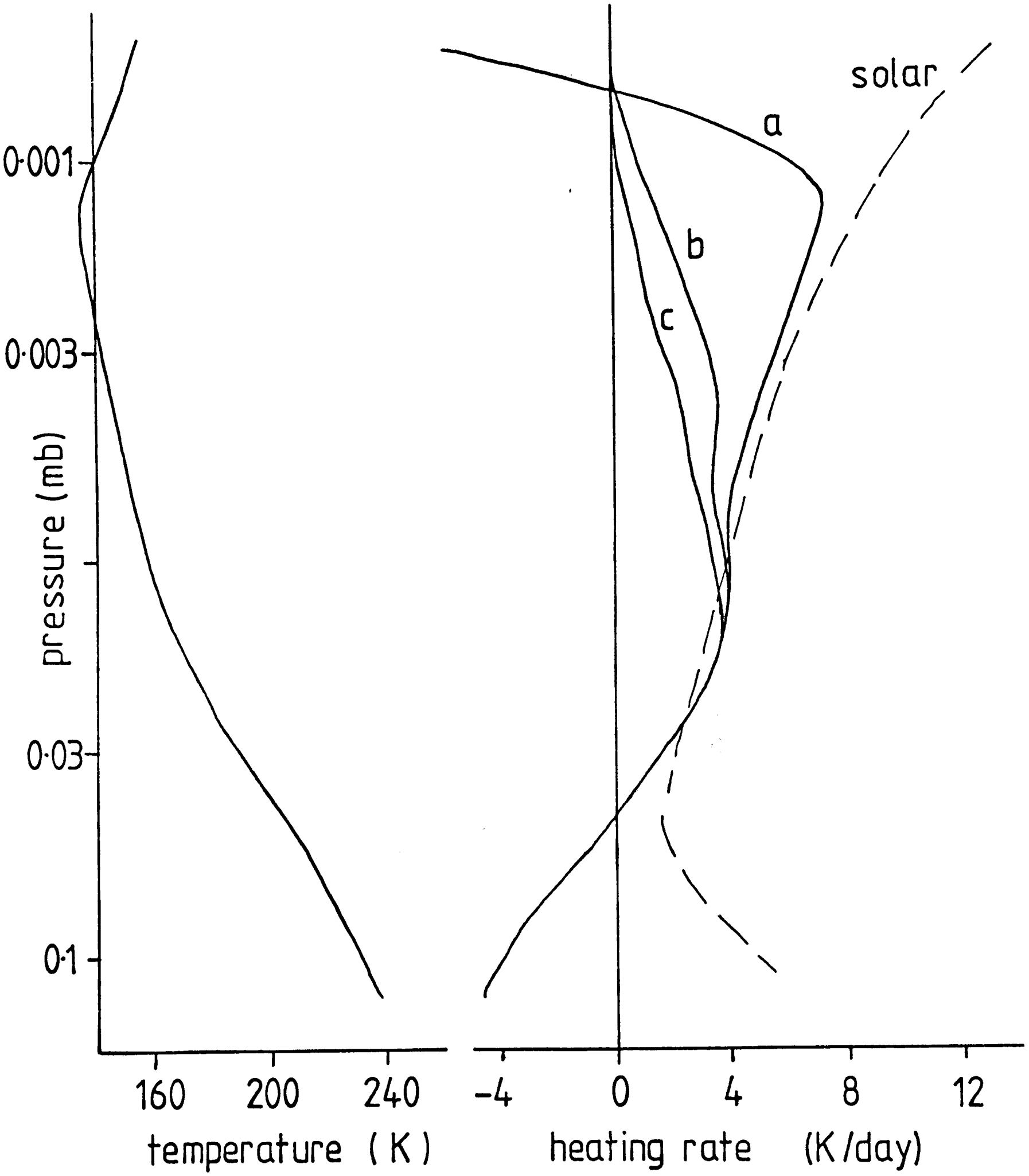

Fig. 4.4 cooling rates for Dec. 70°S.

In the absence of any other cooling mechanisms this extra cooling would have to be balanced by dynamical heating due to an increase in downwards motion of about 0.25 km day^{-1} (= 2.9 mm s^{-1}). There are few reliable measurements of wind in the mesosphere but mean meridional circulations calculated by the Oxford model indicate a maximum downward velocity near the winter mesopause of about 30 mm s^{-1} (see Chapter 8) so the use of the latest τ values might be expected to intensify the meridional circulation by about 10%. However, as is discussed in Chapter 8, the diabatic heating is only one component of the complex system which drives the mesospheric circulation and it is not possible to make such simple assumptions about the effect of changing its value on the circulation calculated. Such analysis does, however, allow the orders of magnitude involved to be appreciated.

In the next two Sections calculations which depend sensitively on the values of collisional relaxation time used will be described.

4.4 A radiative relaxation time for the atmosphere near the mesopause

A quantity which is of interest in the study of the mesosphere is the rate at which radiative processes tend to return a perturbed atmosphere to a radiative mean state. The upper mesosphere is not in radiative equilibrium as is obvious from Figs. 4.3 and 4.4. In high latitudes in winter the insolation is very small (or zero in the polar night) but the relatively warm temperatures lead to a significant ($\sim$ 4 K day^{-1}) cooling by thermal radiation. In summer the absorption of solar radiation is significant ($\sim$ 4 K day^{-1}) but the cold temperatures near 80km result in a net absorption of thermal radiation which gives an additional contribution to the heating of 4 K day^{-1}. Therefore there cannot be a radiative balance. The mechanisms which enable this apparently anomalous temperature

structure to be maintained are discussed in Chapter 8. Here we are interested in evaluating a radiative time constant for the atmosphere near the mesopause.

In Fig. 4.5 a radiative equilibrium temperature profile calculated for 30°N in January is shown by a solid line together with a rather unusual temperature profile in a broken line. This latter profile was measured on January 4th 1976 over southern Spain (37°N) from a rocket and confirmed by other measurements on the same day during the Western European Winter Anomaly Campaign (Offermann et al, 1979). Other data in the same series suggest that this perturbation persisted for some while, being part of a wavelike disturbance with period 7 or 12 days.

Also shown in Fig. 4.5 are the net heating rates (i.e. solar heating + thermal cooling) for the two temperature profiles. The first is, by definition of the temperature profile, approximately zero; the second shows a large cooling (~ 36 K day^{-1}) where the corresponding temperature deviates by +60K from the radiative equilibrium value. Use of the latest τ values, discussed above, has enhanced the magnitude of the calculated cooling rate and as the ozone concentration is inversely correlated with temperature the heating due to absorption of solar u.v. has decreased.

A radiative relaxation time t_r may be defined by the simple expression:

$$\frac{dT}{dt} = \frac{(T - T_e)}{t_r}$$

Where T_e is the equilibrium temperature appropriate to the latitude, date and altitude in question. From the calculations above we find $t_r = 60/36 =$ 1.7 days so a temperature perturbation of this magnitude cannot persist for longer than a couple of days without some kind of continual forcing.

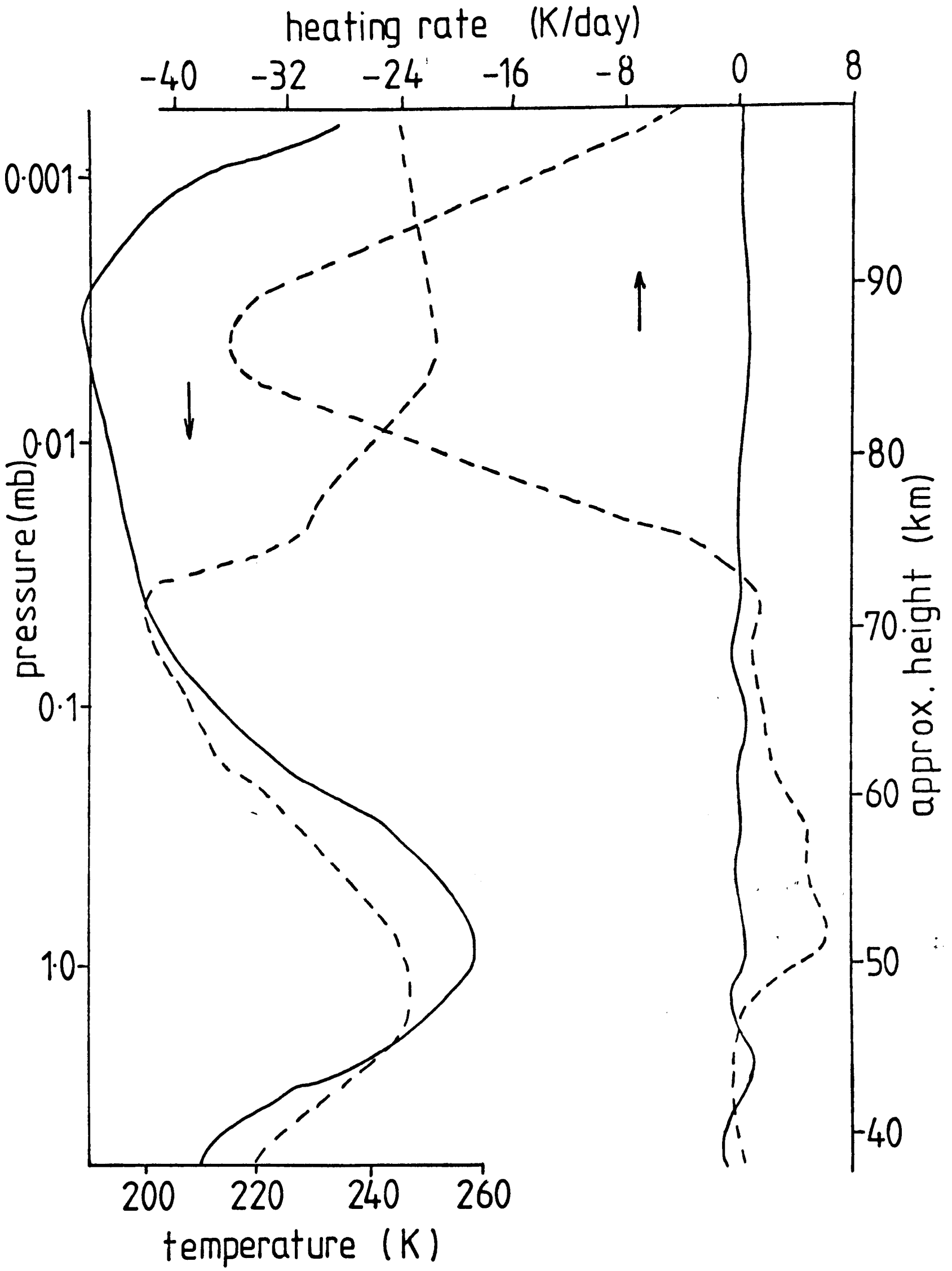
heating rate (K/day)
-40
-32
-24
-16
-8
0
8
0·001
0·01
0·1
1·0
pressure (mb)
90
80
70
60
50
40
approx. height (km)
200
220
240
260
temperature (K)

Fig. 4.5

4.5 Relaxation of the CO_2 (ν_2) vibration by atomic oxygen

It was mentioned in section 4.1 that the collisional relaxation time of a vibrationally excited molecule depends on the characteristics of the molecules with which it collides. For carbon dioxide in the stratosphere and mesosphere the only collision partners of importance are nitrogen and oxygen molecules. However above the mesopause oxygen suffers photo-dissociation and the mixing ratio of atomic oxygen becomes significant. The question arises as to the efficiency of atomic oxygen, as compared with the other constituents of air, in relaxing CO_2 (ν_2).

Crutzen (1970) first pointed out that atomic oxygen might be important in this context and demonstrated the effect of using different values of $\tau_{CO_2 - O}$, together with an assumed O concentration profile, on calculations of the radiative cooling rate.

No direct measurements of τ for a CO_2 - O mixture have been made but values of the rate of vibration - translation energy transfer have been obtained for the collisions of other molecules with free atoms (see e.g. Cramp and Lambert, 1973 or Buchwald and Wolga, 1975). It has become clear that O, Fe, F, Cl and Br atoms are very efficient energy transfer catalysts while H atoms are rather less effecient. Two alternative explanations for this behavious have been advanced:

(i) All the atoms mentioned above, except H, possess resultant orbital angular momentum. This means that energy transfer between the vibrational levels of the molecule and the electronic levels of the atom (e.g. a spin - orbit splitting such as $^2P_{1/2} \leftrightarrow {}^2P_{3/2}$) would be possible.

(ii) Very strong attractive forces would be expected to operate between free atoms and molecules and these (or perhaps a chemical reaction as between CO_2 and H_2O) might be responsible for the efficient transition.

Cramp and Lambert (1973) found that atomic oxygen was about sixteen times as efficient as molecular oxygen in relaxing the CO_2 (ν_3) vibration. It does not follow that the same factor would apply in the case of CO_2 (ν_2) but there is certainly an indication that the value of τ found for CO_2 in N_2 and O_2 would not apply if the mixture contained appreciable amounts of O.

In an attempt to put a value on the efficiency of O, relative to 'air', calculations of the downward flux of radiation in the CO_2 15μm band were calculated and compared to the measurements of Stair et al (1974). The measurements were taken at Poker Flat, Alaska (latitude 65°N) on 22nd March 1973 and gave values of zenith peak spectral radiance at 15μm up to an altitude of about 150 km. Further details of this experiment are given by Stair et al (1975).

The calculations made use of the matrix method described in Chapter 3. However as the fluxes of radiation were required (rather than the divergence of the fluxes to give heating rate) the relevant formula was:

$$\underset{\sim}{F} = (\underset{\approx}{I} - \underset{\approx}{C_F}\,\underset{\approx}{E}\,\underset{\approx}{A})^{-1}\ \underset{\approx}{C_F}\,\underset{\sim}{B}$$

which may be derived from the matrix equations in Chapter 3. A standard March temperature profile (from Groves, 1970, below 115 km and C.I.R.A. 1972, above) was used together with atomic oxygen concentrations and mean atmospheric molecular weights from C.I.R.A. (1972). These parameters are shown in Figs 4.6 and 4.7; also shown, by a broken line, is the U.S.A. standard atmosphere (1962) temperature profile.

A complication which arises in extending the Curtis matrix method above about 100 km is that the CO_2 mixing ratio decreases above this altitude. This is due partly to molecular diffusion and partly to photodissociation. Trinks and Fricke (1978) have measured the ratio of CO_2

Fig. 4.6

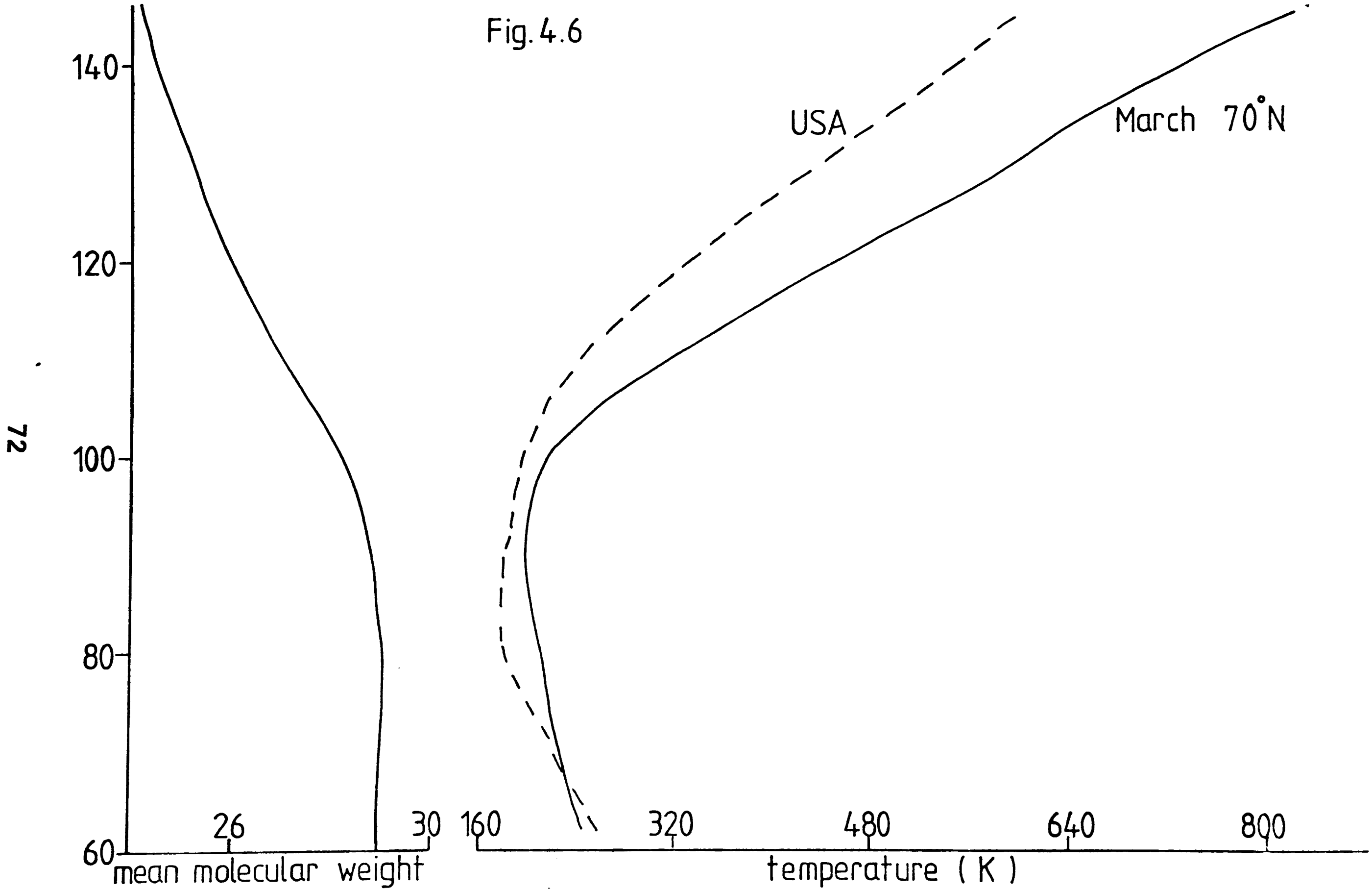
140
120
100
80
60
72
26
30
mean molecular weight
160
320
480
640
800
temperature (K)
USA
March 70°N

Fig. 4.7

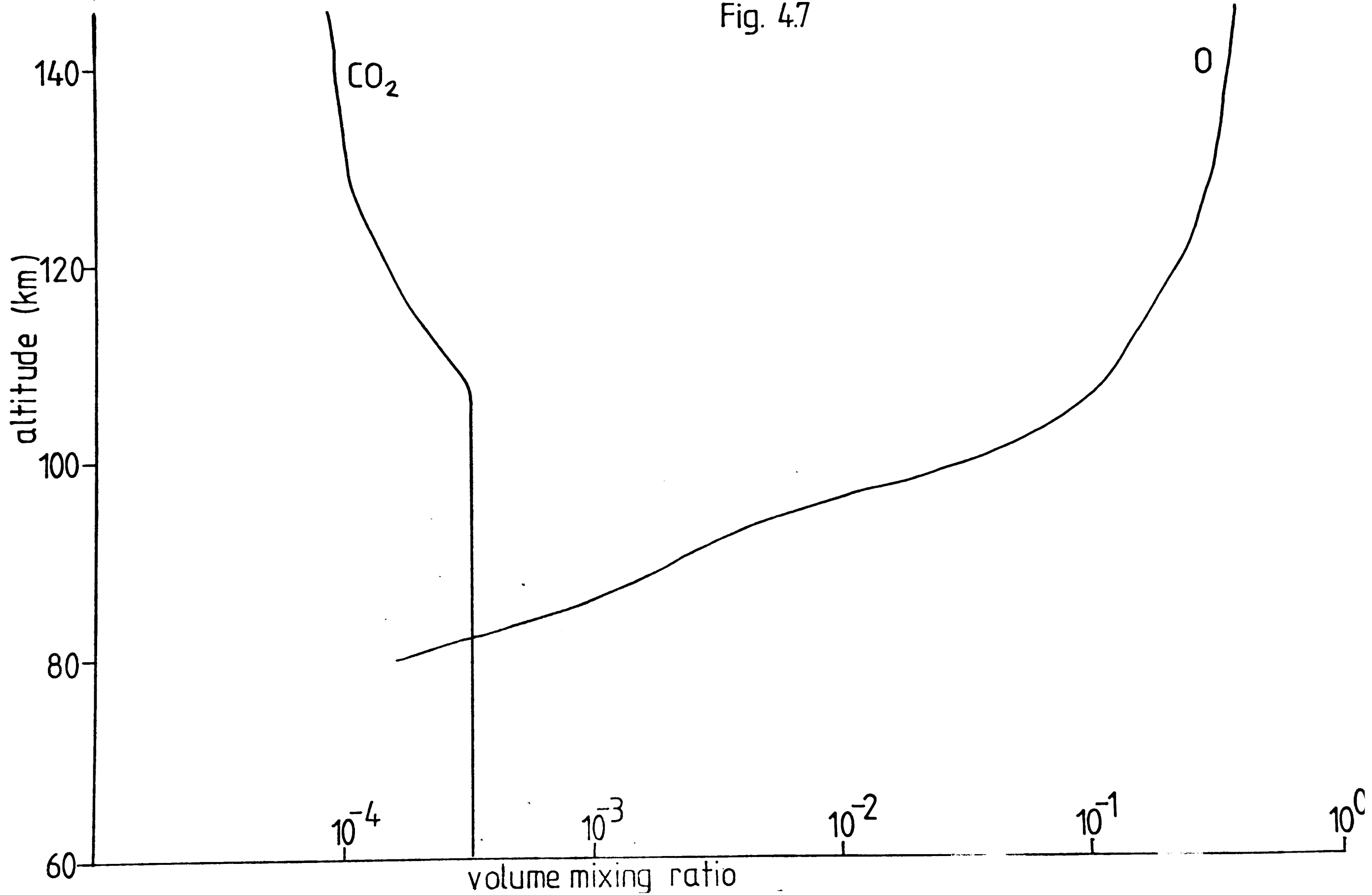
140
120
100
80
60
altitude (km)
CO_2
O
10^{-4}
10^{-3}
10^{-2}
10^{-1}
10^{0}
volume mixing ratio

concentration to Ar concentration up to 150 km using a rocket - borne mass spectrometer. The CO_2 / Ar ratio is a more reliable estimate of CO_2 amounts than a pure CO_2 measurement because the lower thermosphere is subject to pronounced wavelike disturbances which may effect different constituents to greater or lesser extents and as the molecular weight of Ar is only 10% less than that of CO_2 the dynamical effects of any waves should be suppressed in the CO_2 / Ar ratio.

Assuming that the Ar distribution is determined entirely by molecular diffusion and correcting for the difference in temperatures (Trinks and Fricke made their measurements at 30°N in June) we obtain the CO_2 mixing ratio profile shown in Fig. 4.7.

With an altitude - dependent mixing ratio the Curtis - Godson approximations for the mean absorber amount $\bar{m}$, mean pressure $\bar{p}$ and mean temperature $\bar{T}$ of an atmospheric path do not reduce to the simple forms of section 3.4. However, $\int x dp$ and $\int xT dp$ may be found assuming that the mixing ratio x and the product xT vary linearly with $\ln p$ between levels and $\int xp dp$ may be rewritten as $\int x d(\frac{1}{2}p^2)$ so that a similar finite difference method may be used for the integration.

The downward flux was calculated for four cases - for the March temperature profile assuming $\tau_{CO_2-O} = \tau_{CO_2-air}$ and $\tau_{CO_2-O} = \tau_{CO_2-air}/20$ and for the U.S.A. (1962) standard atmosphere using the same two relative relaxation times. The results are shown in Fig. 4.8 together with the measurements of Stair et al (1975). It is obviously inappropriate to compare the calculations for the U.S.A. temperature profile with measurements taken in March at 65°N however the results of these calculations are included to give an indication of the sensitivity to temperature of the flux calculations.

Fig. 4.8

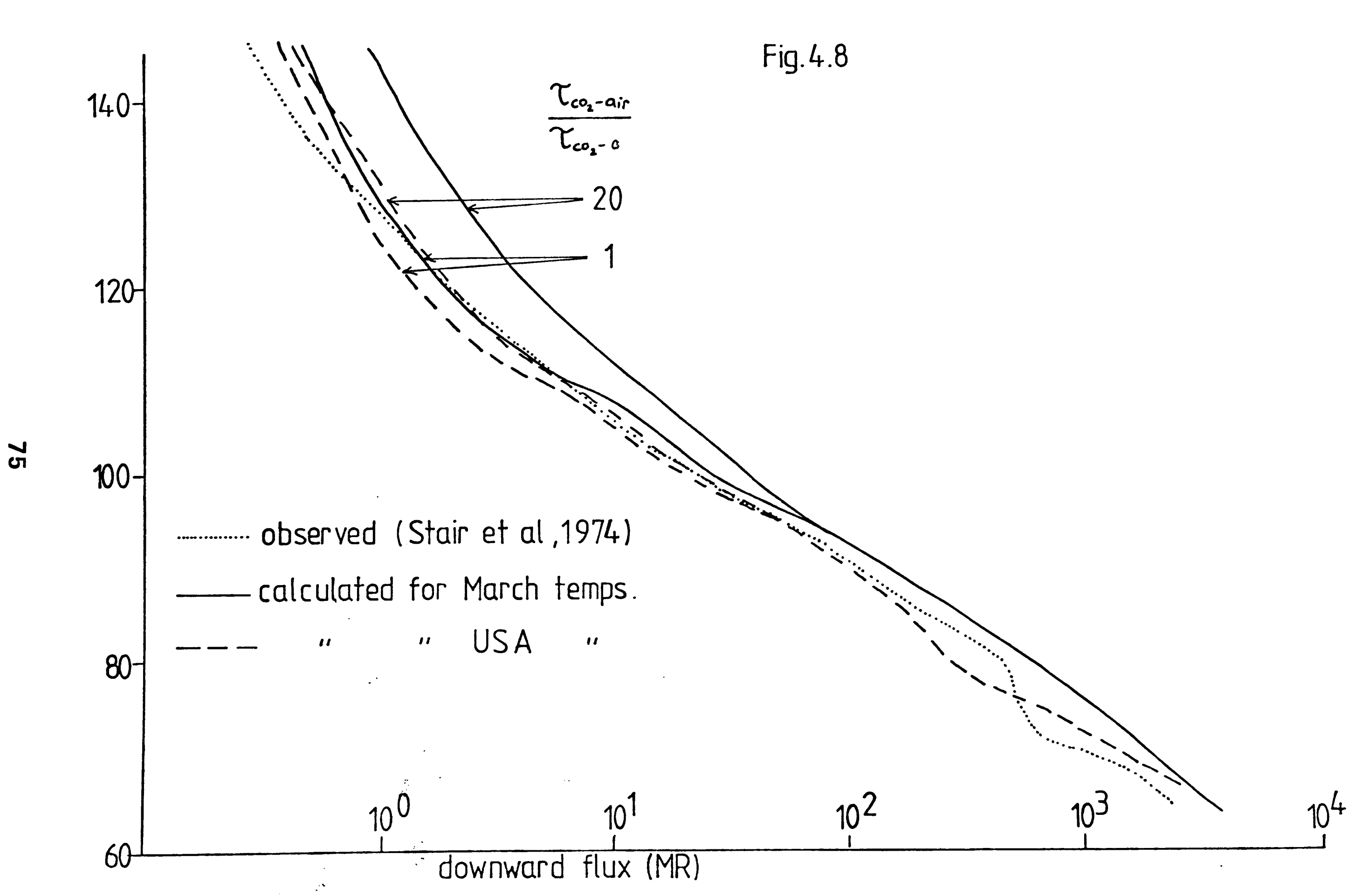
$\frac{\tau_{co_2\text{-}air}}{\tau_{co_2\text{-}o}}$
20
1
140
120
100
80
60
75
..... observed (Stair et al, 1974)
—— calculated for March temps.
— — — " " USA "
10^0
10^1
10^2
10^3
10^4
downward flux (MR)

Given the uncertainty in a number of the parameters used in the calculation (T, $[CO_2]$, $[O]$) the correspondence between measured and calculated fluxes is good and considerably closer than previous calculations (Degges (1974), James and Kumer (1974) and Gordiets et al (1978)). However it is not possible to estimate τ_{CO_2-O} from these results and it would appear that, unless simultaneous measurements of 15μm flux, T, CO_2 and O mixing ratio can be made, it must be measured directly in the laboratory.

CHAPTER 5

The heating of the atmosphere by the absorption of solar radiation

5.1 Introduction

Chapter 3 discussed the transfer of thermal radiation and the resultant atmospheric cooling, mainly in the 15μm band of carbon dioxide but also in the 9.6μm of ozone. However, the major role played by ozone is its absorption of solar radiation in the ultraviolet (2000 - 3500 Å) and, to a lesser extent, the visible (5000 - 7000 Å) wavelength regions. Most of the energy absorbed in this way is converted into kinetic energy, thus heating the atmosphere. The stratopause is formed at the altitude of maximum absorption per unit mass. Molecular oxygen strongly absorbs solar radiation at shorter wavelengths ($<$ 2050 Å). This is important only above about 70 km but a weaker continuum, between 2060 and 2425 Å, causes dissociation of the oxygen molecules near 30 km producing the atoms essential in the formation of ozone.

Solar heating of the atmosphere provides the driving force for the zonal mean circulation. Any variation in the solar input, with latitude, altitude or season, will cause changes in the temperature and wind structure leading to alteration of the transfer properties of the atmosphere and thus the possibility of an entirely different structure. Any dynamical model of the stratosphere must therefore contain an expression or parameterization for solar heating. Several approximations for calculating it without excessive computation have been devised and some of these are considered later in this chapter. First the physical basis for the calculations will be discussed.

The justification for separating atmospheric radiation calculations into two separate regimes : solar and thermal, or shortwave and longwave, is demonstrated by Fig. 5.1. The Planck curve for 6000 K, which is an

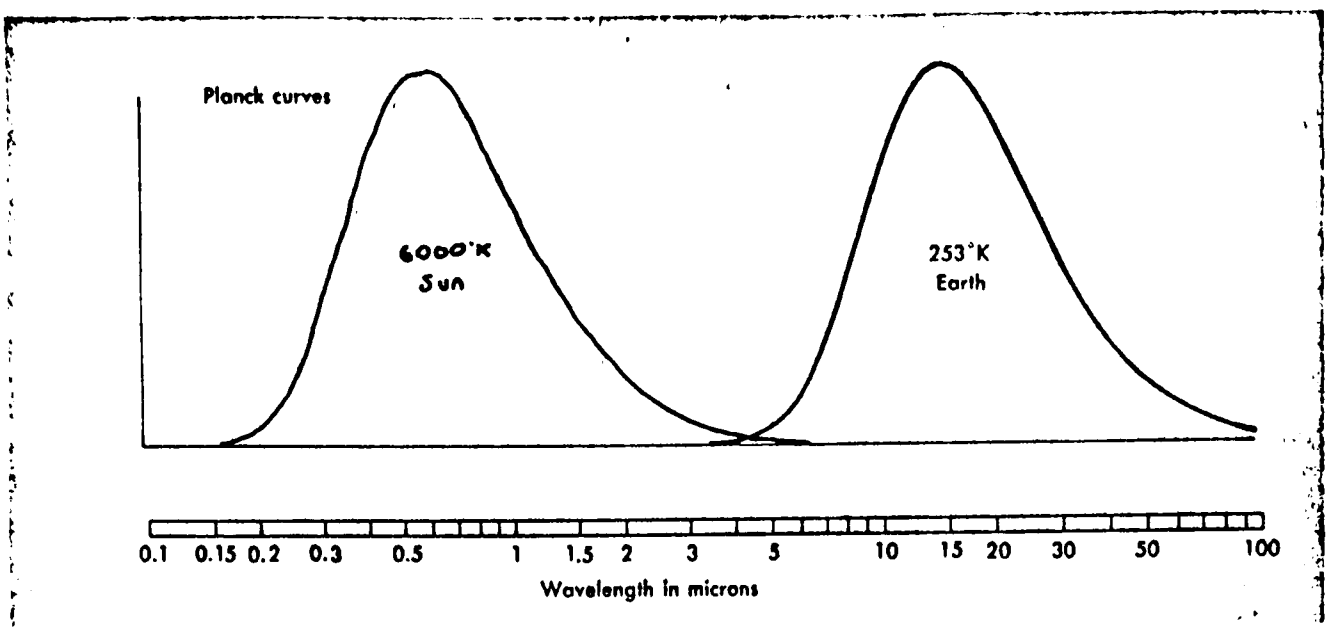

Fig.5.1 Planck curves for Earth and Sun.

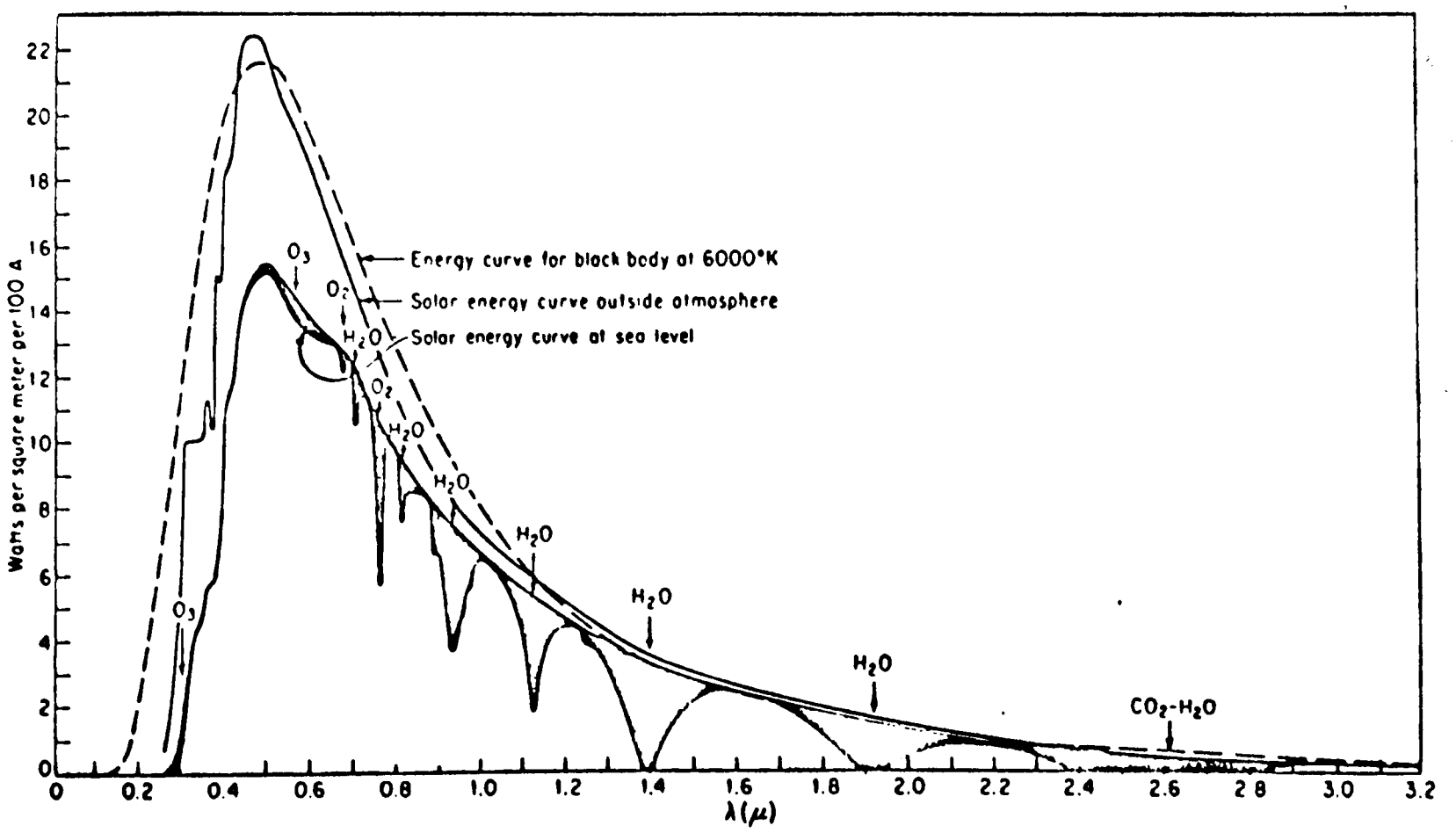

Fig.5.2 Solar flux.

approximation to the radiative flux from the sun, barely overlaps that for 250 K, representing atmospheric temperatures. The division comes at about 4 μm; at longer wavelengths the contribution to the radiation field from direct solar radiation is negligible while at shorter wavelengths the solar radiation dominates. There are a few examples of atmospheric gases having absorption bands in the overlap region (e.g. the 4.3 μm band of carbon dioxide) but these can, in general, be separated into the two components.

5.2 Solar radiation above the atmosphere

Solar radiation arrives at the top of the atmosphere at an average rate, measured normal to the beam, of 1370 W m^{-2} with a wavelength distribution indicated by Fig. 5.2. Its spectral distribution changes as it traverses the atmosphere and the resultant spectrum at the earth's surface is also shown in Fig. 5.2 along with identification of some of the major absorbers. In order to sort out the processes which occur as the sun's radiation penetrates the atmosphere as well as evaluate its wavelength distribution outside the atmosphere it is important to measure the radiation field at many altitudes.

In 1814 Joseph von Fraunhofer published the first spectroscopic observations of the solar spectrum. These showed 574 dark spectral lines and it was not until 1854 that Kirchoff explained these lines as being due to absorption in the atmosphere of the sun. Since then great advances have been made in the fields of instrumentation and data recording and processing. Ground-based measurements have been largely superceded by experiments mounted on balloons and rockets but a recent exception is the work of Labs and Neckel (1973) who used a spectral photometer at Jungfraujock (altitude 3600m) in the Swiss Alps. There have also been some measurements from aircraft.

The advantage of a balloon as a platform is that is allows measurements of solar flux variations with altitude; balloon-borne u.v. spectrometers have been described by Ackerman et al (1971) and Simon (1975). Rocket-borne experiments can measure the shorter wavelength radiation which does not reach the ground or balloon altitudes; rocket - borne spectrometers have been described by Ackerman and Simon (1973), Braodfoot (1972), Rottman (1974) and Heroux and Swirbalus (1976). Rocket - borne spectrographs have been used by Samain and Simon (1975) and Brueckner et al (1976). A rocket-borne spectrometer has been designed to look specifically at the hydrogen Lyman - α line by Vidal - Madjar (1975).

With such great effort apparently put into measuring the solar spectrum it might be assumed that values for solar flux were fairly well established. However, there are quite large discrepancies between different measurements. Although these are undoubtedly partly due to the limitations of accuracy of the instruments used another relevant factor is the variability of the solar flux. Apart from changes due to the well-known eleven year sunspot cycle, the solar flux also varies with the 27-day solar rotation period and annually by 7% due to the ellipticity of the earth's orbit. The most definitive data on ultraviolet variations due to the sun's rotation have been obtained from satellite observations by Heath (1973). Radiation in three relatively broad spectral intervals in the 115 - 300 nm region was monitored for one solar rotation: peak to peak variations were about 25% at 120 nm, 5% at 170 nm and only 0.3% at 260 nm. These results have yet to be corroborated.

Several intercomparisons and tabulations of solar flux data have been made including those of Detweiler et al (1961), Johnson (1954), Thekaekara (1970) and Ackerman (1971). A more recent survey is that of Delaboudinière et al (1978) whose comparisons are reproduced in Figs. 5.3 - 5.6.

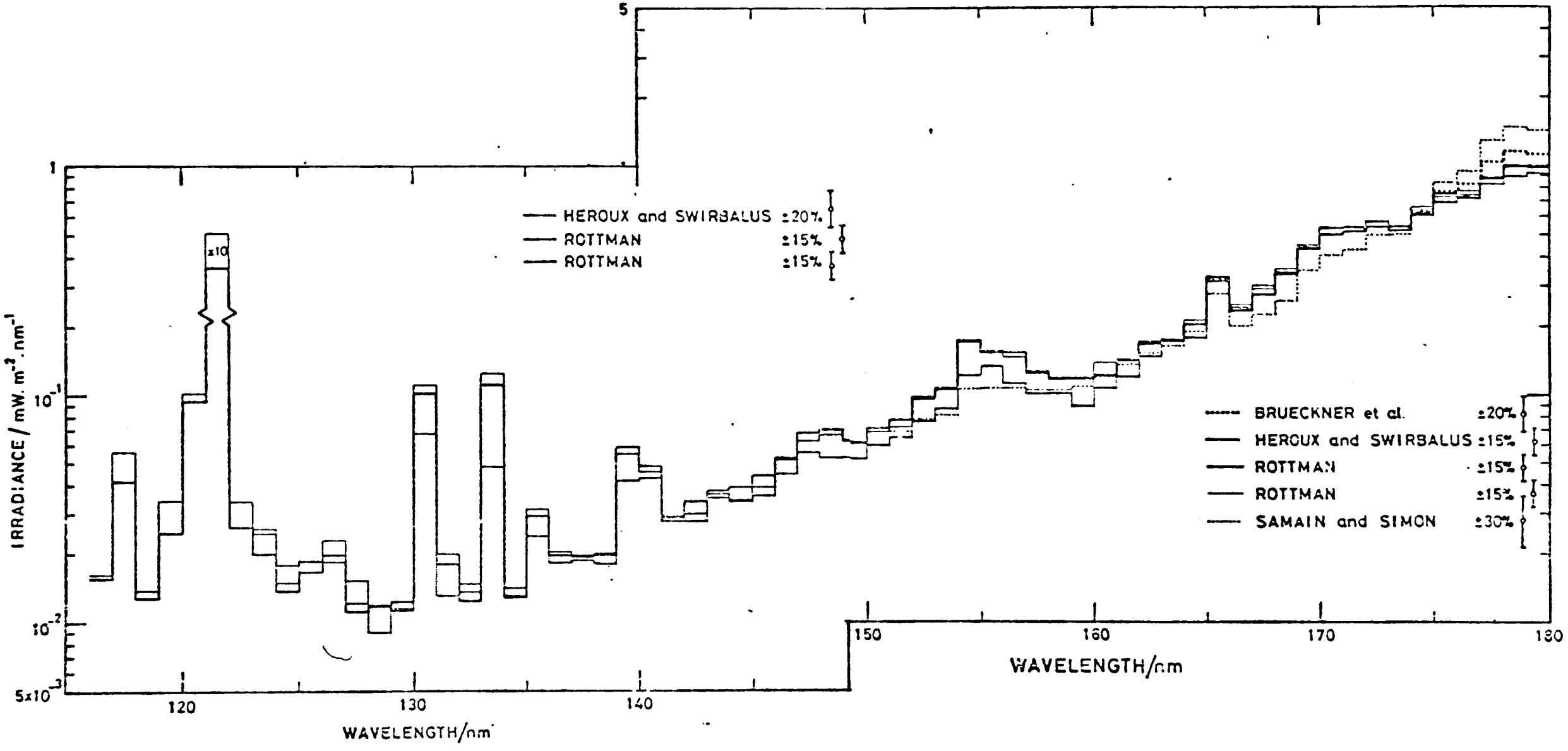

Fig.5.3 Intercomparison of measurements of solar ultraviolet. From Delaboudinière et al (1978). 115-180nm.

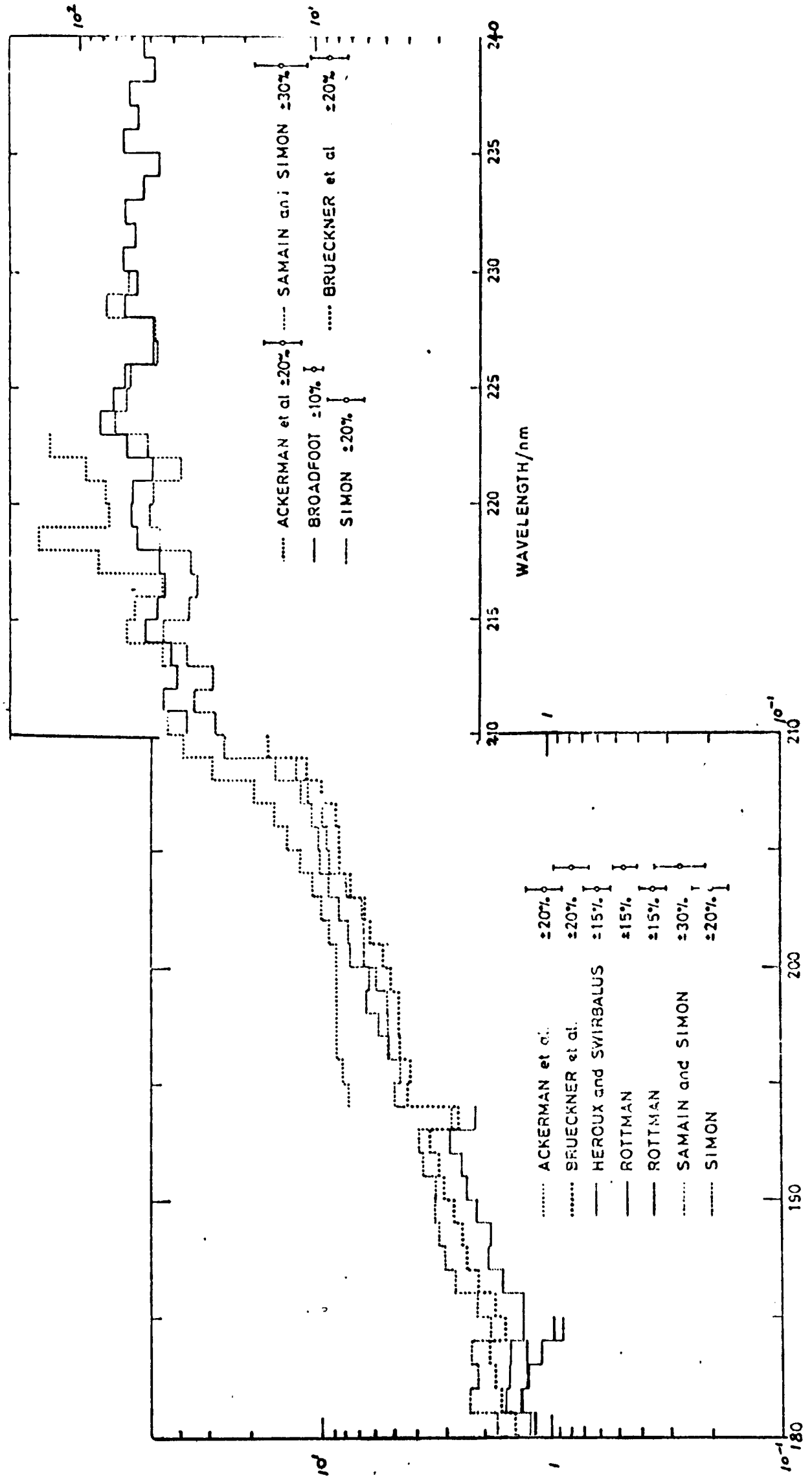

Fig.5.4 As Fig.5.3. 180-240nm.

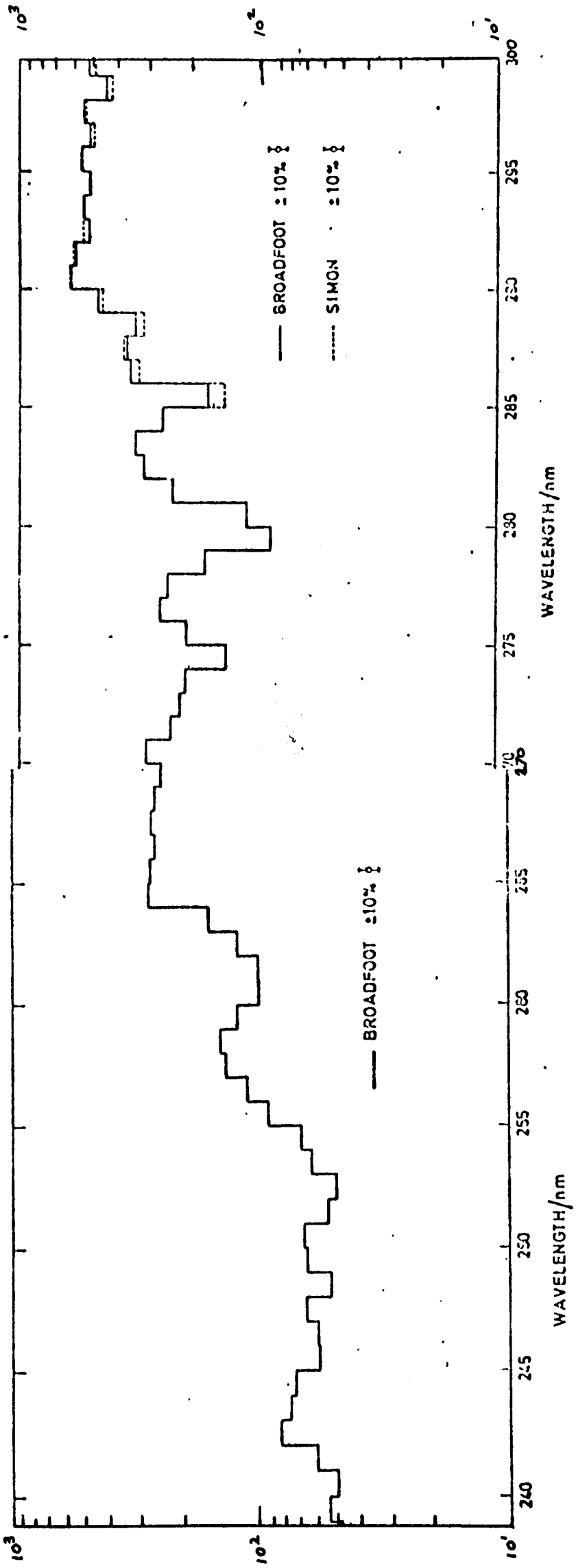

Fig.5.5 As Fig.5.3. 240-300nm.

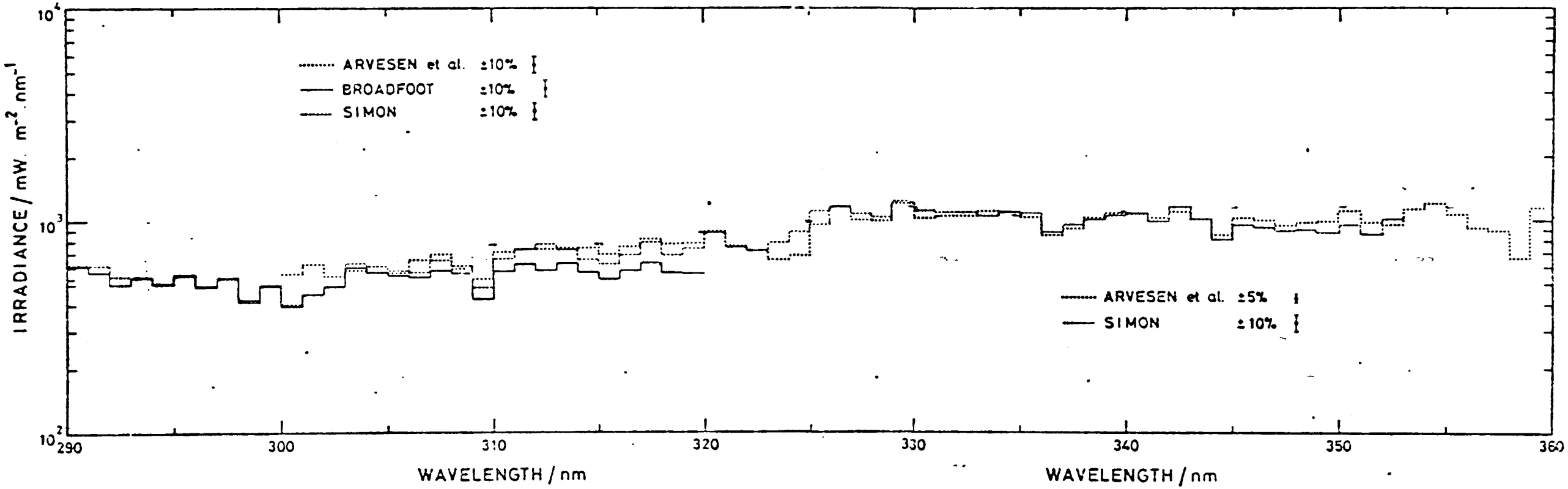

Fig. 5.6 As Fig.5.3. 290-360nm.

In this work the values of Ackerman (1971), modified in the region 200 - 230 nm by the measurements of Simon (1975), have been used because they were an accurate compilation and conveniently already established in the Oxford 2 - Dimensional Model for photochemical calculations. A smoothed representation of these fluxes in terms of the number of photons in a 5 nm wavelength band arriving per unit area per second is given in Fig. 5.7. The flux of photons in the hydrogen Lyman - α line is shown by a cross; its high value, relative to the fluxes at nearby frequencies, is an important factor in the heating of the upper mesosphere as its frequency, 121.6 nm, happens to lie in an atmospheric window. Numerical values of Ackerman's fluxes are given in Appendix B.

5.3 The absorption cross-sections of O_2 and O_3

Figs. 5.8 and 5.9 show the absorption cross-sections of O_3 and O_2 smoothed from the values tabulated by Ackerman (1971). Numerical details of these cross-sections are given in Appendix B.

In the region of 1300 Å ozone has some quite high ($> 10^{-17}$ cm^2) values for its absorption cross-section but these are of little interest in this work as solar radiation at these wavelengths is absorbed by molecular oxygen well above the altitudes of significant ozone mixing ratio. The most important feature in the spectrum of ozone is the Hartley band which extends from 2000 Å to 3000 Å with a peak cross-section of 1.12×10^{-17} cm^2 at 2550 Å. The cross-sections are not very sensitive to temperature varying by less than 10% between 181 K and 291 K according to Vigroux (1953). The Hartley band is responsible for the majority of the absorption of solar radiation which occurs in the upper stratosphere and lower mesosphere.

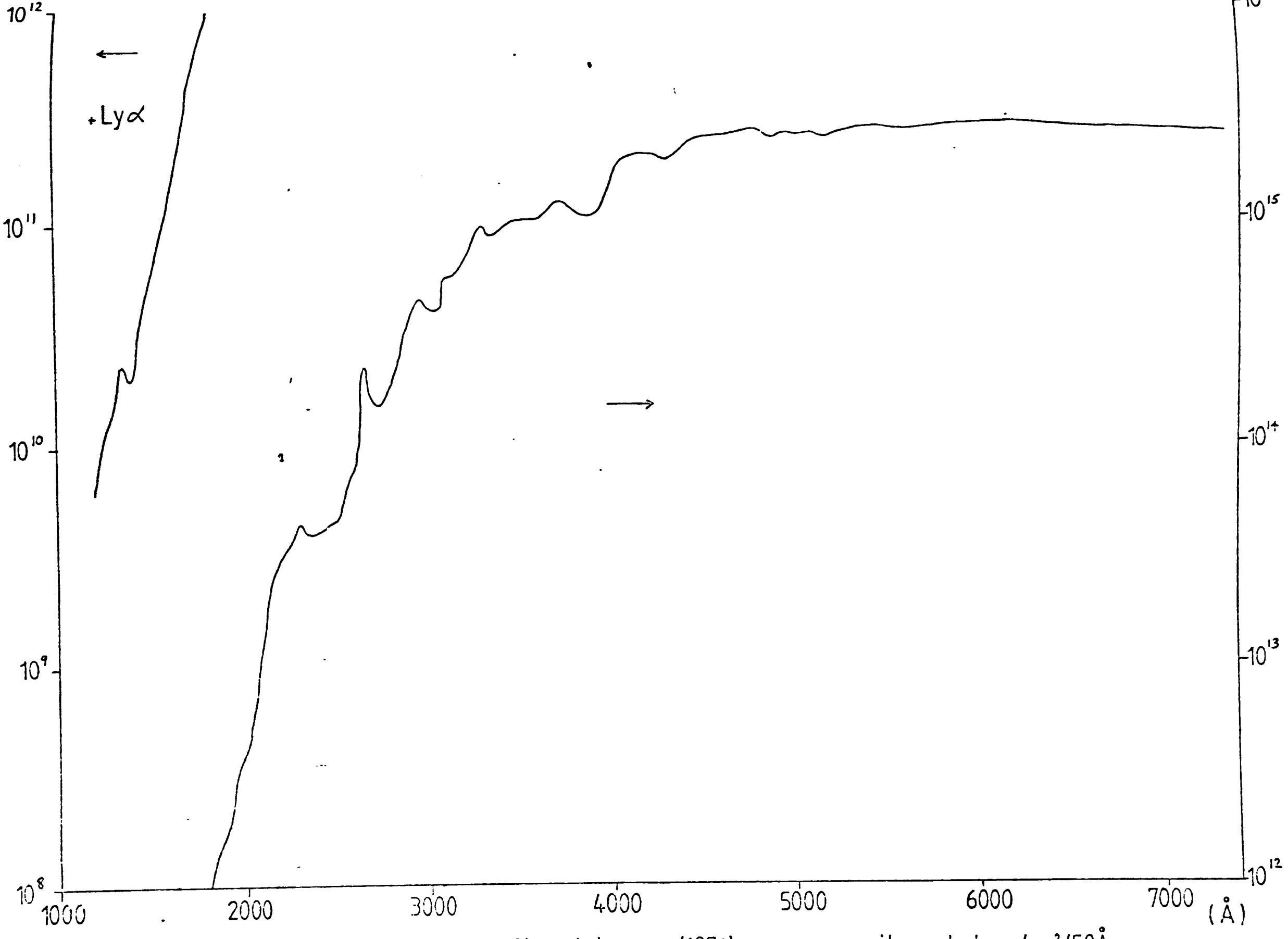

Fig. 5.7 Solar flux at 1AU, after Ackerman (1971) units: photons/cm²/50Å

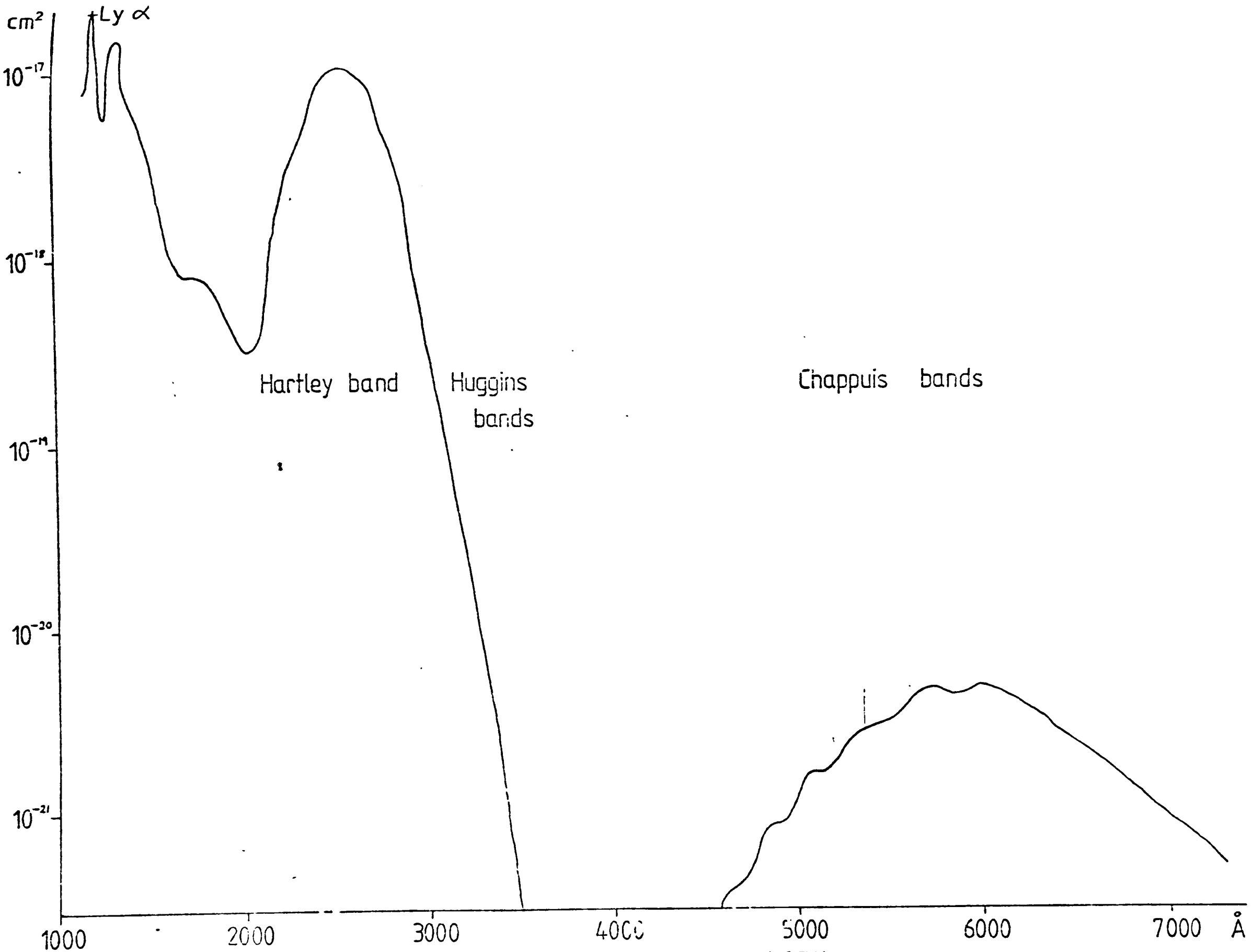

Fig 5.8 O_3 absorption cross-sections, after Ackerman (1971)

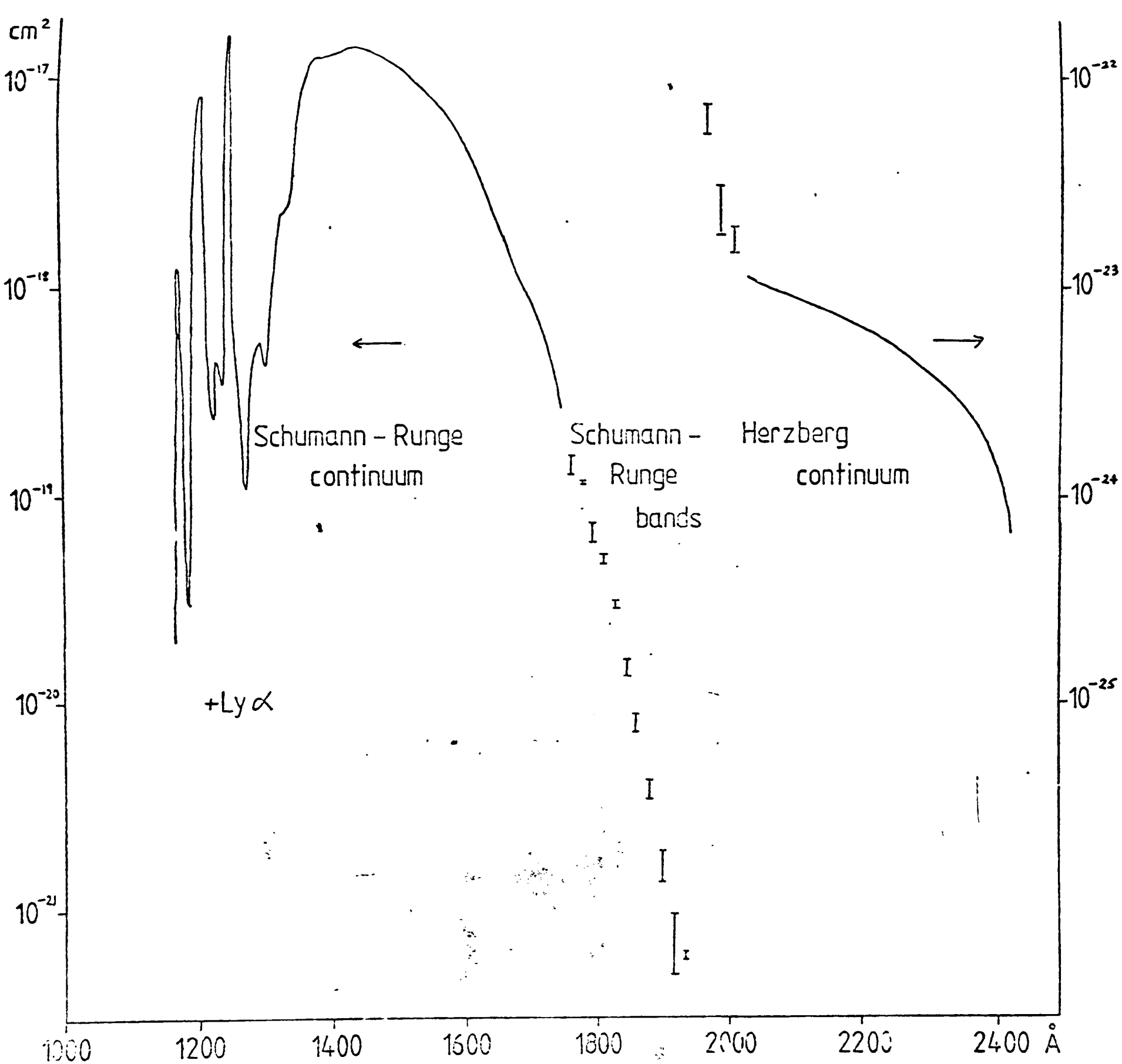

Fig. 5.9 O_2 absorption cross-sections, after Ackerman (1971)

Adjoining the Hartley band are the weaker Huggins bands, between 3000 Å and about 3500 Å, which are responsible for flux depletion in the middle stratosphere. Vigroux (1953) found that absorption in these bands is sensitive to temperature with a different dependence in absorption maxima and minima. For the maxima the ratio $\sigma(T)/\sigma(291)$ varies between 0.51 at 181 K and 3295 A and 4.25 at 393 K and 3421 A. The same magnitude of variation applies to the minima but at different wavelengths. These extreme values of the ratio are confined to the extremes of temperature which are not typical of atmospheric temperatures in the altitude region of interest here. The wavelength interval of 50 Å used by Ackerman (1971) is too large to resolve the maxima and minima of the Huggins bands and thus any attempt at determining a temperature dependence for Ackerman's coefficients is futile.

The Hartley and Huggins bands of ozone are responsible for shielding the earth's surface from the biologically harmful radiation in the wavelength region 2800 - 3200 Å.

At visible wavelengths, around 4500 - 7500 A, are the Chappuis bands with maximum cross-section $4.89 \times 10^{-21} cm^2$ at 6000 Å. Vigroux (1953) found no temperature dependence for the absorption in these bands. The major contribution of the Chappuis bands occurs in the lower stratosphere.

In all the ultraviolet and visible bands of ozone absorption is found to be independent of pressure.

The absorption cross-section spectrum of molecular oxygen shows some sharp peaks and troughs at wavelengths shorter than 1300 Å. Solar radiation at frequencies corresponding to the peaks is absorbed well above the mesopause but in the troughs it may contribute to the thermal budget as low as 85 km. The cross-section at 1216 Å, which is the wavelength of strong solar output due to emission in the hydrogen Lyman -α line, is

particularly small at about 10^{-20} cm^2 and thus radiation at this wavelength is important at altitudes significantly lower than the mesopause. Between 1300 Å and 1750 Å is the strong Schumann - Runge continuum which extinguishes radiation in this wavelength band well above the region of interest here.

From 1750 Å to 2026 Å is an area of particular importance but also considerable uncertainty. Absorption in this region by O_2 is due to the Schumann - Runge bands. This absorption is particularly sensitive to temperature (Ackerman et al (1970), Kockarts (1971)) as it depends on the relative population of the first excited vibrational level $v'=1$, of the ground state; as the temperature decreases the $v'=1$ bands tend to disappear. Another reason for the temperature sensitivity is the relative intensities of the rotational lines of the P and R branches inside a specific band; this effect can only be seen at resolution of about 0.5 cm^{-1} as at wider waveintervals the difference is smoothed out. The absorption cross-sections in this wavelength band shown in Fig. 5.9 are those of Kockarts (1971) with the length of the bar indicating the difference between the values at 160 K and 300 K. In this work a linear interpolation is used between these temperatures at each wavelength interval to find the cross-section at an intermediate temperature. Because of the very fine structure of the Schumann - Runge Bands the use of absorption cross-sections averaged over 50 Å may lead to errors in calculating the absorption at a particular wavelength. This is of great importance in the estimation of the photodissociation coefficients of e.g. H_2O and CO_2 (see Kockarts, 1976) but not of significance in heating rate calculations. Further complications at these wavelengths arise from uncertainty in the magnitude of the solar flux (see Fig. 5.4). The Schumann - Runge Bands are the main source of heating in the upper mesosphere.

Between 2026 Å and 2420 Å lies the Herzberg continuum, competing for radiation with the shorter wavelength end of the Hartley band of ozone. It contributes a small amount to the heat budget of the upper stratosphere and mesosphere but is more important for the oxygen atoms it produces in the region of ozone formation. Absorption by O_2 and O_3 in all the other wavelength intervals mentioned in this section can also lead to photodissociation of the molecule. Calculations of heating rates, therefore, may not assume that all the absorbed radiative energy is immediately transferred into kinetic energy.

5.4 Optical depths and heating rates

In order to simplify the radiative transfer equation for short wave radiation we may neglect the contribution to the source function from thermal radiation in the atmosphere. A further simplification can be made by neglecting the scattering and reflection of radiation.

Scattering in the atmosphere is usually considered to take place by one of two methods. Firstly there is Rayleigh, or molecular, scattering for which the radius of the scattering centre (in this case an air molecule) is much smaller than the wavelength of the radiation. Dave and Furukawa (1967) found that the inclusion of Rayleigh scattering would increase the amount of solar radiation absorbed above 5 mb by 3 - 4%. They concluded that the effect of reflection from the ground was far more significant. Edwards (1970) developed this idea and studied the effect of different surface and cloud albedos on heating rate calculations. He found that varying the height of the cloud made little difference but that by varying its albedo from 0.2 to 0.9 a maximum increase of about 0.9 K day^{-1} at 30 km was obtained in the heating rate. Lacis and Hansen (1974) concluded from their detailed multiple scattering calculations that diffuse

solar radiation can be modelled by a pure absorption region above a purely reflecting layer of which the albedo is determined from the ground reflectivity and lower atmosphere albedo. They showed that the reflecting layer could have a significant ($\lesssim$ 1 K day^{-1}) effect on the heating rate between about 15 and 35 km.

The second form of scattering is that by atmospheric aerosols which have radii of the order of or larger than the wavelength of the radiation. There is still considerable uncertainty in the size distribution, composition, optical properties and variation of concentration with altitude of aerosols (see e.g. Cadle, 1977) so it is difficult to make an accurate assessment of their effect on the transmission of radiation. Cadle and Grams (1975) have calculated the percentage reduction in the solar constant as a function of particle radius and imaginary reflective index, their maximum depletion is about 2% for zenith angle 60°.

Scattering and reflection also affect the calculation of photodissociation coefficients but they have not been included in any of the heating or photochemical schemes used in the Oxford Model and this is a problem that remains to be tackled.

The neglect of scattering reduces the radiative transfer equation to the simple form

$$S(z,\lambda) = S(\infty,\lambda)\, e^{-\tau(z,\lambda,\theta)} \qquad (5.1)$$

where $S(\infty,\lambda)$ is the solar flux at wavelength λ outside the atmosphere and $S(z,\lambda)$ is its value at an optical depth $\tau(z,\lambda,\theta)$ into the atmosphere. θ is the solar zenith angle at altitude z.

This is the Bouguer - Lambert Law first used in 1760. The local heating rate may be obtained from the convergence of the fluxes:

$$\frac{\partial T}{\partial t}(z,\lambda,\theta) = \frac{1}{\rho(z) c_p \sec\theta} \frac{\partial S}{\partial z}(z,\lambda)$$

$$= \frac{-1}{\rho(z) c_p \sec\theta} S(\infty,\lambda) \frac{\partial \tau}{\partial z}(z,\lambda,\theta)\, e^{-\tau(z,\lambda,\theta)} \qquad (5.2)$$

Thus a knowledge of the solar spectrum outside the atmosphere, the distribution of absorbing gases and their frequency - dependent absorbing properties makes possible a calculation of heating rates throughout the atmosphere.

The absorption cross-section $\sigma(\lambda,z)$ is defined by the equation

$$\tau(\lambda,z,\theta) = \int_z^\infty \sigma(\lambda,z')\, n(z')\, dz' \sec\theta \qquad (5.3)$$

where $n(z')$ is the number density of the gas at altitude z'. σ is a function of z through its dependence on temperature and pressure, it may also depend on the number density (see discussion of the work of Strobel (1978) in Section 5.5).

Separating the ozone and oxygen contributions to the optical depth equation (5.3) becomes:

$$\tau(\lambda,z,\theta) = \int_z^\infty \sigma_2(\lambda,z') n_2(z') dz' \sec\theta + \sigma_3(\lambda) \int_z^\infty n_3(z')\, dz' \sec\theta$$

where the suffix 2 indicates O_2 and 3 O_3. The absorption cross-section of ozone is assumed independent of temperature and pressure and therefore of z.

In finite difference form we obtain:

$$\tau_{i,k}(\theta) = \Delta z \sec\theta \left\{ \sum_{j=k}^{\infty} \sigma_{2_{i,j}} n_{2_j} + \sigma_{3_i} \sum_{j=k}^{\infty} n_{3_j} \right\}$$

where i indicates a wavelength interval and the summations occur over layers each of vertical thickness Δz. $\sigma_{2_{i,j}}$, n_{2_j} and n_{3_j} have constant values over each layer and $\sigma_{2_{i,j}}$, σ_{3_i} have constant values over each wavelength interval i. In practice it is not possible to sum to infinity and a further approximation can be made by specifying the optical depth $\tau_{i,t}$ above the highest level of interest t:

$$\tau_{i,k}(\theta) = \Delta z \sec\theta \left\{ \sum_{j=k}^{t} \sigma_{2_{i,j}} n_{2_j} + \sigma_{3_i} \sum_{j=k}^{t} n_{3_j} \right\} + \tau_{i,t}(0) \sec\theta \qquad (5.4)$$

Because of the curvature of the earth's surface the solar zenith angle θ at altitude Z is not the same as the zenith angle θ_s at the earth's surface. The relationship between the two is:

$$\cos\theta = \left\{ 1 - \frac{(1 - \cos^2\theta_s)}{(1 + z/a)^2} \right\}^{1/2}$$

where a is the radius of the earth

which may be approximated by:

$$\sec\theta = (1 + z/a)\left(\cos^2\theta_s + 2z/a\right)^{-1/2} \qquad \text{for } z/a \ll 1$$

Houghton (1963)

Optical depths have been calculated for $\theta_s = 0^\circ$ and 81.6°. Using a midlatitude summer temperature profile and the ozone mixing ratio profile constructed by Edwards (1970). The height intervals were fixed by $\xi = n/2 + 1/4$ $n = 0, 1, 2 \ldots, 28$ $\left(\xi \equiv -\ln \frac{p}{p_s}\right)$ with the height of level t ($\xi = 14.25$) being approximately 95 km. $\tau_{i,t}(0)$ was specified from the data of Kock arts (1971).

Fig. 5.10 shows the frequency dependence of the heights at which the optical depth is 0.1, 1.0 and 10.0 for a zenith angle of 0°; Fig. 5.11 presents the same for $\theta_s = 81.6^{\circ}$. The numbers along each abcissa indicate the wavelength interval specified in Appendix B; the horizontal scale is therefore not linear throughout the range of wavelengths.

The penetration of Lyman -α radiation can be seen clearly. For an overhead sun this radiation reaches about 75 Km before it has traversed one optical depth. In the Schumann - Runge continuum the radiation has crossed more than ten optical depths above 100 km. The position of the Hartley band is clearly shown by the increase in altitude of the position of unit optical depth in the 2000 - 3000 Å region. The effect of the Chappuis bands is only just in evidence with the position of $\tau = 0.1$ appearing at 27 Km near 5900 Å for the large zenith angle.

A form of equation (5.2) suitable for numerical evaluation is:

$$\left(\frac{\partial T}{\partial t}(\theta)\right)_{i,j} = \frac{S_{i,j}}{\Delta z\, \rho_j\, c_p \sec\theta} \left(\tau_{i,j}(\theta) - \tau_{i,j+1}(\theta)\right) \qquad (5.5)$$

where the values of $\tau_{i,j}(\theta)$ are obtained from equation (5.4). The total heating rate for all wavelengths when the sun has zenith angle θ is

$$\left(\frac{\partial T}{\partial t}(\theta)\right)_{j} = \frac{1}{\Delta z\, \rho_j\, c_p \sec\theta} \sum_{k} S_{k,j} \left(\tau_{k,j}(\theta) - \tau_{k,j+1}(\theta)\right) \Delta\lambda_k$$

where $\Delta\lambda_k$ is the size of wavelength interval k. The solar zenith angle depends on the time of year (declination angle δ), the time of day (hour

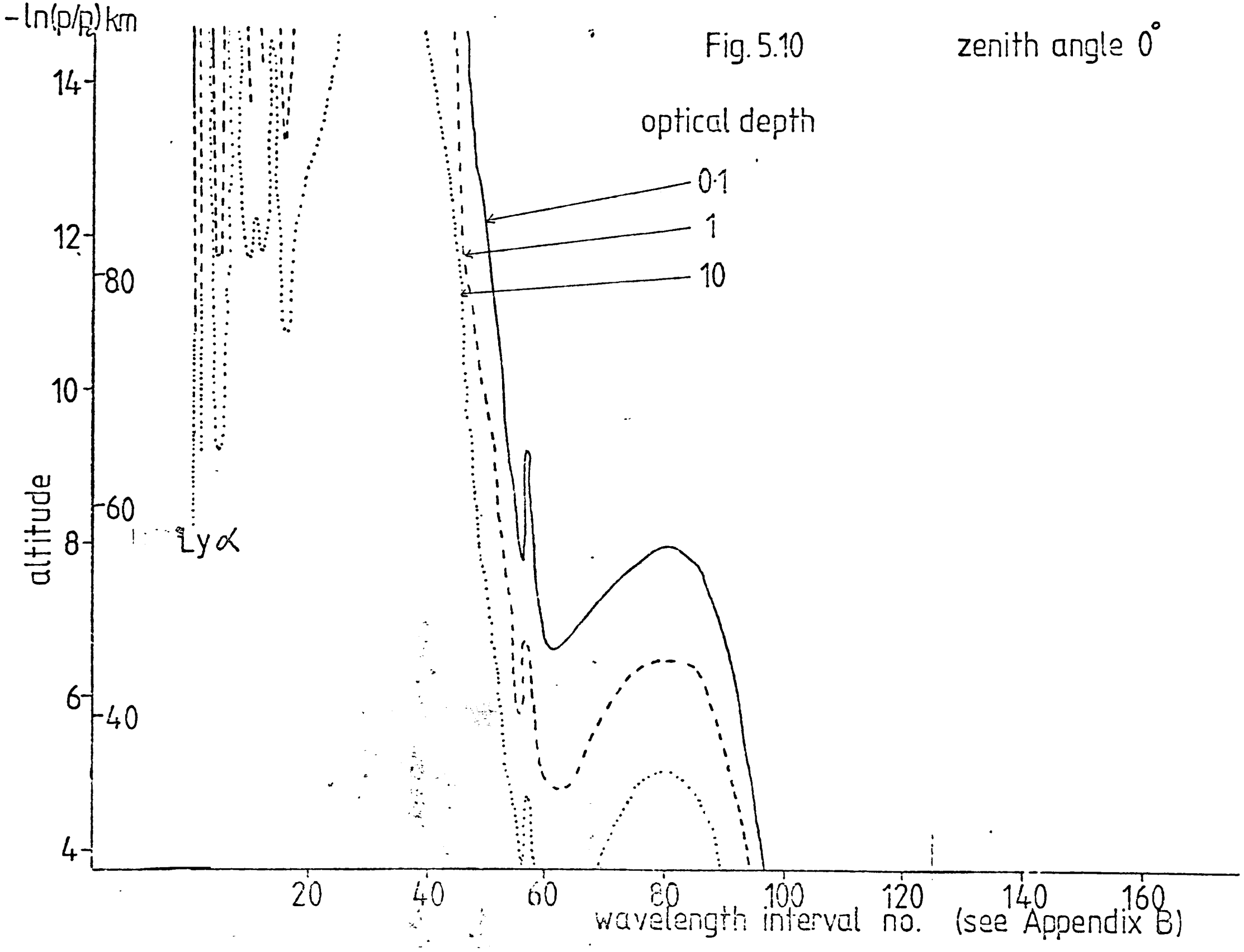

Fig. 5.10 zenith angle 0°

Fig. 5.11

zenith angle 81·6°

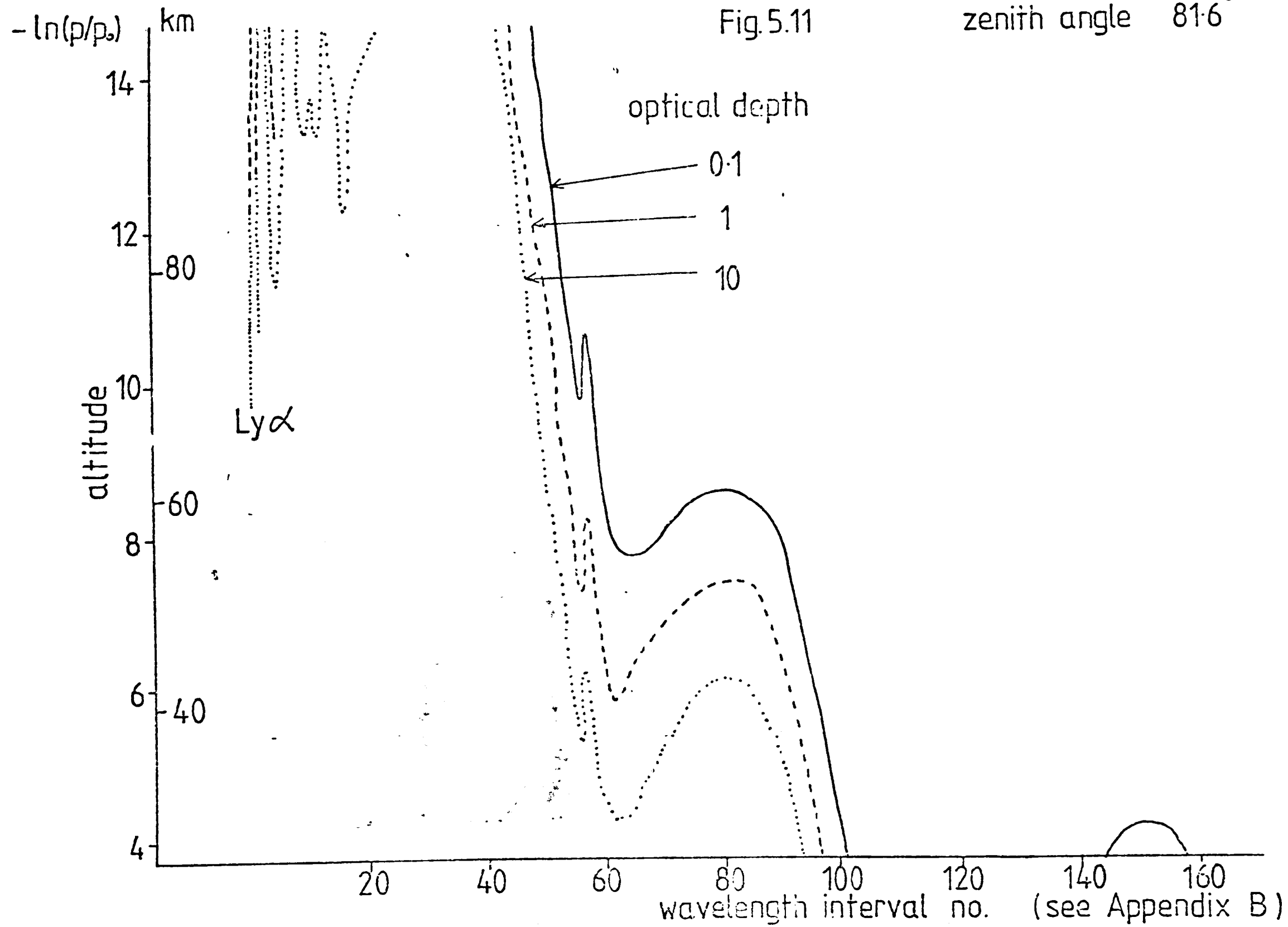

angle h) and the latitude ϕ of observation according to:

$$\cos\theta = \cos\phi \cos\delta \cos h + \sin\phi \sin\delta$$

For one daylight period (i.e. assuming constant δ) at a particular latitude the average heating rate may be calculated using a Gaussian average of the heating rate between sunrise and sunset with hour angle as the variable. Net heating over the day may then be found by multiplying the average rate by the fraction of the day for which the sun is shining.

A scheme based on the above method was used to calculate heating due to the absorption of solar radiation by O_2 and O_3 between about 25 km and 95 km. All the radiation absorbed was assumed to have become kinetic energy directly. This is not a realistic assumption as some of the energy absorbed is used in photodissociating the molecule and at high altitudes the resulting oxygen atoms may be transported some distance before a chemical reaction or recombination causes the release of the stored energy. However, Fukuyama (1974), using a vertically diffusive - photochemical model, concludes that at 80 km (though not at 120 km) the energy released by various hydrogen-oxygen and oxygen-oxygen reactions together with that released by collisidal quenching almost exactly balances that used in dissociation and excitation of the products. Thus the heating rates given in this section should be reasonably accurate below the mesopause and increasingly overestimated above.

The result of such a heating rate calculation is shown in Fig. 5.12 for March conditions and Fig. 5.13 for the situation in June. Maximum heating occurs at about 47 km near the summer pole corresponding to the altitude at which a large part of the spectrum of solar radiation reaches unit optical depth and the date and latitudes for which the insolation

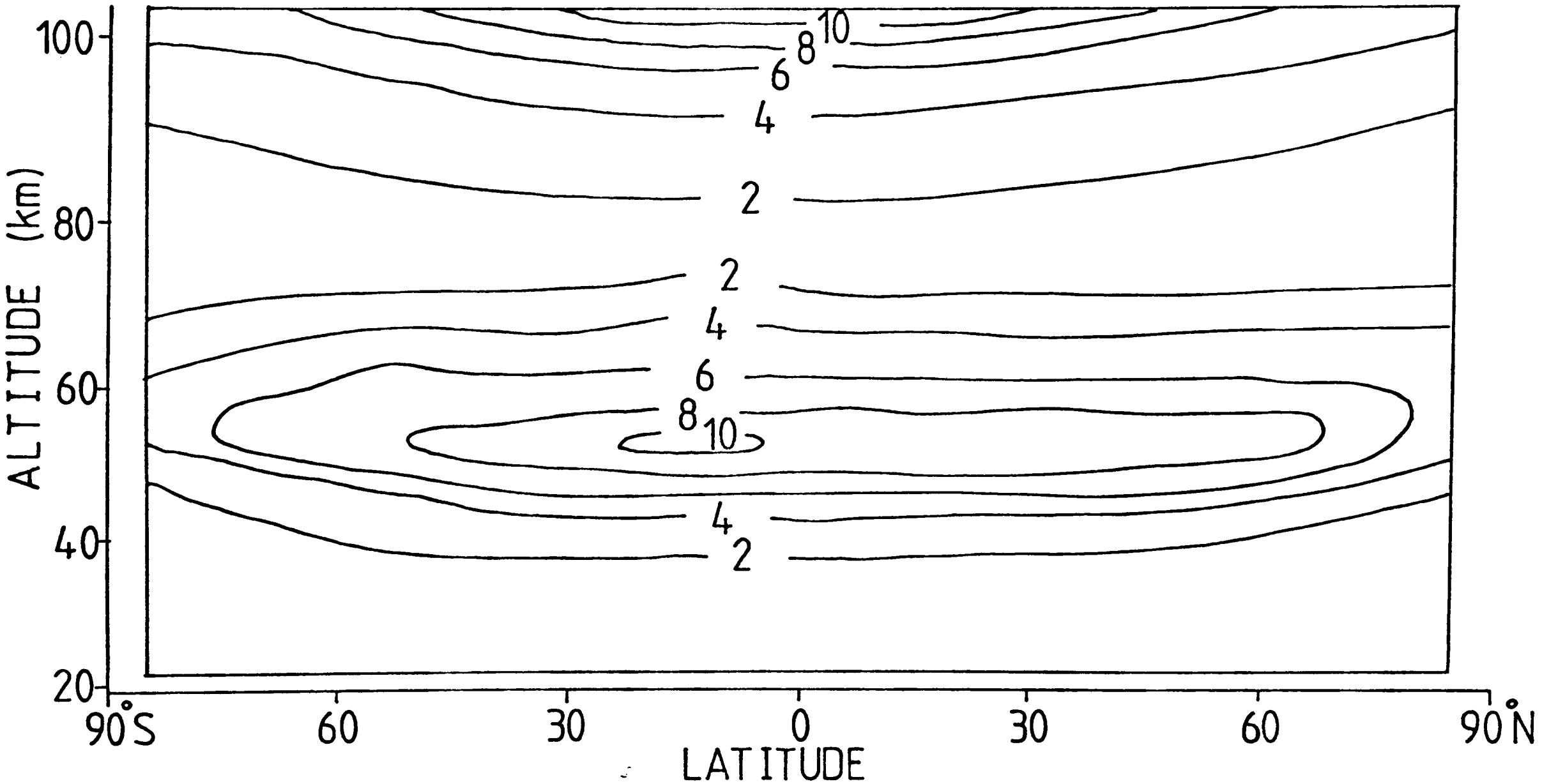

Fig. 5.12 Heating rate (K/day) due to absorption of solar radiation by O_3 and O_2 , March.

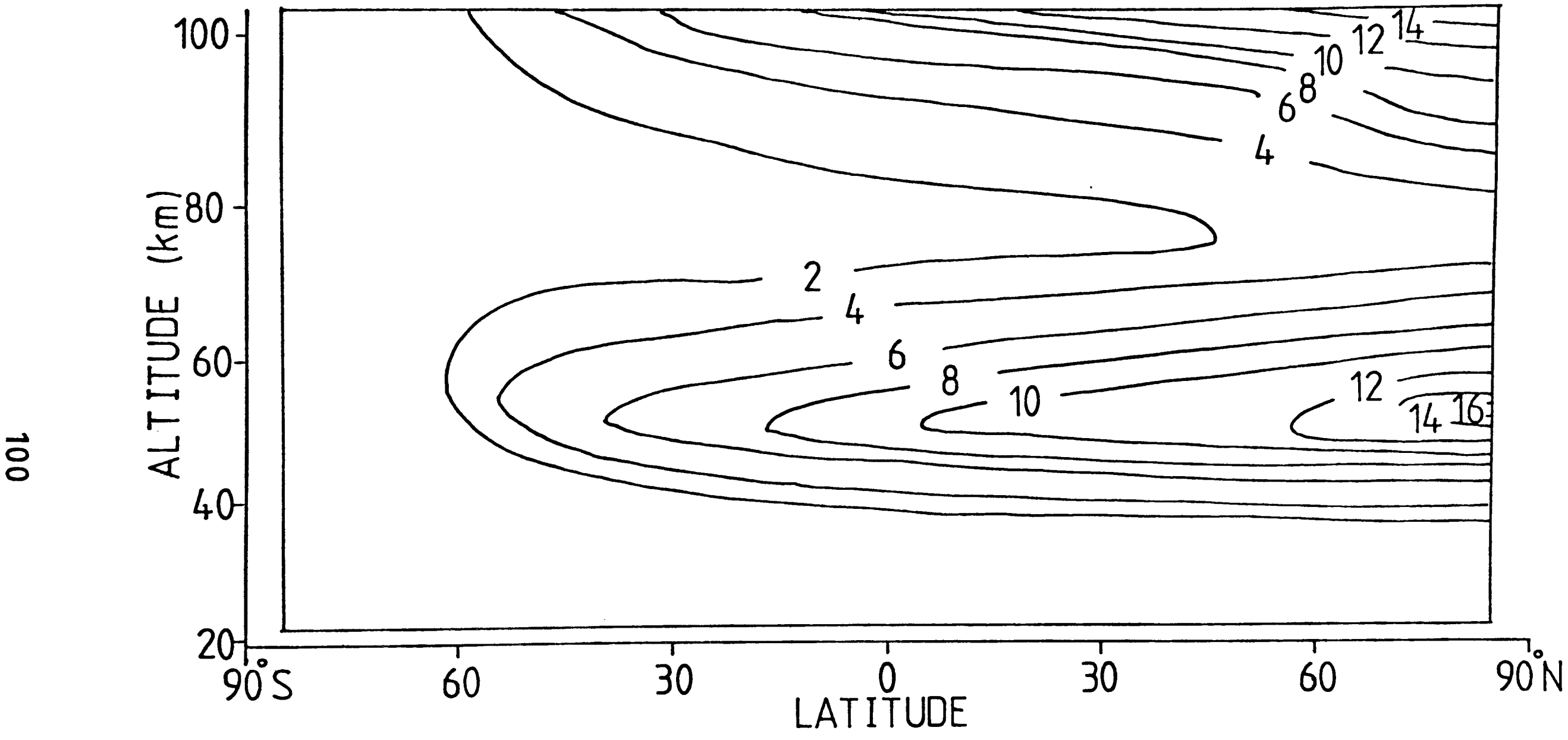

Fig. 5.13 Heating rate (K/day) due to absorption of solar radiation by O_3 and O_2 , June.

lasts most, or all, of the day.

Within the limits of the theory and the experimental accuracy of the measurements of fluxes and cross-sections the above method for calculating heating rates may be considered 'exact' i.e. there have been no approximations made solely for the purpose of shortening the calculations involved. For use in numerical models, however, this method is impractical because of the large amounts of computing time required to calculate the flux depletion and heating rate in each wavelength interval at each height level several times per model day. For this reason several workers have suggested parameterisations which calculate heating rates without such exhausive computation but within a given margin of error. Some of these methods will now be considered.

5.5 Parameterisations of the absorption of solar radiation

There have been only two fundamentally different methods used in solar heating parameterisations. The first, developed by Lindzen and Will (1973) for ozone absorption and extended to incorporate oxygen absorption by Strobel (1978), assumes that the absorption cross-sections are either constant or have exponential variation over a given (wide) wavelength interval. The incoming solar radiation is also given a constant value in each of the intervals.

Lindzen and Will (1973) found that by using constant values for the absorption cross-sections in the regions 2375 - 2750 A, representing the Hartley band, and 5150 - 6800 A, representing the Chappuis bands and an exponential decay in the Huggins bands 2750 - 3400 A they could calculate atmospheric heating due to absorption by ozone to within 5% of an 'exact' calculation. Strobel (1978) divided the Huggins bands into two parts each with a different exponential factor. He also parameterised absorption by

molecular oxygen. The Herzberg continuum was incorporated into that part of the Hartley band with which it overlaps and the Schumann - Runge continuum was divided into two sections: one (1250 - 1520 Å) of constant and one (1520 - 1750 Å) of exponentially decreasing cross-section. For transmission in the Schumann - Runge bands Strobel considers that both weak line (linear) and strong line (square root) absorption should be included and his parameterisation for the heating rate is given as a function of N and $N^{\frac{1}{2}}$ (N is column density O_2). With this scheme Strobel attains an accuracy in calculating heating rates of 5% in the altitude range 15 - 120 km.

The second method used in parameterisations is to find analytic expressions for absorption in terms of absorber amount by numerical fits to exact calculations. Exact absorption curves have been compiled by Craig (1951) and Kennedy (1964). Kennedy used solar flux data from Tousey (1963) and Johnson (1954) and absorption coefficients from Inn and Tanaka (1957) and Vigroux (1953). An empirical formula to fit Kennedy's curve was produced by Harwood, Pyle and Rendel (1972). This is the formula, given in section 2.5.1, which was used in the Oxford Model for solar heating calculations. Lacis and Hansen (1974) used the spectral distribution of solar flux given by Labs and Neckel (1968) and the ozone absorption coefficients of Howard et al (1961) to calculate exact absorption curves for the ultraviolet and visible regions separately. They then fitted an algebraic expression to each of the curves with a maximum error of 0.5%. The formulae they obtained are:

$$A_{vis} = \frac{0{\cdot}02118\,x}{1 + 0{\cdot}042x + 0{\cdot}000323x^2}$$

$$A_{uv} = \frac{1{\cdot}082x}{(1 + 138{\cdot}6x)^{0{\cdot}805}} + \frac{0{\cdot}0658x}{1 + (103{\cdot}6x)^3}$$

where A_{vis} is the fraction of the incident solar flux at visible wavelengths absorbed by a pathlength x atmo-cm of ozone
and A_{uv} is the same at ultraviolet wavelengths.

Although this method can produce very accurate parameterisations it has the disadvantage that to incorporate any revised solar flux or cross-section data the fitting procedures must be repeated, thus making it rather inflexible. As improved measurements have been carried out since Kennedy's work it was felt that Rendel's formula in the Oxford model should be replaced. The inclusion of the data compiled by Ackerman (1971) also makes sure that the model is internally consistent as these values are used in the photochemical schemes.

5.6 An 'almost exact' method

The method described in section 5.4 was used to calculate the heating rate due to each wavelength interval (see Sppendxi B) at each altitude level ($-\ln p/p_s = n/2 + 1/4$, $n = 7, 8, \ldots, 28$) so that its relative contribution could be assessed. Fig. 5.14 shows those intervals which are responsible for 10, 1, 0.1 and 0.01 % of the total heating rate at each level. One obvious feature is the general trend of increase in wavelength with decrease in altitude - as would be expected the shorter wavelengths are more important at high altitudes. Another feature is the lack of contribution, in the height range considered, by wavelengths in the 1330 - 1640 Å and 3620 - 4080 Å, this just reflects the properties of the cross-sections discussed in section 5.3. Another point mentioned

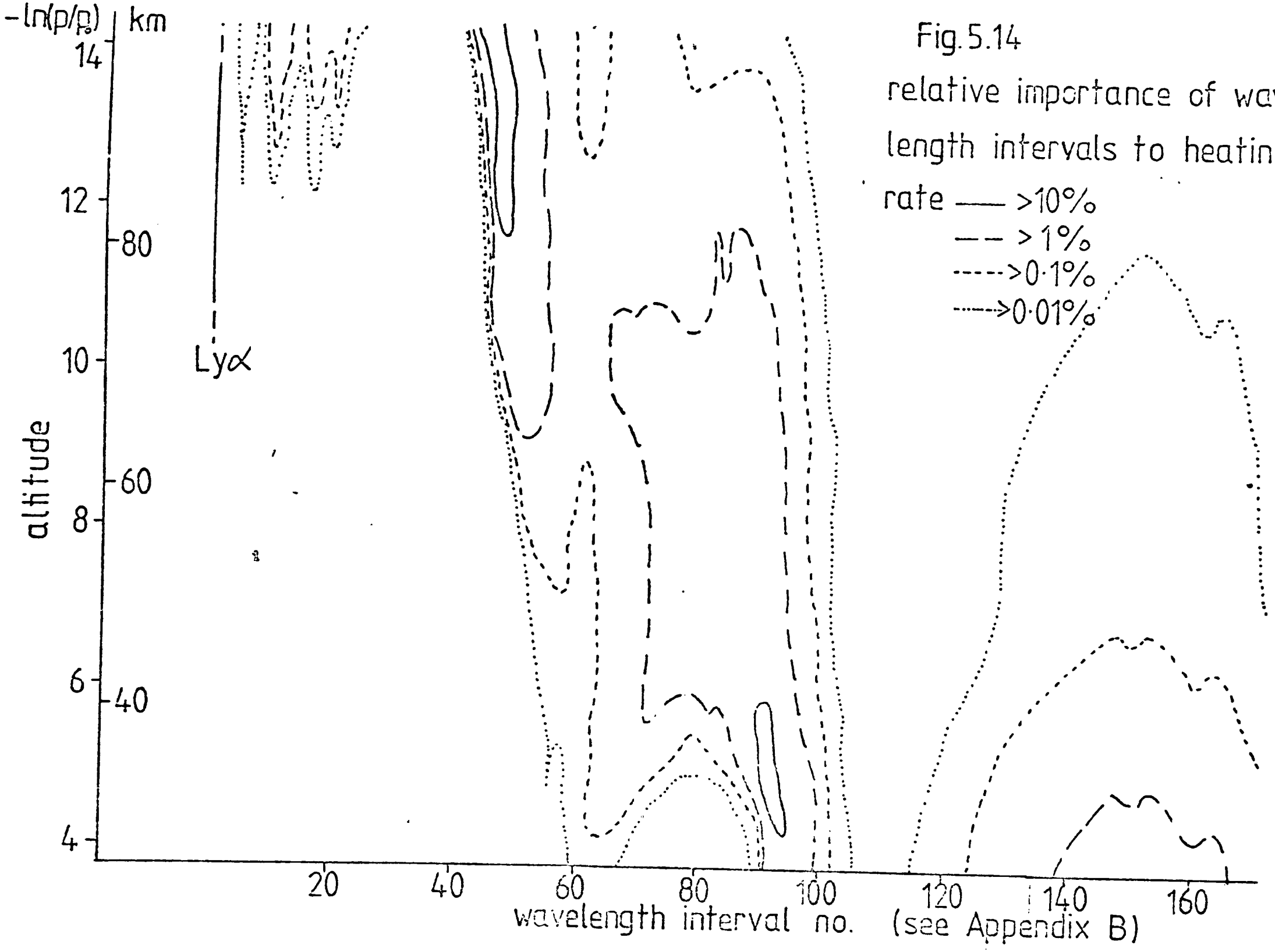

Fig. 5.14
relative importance of wave-length intervals to heating rate —— >10%
— — >1%
-----> 0·1%
·····> 0·01%

earlier is clearly demonstrated in the important role played by the radiation of the hydrogen Lyman-α line. Between 75 and 95 km it is responsible for at least 10% of the energy absorption.

In order to cut down the computing time needed for the calculation of heating rates by this method experiments were carried out in which various wavelength intervals were neglected either throughout the altitude range or for selected heights only. Table 5.1 indicates the intervals used in three of the experiments, chosen so as to coincide with the most important regions indicated in Fig. 5.14. The long wavelengths were only included at low levels; this saves time in calculating heating rates at higher altitudes but does not, of course, remove the necessity of calculating the depletion of the solar flux as it travels down through the higher levels.

Table 5.1

Experiment	Wavelength intervals (see Appendix B)	Approx. height range (Km)
1	1 - 24	65 - 95
	41 - 102	25 - 95
	124 - 171	25 - 50
2	41 - 102	25 - 95
	124 - 171	25 - 50
3	1 - 62	50 - 95
	63 - 102	25 - 95
	124 - 171	25 - 50

Experiment 1 takes approximately 68% of the computing time needed for the exact calculation while experiments 2 and 3 need about 61% and 74% respectively. Table 5.2 shows the errors incurred at each height from

using the three different schemes. Experiment 1 has a maximum error of 2.0% at 50.8 km. This is an altitude of relatively large heating rate but even for its maximum value ($\sim$20 K day^{-1}) the error is less than 0.5 K day^{-1}. This is quite satisfactory for current purposes but the three separate wavelength regions and altitude ranges makes this scheme somewhat complex. Experiment 2 shows the result of neglecting radiation in the Schumann - Runge continuum and the hydrogen Lyman-α line. Errors as high as 16% occur in the region of the mesopause. This is not sufficiently accurate for our heating rate calculations and the reduction in computing time ($\sim$ 7%) is not large enough to justify such inaccuracy.

Experiment 3 needs slightly more time than experiment 1. However, the reduction in the number of height ranges to two simplifies the calculation and although the accuracy is slightly reduced below 48 km it is increased above 82 km. For these reasons the scheme used in experiment 3 was adopted for the Model and the results of using it are discussed in Chapter 6.

Table 5.2

Altitude		Errors incurred (%)		
$-\ln p/p_s$	km	Expt. 1	Expt. 2	Expt. 3
14.25	95.3	< 0.1	10.9	< 0.1
13.75	92.4	0.2	12.5	< 0.1
13.25	89.5	0.3	14.3	< 0.1
12.75	86.8	0.5	13.3	< 0.1
12.25	84.1	0.3	15.4	0.1
11.75	81.4	0.2	16.7	0.2
11.25	78.6	0.3	15.2	0.3
10.75	75.8	0.4	11.9	0.4
10.25	72.7	0.6	7.1	0.6
9.75	69.5	0.9	2.9	0.9
9.25	66.1	1.3	1.4	1.3
8.75	62.5	1.4	1.4	1.4
8.25	58.7	1.5	1.5	1.5
7.75	54.8	1.7	1.7	1.7
7.25	50.8	2.0	2.0	2.0
6.75	46.9	< 0.1	0.1	0.5
6.25	43.0	< 0.1	0.1	0.4
5.75	39.2	< 0.1	0.1	0.5
5.25	25.6	0.1	0.1	0.5
4.75	32.3	0.2	0.2	0.5
4.25	28.8	0.4	0.4	0.5
3.75	25.5	0.5	0.5	0.6

CHAPTER 6

The Response of the model to different radiation schemes

6.1. Model results using the radiation schemes described in chapter 2

6.1.1 Basic Fields

In setting up a numerical model of the type established at Oxford the aim must be to reproduce as closely as possible the observed fields of atmospheric variables such as winds, temperature and minor constituents and their seasonal and latitudinal variations. If there is a close correspondence between the model results and the observed values then it may be assumed that the theory behind the model equations is valid and that the driving forces of the natural atmosphere are fairly well understood. Further one may feel justified in conducting experiments with the model in which the atmosphere is artificially perturbed in order to predict its state under various possible conditions (e.g. increasing the amount of carbon dioxide in the model atmosphere to simulate the possible effects of the burning of fossil fuel and deforestation.) If the model fields do not correspond well with their observed counterparts then the conclusion must be either that at least part of the model is incorrectly formulated or that there are some other processes which have not been included and which have a significant effect.

Before the response of the model to different radiation schemes is considered the merits and deficiencies of the results of the model set up as described in chapter 2 will be discussed. This basic experiment will be called Run A.

Figs. 6.1 and 6.2 show the temperature and zonal wind fields for 21st December near the end of the second year of Run A. Previous work by Harwood and Pyle (1977) has shown that the model takes about one year to

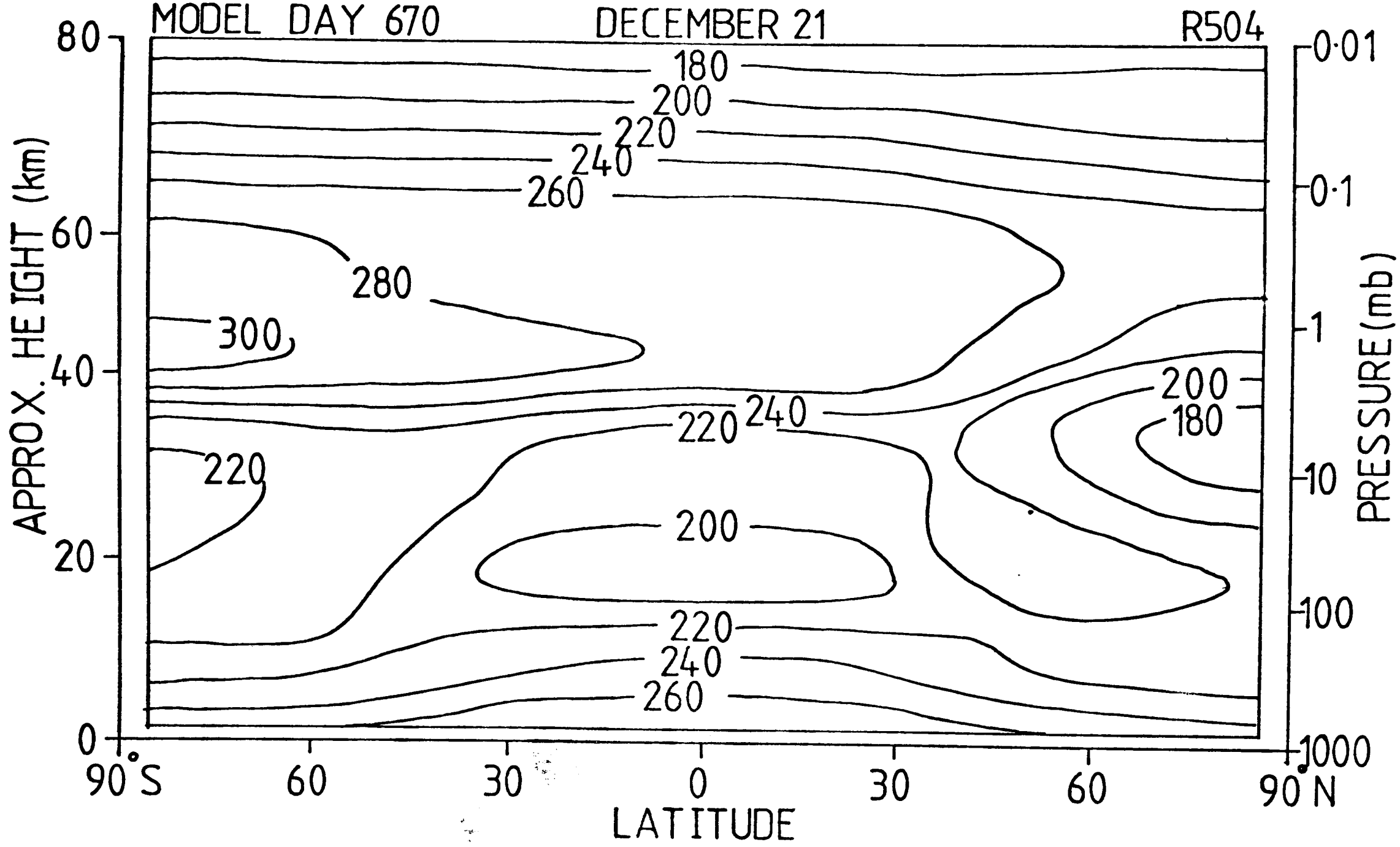

Fig. 6.1 Temperature (K) Run A

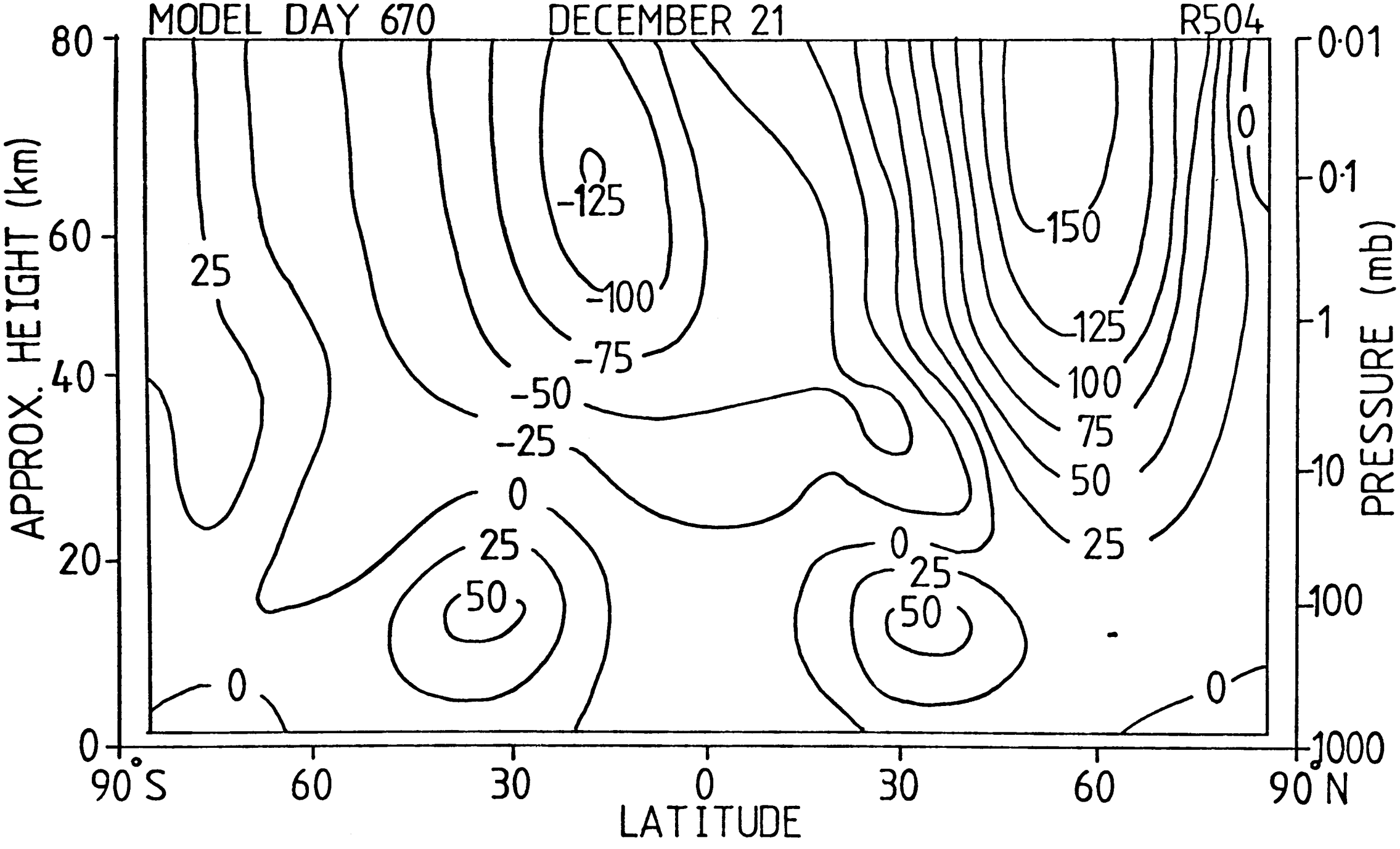

Fig. 6.2 Zonal wind (m/s) Run A

reach a state in which an annually reproducible distribution is established and thus the results depicted in these Figures represent the situation after the model has 'settled down'.

The temperature field in Fig. 6.1 shows the general features of the atmosphere (c.f. Fig. 1.1) but with some differences. The stratopause has an unrealistic wide plateau-like shape and its altitude is slightly low in the summer hemisphere. The peak temperature of 311K at the summer pole is rather high. There is an anomalous cold cell in the lower stratosphere in summer high latitudes. The shape of the tropopause and the temperature values in this region are well reproduced. There is only the slightest indication of the reversal in horizontal temperature gradient which occurs above about 65 km.

The zonal wind field, shown in Fig. 6.2, is linked to the temperature field through the thermal wind equation. Comparison of these winds with the representative values of Fig. 1.2 shows that the subtropical jets are reproduced, although rather too strong, and there are easterly components in the troposphere in equatorial and polar regions. In the stratosphere and mesosphere there are easterlies in summer and westerlies in winter and, as observed, the easterly regime encroaches into the winter hemisphere. The westerly region is separate from the sub-tropical jet. Consistent with the very small reverse temperature gradient at 80 km the peak values of both easterly and westerly regions occur at too great a height and are overestimated by about a factor two i.e. the jets do not close sufficiently. The westerlies apparent in Fig. 6.2. at summer high latitudes above about 20 km are not observed in the atmosphere or in the modelled zonal wind fields for the northern hemisphere summer. This asymmetry is due to the difference between the horizontal eddy momentum fluxes specified in December and June. The weak easterlies in the mesosphere

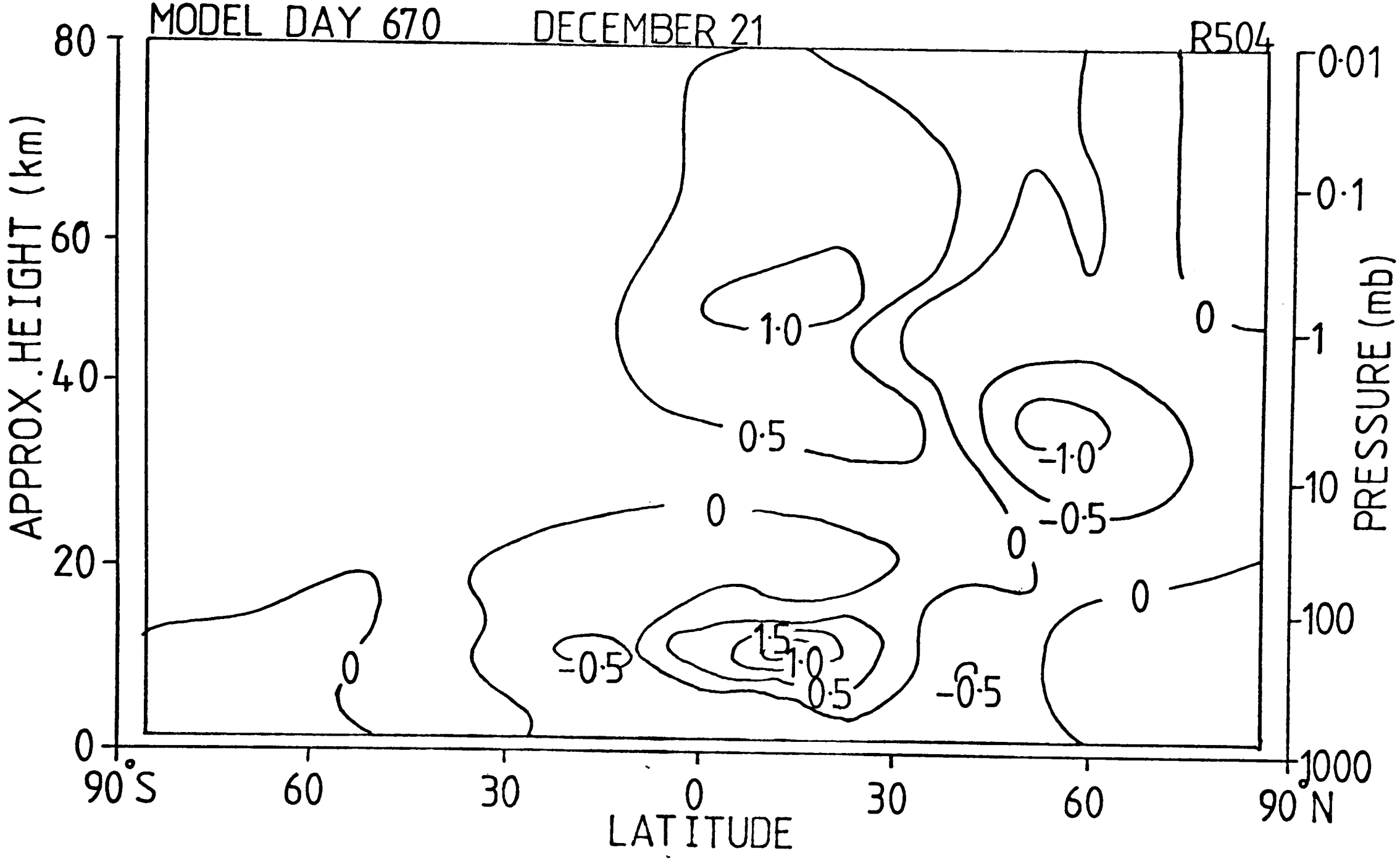

Fig. 6.3 Meridional wind (m/s) Run A

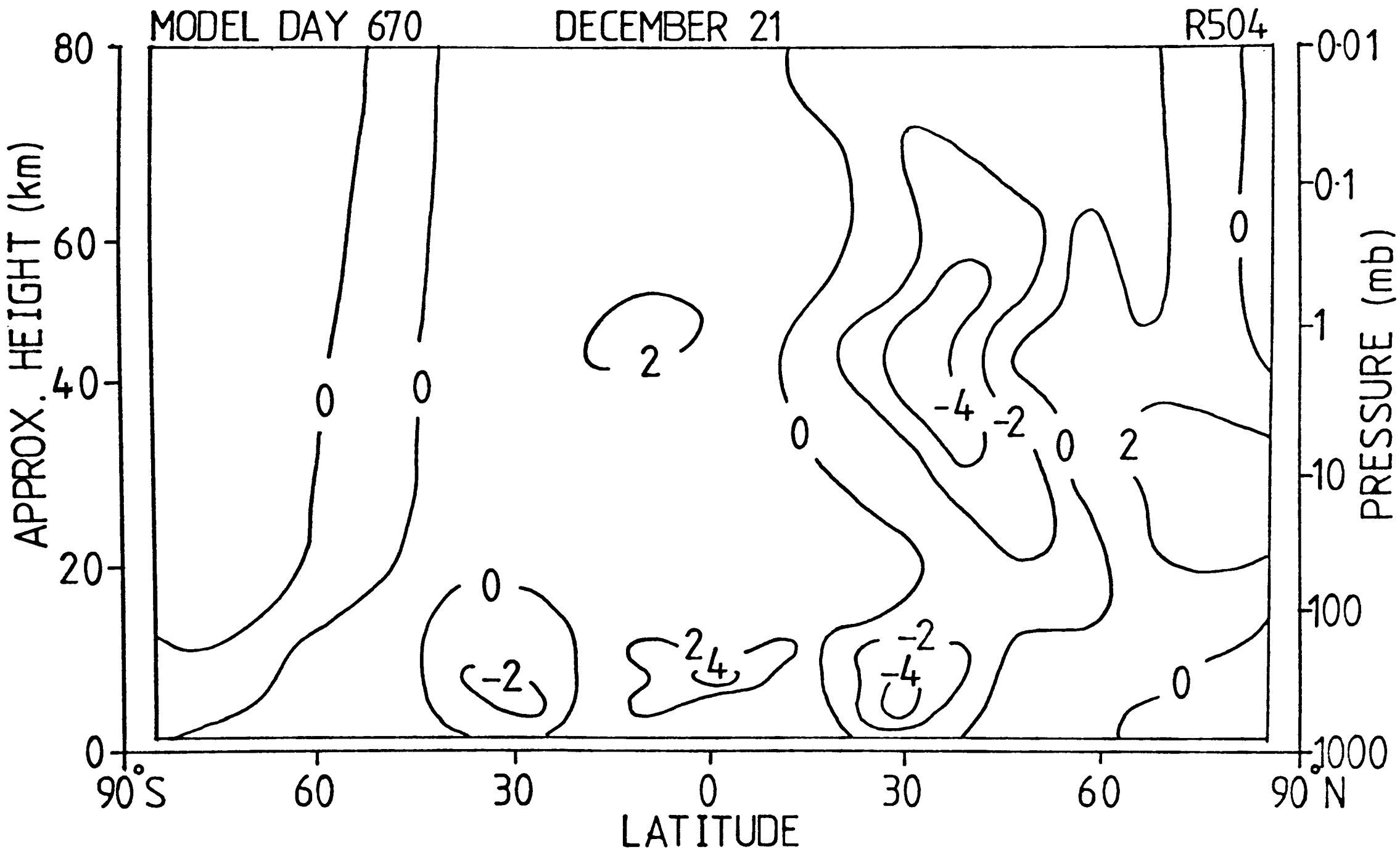

Fig. 6.4 Vertical wind (mm/s) Run A

near the winter pole are observed in the atmosphere; their presence in the model is again due to the divergence of the horizontal eddy momentum fluxes.

The model fields of meridional and vertical velocities are given in Figs. 6.3 and 6.4. The meridional circulation in the troposphere is well reproduced with a Hadley cell, Ferrel Cell and high latitude direct cell in each hemisphere. In the stratosphere there is rising motion to the summer side of the equator and sinking in winter mid-latitudes, there is also rising motion at the winter pole thus creating a two cell system. Above 25 km there is a net flow from the summer to the winter hemisphere. These features correspond well with the winter stratosphere observations of Vincent (1968) (see Fig. 1.3 and Harwood and Pyle, 1980). The reverse cell in winter high latitudes is a wave-induced cell; it has been forced in order to identically cancel the eddy fluxes of the waves themselves and thus has no effect on mass transport. Harwood and Pyle (1977) showed a near cancellation between the fluxes of ozone due to mean motions and eddies in winter high latitudes and Dunkerton (1978) has identified the motion of tracers with the Lagrangian mean meridional circulation. This circulation differs from the Eulerian mean circulation (described above) in that it has no reverse cell near the winter pole - it consists of rising motion at the summer pole, strong horizontal motion from summer to winter hemispheres in the upper stratosphere and mesosphere and sinking in winter high latitudes. It is determined by diabatic heating alone.

Fig. 6.5a shows the model field for ozone concentration on March 21st. This may be compared with the observations of Dütsch (1971) (see Fig. 1.4). The model clearly demonstrates the transition from the region above about 30 mb where the ozone distribution is determined by photochemical processes with maximum values in equatorial latitudes to the region below where

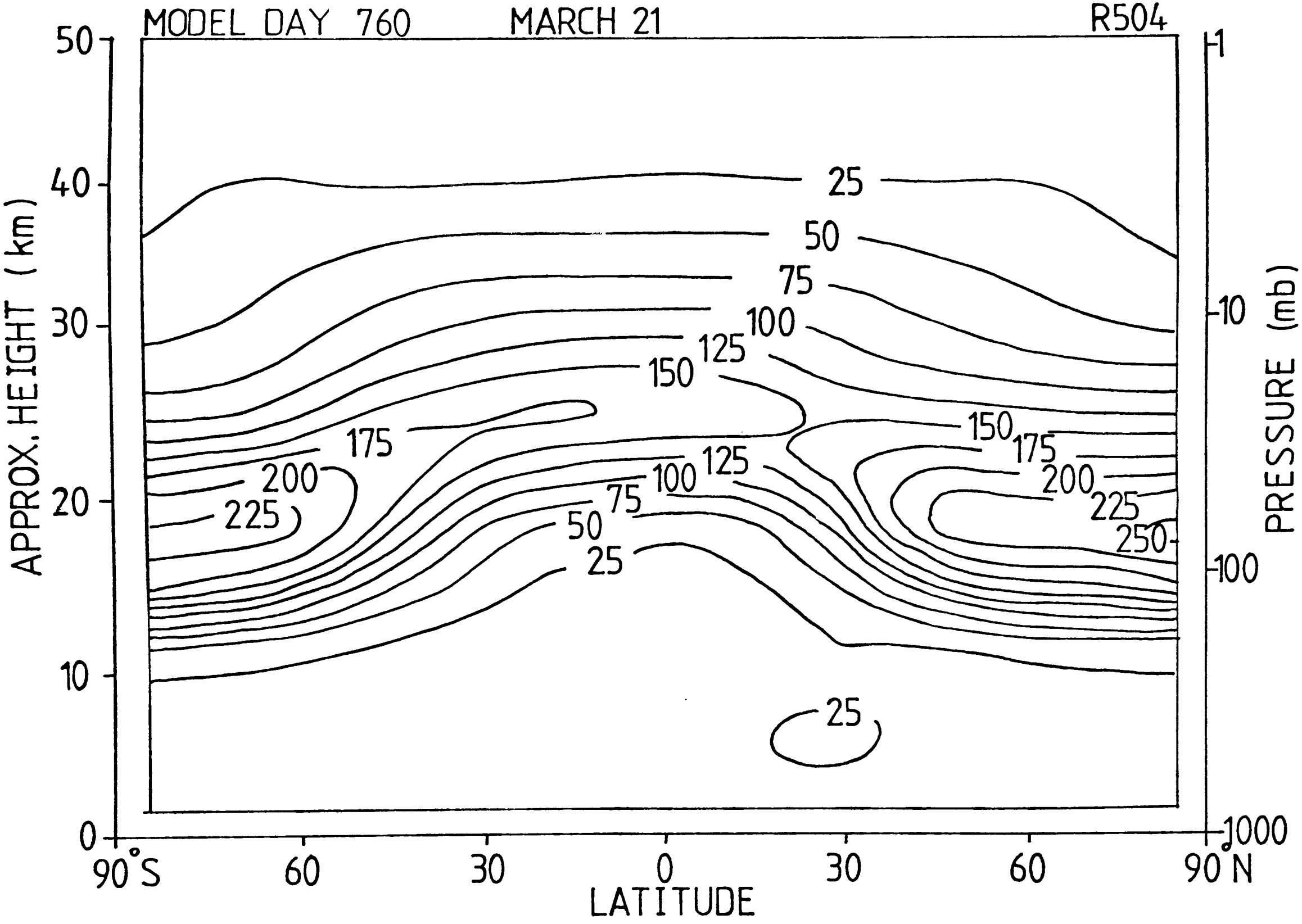

Fig.6.5(a) Ozone partial pressure (nb) Run A

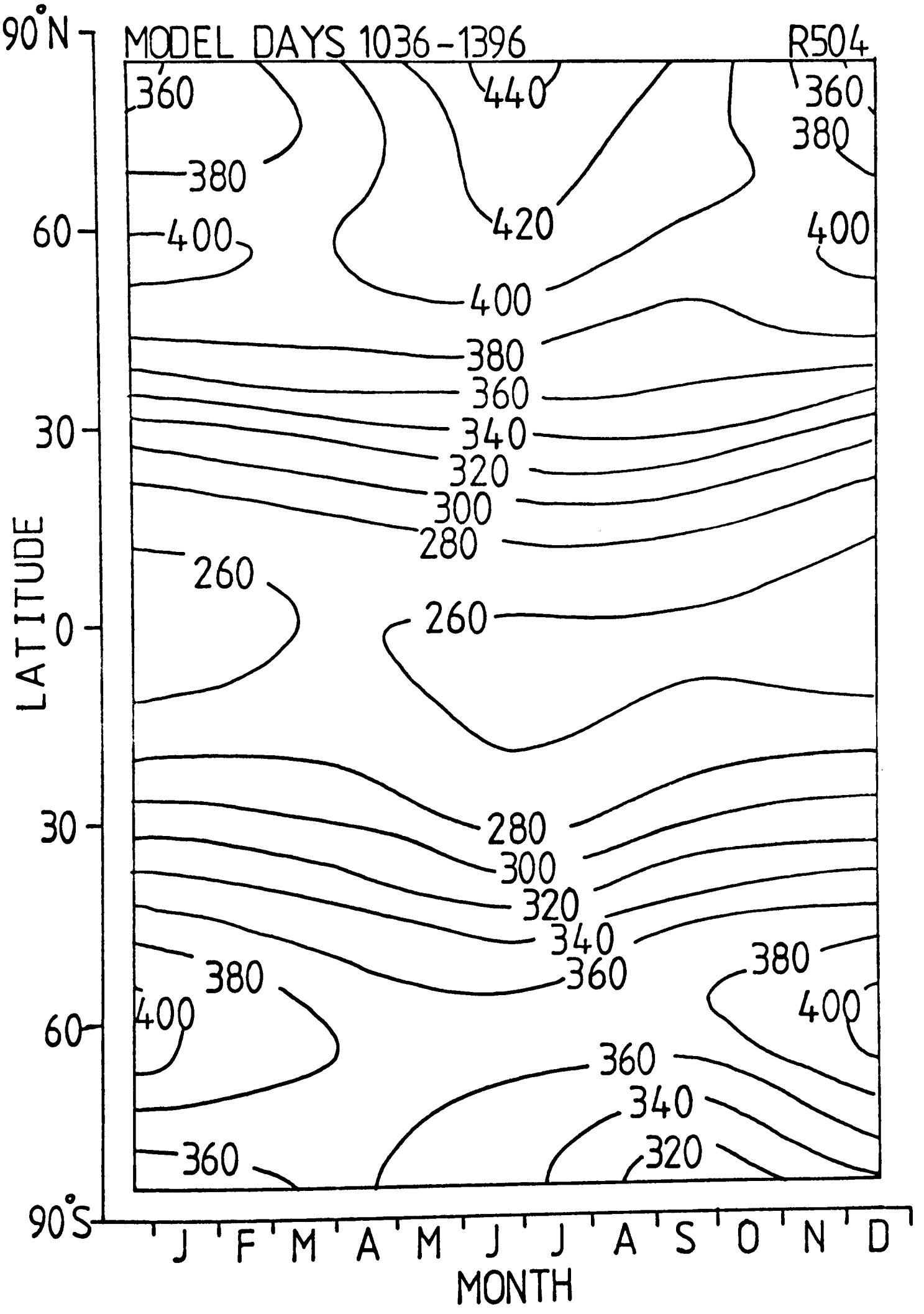

Fig.6.5(b) Ozone column density (Dobson units) Run A

dynamical effects are more important, leading to maximum values in high latitudes. The peak values at the spring pole agree well with Dütsch's measurements in magnitude and altitude however the values at the autumn pole appear to be rather too large. Investigation of the changes in ozone concentration throughout the year (see Fig. 6.5b) shows that the model reproduces well the total ozone amounts including the hemispheric asymmetries. However, the model lags behind the observed changes by about two months, predicting maximum values in the northern hemisphere in June when in fact they occur in April. This is due to the use of the time-constant approach in the linearised photochemical scheme which overestimates the relaxation time for regions in which the ozone concentration is larger than its equilibruim value. This also explains why the modelled ozone cross-section is more latitudinally symmetric than Dütsch's observations.

6.1.2 The heat budget

In this chapter the effect on the model of using different radiation schemes will be studied. These schemes give a value for the diabatic heating function, q, which is then used in the thermodynamic equation (Eq. 2.9) to find the local rate of change of temperature. It is interesting to look at the magnitudes of the different contributing factors to dT/dt in Run A. Fig. 6.6 shows the heating rate due to the absorption of solar radiation by ozone, Fig. 6.7 the cooling due to infra-red radiation by CO_2 and O_3 and Fig. 6.8 the sum of these plus latent heat release (i.e. the net diabatic heating). The rates of change of temperature due to mean motions and horizontal eddy heat fluxes are presented in Figs. 6.9 and 6.10. (N.B. The horizontal convergence of eddy heat fluxes far outweighs the vertical convergence below 50 km).

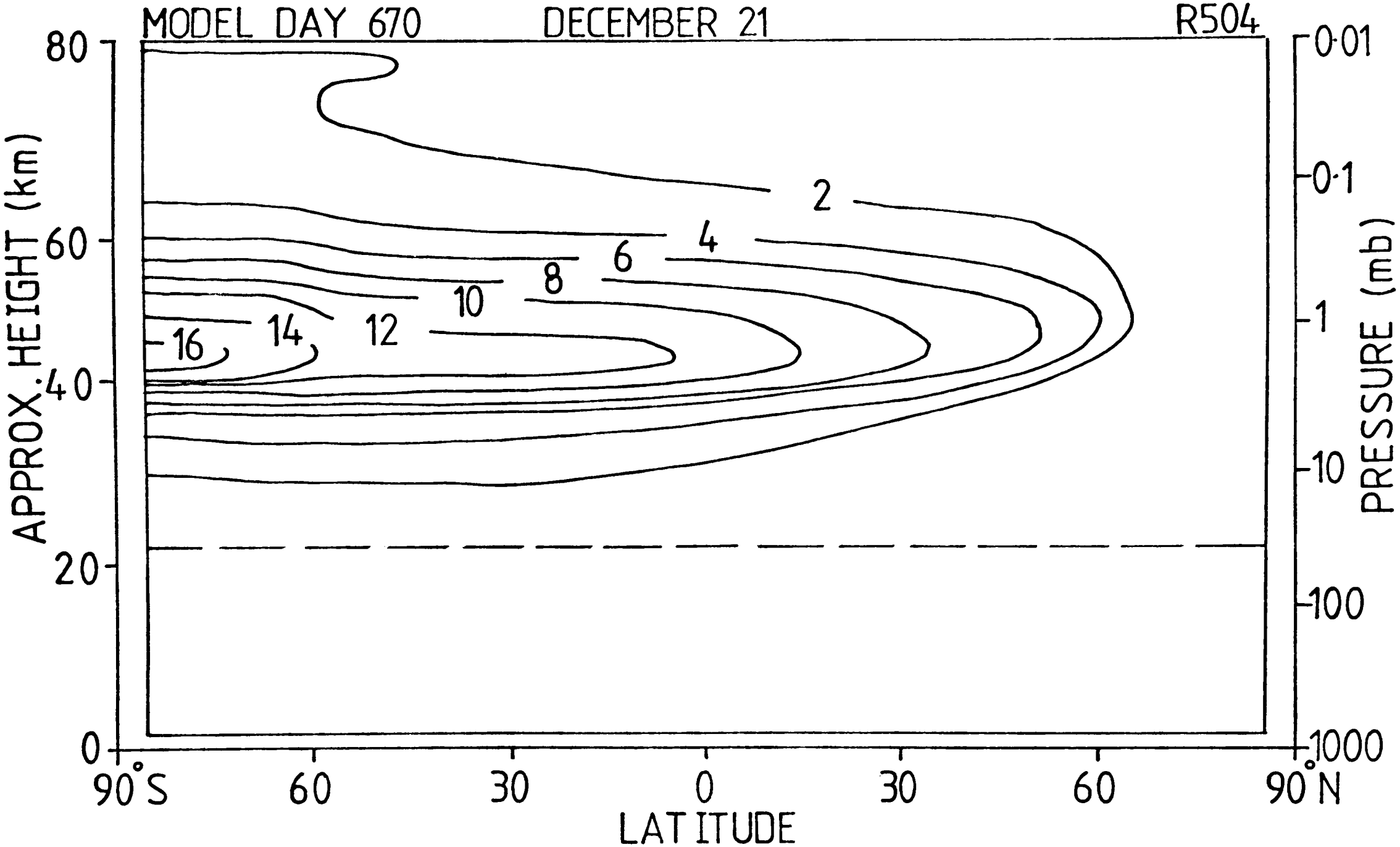

Fig. 6.6 Solar heating rate (K/day) Run A

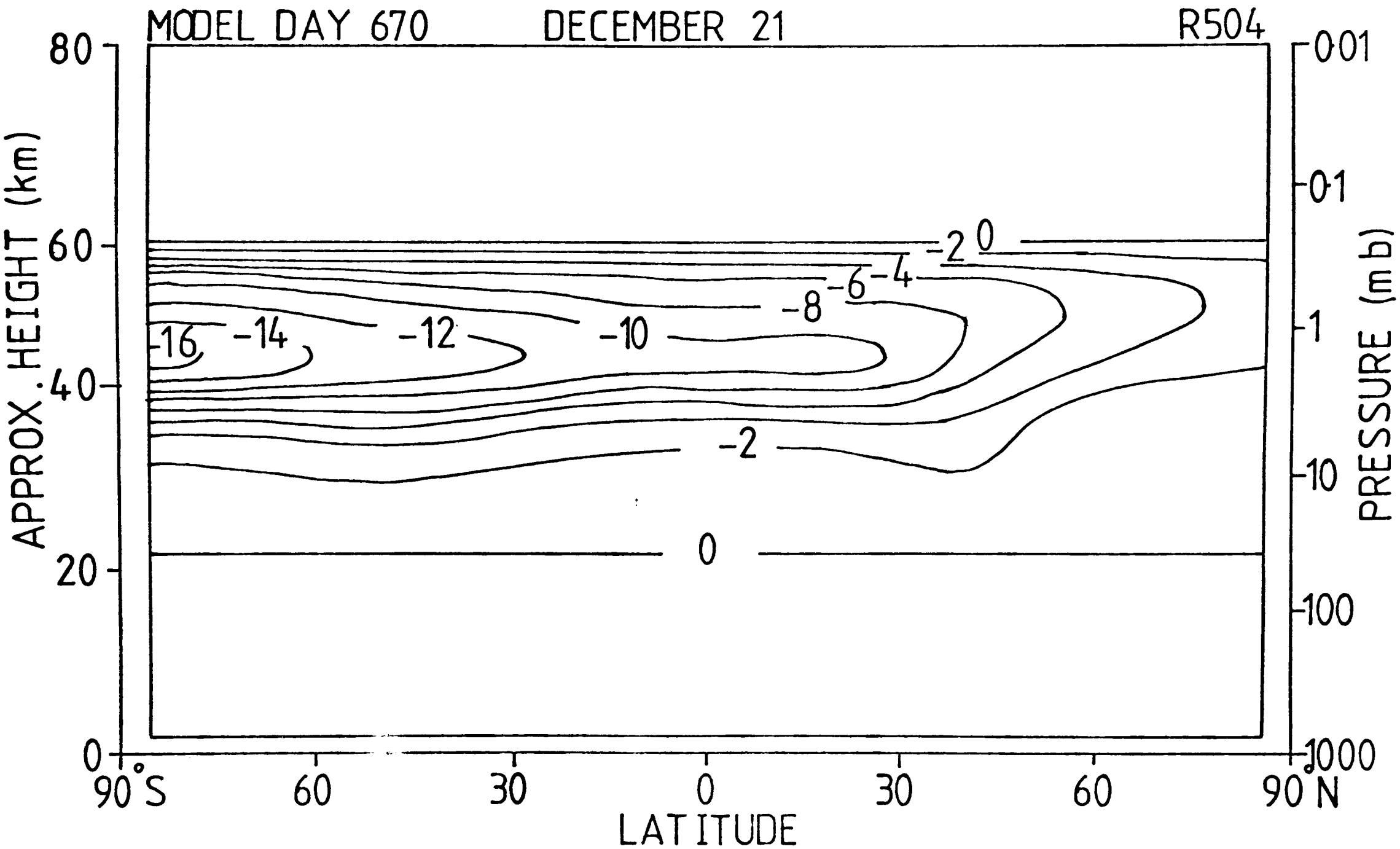

Fig. 6.7 Heating rate - thermal radiation (K/day) Run A

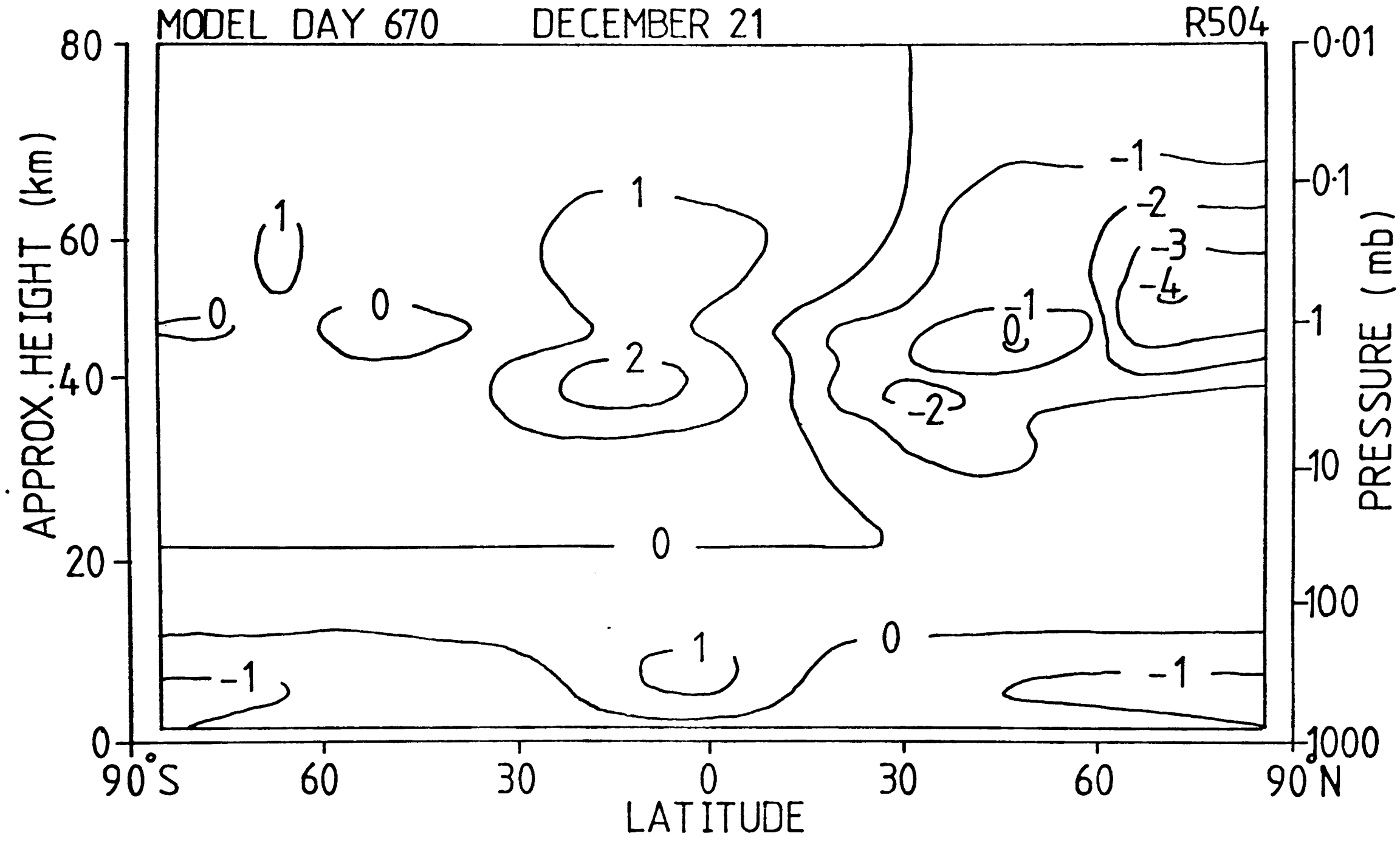

Fig. 6.8 Net diabatic heating rate (K/day) Run A

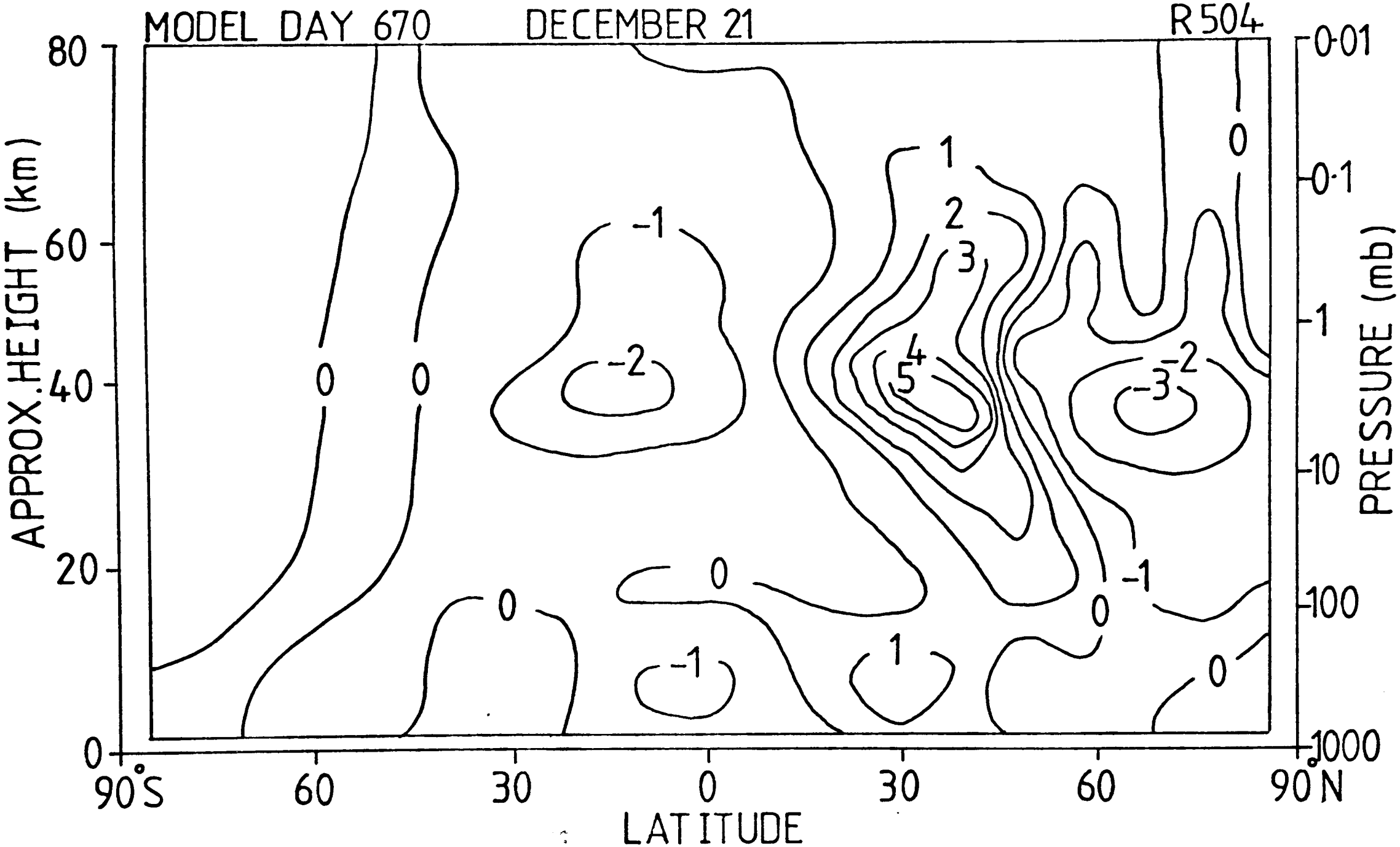

Fig. 6.9 $\partial \bar{T}/\partial t$ due to mean circulation (K/day) Run A

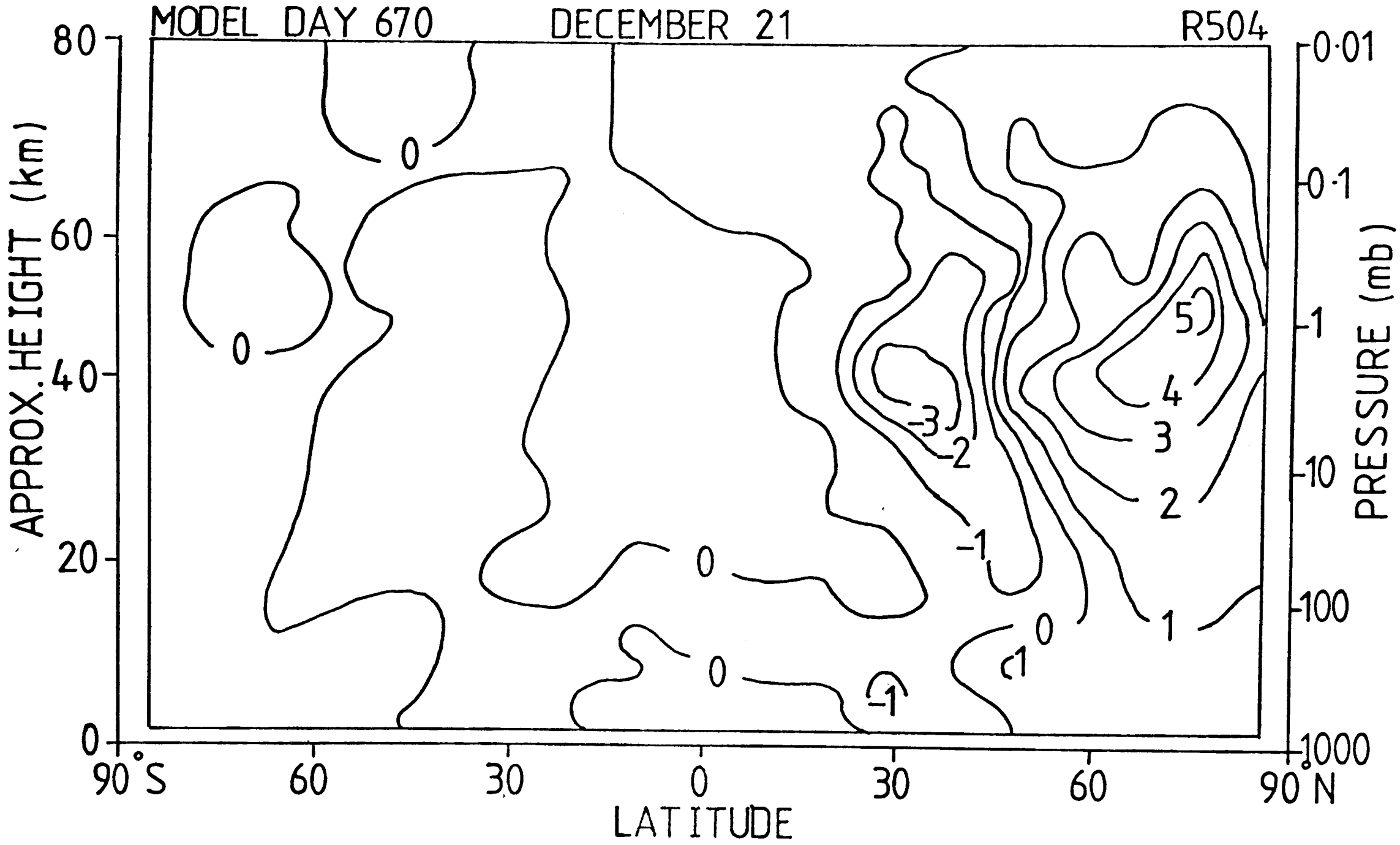

Fig. 6.10 $\partial \bar{T}/\partial t$ due to horiz. eddy heat fluxes Run A

The radiative heating and cooling have their largest individual terms in the summer hemisphere, however these effectively cancel leaving the summer high latitude stratosphere and mesosphere in approximate radiative equilibrium. Harwood and Pyle (1980) argue that the model is correct in predicting near radiative equilibrium at the summer stratopause as there is insufficient eddy activity to remove excess heat and continuity arguments preclude the possibility of large amounts of excess heat being advected upwards. This is in conflict with the radiation calculations of Murgatroyd (1969) which show a net heating of 5 K day^{-1} at 50 km at the summer pole. However, the solar heating in these calculations varies almost linearly with ozone concentration and while Murgatroyd used a fixed O_3 distribution the model's ozone field is dependent on local temperature and wind fields which in turn depend on the solar absorption. Thus the model is internally consistent and it is probable that this feedback produces lower ozone concentrations that those used by Murgatroyd.

Harwood and Pyle (1980) have pointed out that the small net heating at the summer stratopause, and the concomitant small vertical velocities, preclude the possibility that the low temperature of the summer mesopause is caused by the adiabatic cooling of ascending air. However Crane et al (1980) have shown that at 80 km the temperature, zonal and meridional wind structure are largely determined by a Rayleigh friction parameter and that radiative effects are of secondary importance at this altitude. This will be discussed more fully in chapter 8.

In equatorial regions in the upper stratosphere the net diabatic heating is of the order of 2 K day^{-1}; this heating causes the upward motion shown in Fig. 6.4. As there is virtually no eddy heat transfer

in this part of the atmosphere the diabatic heating is almost exactly balanced by the cooling due to the upward motion which is shown in Fig. 6.9. In the winter hemisphere the eddy heat transfer is more significant, as indicated in Fig. 6.10. Comparison of this diagram with Figs. 6.8 and 6.9 reveals that the transport of heat by the eddies from middle to high latitudes and the radiative cooling are balanced by the heat transport from pole to mid-latitudes by the mean motions. Thus, as expected from the Ψ equation (Eq. 2.16) the meridional circulation adjusts to maintain thermal wind balance between the zonal wind and the meridional temperature gradient against the perturbing effects of the heating and eddy fluxes. The resulting value of $d\overline{T}/dt$ is very small everywhere giving the observed slow change with time of $\overline{T}$.

6.2 The effect of replacing the thermal radiation scheme

In Run B the thermal radiation scheme for the CO_2 15μm band was replaced by the Curtis matrix method described in chapter 3. Because the solar heating scheme could only be used accurately below 80km the net heating above this altitude was specified by a linear decrease from its 80km value to zero at the upper boundary. The model specifications were otherwise as in Run A.

The temperature and wind fields produced by Run B for December 21st are shown in Figs. 6.11 to 6.14. Comparison of the temperature structure of Run B (Fig. 6.11) with Run A (Fig. 6.1) shows that in the troposphere and lower stratosphere the new scheme has had little effect although the cold cell at about 25km in summer high latitudes has intensified slightly. The structure of the stratopause region has been improved, having a more realistic curvature, and the temperature at the summer polar stratopause has decreased to 299K. Both these modifications make for quite a good

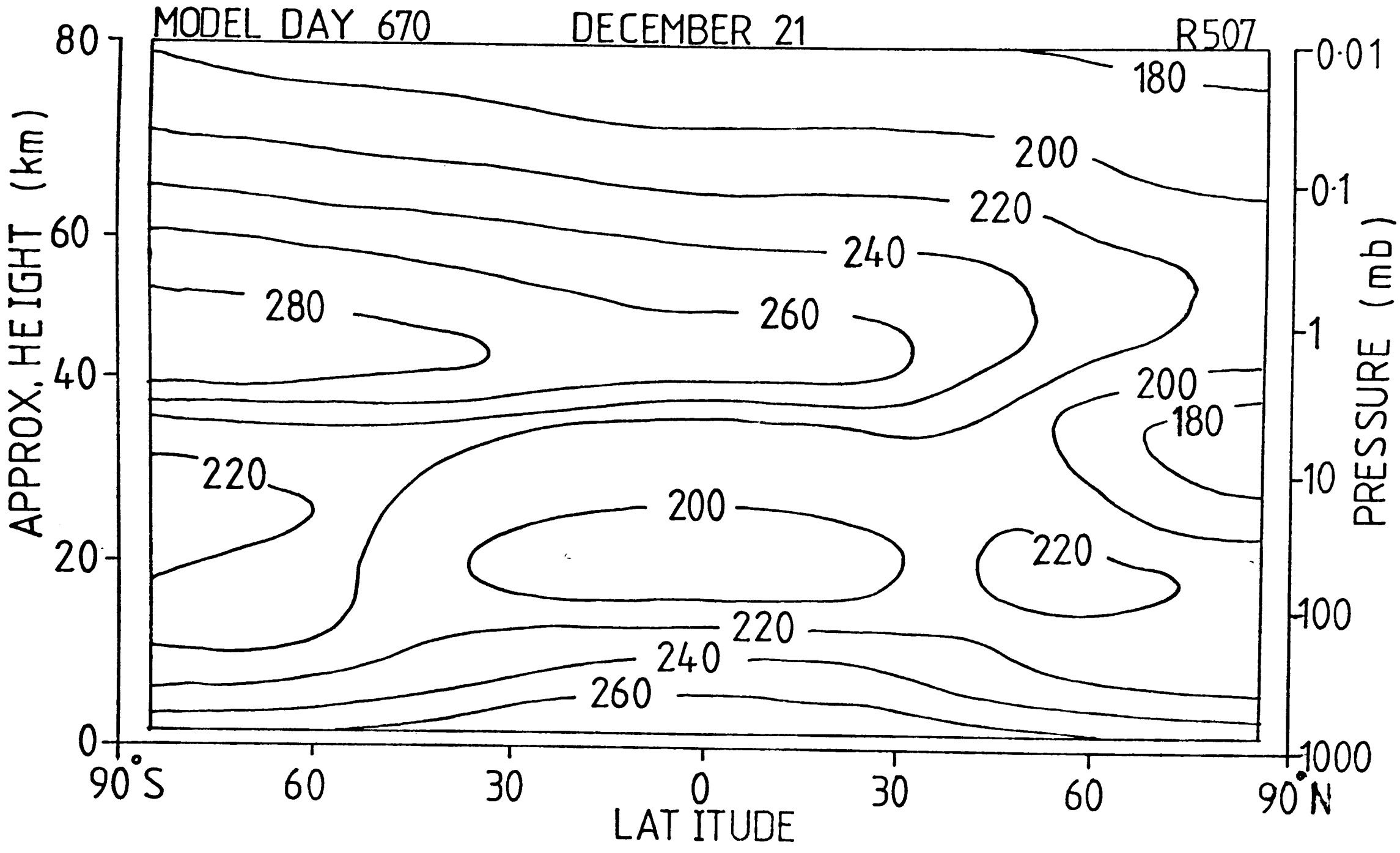

Fig. 6.11 Temperature (K) Run B

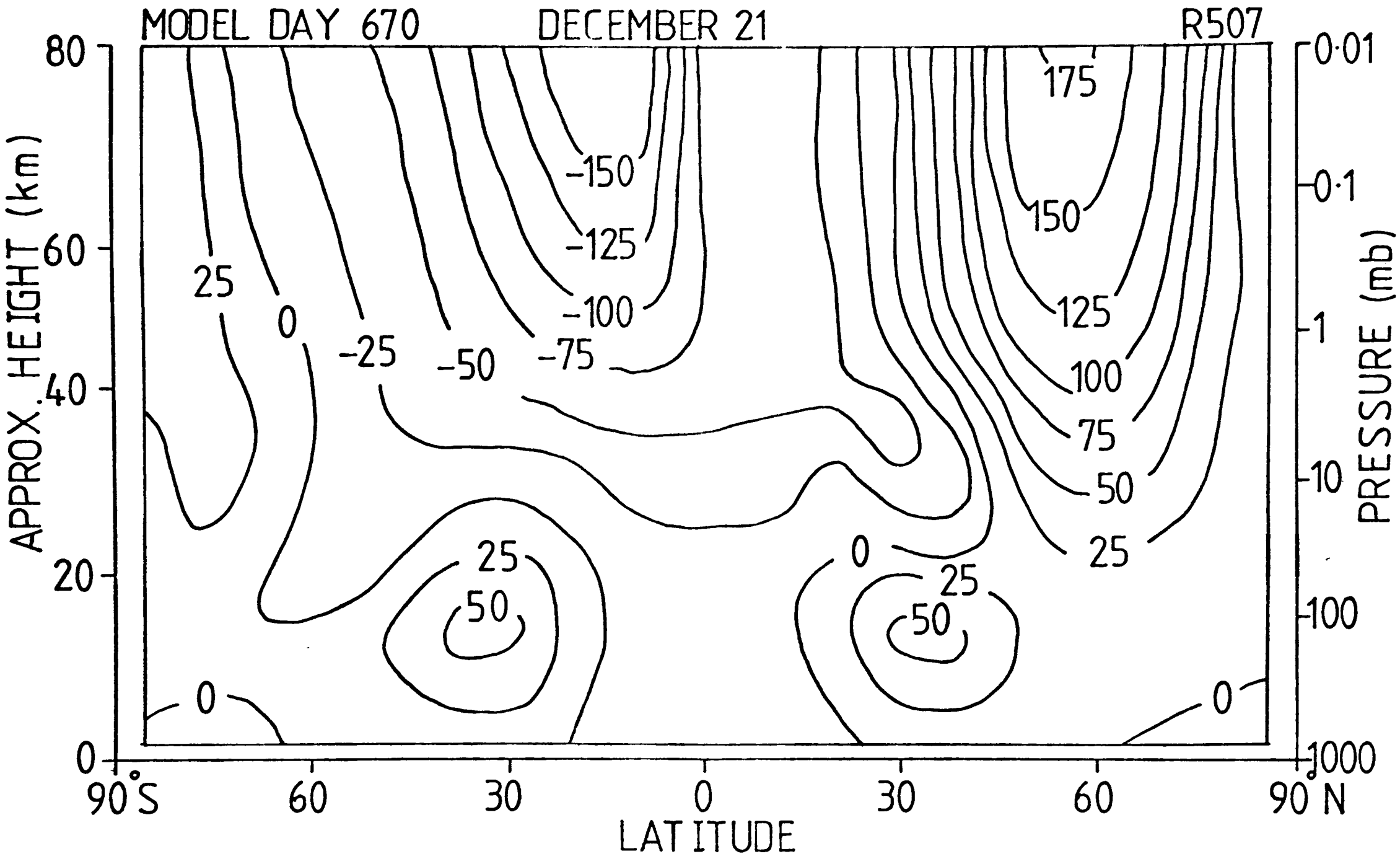

Fig. 6.12 Zonal wind (m/s) Run B

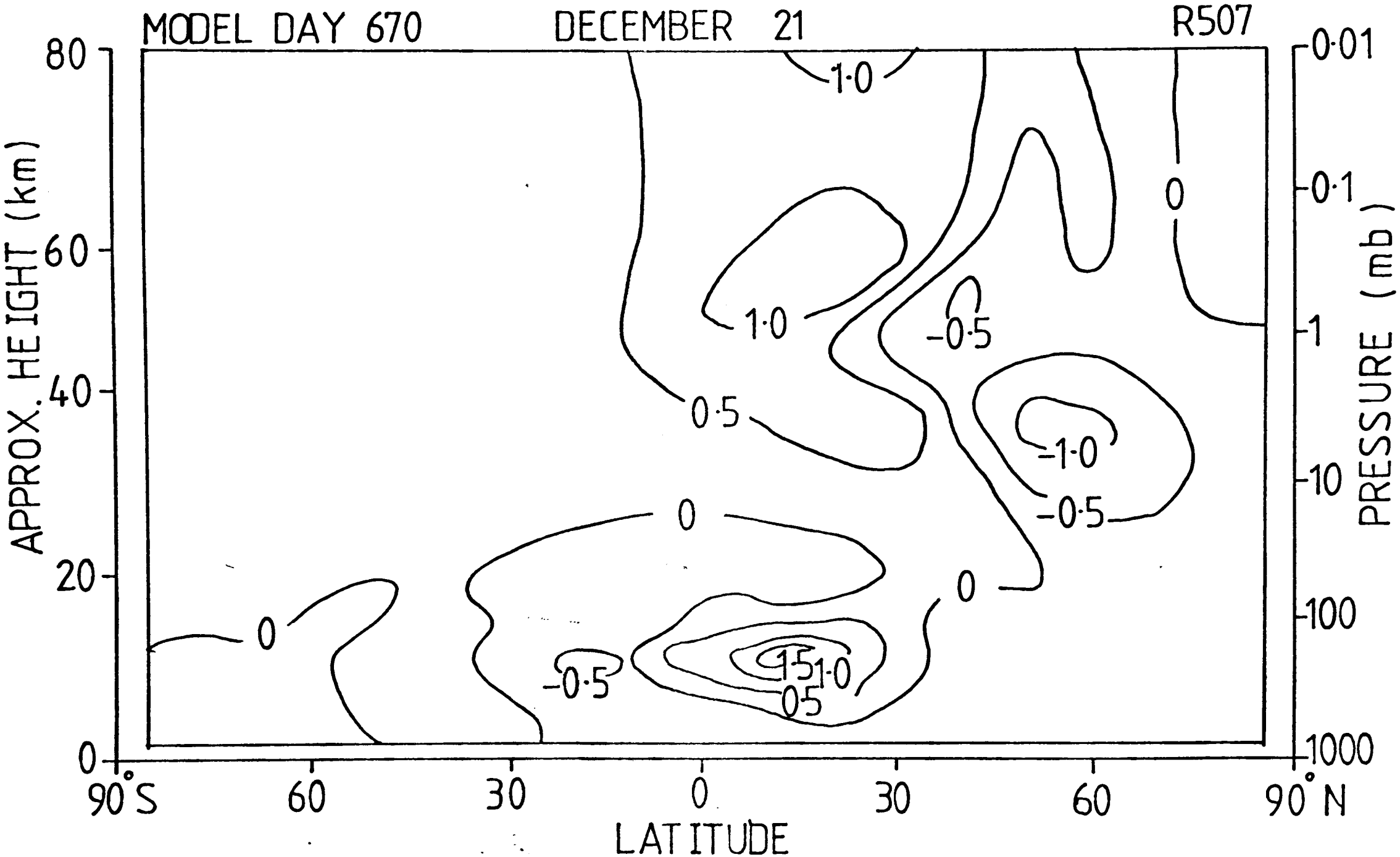

Fig. 6.13 Meridional wind (m/s) Run B

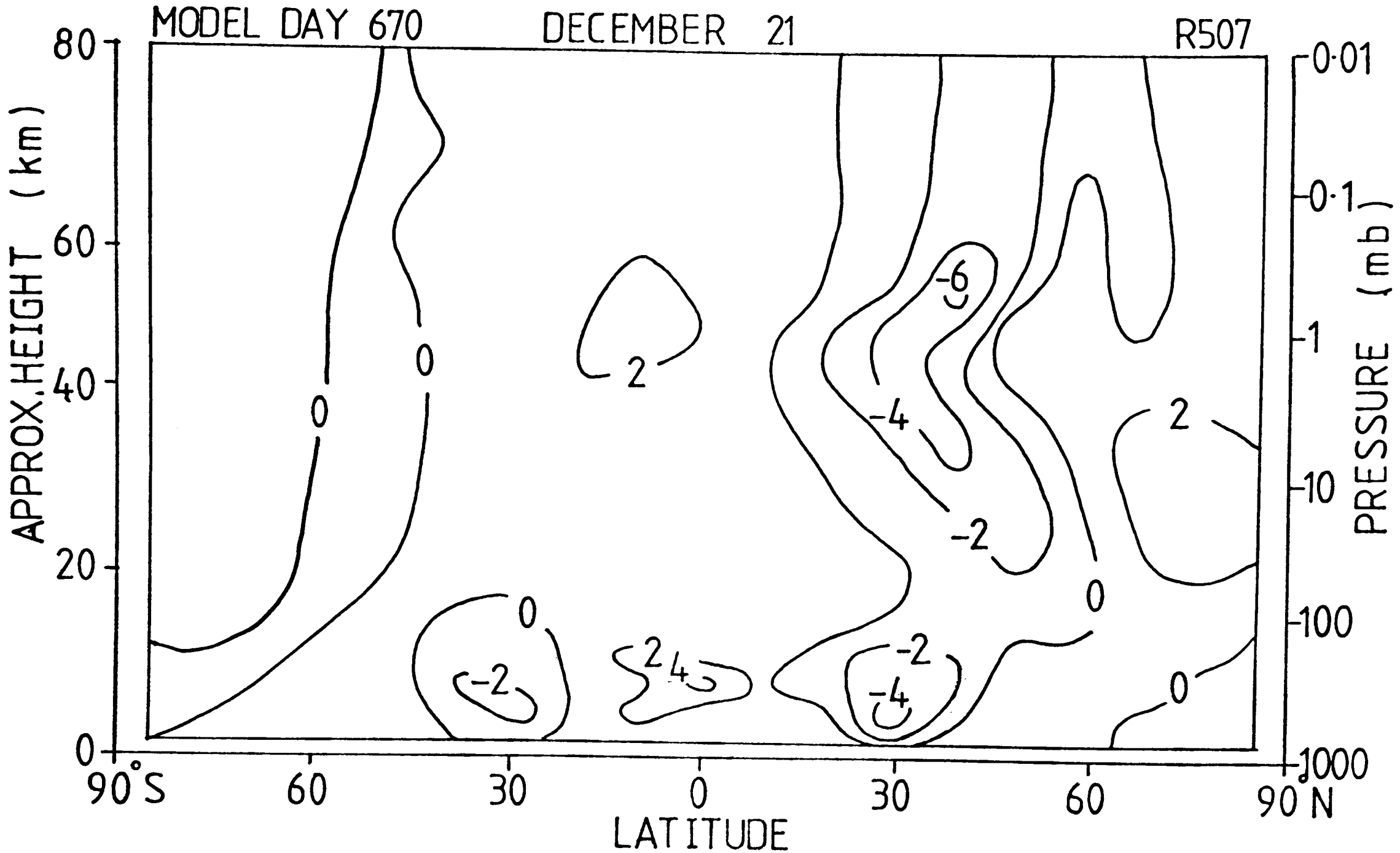

Fig. 6.14 Vertical wind (mm/s) Run B

representation of the temperature field. However, the altitude of the stratopause is still too low in the summer hemisphere and there has been a considerable reduction (from 248K to an unrealistic 219K) in the temperature of the winter polar stratopause. The lower mesosphere has been modelled more accurately but there is no reverse in the horizontal temperature gradient above 70km. This results in the zonal wind structure shown in Fig. 6.12 with no sign of either westerly or easterly jet closing; thus the representation of the upper mesosphere is quite poor. However, the change in temperature structure in the stratosphere has meant a slightly smaller increase of zonal wind with height here making the winds in the stratosphere quite realistic.

The meridional and vertical winds (Figs. 6.13 and 6.14) are virtually unchanged in Run B, the only difference being a stronger circulation in the upper mesosphere.

The components of the heat budget in Run B are shown in Figs. 6.15 to 6.19. Associated with the decrease in temperature in the summer hemisphere upper stratosphere and mesosphere there has been an increase in ozone concentration which has resulted in a slight increase in solar heating. Again this heating is almost exactly balanced by the long-wave cooling. In chapter 3 it was noted that although the thermal radiation schemes used in Runs A and B produced similar results below about 48km above this altitude the Curtis matrix scheme gives much larger cooling rates for the same temperature profile. Thus in Run B the balance between solar heating and long-wave cooling at the summer stratopause occurs at a lower temperature.

At the winter polar stratopause, which cannot be in radiative equilibrium, the cooling rate has increased by about 0.5 K day^{-1} resulting in the large temperature decrease mentioned above. The steeper horizontal

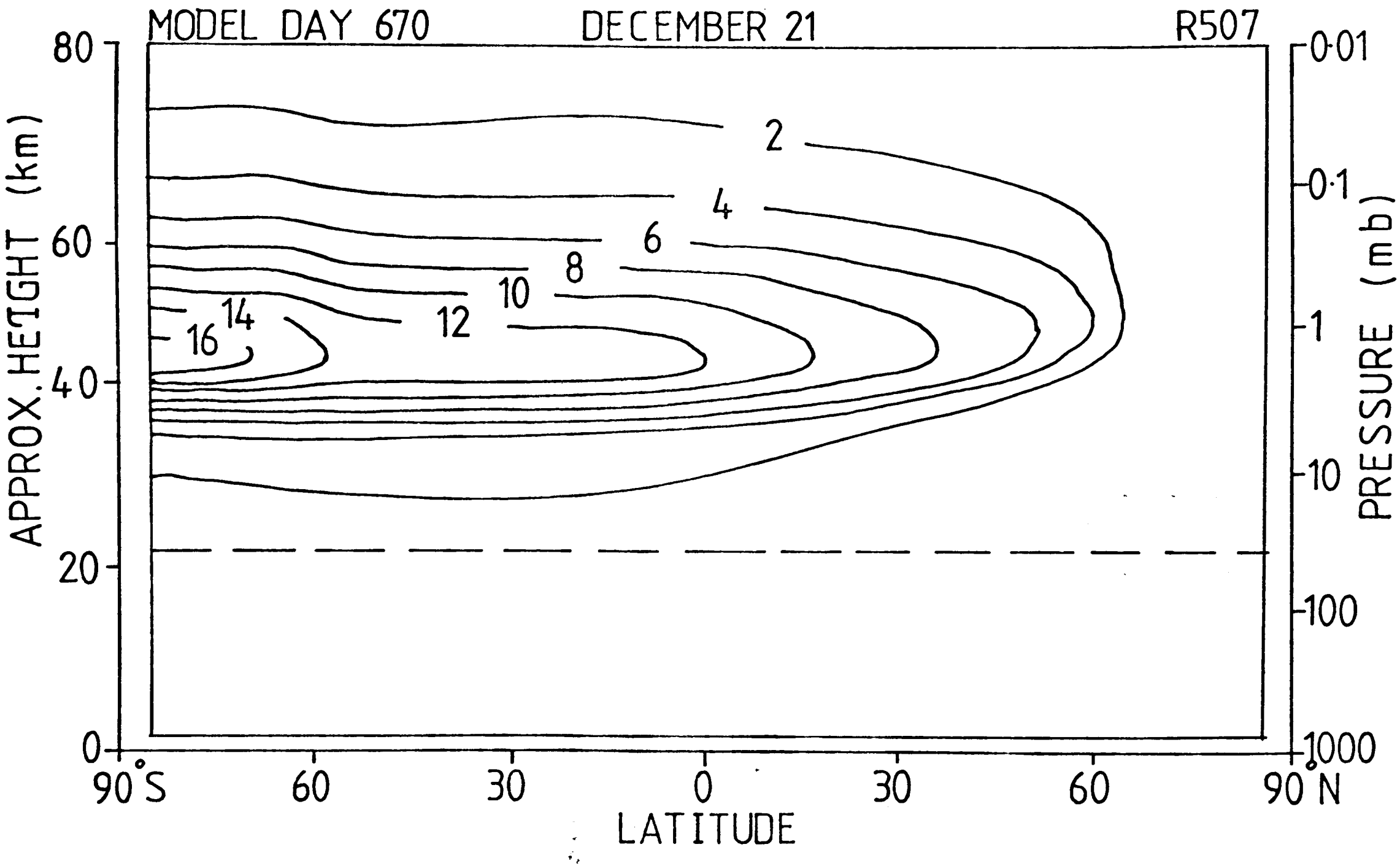

Fig. 6.15 Solar heating rate (K/day) Run B

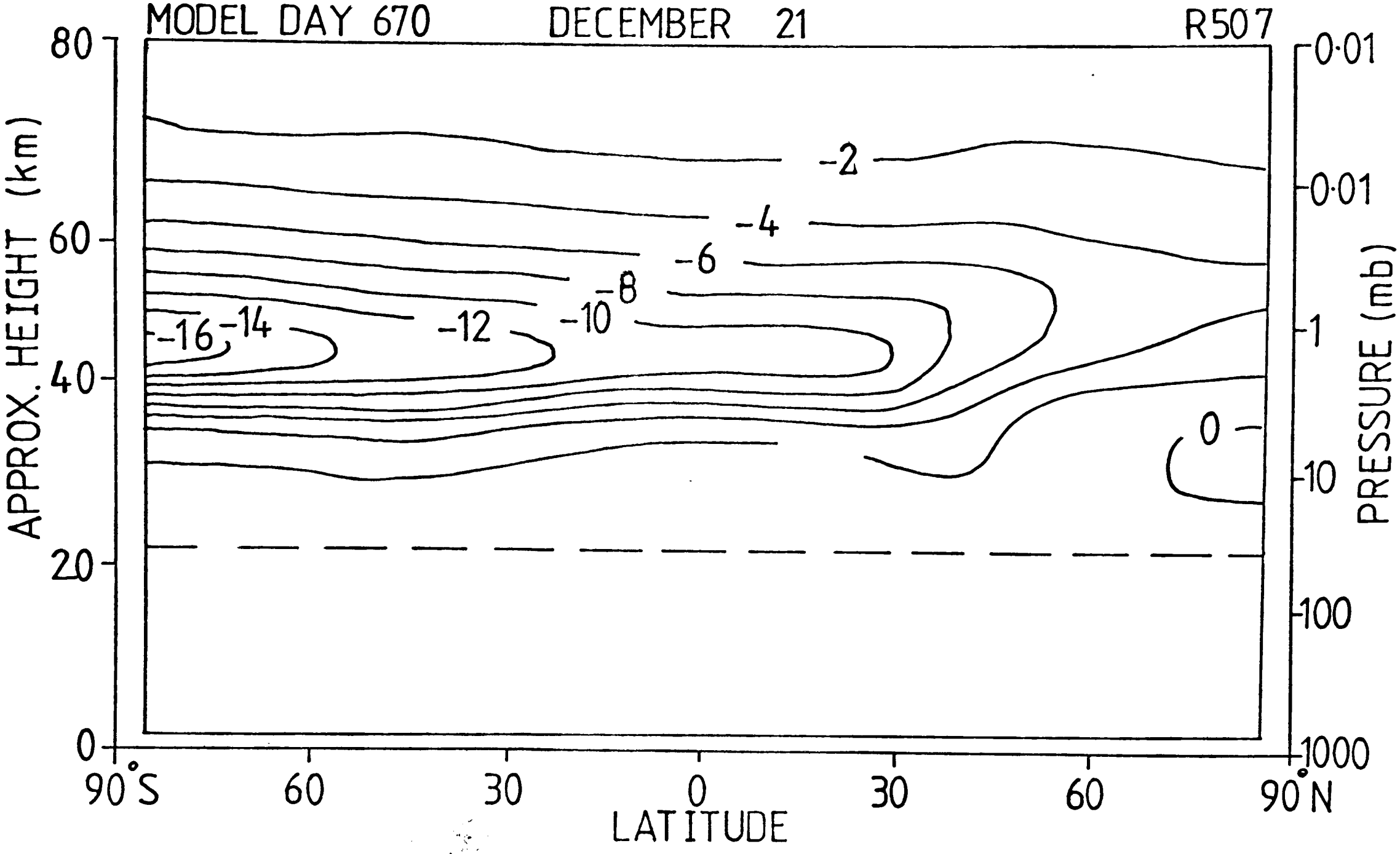

Fig. 6.16 Heating rate – thermal radiation (K/day) Run B

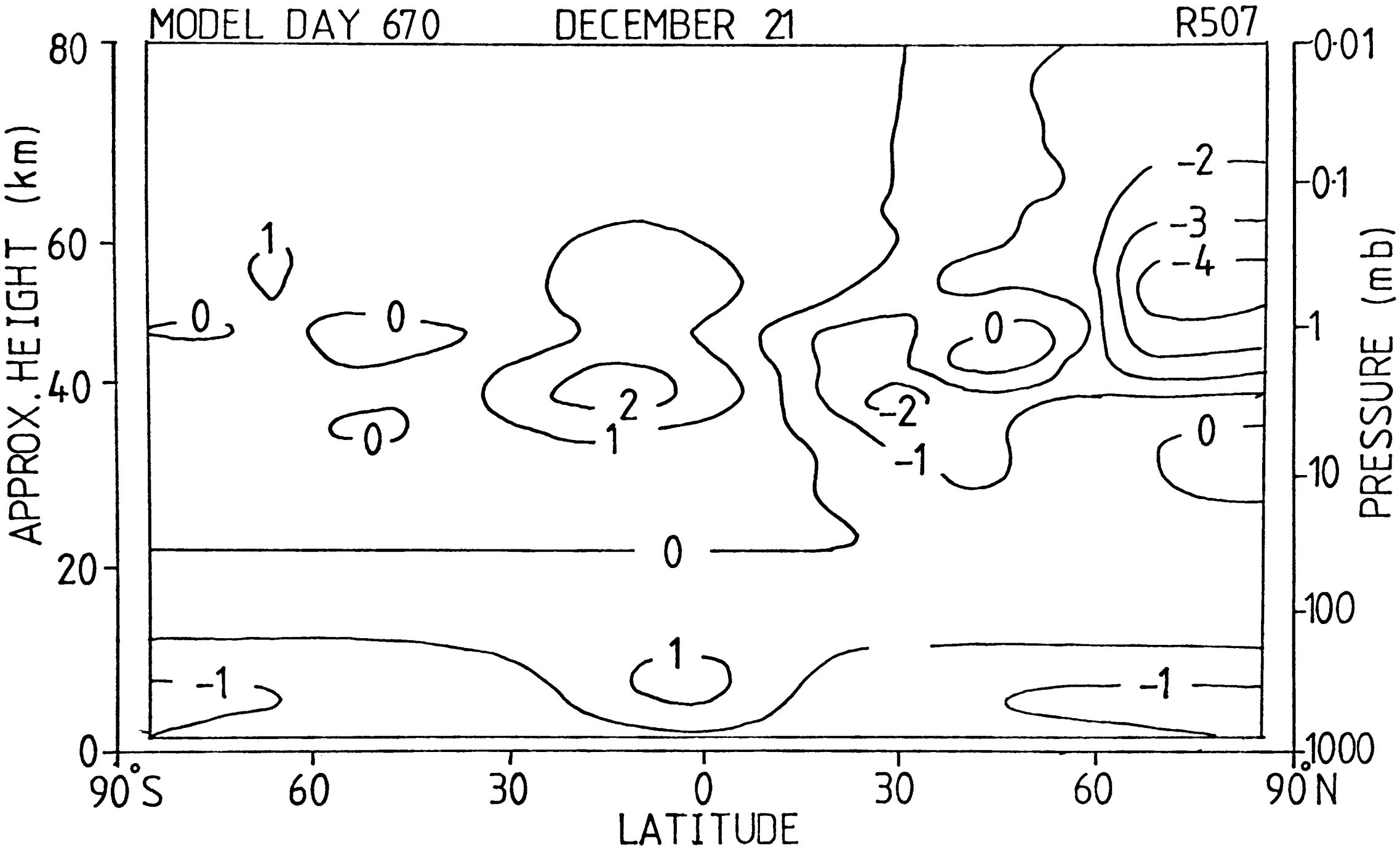

Fig. 6.17 Net diabatic heating rate (K/day) Run B

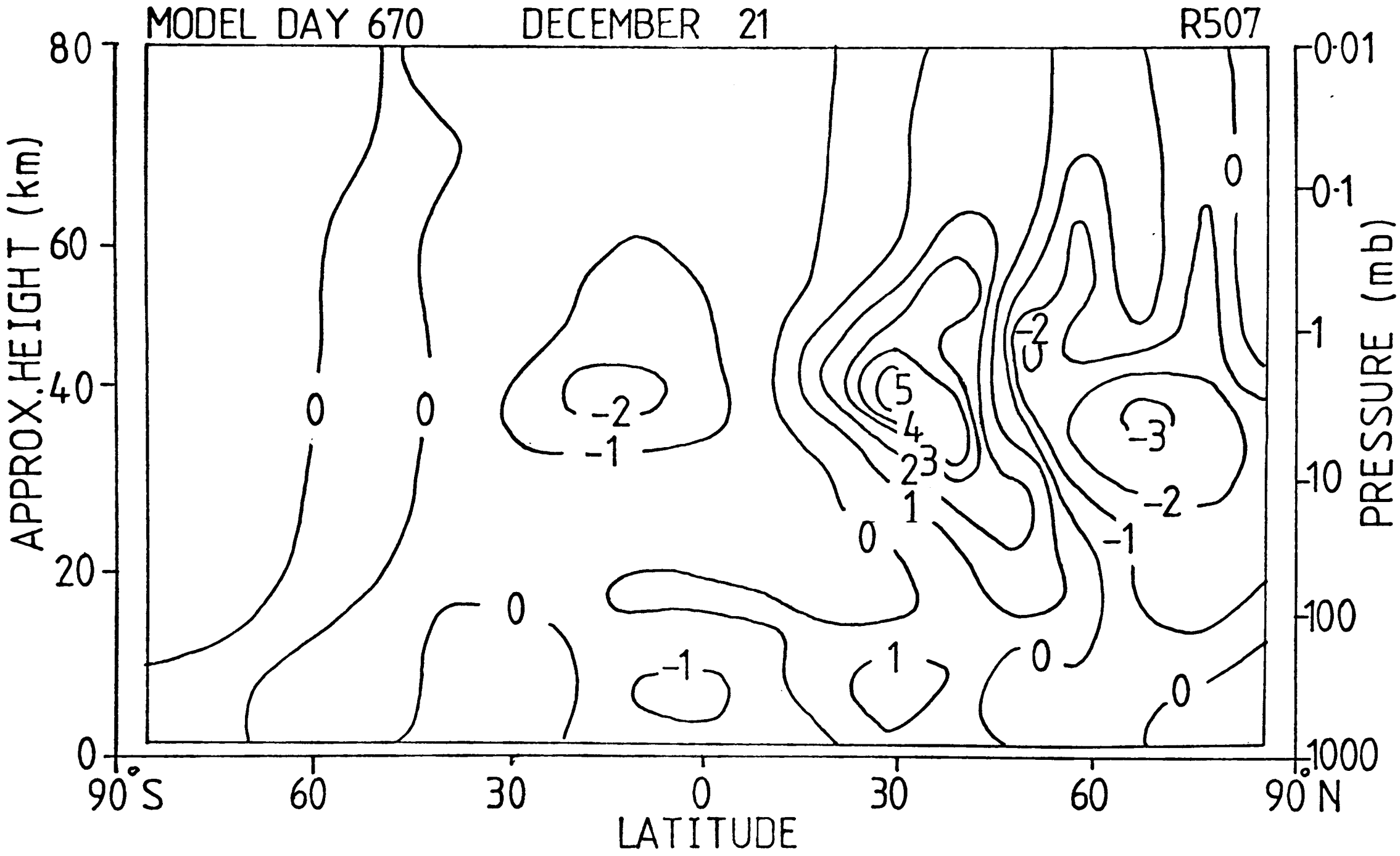

Fig. 6.18 $\partial\bar{T}/\partial t$ due to mean circulation (K/day) Run B

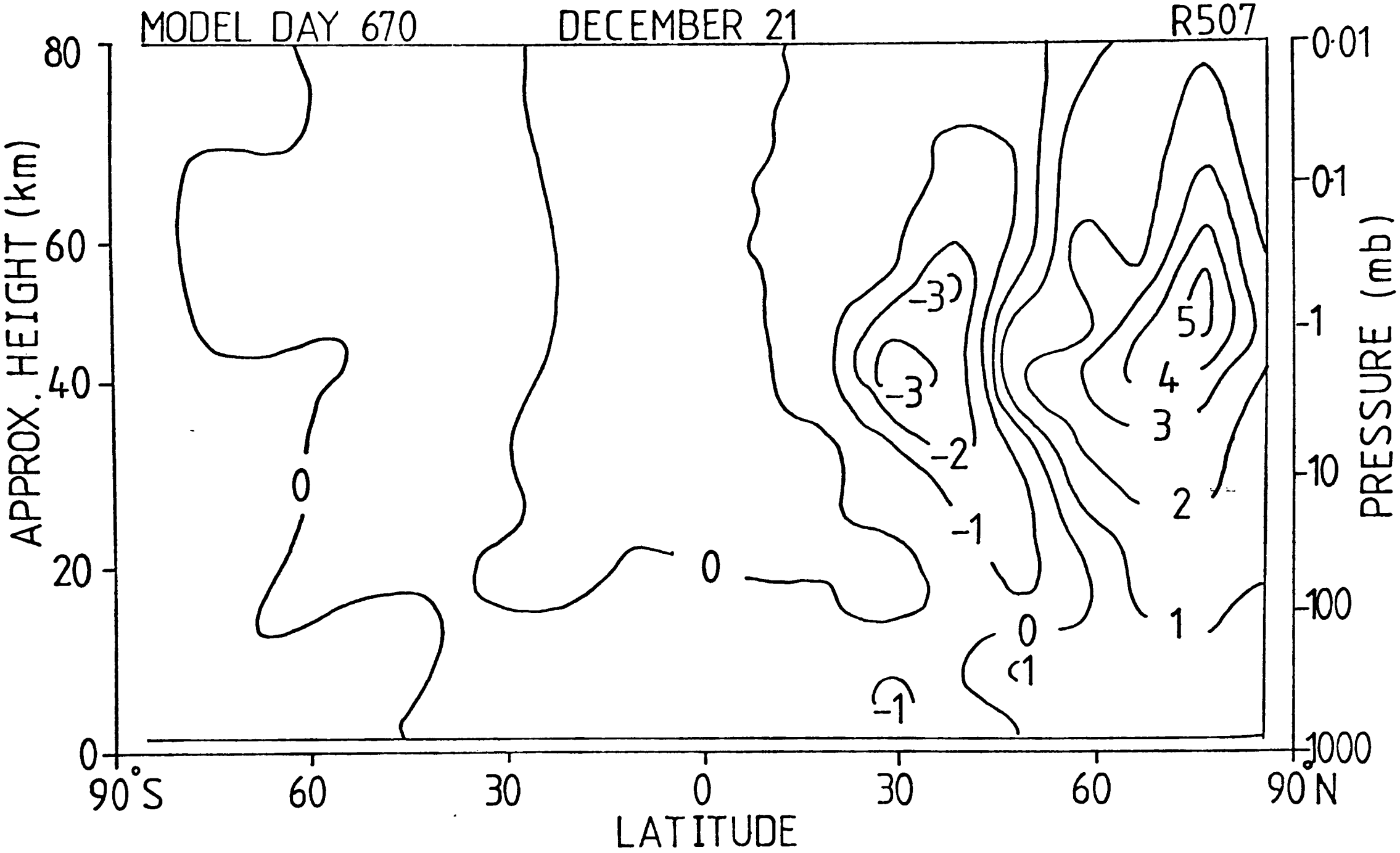

Fig. 6.19 $\partial\bar{T}/\partial t$ due to horiz. eddy heat fluxes (K/day) Run B

temperature gradient has slightly increased the eddy heat flux and the mean motion contribution to the heat budget.

It was noted above that there is an increase in ozone concentration associated with the decrease in temperature. The magnitude of the changes are shown in Fig. 6.20 which indicates large percentage increases at around 60km especially in winter where the temperature decreases are greatest. However, changes are small at altitudes of significant ozone mixing ratio and the increase in O_3 column density is less than 2% at all latitudes.

The Curtis matrix method calculates thermal cooling more accurately than the previous scheme in the upper stratosphere and mesosphere and, in general, has enabled the model to produce more realistic fields in these regions. The exceptions are the high latitudes in winter and the upper mesosphere however in these regions the lack of success must be attributed to deficiencies in the model other than the radiation schemes. Eddy fluxes are important in winter polar regions and at the mesopause the direction of the temperature gradient indicates that local radiative heating does not exert great influence.

6.3 The effect of replacing the solar heating scheme

In Run C the method of calculating heating rates due to the absorption of solar radiation was replaced by the 'almost exact' method detailed in chapter 5. The model was otherwise as in Run A so the thermal radiation scheme limited calculation of net heating to below 60km. Because of this, and to save computing time, the absorption of solar radiation by molecular exygen in its Schumann - Runge bands and at shorter wavelengths was omitted from the solar heating scheme. It was shown in chapter 5 that this should incur negligible errors below 60km. The net heating rate was reduced

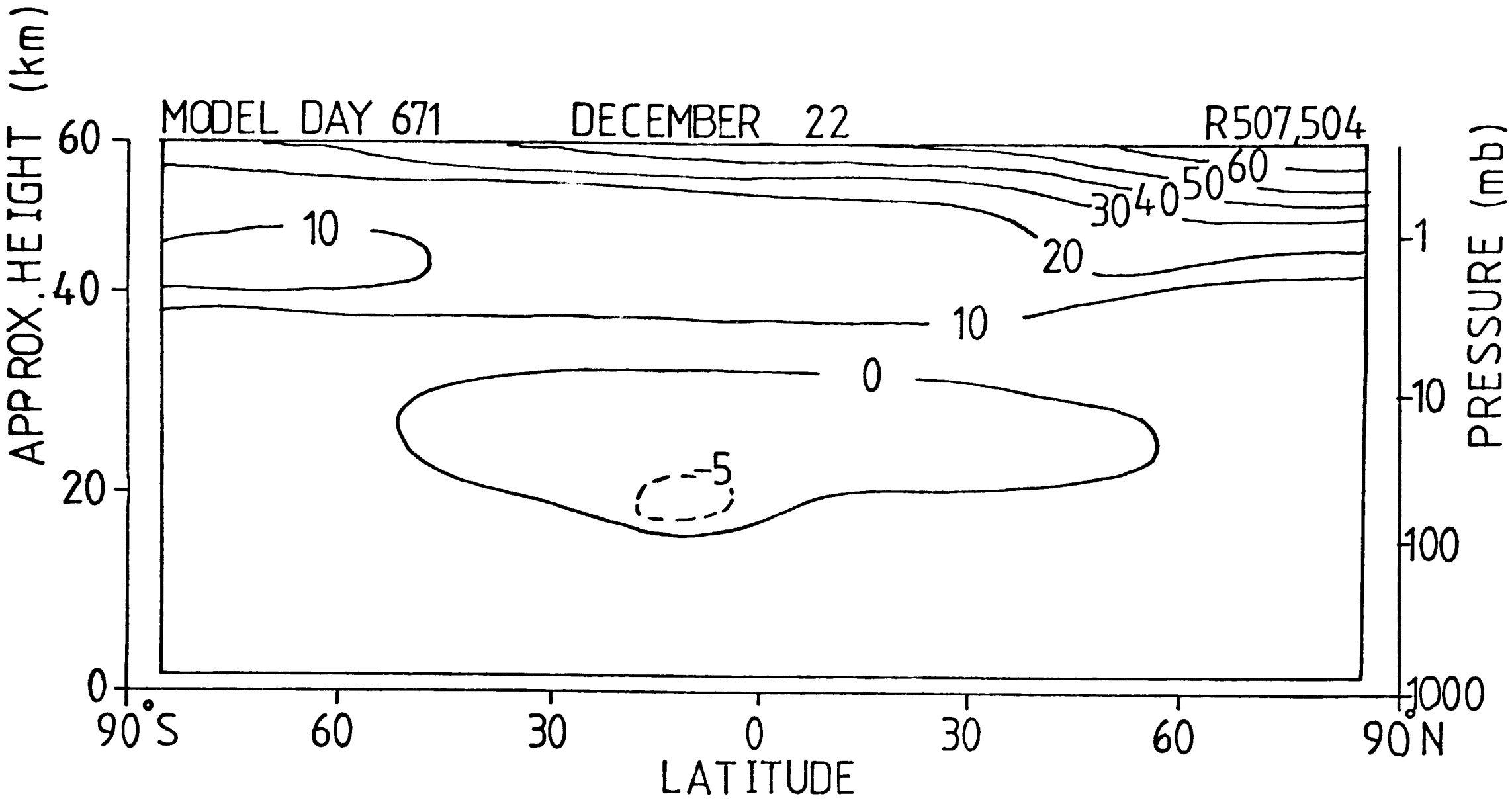

Fig. 6.20 Percentage increase in ozone Runs B,A

smoothly from its value at 60km to zero at 80km as in Run A.

The main effect of introducing the new solar heating scheme is to increase the temperatures throughout the stratosphere and mesosphere (no figure). In middle and high latitudes in the winter hemisphere the in - creases range from 1 to 7K with greatest changes at the stratopause. In low latitudes and in the summer hemisphere the increases are of the same magnitude at most altitudes but at around 33km the temperatures rise by about 10K thus weakening the cold cell described in section 6.1.1. The summer stratopause temperature is now calculated as nearly 320K. As the previous heating rate scheme was as accurate a parameterisation as re- quired in the model the increased temperatures must be due to the different solar flux and ozone cross-sections used as a basis for the calculations.

Apart from increases in magnitude the general structure of the temperature field in Run C is very similar to that of Run A. The height of the stratopause is too low in the summer hemisphere and has the same distorted shape as in Run A. The troposphere is unchanged. Associated with the changes in temperature the zonal wind field has intensified by about 8% in the upper stratosphere.

The ozone concentration is slightly lower in the upper stratosphere in Run C but there is almost no change in the lower stratosphere in spite of the increases in temperature there. This is due to the long time constant for the relaxation of the ozone concentration back to temperature - dependent equilibrium values specified by the photochemical scheme at this altitude.

In general the replacement of the solar heating scheme has had only a slight effect on the model fields and the parameterisation discussed in chapter 2 would be quite sufficient if calculations were limited to below the mesopause. However above this altitude absorption by molecular oxygen

needs to be considered. The other advantage of the new scheme is that is makes the model more internally consistent to use the same solar flux and absorption cross-sections in the heating scheme as in the more complete photochemical scheme used in some Runs.

6.4 Extension of the radiation calculations to 95km

6.4.1 Other components of the heat budget

The replacement of both thermal and solar radiation schemes enables the calculation of diabatic heating rates to be carried out up to the top of the model grid, i.e. about 95km. This is because of the inclusion of non - L.T.E. effects in the long-wave calculations and absorption by molecular oxygen in the short-wave calculations.

However in the upper mesospause and lower thermosphere there are other mechanisms which cause heating or cooling and which have not yet been mentioned in this work. These include the absorption of solar radiation by carbon dioxide in its 4.3μm band and 2.7μm combination band, the transfer of thermal radiation in these same bands, the emission of radiation by vibrationally excited OH and by oxygen in the transition $^3\Sigma_g^- - {}^1\Delta_g$ (two of the so-called airglow emissions) and other processes such as the release of chemical energy and the viscous dissipation of gravity waves.

Most of these effects only become significant well above the mesopause so an accurate parameterisation of each process, even if possible, is unnecessary for use in the model. However, in the context of the diabatic heating of the atmosphere, it is interesting to take a brief look at the relative importance of each mechanism in the region 80 - 100km.

6.4.2 Heating in the near-infrared bands of carbon dioxide

Although the solar flux is comparatively small at 2.7μm and 4.3μm a considerable amount of energy is absorbed at these wavelengths by the vibration-rotation bands of CO_2. Calculations of the heating rates due to absorption in these bands and the cooling rates due to transfer of thermal radiation by them have been made by M^{c}Clatchey (1966, 4.3μm fundamental band only), Houghton (1969) and Williams (1971). Williams' results for solar absorption under equinox and solstice conditions are shown in Fig. 6.21. The maximum heating is about 1 K day^{-1} near 85km at the summer pole. These results correspond well with those of M^{c}Clatchey but Houghton estimates somewhat higher values. The thermal cooling is small, estimated by Houghton and by Williams to be about 0.4 K day^{-1} at 50km and less at other altitudes.

6.4.3 Airglow cooling

The term 'airglow' covers a wide range of atmospheric emissions which are, in general, weak, widespread, steady and always present although to a varying degree. The spectrum extends from the hydrogen Lyman - α line at 1215 Å through the visible emissions by atomic oxygen, sodium, ionized nitrogen molecules and other gases to infrared emissions by molecular oxygen and hydroxyl radicals in their vibration-rotation bands.

Of these the only emissions significant to the heat budget of the atmosphere are the infrared components. Absorption of solar radiation produces photodissociation of O_2 and O_3 molecules and the oxygen atoms formed may recombine to form several different excited states of the O_2 molecule. In particular O_2 ($^1\Delta_g$) may be formed and, in transferring to the $^3\Sigma_g^-$ state, emit radiation at 1.27μm and, to a lesser extent, 1.58μm and 1.9μm. This radiant energy has never been shared with the kinetic

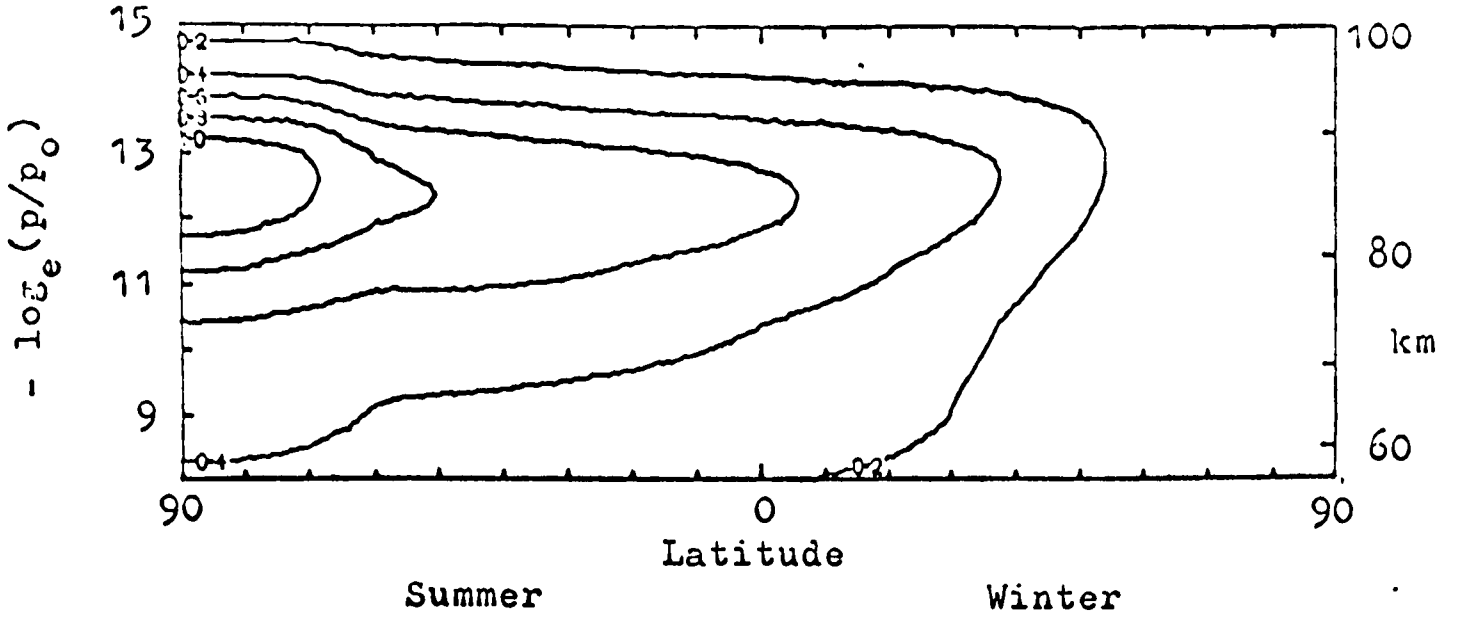

Climatological distributions of solar heating at 4.3μ and 2.7μ.

Fig. 6.21 from Williams (1971)

energy of the molecules: it has been stored as chemical energy before re-radiation. Thus, in considering the heat budget, it would be more correct to subtract it from the incoming solar radiation. However, it is instructive to calculate the effective cooling rate due to these processes. Fukuyama (1974) estimated that radiation by O_2 in its 1.27μm band results in a maximum cooling rate of about 2 K day^{-1} in the region 85 - 90km at 30^{o} latitude in winter representing about 30% of the apparent solar energy input at this altitude. Hunt (1972) calculated a maximum cooling for the same process of 1 K day^{-1} for equatorial equinox conditions at 85km.

The oxygen atoms formed by the photodissociation of O_2 molecules may also combine with other oxygen molecules to form ozone. O and O_3 may then contribute to the excitation of hydroxyl radicals:

$$OH + O \rightarrow H + O_2$$

$$H + O_3 \rightarrow O_2 + OH^*$$

where the asterisk indicates a molecule in an excited state. The maximum possible excitation energy is equal to the energy of reaction and is slightly less than the energy of the tenth vibrational level of OH in its electronic ground state. Thus the OH bands observed in the airglow correspond to transitions between the first nine vibrational levels and extend from 0.4 to 4.0μm. Again the energy released in this radiation has never been part of the kinetic energy of the molecules and so it may not be considered as <u>directly</u> cooling the atmosphere but it effectively leads to a maximum cooling rate of $\sim$ 6 K day^{-1} in the lower thermosphere at 30^{o} in winter (Fukuyama, 1974). Hunt (1972) has estimated this cooling rate as diurnally varying between 3 and 9 K day^{-1} at 85km in low latitudes; Crutzen (1971) calculates 2.7 K day^{-1} at 90km in summer high latitudes and Houghton (1965) 1.2 K day^{-1}. That these authors should produce different results is not surprising if the variety of their methods is considered:

for example Crutzen takes into account that the excited OH may be physically deactivated or react with $O(^3P)$ before it has radiated whereas Hunt (1972) and Fukuyama (1974) assume that all the excitation energy is lost in the airglow.

As far as the model is concerned the heating rate in the upper mesosphere is of interest and emissions from the OH bands originate between 56 and 100km. The energy radiated by these bands has been estimated by Wallace (1962) as about $0.2\mu W\ cm^{-2}$; from this an order-of-magnitude calculation for the peak airglow cooling may be made:

Downward flux at surface $$F_s = -\int_0^\infty \rho(z)\, c_p\, \frac{\partial T}{\partial t}(z)\, dz$$

Now $$\rho(z) = \rho(z_0)\, e^{-(z-z_0)/H}$$ H is the density scale height in the region of z_0

The OH emission is confined to the region of the mesopause and an arbitrary shape may be specified for dT/dt:

$$\frac{\partial T}{\partial t}(z) = \frac{\partial T}{\partial t}(z_0)\, e^{-r^2(z-z_0)^2}$$

so that the heating rate peaks at $z=z_0$ and decreases to half its peak value at $z = z_0 \pm \sqrt{\ln 2}/r$.

This gives for the flux:

$$-F_s = \rho(z_0)\, c_p\, \frac{\partial T}{\partial t}(z_0) \int_0^\infty e^{-(z-z_0)/H}\, e^{-r^2(z-z_0)^2}\, dz$$

$$= \rho(z_0)\, c_p\, \frac{\partial T}{\partial t}(z_0) \int_{-z_0}^\infty e^{-x/H}\, e^{-r^2x^2}\, dx \qquad x \equiv z-z_0$$

$$\simeq \rho(z_0)\, c_p\, \frac{\partial T}{\partial t}(z_0) \int_{-\infty}^\infty e^{-x/H}\, e^{-r^2x^2}\, dx$$

where it has been assumed that the integrand is only of significant magnitude in the region $|z - z_0| \ll z_0$.

$$- F_s = \rho(z_0)\, c_p\, \frac{\partial T}{\partial t}(z_0)\, \frac{\sqrt{\pi}}{r}\, \exp\left(1/4 r^2 H^2\right)$$

For emission by OH $F_s \sim 0.2\ \mu W\ cm^{-2}$ (Wallace 1962)

$z_0 \sim 85$ km

$\rho(z_0) \sim 4.8 \times 10^{-6}$ kg m^{-3}

$H \sim 5.3$ km $(T = 180\,K)$

$r \sim 0.17$ to 0.08 km^{-1} (half-width 10 to 20 km)

Which gives $$- \frac{\partial T}{\partial t}(z_0) \sim 0.4 \text{ to } 2.5 \text{ K day}^{-1} .$$

This very approximate calculation suggests that the peak cooling rates estimated by Hunt and Fukayama are rather high. However, the flux may vary with latitude and season and more measurements are required along with modelled estimates of OH concentrations.

6.4.4 Heating through chemical reactions

As mentioned above dissociation and excitation energy, acquired through the absorption of solar radiation, may be stored as chemical energy. This may be released thro ugh chemical reaction, recombination and quenching leading to thermal energy possible in regions far from the place of initial solar absorption. The chemical reactions significant in the upper mesosphere and lower thermosphere are many and are discussed by e.g. Hesstvedt (1971) and Hunt (1972). Their effect on the energy budget is studied by Crutzen (1971), Hesstvedt, Hunt and Fukuyama (1974). It is difficult to assess how much of the chemical energy created is converted into kinetic energy but the major contributions come from the recombination

of atomic oxygen:

$$O + O + M \rightarrow O_2 + M \qquad [6.1]$$

and the formation of ozone:

$$O + O_2 + M \rightarrow O_3 + M \qquad [6.2]$$

Hesstvedt calculates that reaction [6.1] will cause a maximum heating rate of about 4 K day^{-1} at 90-95km whereas the estimate of Hunt for this source is about 1 K day^{-1} and that of Fukuyama less than 0.5 K day^{-1}. The authors agree more closely on the heating rate due to reaction [6.2] which is calculated to be 5 K day^{-1} in the region of 87km and about 2 K day^{-1} at the mesopause. Kellogg (1961) proposed that the warm winter mesopause temperatures might be due to the recombination of oxygen atoms

brought downward by the mean motion of the atmosphere. However, Houghton (1978) has suggested that this heating may be balanced by cooling due to enhanced de-excitation of the CO_2 (ν_2) vibration by the extra oxygen atoms present.

Hunt and Fukuyama also consider the heating rate due to quenching of excited atoms and molecules. In the lower thermosphere the largest contribution comes from the collisional quenching of $O(^1D)$ with peak heating rates of about 6 K day^{-1} at 87km and 1-2 K day^{-1} at 80km.

6.4.5. Dynamical heating

Another possible source of heat in the lower thermosphere is the dissipation of internal atmospheric gravity waves, which have propagated upwards from the surface, and of the atmospheric tides driven by the absorption of solar radiation by ozone in the stratosphere and water vapour in the troposphere.

The first estimate of heating due to the dissipation by molecular viscosity of internal gravity waves was made by Hines (1963) and implied a

value of a few degrees per day at 95km. However this estimate depended sensitively on the spectrum that was assumed for the distribution of wave energy and this could only be estimated crudely. Kochanski (1964) produced an analysis of the vertical variation of wave amplitude as revealed by numerous rocket-released vapour trails and noted that the wave energy density (ρu^2, ρ = density, u = horizontal wind speed) did not remain constant with height, as would be predicted by theory for a non-dissipative atmosphere, but decreased exponentially between 70 and 140km with a scale height of 7.6km. Kochanski also showed that the bulk of gravity wave energy resides in modes of vertical wavelength of the order of 10km and that the mean value of u at 95km is 40 ms^{-1}.

Hines (1965) used this information to calculate the rate of energy loss of the waves and thus a net heating rate of about 10 K day^{-1} at 95km. Roper (1966), using a similar method but assuming turbulent dissipation rather than molecular viscous damping, estimated a heating rate of about 2 K day^{-1} at this altitude. Justus (1967, 1969) considered the energy budget of turbulent kinetic energy and inferred a heating rate increasing from 3 K day^{-1} at 90km to 10 K day^{-1} at 100km. Lindzen and Blake (1970) considered only the tidal component and decided the most tidal energy in the semi-diurnal mode is dissipated in the region 120-160km. Zimmerman and Rosenberg (1972) used an analysis of seventy wind profiles to predict a mean heating rate of about 20 K day^{-1} between 90-110km due mainly to waves of vertical wavelength less than 5km.

The latitudinal and seasonal variations of gravity-wave excitation and propagation are not well known. Planetary-scale waves are much stronger in winter than in summer, as explained by Charney and Drazin (1961), but there is little evidence that this is the case with small-scale waves. Roper and Elford (1963) suggest that the turbulent energy in the lower

thermosphere peaks in March and September.

Though estimates of the magnitude of this form of dynamical heating vary considerably none of the authors mentioned above have calculated large heating rates at 80km from this source. However, in the lower thermosphere in winter high latitudes, when there is no heat input due to solar absorption, the viscous dissipation of gravity waves may be significant.

6.4.6 Model results using both new radiation schemes

In Run D the Curtis matrix scheme for CO_2 15μm cooling and the 'almost exact' method for absorption of solar radiation were both used in the model up to its top level. Generalising the result of Fukuyama (1974) it was assumed that the heating due to chemical reactions and quenching plus the initial direct solar heating are equal to the apparent total absorption of solar energy (i.e. that which is calculated in the new solar heating scheme). An airglow cooling was specified above 80km with, because of the lack of any further information, latitude and season-independent values equal to Fukuyama's results for 30° latitude in winter. Heating due to the dynamical sources discussed in section 6.4.5. was ignored.

With these specifications the model produced very low temperatures at about 85km and high temperatures at the upper boundary so that by model day 315 the vertical temperature gradient was too great to allow a convergence in the relaxation scheme for the solution of the Ψ equation (Eq. 2.19) and Run D was prevented from continuing.

In order to circumvent this the airglow array was modified as shown in Fig. 6.22 for Run E. There is no physical justification for this but it is necessary to keep the model fields stable. As we are mainly interested in results below the mesopause and above this the fields may be affected by the upper boundary we feel justified in maintaining model stability using the 'airglow' array in the lower thermosphere.

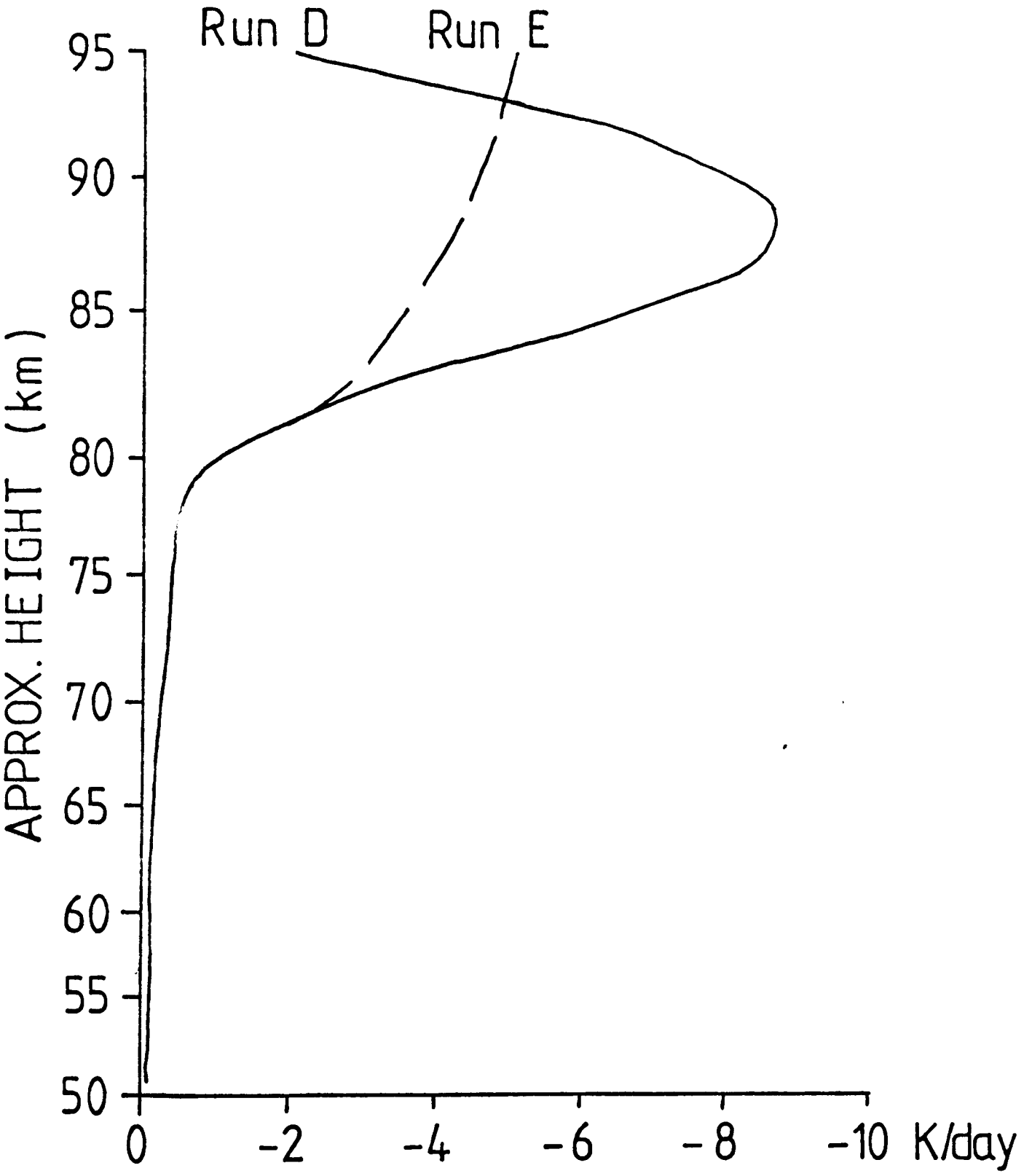

Fig.6.22 Airglow heating rate

The fields of temperature and zonal wind produced by Run E for December 21st are shown in Figs. 6.23 and 6.24. As might be expected they show a combination of the effects given in Runs B and C. Thus the temperature field shows the improvements of structure and general cooling in the upper stratosphere and lower mesosphere demonstrated in Run B and also a tendency to the overall increase in temperature produced in Run C. The altitude of the stratopause is still too low in the summer hemisphere and its temperature varies from a rather high 305K (still an improvement on the 311K of Run A) at the summer pole to a rather low 224K at the winter pole. In the upper mesosphere, apart from a slight reverse in winter low latitudes, the temperature increases strongly from the winter to the summer pole reflecting the radiant heat input. Again, therefore, the zonal wind field does not show closed jets.

As an order of magnitude experiment an attempt was made to assess the contribution of a hypothetical extra diabatic heat source necessary to close the stratospheric jets. It was found that using twice the 'airglow' values of Run E at the summer pole and varying cosinusoidally with time and linearly with latitude to minus twice its values at the winter pole an artificial closing of the jets could just be obtained. Thus at 85km an extra heating of about 16K day^{-1} is required at the winter pole with respect to the summer pole. It is difficult to explain a value of this magnitude in terms of the processess discussed earlier in this chapter and in such a situation it is difficult to envisage how a thermally indirect mean meridional circulation could be maintained. It must be concluded that there are other mechanisms not accounted for which produce the closing of the jets and the reverse temperature gradient. This topic is discussed further in chapter 8.

The meridional wind and ozone fields in Run E are very similar to those of Run B.

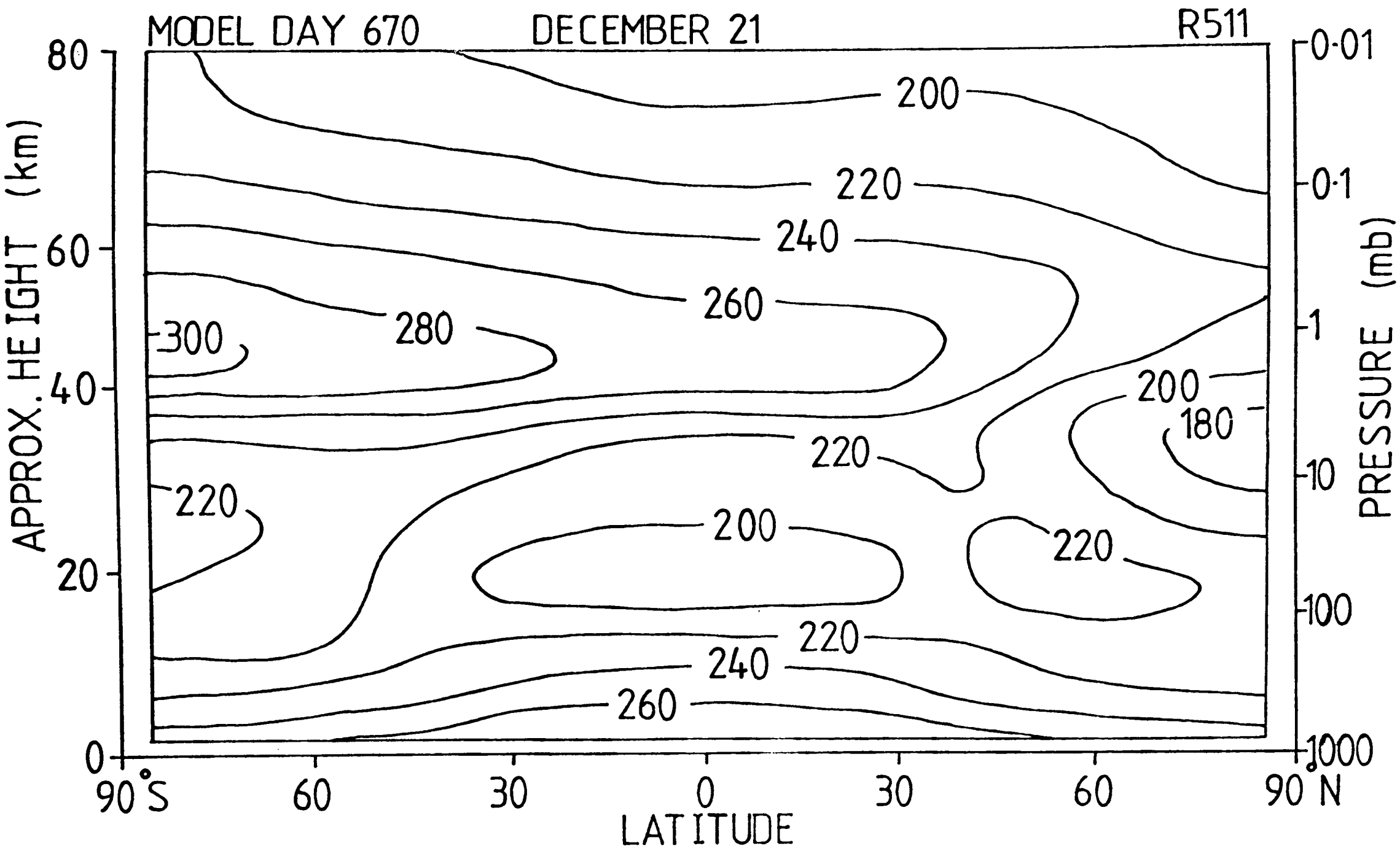

Fig. 6.23 Temperature (K) Run E

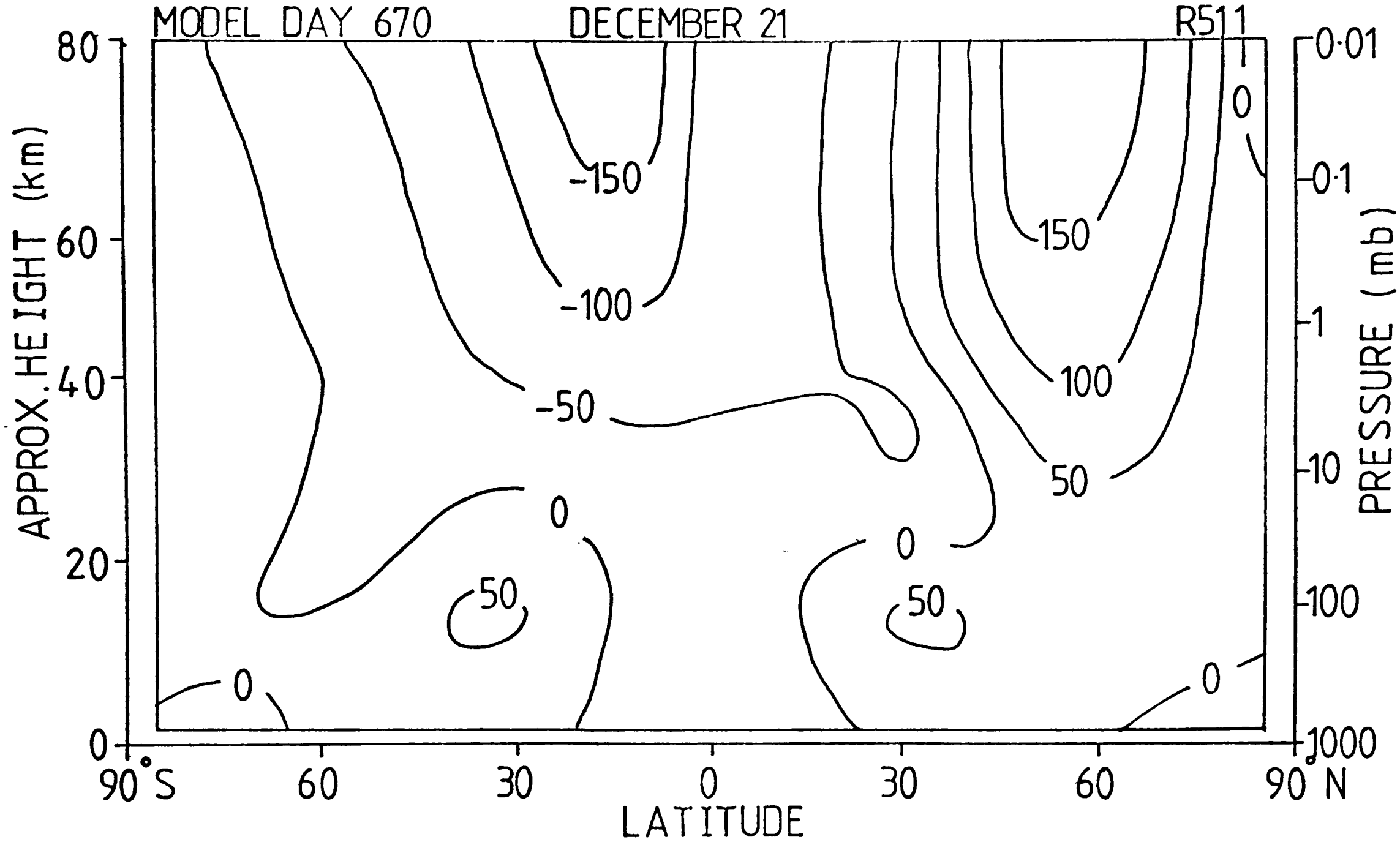

Fig. 6.24 Zonal wind (m/s) Run E

6.5 Use of the more complete photochemical scheme

Although the development of photochemical schemes was not part of the work described in this thesis in order to provide a better picture of the current model calculations and a description of the model used as a base for the experiments of chapter 7 it is important to consider here the results of using the new radiation schemes together with the better photochemistry described by Pyle (1980) and outlined in chapter 2.

The latitudinal and seasonal dependence of the ozone concentration predicted by Run A has been described earlier in this chapter and it was observed that the new radiation schemes do not have a significant effect on them. However, the improved photochemical scheme does alter their structure. Run F included the new radiation and photochemical schemes and Fig 6.25a shows the vertical cross-section of ozone concentration it produced for March 31st. There are two major differences from the results of Run A (Fig. 6.5a). Firstly, the latitudinal symmetry has disappeared with a higher ozone maximum in spring high latitudes than in autumn; this is in good agreement with the measurements of Dütsch (1971). Secondly, the absolute values of ozone concentration have decreased at high latitudes in both hemispheres giving amounts rather lower than those of Dütsch. Pyle (1980) suggests that this may be due to an underestimate of the eddy transport of ozone to high latitudes in late winter which would suggest that an explanation of the low temperatures in the high latitude lower stratosphere might be an underestimate of eddy heat fluxes too. The low ozone values are reflected in the time-latitude cross-section of ozone column density (Fig 6.25b) which barely reaches 400 Dobson units for the spring maximum in the northern hemisphere. However, the major improvement shown in Fig. 6.25b is the timing of the maxima in both hemispheres. In

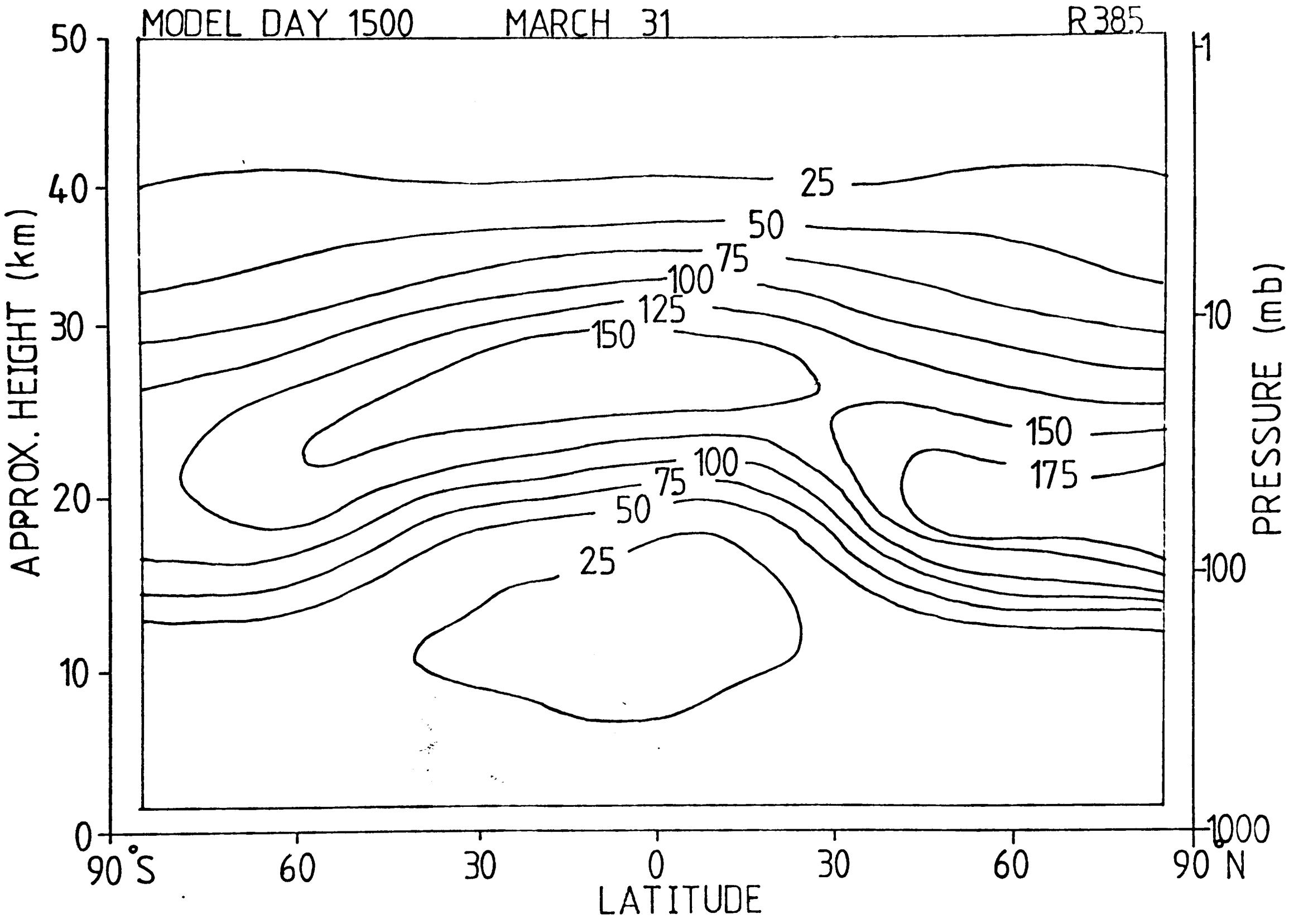

Fig. 6.25(a) Ozone partial pressure (nb) Run F

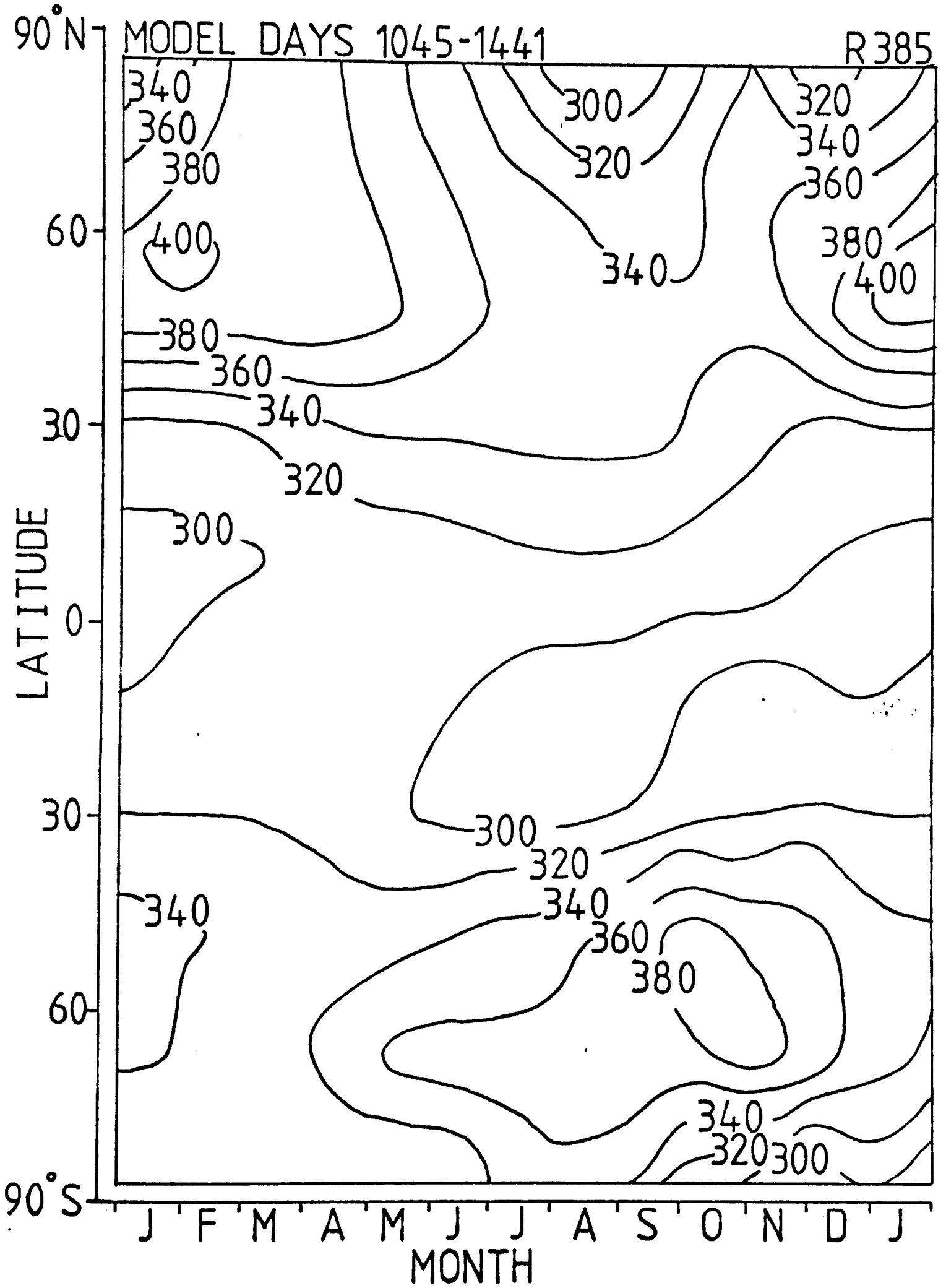

Fig.6.25(b) Ozone column density (Dobson units) Run F

Run A the maxima occurred abouth two months later than observed but in Run F they appear in spring as expected.

The changes in ozone concentration affect the absorption of solar radiation and therefore the temperature structure. The temperature field for Run F is shown in Fig. 6.26. A comparison of this diagram with Fig. 6.23 (for Run E) shows that the level of the summer stratopause has been raised to about 47km - a more realistic height than the 43km predicted in Run E. Also the value of the summer stratopause temperature has been slightly lowered and that of the winter stratopause slightly raised. The zonal wind field, shown in Fig. 6.27 is very similar to that of Run E.

The most important aspect of the model as it now stands is that it allows for feedback between the radiation field, the various chemical species and the dynamical transports. The sensitivity of this coupling is crucial in determining atmospheric structure and composition and its neglect in any calculation will result in errors which are difficult to predict but which may be observed. For example, the net radiative heating rates at the summer pole estimated by Murgatroyd (1969) are much larger than those computed in the model although the radiation calculations are of similar accuracy. In chapter 7 the feedbacks observed after particular cases of perturbation to the temperature and photochemcial fields are studied.

6.6 Model response to changes in the heating rates in the lower stratosphere

Harwood and Pyle (1980), using a version of the model similar to that in Run A, showed that small changes in the net diabatic heating rates in the lower stratosphere can significantly alter the ozone field. This model used the simpler photochemical scheme in which the ozone equilibrium values and relaxation times are specified and so do not respond to changes

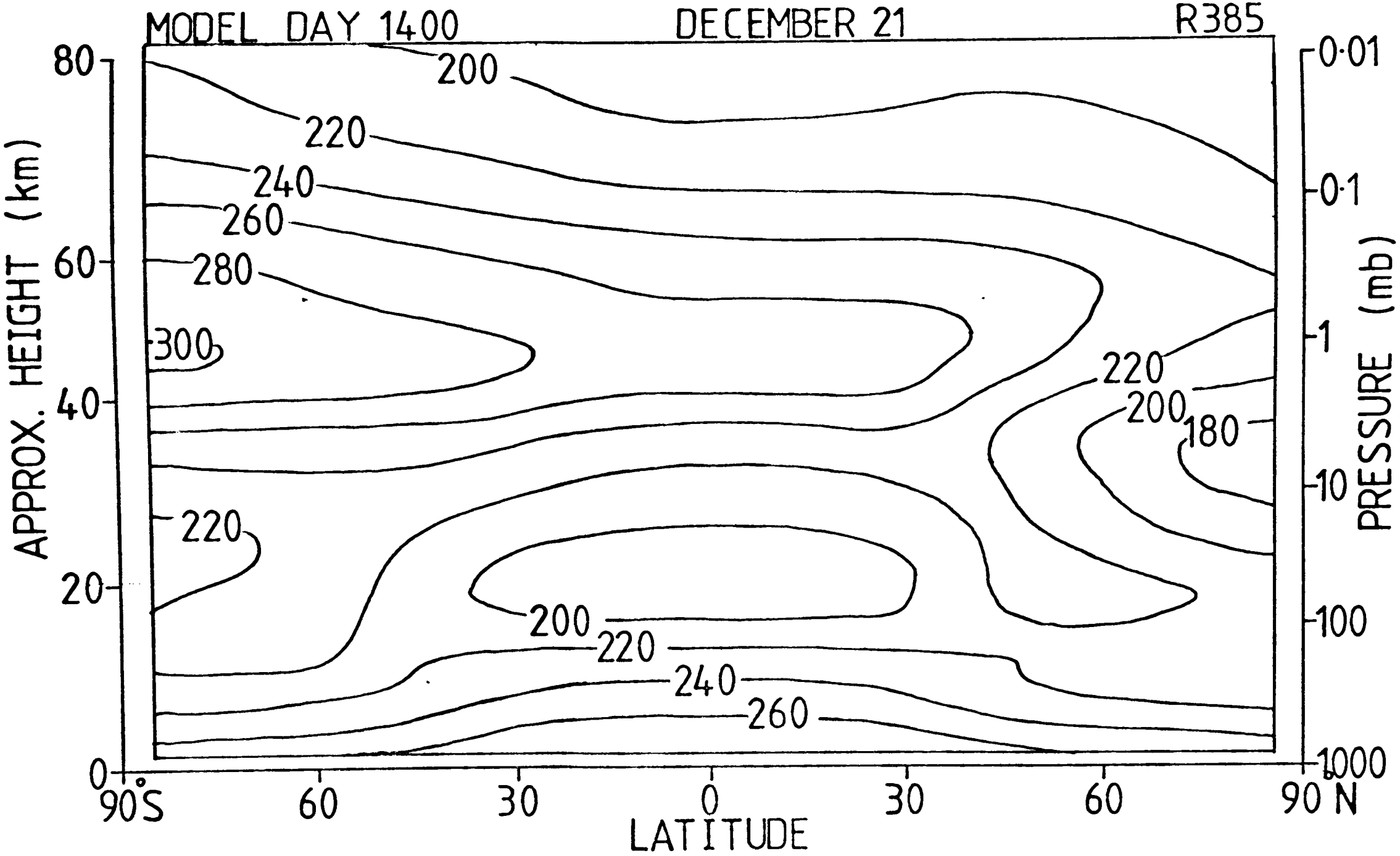

Fig. 6.26 Temperature (K) Run F

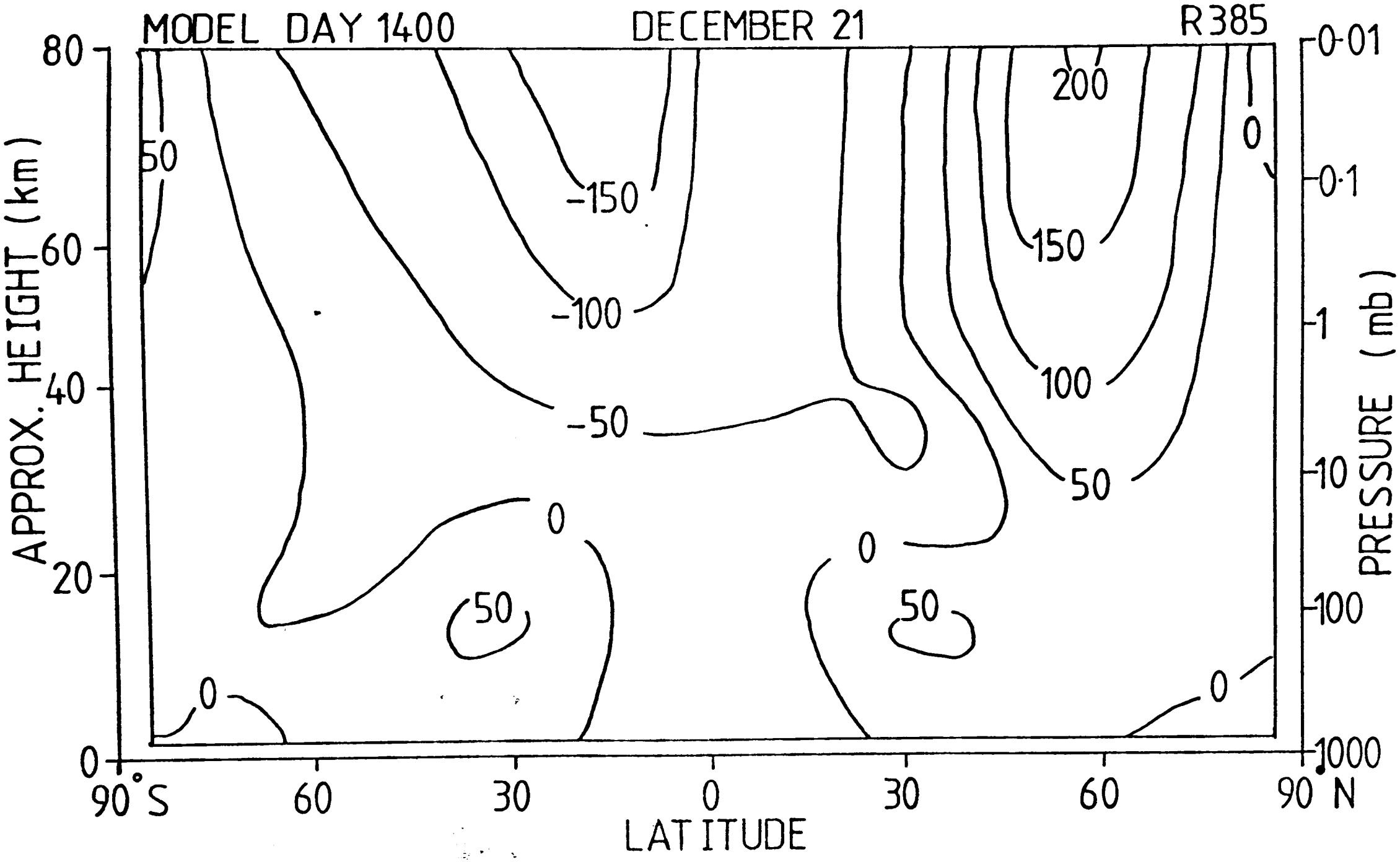

Fig.6.27 Zonal wind (m/s) Run F

in the model temperatures and also cannot respond to any simultaneous changes in the other chemical species.

For Run G the assumptions made in Run F of radiative equilibrium in the lower stratosphere and constant cooling rates in the troposphere were replaced by the seasonal net heating rates calculated by Rodgers (1967). This is the same experiment as carried out by Harwood and Pyle except that now the rates of creation and destruction of ozone depend on the temperature-dependent concentrations of the other species. The magnitude of Rodgers' net heating rates never exceeds 2 K day^{-1} in the troposphere or a few tenths of 1 K day^{-1} in the lower stratosphere but they are negative throughout the year in high latitudes and positive, though smaller in magnitude, in low latitudes.

The inclusion of these net heating rates results in large temperature decreases in the lower stratosphere and a strengthening of the mean meridional circulation which leads to small temperature decreases (despite the extra net heating) in low latitudes. The combination of decreased temperatures and increased transport results in increases in ozone column density in high latitudes of over 100 Dobson units in places. A latitude-time section of O_3 column density for Run G is shown in Fig. 6.28. There is also an ozone increase in low latitudes. This may be due to decreased O_3 destruction in the NO_x cycle as NO_2 concentrations have decreased. At all latitudes and dates the O_3 columns are much greater than the corresponding observed values (c.f. Fig. 1.5).

The results of Harwood and Pyle also show large changes in ozone column density although negative in the northern summer. The difference must be ascribed to the better photochemistry used in Run G as ozone is predominantly dynamically controlled in the lower stratosphere and temperature feedback on ozone concentration should not be too significant.

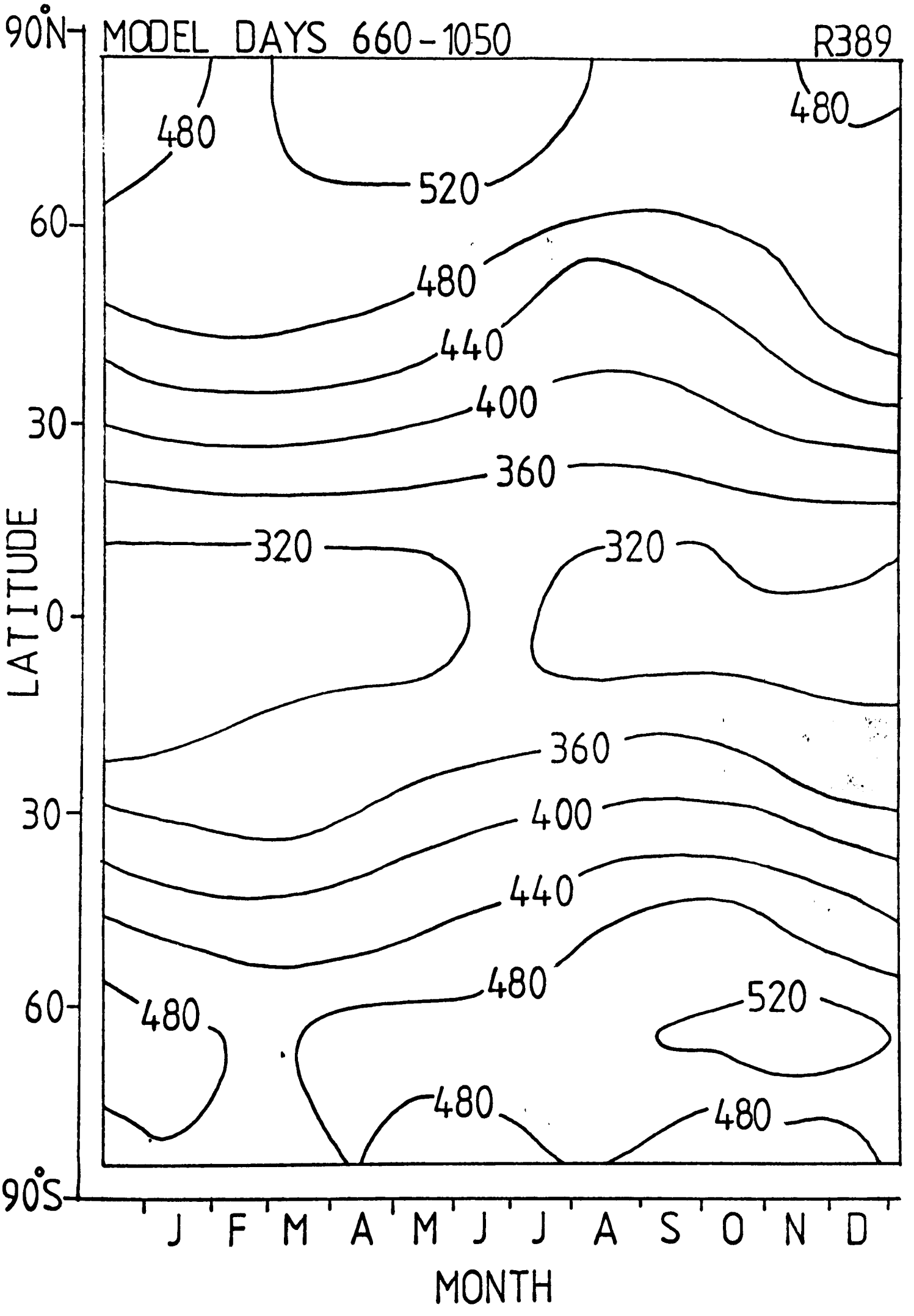

Fig.6.28 Ozone column density (Dobson units) Run G

The most important result of this experiment is that the modelled ozone amounts are extremely sensitive to the heating rates in the lower stratosphere. As these heating rates are the small residues of large positive and negative components each contribution to the diabatic heating in this region (including the CO_2 near infrared and water vapour bands) would have to be calculated accurately and in a model-dependent fashion for a reliable value of q to be obtained. This remains for future work; all the remaining experiments described in this thesis assume radiative equilibrium in the lower stratosphere.

CHAPTER 7

The effect of increased carbon dioxide concentrations on stratospheric ozone.

7.1 Observations of atmospheric carbon dioxide

The carbon dioxide content of the atmosphere has been measured for nearly two centuries. Fig. 7.1, compiled by Fonselius et al (1956), shows measurements of CO_2 volume mixing ratio made between 1800 and 1955. The large scatter in early values is probably due to the rather crude and incomplete techniques of analysis used during the first fifty years, possible with systematic positive errors. By the end of the nineteenth century the values have settled around a value rather lower than 300 ppm and after 1900 a positive trend is discernable. Callendar (1938) observed this increase and attributed it to the industrial combustion of fossil fuels in western Europe. Fig. 7.2 shows more recent measurements (a) in Hawaii (Ekdahl and Keeling, 1973) and (b) over the north Atlantic (Bischof, 1977). Both clearly show an annual cycle of magnitude 6 ppm and an overall increasing trend of from 0.5 to 1.5 ppm per year. In the period when they overlap the data agree well. Bolin and Keeling (1963) have studied the seasonal and latitudinal variation of CO_2 mixing ratio and found that, on annual average, the northern hemisphere has a value of a few parts per million more than the southern hemisphere - reflecting the higher rates of production of industrial CO_2 there. The annual cycle shows a peak value in spring and minimum in late summer; this is thought to be due to the annual variation in the photosynthesis rate of plant life on the earth's surface. Bolin (1977) suggested that changes in land usage, e.g. the destruction of forests, might also contribute to the increase of atmospheric CO_2.

Measurements of the CO_2 concentration in the stratosphere have been few. It has been generally accepted that its mixing ratio is constant with height from the surface to about the mesospause where photodissociation

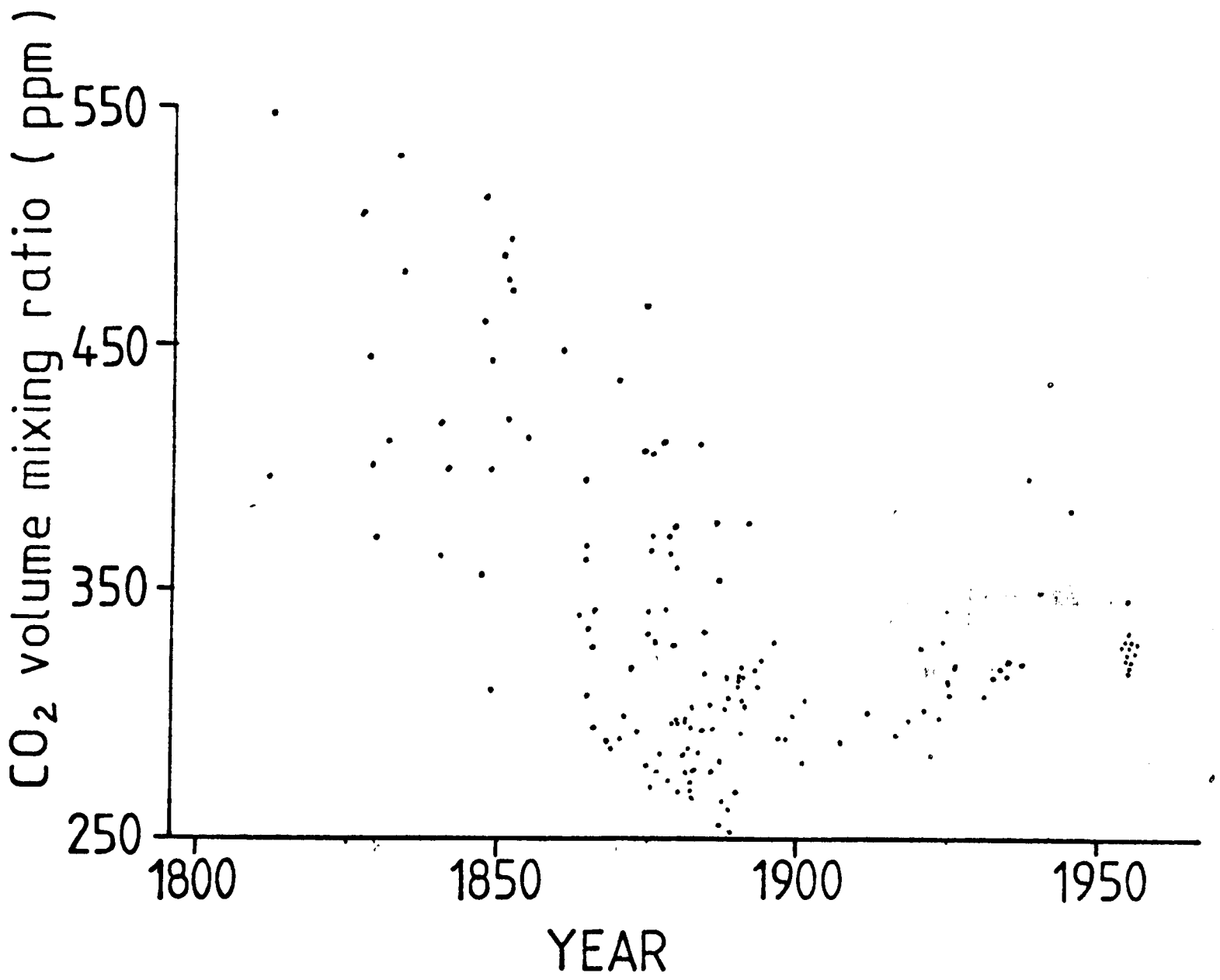

Fig.7.1 from Fonselius et al (1956)

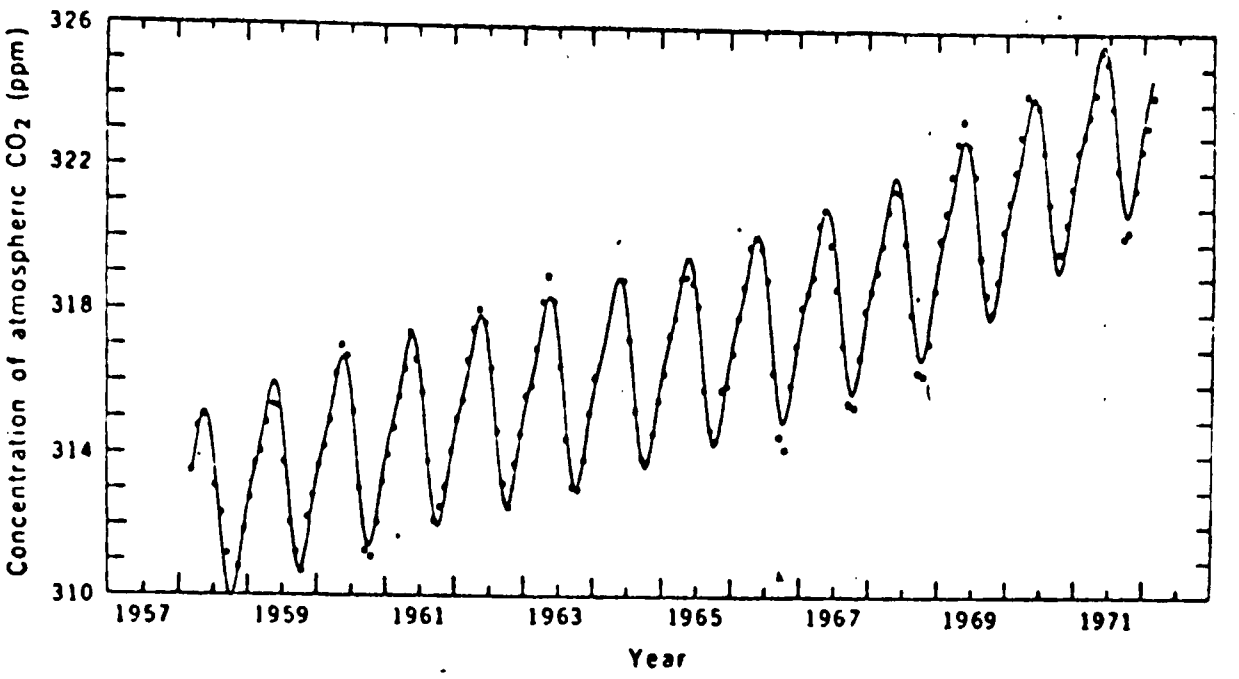

(a) At Hawaii. From Eckdahl and Keeling (1973).

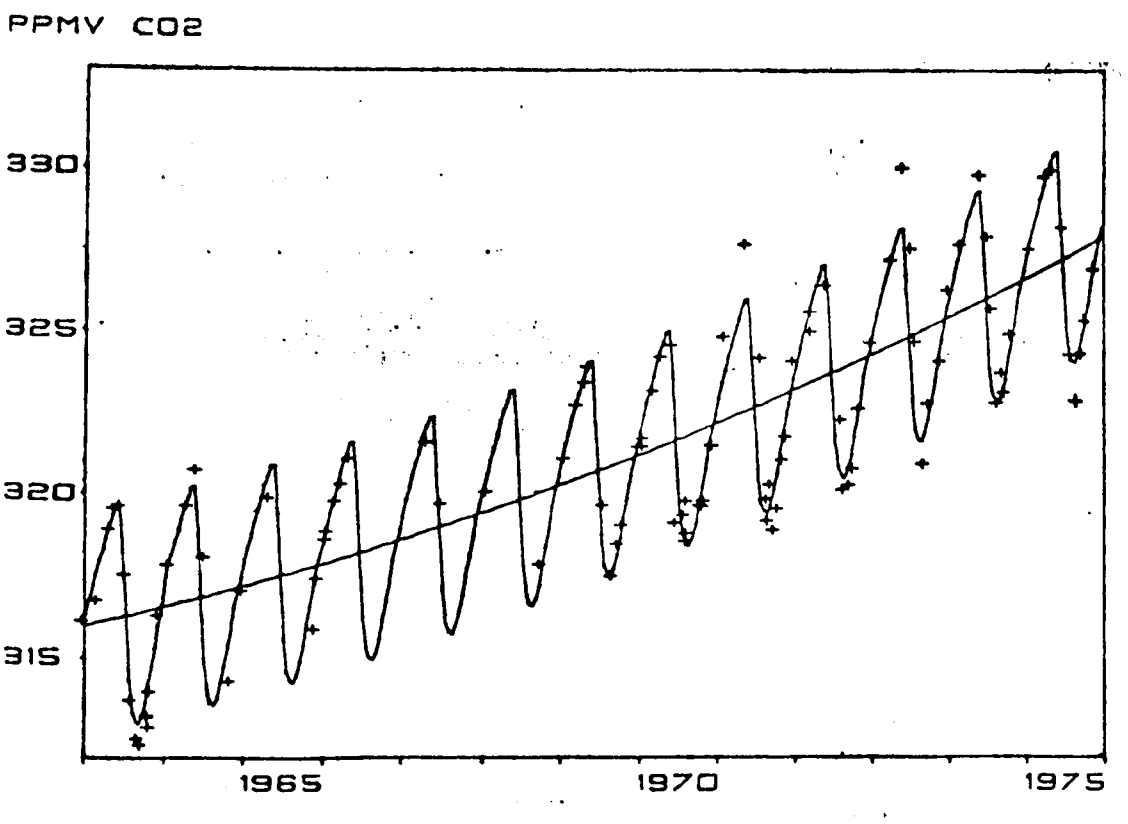

(b) Over the North Atlantic. From Bishof(1977).

Fig.7.2 CO_2 measurements.

becomes important (Scholz and Offermann, 1974). Recent observations, however, suggest a discontinuous decrease at the tropopause (Volz et al, 1977). The possibility of a vertical gradient is discussed in section 7.6.

7.2 CO_2 increases and the carbon cycle

7.2.1 The solid earth

By far the largest reservoir of the earth's carbon is the carbonate sediment in the solid earth. This reservoir may exchange carbon with the atmosphere and oceans through weathering and erosion but on a time scale far greater than that operating the atmosphere - ocean - biosphere system and may be neglected if we are considering periods of the order of hundreds of years. The factors controlling the amount of CO_2 in the atmosphere are the rate of combustion of fossil fuels and the rates of exchange with the ocean and biosphere.

Bolin (1970) and Bacastow and Keeling (1973), among others, have studied the carbon cycle in detail and a highly simplified version, along with some approximate magnitudes, is given in Fig. 7.3. Keeling (1973) has given a detailed breakdown of the annual emission of CO_2 by fossil fuel combustion and due to other industrial sources.

7.2.2 The biosphere

Although plants are believed to photosynthesise at a faster rate under conditions of higher CO_2 concentration Woodwell et al (1978) suggest that the land biomass acts as a net source, rather than a sink, of CO_2 at least during periods of agricultural expansion and deforestation as have occurred over the past century. Wilson (1979) and Stuiver (1978) have been able to assess the amount of atmospheric CO_2 due to the decay or

destruction of organic material by studying the fractions of ^{14}C and ^{13}C in the wood of tree rings. Oil, coal and other fossil fuels are much older than the half-life of ^{14}C (5730 years) and they therefore contain essentially no ^{14}C. Thus a significant release of CO_2 from fossil fuels could be expected to dilute the ^{14}C content of the atmosphere (Suess, 1955). In fact, the atmospheric ^{14}C reduction is smaller than expected due to isotopic exchange. During photosynthesis plants discriminate against ^{13}C in favour of ^{12}C and so $^{13}C/^{12}C$ ratios of organic materials are lower than those of the atmosphere and fossil fuel CO_2 not only completely lacks ^{14}C but also contains reduced amounts of ^{13}C. Thus the anthropogenic release of CO_2 from both fossil fuels and the biosphere reduce ^{13}C levels in the atmosphere but the ^{14}C content is affected only by fossil fuels. The biospheric release may be calculated from the difference of the two effects. There is some dispute as to the interpretation of the results. Broecker et al (1979) interpret Stuiver's calculations as indicating no decrease since 1958 in the carbon content of the biomass and thus that for the past two decades the biosphere has not been a source of atmospheric CO_2.

7.2.3 The oceans

If the biosphere is a source rather than a sink of CO_2 any excess released into the atmosphere must either stay there or be absorbed into the surface of the oceans. The airborne fraction might well increase with time as the acidity of the surface layers of the oceans increase making further solution more difficult. The rate of exchange between the surface layer and the deep ocean is important here but data on oceanic mixing seem to show that the oceans have a limited capacity for absorbing CO_2 on a time scale of years or decades. Any increase in the temperature of the ocean surface will also reduce the solubility of CO_2.

7.2.4 Predictions of CO_2 increase

Attempts to evaluate the airborne fraction and to predict future levels of CO_2 in the atmosphere have been made by Bacastow and Keeling (1973), Machta (1973), Smil and Milton (1974), Hoffert (1974) and Keeling and Bacastow (1978). These authors use widely differing assumptions as to the rate of increase of fossil fuel burning and the effect of the biosphere but all predict doubling of the atmospheric CO_2 in less than 100 years unless current trends are halted. The uncertainties involved in these calculations, however, make the predictions very approximate.

7.3 The possible consequences of increasing atmospheric CO_2

7.3.1 Temperature

The earth's surface is heated by radiation from the sun. This energy is re-radiated at longer wavelengths which may be absorbed by gases in the lower atmosphere. These gases will emit the radiation isotropically so much of the energy is trapped near the earth's surface. This phenomenon, in which the surface temperature of a planet is increased because the atmosphere is translucent to solar radiation but opaque to infrared radiation is known as the 'greenhouse effect'. The amount of long-wave radiation absorbed and the resultant warming of the lower atmosphere depends on the distribution of infrared absorbers. These are principally water vapour, carbon dioxide and ozone.

As the carbon dioxide mixing ratio increases the opacity of the atmosphere increases in the infrared but is unaffected in the ultra-violet and visible regions of the spectrum so, if all other factors remain the same, the temperature of the troposphere would be expected to increase. Arrhenius (1896) calculated "The influence of the carbonic acid in the air upon the temperature of the ground" in an attempt to explain periods of glaciation.

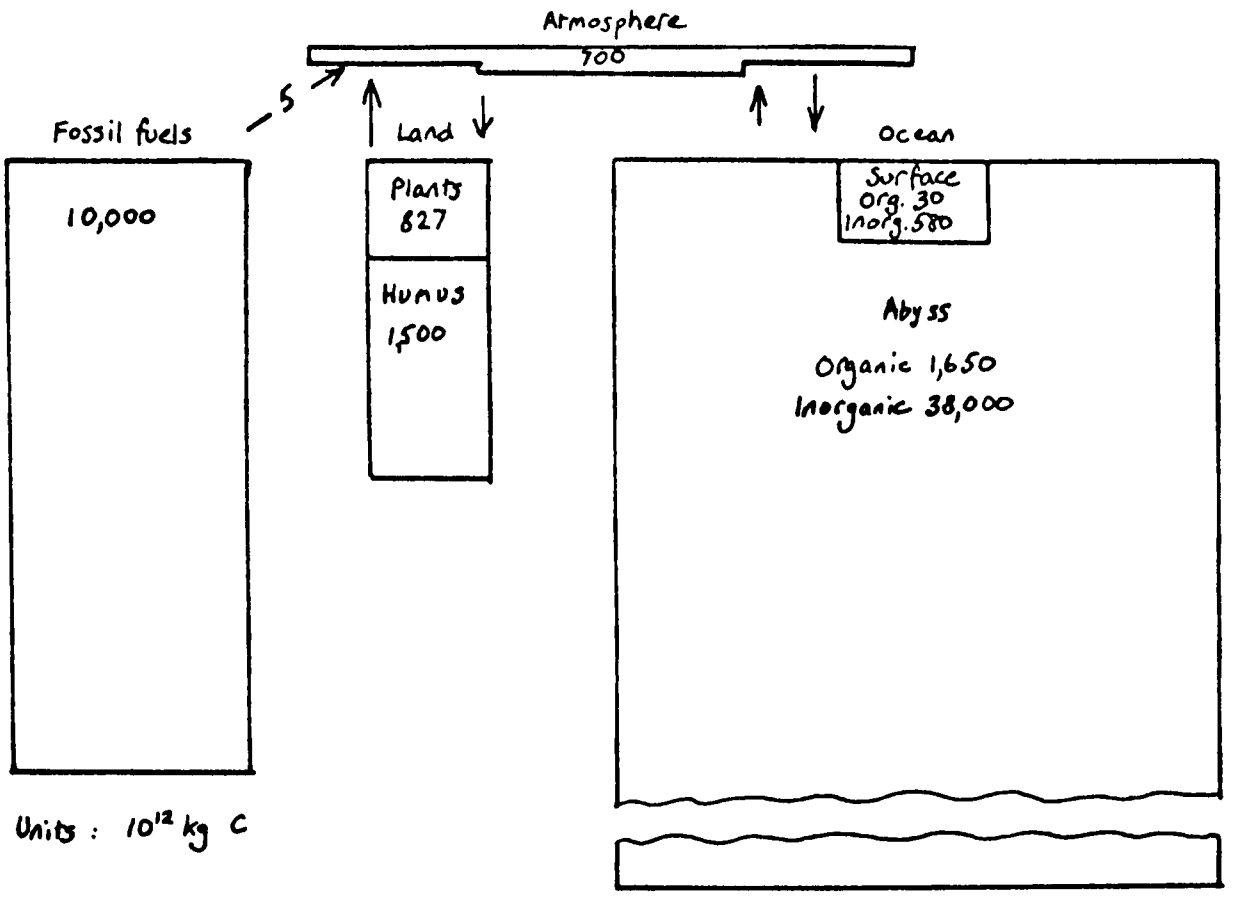

Fig. 7.3 The world carbon budget after Woodwell et al (1978)

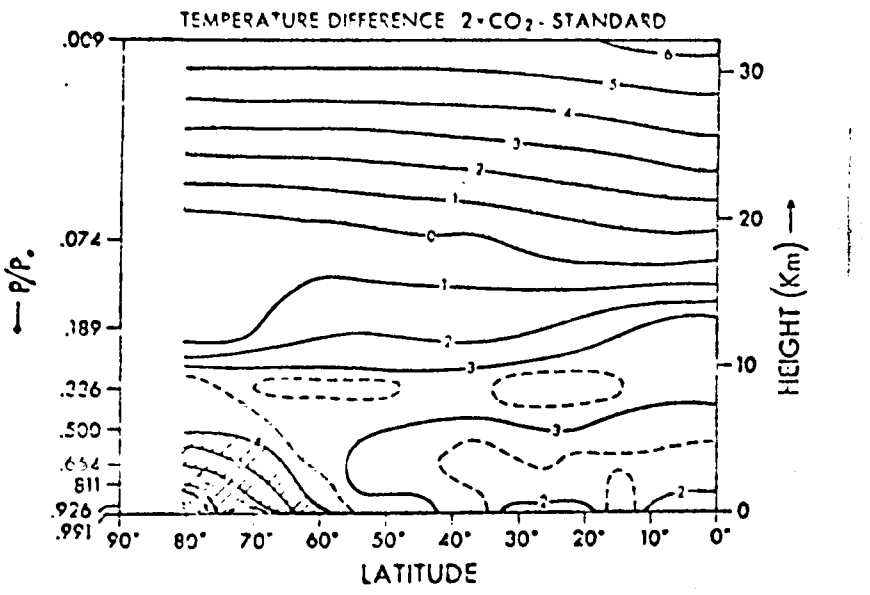

Fig.7.4 Temperature changes due to doubling CO_2 from Manabe and Wetherald (1975)

Chamberlin (1899) and Callendar (1938) extended his work. These studies all look at the carbon dioxide effect in isolation whereas the increase in tropospheric temperatures might bring about other changes which could amplify or reduce the initial increase. For example, higher temperatures will increase the evaporation rate leading to greater humidity and possibly more cloud cover. The change in humidity would affect the transfer of thermal radiation and the absorption of solar radiation while increased cloudiness would raise the earth's albedo. Another effect of increasing surface temperatures might be the reduction of the earth's snow and ice cover and therefore its albedo.

Various authors (Plass, 1956; Kaplan, 1960; Möller, 1963) improved the accuracy of the radiation calculations and included some of the feedback effects. In the case of Möller the inclusion of the water vapour 'greenhouse effect' led to a self-amplifying situation in which large, almose arbitrary, temperature changes occurred. Manabe and Wetherald (1967) constructed a one-dimensional model including most of the factors mentioned above (but not snow cover) along with fluxes of latent and sensible heat, constant relative humidity and a system of radiative-convective equilibrium. They calculated an increase in surface temperature of 2.3K for a doubling of CO_2 and also, of interest to this work, decreased temperatures in the stratosphere. As most of the infrared flux emitted upwards in the stratosphere is radiated to space (Rodgers and Walshaw, 1966), increased CO_2 amounts there result in greater cooling rates and therefore lower temperatures.

The combustion of fossil fuels and slash-and-burn agriculture also increase the number of smoke and soot particles in the air. Rasool and Schneider (1971) included in their calculation the effects of increasing aerosol concentrations and found that the back-scattering of solar radiation

exceeded the trapping of thermal radiation by the particles and thus the predicted surface temperature increase for doubled CO_2 was less than that of Manabe and Wetherald. Recently, however, it has been pointed out that most of these aerosols exist over land, where they are produced and that they are sufficiently absorbing to reduce the relatively high albedo there (Kellogg et al, 1975). Aerosols may also act as condensation and freezing nuclei.

Newell and Dopplick (1979) suggest that the temperature increases may not be as large as predicted in previous calculations for a different reason. Using a static radiative flux model which included water vapour bands, CO_2 15μm and near infrared bands and O_3 9.6μm band they show an increase in surface temperature of 0.25K. They emphasise that water vapour dominates CO_2 in the radiation budget of the troposphere and suggest that the larger value obtained by Manabe and Wetherald might be due to an exaggerated feedback between temperature and humidity.

The warming that should have already occurred due to fossil fuel burning has not been observed, in fact for the past forty years there has been a general downward trend in surface temperature. Broecker (1975) explains this as the effect of a 'natural' temperature cycle which has been observed in 800 years of $^{18}O/^{16}O$ data from Greenland snow. This cycle shows periods of 80 and 180 years and has been on a cooling trend recently, overcoming the CO_2 effect. However as reversal is predicted in the cooling curve for 1985 after which this 'natural' cycle would combine with the CO_2 effect to produce large surface temperature increases. In a similar study Hoyt (1979) has correlated surface temperature changes with solar luminosity and found that anthropogenic sources have probably caused an increase of 0.4K between 1880 and 1970 although this has been overshadowed by changes due to variations in the solar constant. An extrapolation indicates that a doubling of CO_2 would result in a 2-3K surface temperature rise.

Hoffert (1974) discusses the latitudinal asymmetry of anthropogenic CO_2 production and its possible implications for the circulation of the atmosphere and oceans. If the temperature changes produced by the CO_2 increase are not independent of latitude the zonal and meridional wind structure of the atmosphere might be affected. Also changes in the static stability of the stratosphere might alter the vertical propagation of planetary waves and even the tropospheric circulation (Bates, 1977). It is evident that one-dimensional models cannot deal with such questions.

Manabe and Wetherald (1975) studied the effect of increasing CO_2 on a three-dimensional general circulation model. This model includes a treatment of the hydrologic cycle, including snow cover, and an explicit calculation of heat transport by large scale eddies. Results are given as zonal means and averaged over 100 model days for two CO_2 concentrations: (i) a value of 0.456 g kg^{-1} (≈ 300 ppmv) and (ii) double this value. In both cases the CO_2 is mixed uniformly throughout the model atmosphere. The temperature difference between the two cases is shown in Fig. 7.4. There is a general warming in the troposphere and cooling in the stratosphere with a global average surface temperature increase of 2.9K. The increases near the surface vary considerably with latitude - at 80° the temperature has risen by over 10K while at the equator the difference is 2K. Manabe and Wetherald explain this as due to a decrease in snow cover, and hence albedo, at high latitudes. The latitudinal variation does not extend very high in the troposphere because vertical mixing by turbulence is suppressed by the stability of the polar region - this serves to amplify the warming near the surface. Other results are an increased intensity of the hydrologic cycle and a reduction of eddy kinetic energy in the lower troposphere with an increase in the upper troposphere and lower stratosphere.

Manabe and Stouffer (1979) have included a mixed layer ocean, global domain, realistic geography and seasonal variation of insolation. They predict a mean global warming of about 2K for the doubling of CO_2 content but emphasise the importance of seasonal and interhemispheric asymmetries. Manabe and Wetherald (1980) have assessed the distribution of climatic change resulting from CO_2 increases using a model similar to that described in their 1975 paper.

Table 7.1

The basic chemistry of ozone

$O_2 + h\nu$	$\rightarrow$	$O + O$	J_2
$O + O_2 + M$	$\rightarrow$	$O_3 + M$	k_2
$O_3 + h\nu$	$\rightarrow$	$O + O$	J_3
$O_3 + O$	$\rightarrow$	$2O$	k_3
$O + O + M$	$\rightarrow$	$O_2 + M$	k_1
$O + OH$	$\rightarrow$	$H + O_2$	k_8
$H + O_2 + M$	$\rightarrow$	$HO_2 + M$	k_9
$HO_2 + O$	$\rightarrow$	$OH + O_2$	k_{10}
$H + O_3$	$\rightarrow$	$OH + O_2$	k_{12}
$NO + O_3$	$\rightarrow$	$NO_2 + O_2$	k_{17}
$NO_2 + O$	$\rightarrow$	$NO + O_2$	k_{16}

J_i , k_i are the dissociation and reaction rate constants.

7.3.2 Ozone

In the upper stratosphere the ozone concentration is determined mainly by photochemical processes. The simple oxygen only (Chapman) cycle was described in section 2.6.1 and a expression for the equilibrium ozone concentration due to this scheme stated. Table 7.1 shows the Chapman reactions together with the HO_x and NO_x reactions which catalytically destroy odd oxygen (i.e. $O + O_3$). Barnett et al (1975), considering the reactions in Table 7.1 and assuming that the species in each cycle were in equilibrium, showed that the equation for the rate of change of ozone is :

$$\frac{1}{2}\frac{d[O_3]}{dt} = J_2[O_2] - \frac{k_3}{k_2}\frac{J_3}{[O_2][M]}[O_3]^2$$

$$- \frac{k_8}{k_2}\frac{[OH]\ J_2\ [O_3]}{[O_2]\ [M]} - k_{17}[NO][O_3] \qquad (7.1)$$

where the third and fourth terms on the right hand side are due to the HO_x and NO_x cycles respectively. Barnett et al investigated the temperature dependence of ozone due to the three cycles individually and found that in each case it was of the form

$$\frac{d\ ln[O_3]}{d\ T^{-1}} = c$$

where c = 1330 - 1675 for the Chapman scheme

330 - 500 if HO_x destruction dominates

1200 if NO_x destruction dominates

using recent estimates of the temperature dependent reaction rates (see Table 2.1). When no one scheme dominates an intermediate temperature dependence is obtained. This theory was found to correlate well with satellite observations of ozone and temperature.

From the above we see that in the upper stratosphere a decrease in temperature implies an increase in ozone concentration and it is for this reason that changes in CO_2 concentrations may affect O_3 amounts. As CO_2 levels increase infrared cooling-to-space is enhanced and the temperature decreases. This leads to an increase in O_3 concentration, and therefore in the absorption of solar ultra-violet radiation, which tends to counteract the effect on temperature of the extra long-wave cooling. This is an example of negative feedback through photochemical - radiative coupling.

In the lower stratosphere the ozone distribution is determined by atmospheric motions. The transport by the mean meridional circulation and by eddy motions almost cancel but the tendency is for the mean motions to move O_3 to mid-latitudes and horizontal eddies to transport it towards the poles (Harwood and Pyle, 1977). Changes in the radiative balance of the lower stratosphere may produce changes in the circulation which could drastically alter the O_3 concentration there (Harwood and Pyle, 1980).

The possibility of changes in ozone concentration is of concern because of the important role it plays in the heat balance of the atmosphere and also because it shields the earth's surface from ultra-violet radiation which may be biologically harmful (Mole, 1980).

One-dimensional studies of stratospheric CO_2 - O_3 coupling have been made by Luther et al (1977), Boughner (1978), Groves et al (1978), Groves and Tuck (1980 a, b) and Isaksen et al (1980). These all include complex photochemical schemes and most include detailed radiation calculations but they represent dynamical processes by specifying vertical profiles of an eddy diffusion coefficient. The O_3 mixing ratios predicted for the lower stratosphere are strongly dependent on the choice of these coefficients.

The temperature and ozone changes predicted by Luther et al and Boughner for a doubling of the CO_2 mixing ratio (though starting with different $[CO_2]$ values - see Table 7.2) are shown in Fig. 7.5. The temperature differences of Manabe and Wetherald (1975) at 35° latitude from 10 to 30 km are also given. Although Luther et al give temperature differences at only two altitudes it can be seen that their decreases are greater than Boughner's and correspondingly their increases in ozone are greater. The difference between the temperature calculations is due to the use of different radiative transfer schemes. Both calculations show a maximum O_3 increase at about 42 km (of 15% for Boughner and 27% for Luther et al) and decreases in O_3 in the lower stratosphere. These decreases occur because the higher concentrations of O_3 in the upper stratosphere have absorbed more ultra-violet radiation thus J_2 is decreased at lower levels and the production of O_3 reduced through the first term on the right hand side of Equation 7.1. The results of Groves et al, who included diurnal and seasonal variations of insolation, are shown in Fig. 7.6. The temperature changes at 42 km vary between those predicted by Boughner and those of Luther et al with maximum decrease in summer. The largest ozone increase occurs at about 45 km and varies between about 17% in winter and 22% in summer. No O_3 decrease in the lower stratosphere is observed.

The percentage changes in O_3 column density predicted by the various authors are given in Table 7.2. Their estimates vary, for a doubling of CO_2 mixing ratio, from 1.2% given by Boughner for a particular K_z profile to about 4.5% (seasonal average) from Groves et al who suggest their value may be larger because of the use of different photochemical constants in calculating the dissociation rate of N_2O. Part of the difference between the models of Boughner and Luther et al may also be attributed to photochemistry.

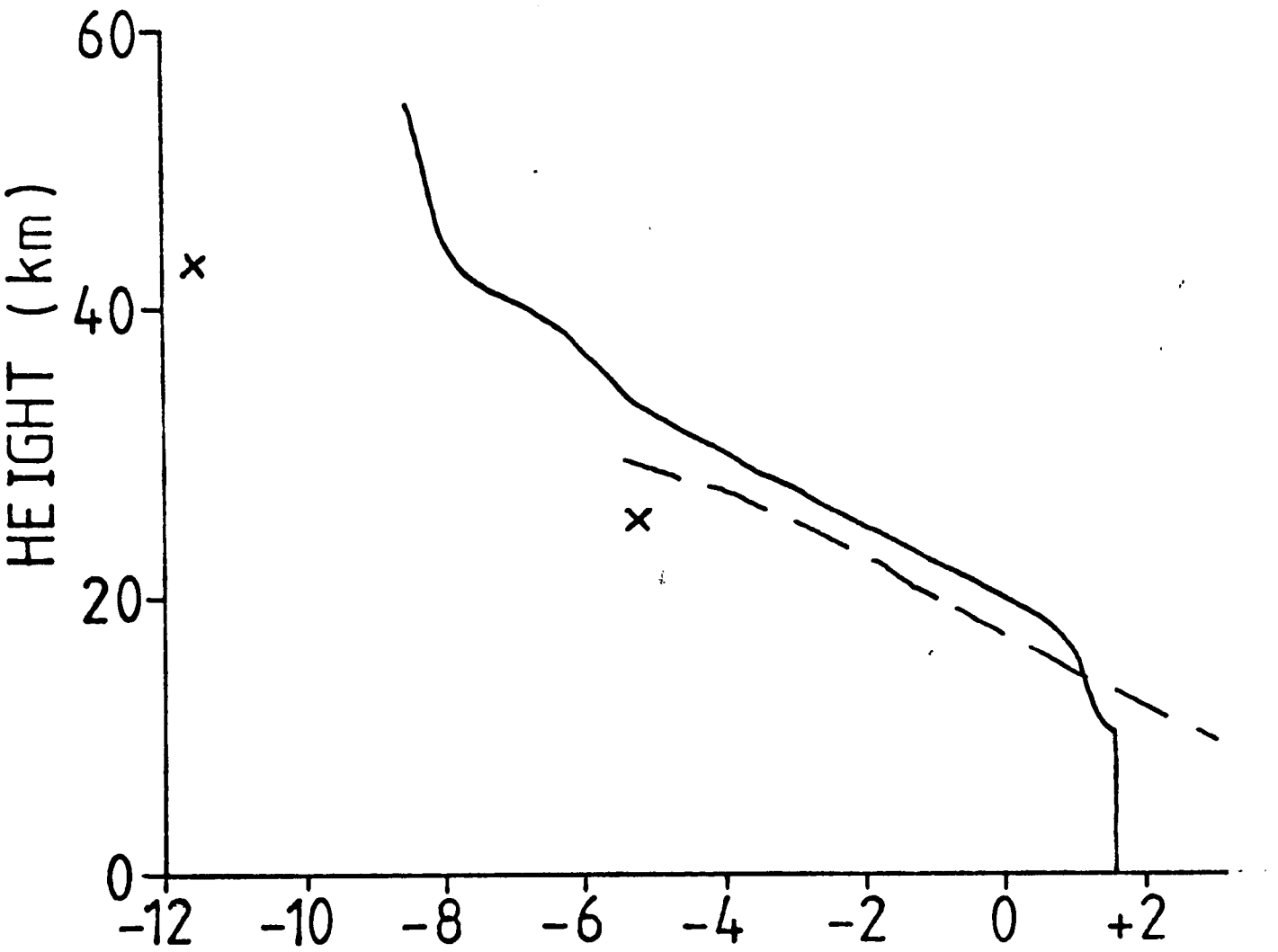

Fig.7.5 Change in temperature (K)

——— Boughner (1978)

— — Manabe and Wetherald (1975) 35°N

x Luther et al (1977)

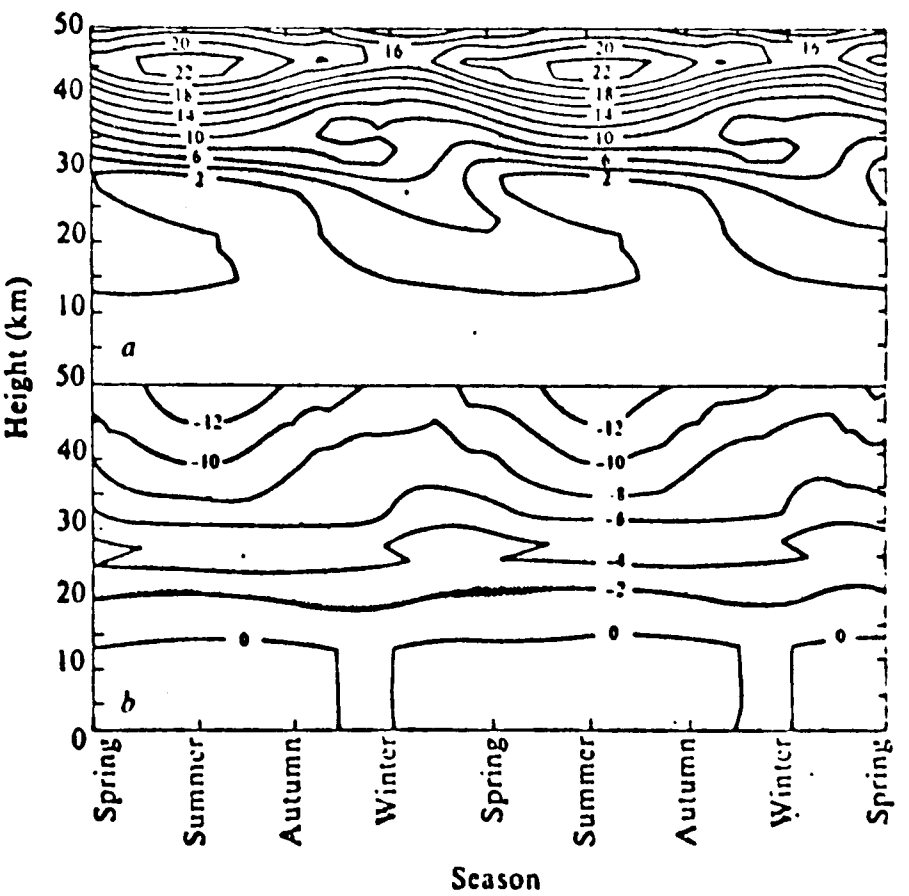

Fig.7.6 a.% difference in O_3 v.m.r.
b.Difference in temperature.

due to increase of CO_2 v.m.r.
from 290p.p.m. to 600p.p.m.

From Groves et al (1978).

The model described by Groves and Tuck (1980a) is the same as that of Groves et al (1978) while in the work of Groves and Tuck (1980b) and Isaksen et al (1980) natural chlorine-containing species have been included.

Table 7.2

Ozone increases predicted in one dimensional models

Author	Initial - final CO_2 volume mixing ratio (ppm)	Percentage increase in O_3 column density
Luther et al (1977)	300 - 600	2.9
Boughner (1978)	320 - 640	1.2 ↔ 2.5
Groves et al (1978)	275 - 600	5.5
"	290 - 600	4.7
"	325 - 600	4.2
Groves and Tuck (1980b)	275 - 600	3.2
Isaksen et al (1980)	300 - 600	4.3

7.4 A two-dimensional calculation

The one-dimensional models reviewed so far have all shown an increase in stratospheric ozone as a result of increasing CO_2. Because of the limitations of the treatment of transport used in these models, however, they are unable to represent latitudinal and seasonal variations accurately. They are also unable to include coupling between radiative sources and sinks and the mean circulation. Pyle (1978, 1980) has shown the importance of including these factors in assessing the possible effects of chlorofluorocarbons

on the ozone layer. An experiment to assess the changes in temperature structure throughout the stratosphere and the effect on ozone of increasing CO_2 in a two-dimensional model will now be described.

The basic model was Run F, described in Chapter 6. In a similar experiment, described by Haigh and Pyle (1979), a model with slight differences in some of the reaction rates, eddy diffusion coefficients and radiative cooling in the 9.6μm O_3 band was used. Run F includes the detailed photochemical scheme (without chlorine species) and the Curtis matrix method for calculating radiative transfer in the 15μm band of CO_2 assuming a volume mixing ratio of 320 ppm. For Run H new Curtis matrices were calculated for CO_2 mixing ratios of 400, 500 and 625 ppm appropriate to approximately the years 2000, 2020 and 2040. As simulating 80 years is very expensive in computer time it was decided to increase the CO_2 in the model at four times the expected rate in the atmosphere and the matrices were therefore used as follows :

Model days	Simulated years	CO_2 v.m.r (ppm)
0 - 1800	1965 - 1985	320
1800 - 3750	1985 - 2005	400
3750 - 5500	2005 - 2025	500
5500 - 7250	2025 - 2045	625

Thus we have a crude representation of the increase of CO_2 with time. Fig. 7.7. shows how this step function corresponds to predictions of CO_2 increase by various authors. All the matrices were calculated using the U.S.A. Standard Atmosphere temperature profile. As the temperature reductions predicted are less than the latitudinal variation of temperature at any altitude the errors introduced by using the standard atmosphere are no greater than those due to the use of one matrix for all latitudes (see Chapter 3). The cooling-to-space approximation was retained for the 9.6μm O_3 band with cooling

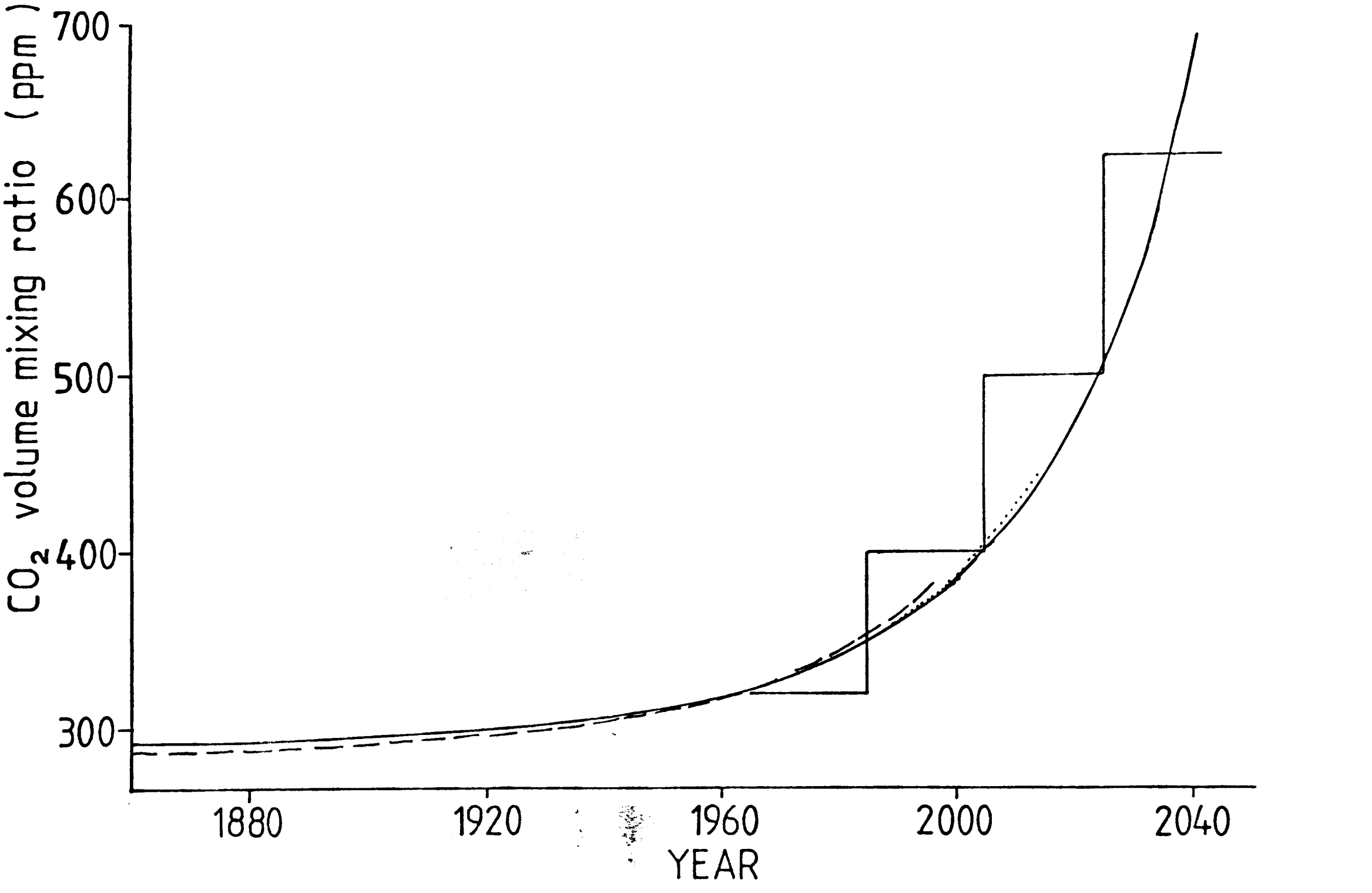

Fig.7.7 ——— Bacastow and Keeling (1973) – – – – – Machta (1973)
step function - Run H ..... Broecker (1975)

dependent only on changes in temperature and not on changes in ozone concentration. This should not introduce serious error as the majority of the long-wave cooling in the stratosphere and mesosphere is due to the 15μm CO_2 band.

The lower stratosphere was assumed to remain in radiative equilibrium. Calculations of changes in heating rates in the 15μm and near infrared bands of CO_2 due to doubling its mixing ratio indicated a net cooling of a few tenths K day^{-1} in the lower stratosphere. The meridional circulation, and hence ozone amounts, of the model are extremely sensitive to such heating rates at these altitudes (see discussion in Section 6.6.). However, it was felt that, given the difficulty of these calculations in the lower stratosphere and the fact that no allowance was made for changes in water vapour mixing ratio, they should not be included. The need for accurate calculations of heating rates in the lower stratosphere has been stressed by Houghton (1978).

The net heating rates in the troposphere were likewise unchanged but the sea surface temperatures were modified, in step with the CO_2 mixing ratio, to match the results of Manabe and Wetherald (1975) for doubled CO_2. The tropospheric temperatures could then be altered by the convective adjustment scheme.

7.5 Results

The cross-section of temperature for April (day 7000) of control Run F is shown in Fig. 7.8. The temperature difference between Runs H and F on this day are shown in Fig. 7.9. Day 7000 corresponds to some 77 years in the future. In common with other authors' results there is warming in the troposphere and cooling in the stratosphere. The changes in the troposphere agree well with the results of Manabe and Wetherald (1975), shown in Fig. 7.4, having largest increases near the surface in high latitudes. The height of

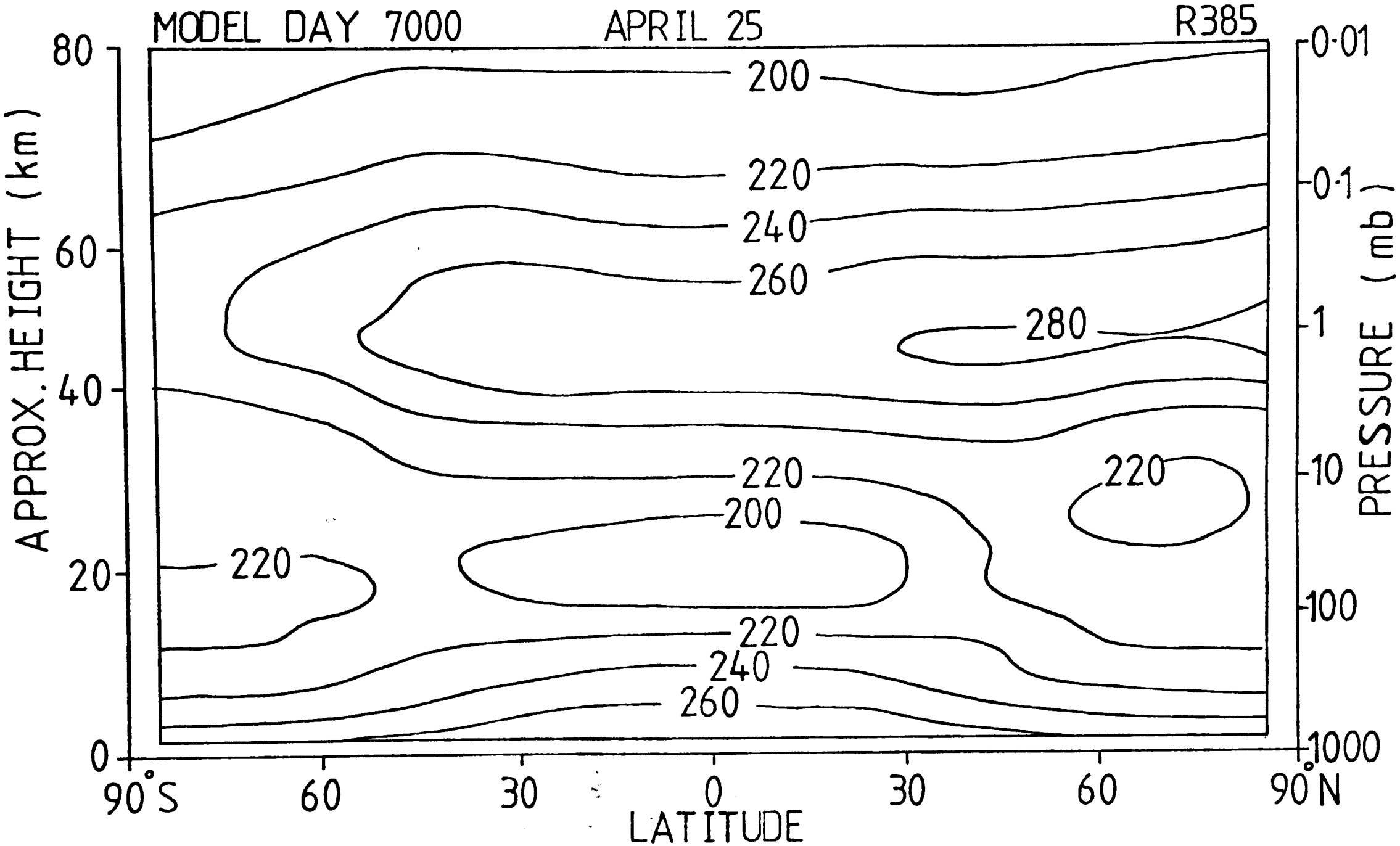

Fig. 7.8 Temperature (K) Run F

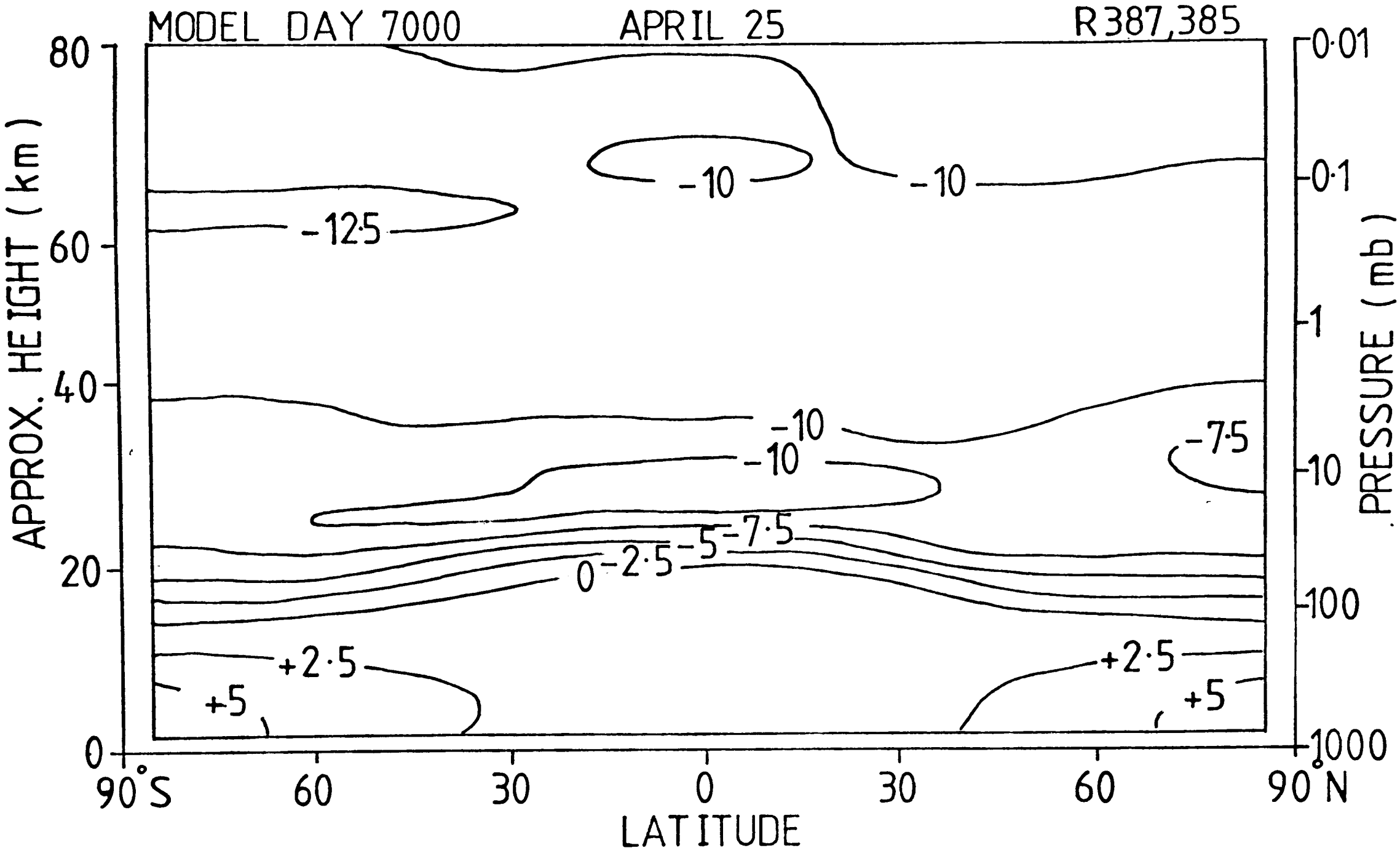

Fig.7.9 Change in temperature (K) Runs H,F

zero temperature change, however, slopes towards the equator in Manabe and Wetherald's results where in the present work it follows the tropopause. The results of Manabe and Wetherald (1980) show the same gradient as in the present work. In the stratosphere the temperature change increases with height more steeply than in previous works, especially in low latitudes where it reaches -10K at 26 km. The lower temperatures of the equatorial lower stratosphere reflect the marked 'reverse self-healing' effect in the ozone field (see below). At the stratopause the value of -12K is similar to that of Luther et al (1977) and Groves et al (1978) though larger than that of Boughner (1978).

Investigation of the cross-section of changes in temperature throughout the year reveals little variation below 30 km or above 45 km but an annual cycle in the middle stratosphere with temperature decreases 3 - 4K larger in summer than in winter. Groves et al (1978) show a similar cycle but its amplitude increases with height up to 50 km. This difference is probably due to the different sensitivity of each model to photochemical - radiative feedback. Fig. 7.10 shows long-wave cooling and solar heating for Run F in December (model day 7250) and Fig. 7.11 shows the same for Run H. The larger amounts of CO_2 in Run H have increased the long-wave cooling from -16.9 K day^{-1} to -18.9 K day^{-1} at the summer stratopause but the increase in ozone concentration at this level (which will be described shortly) has given an exactly compensating increase in solar heating from 17.3 K day^{-1} to 19.3 K day^{-1}. The net cooling is also the same in both runs at the winter stratopause because the decreases in temperature tend to reduce the cooling due to the extra CO_2. Thus the feedback mechanisms produce a situation in which the temperature reduction near the stratopause is independent of latitude and season. In the middle stratosphere the increases in ozone in summer high

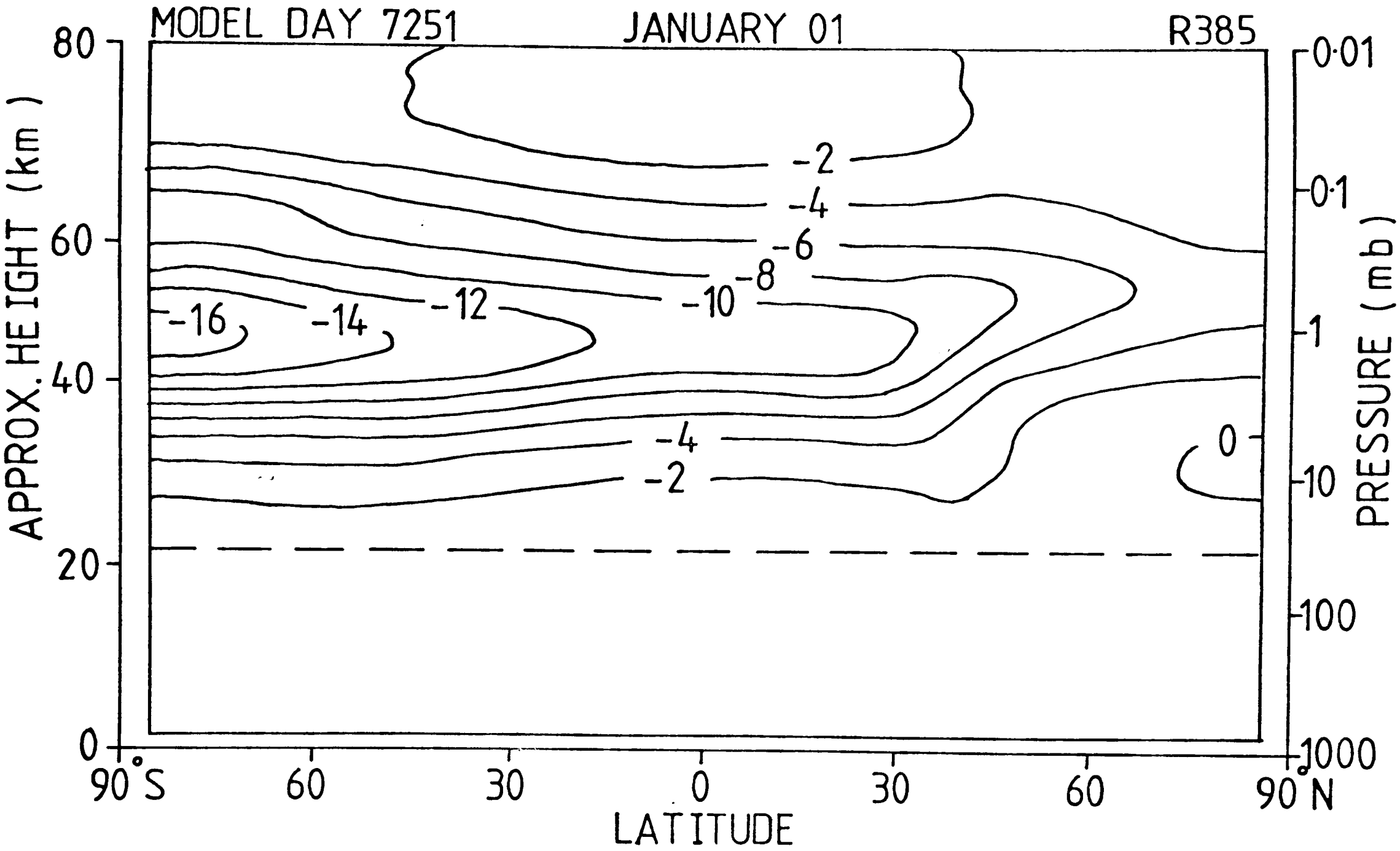

Fig.7.10(a) Heating rate - thermal radiation (K /day) Run F

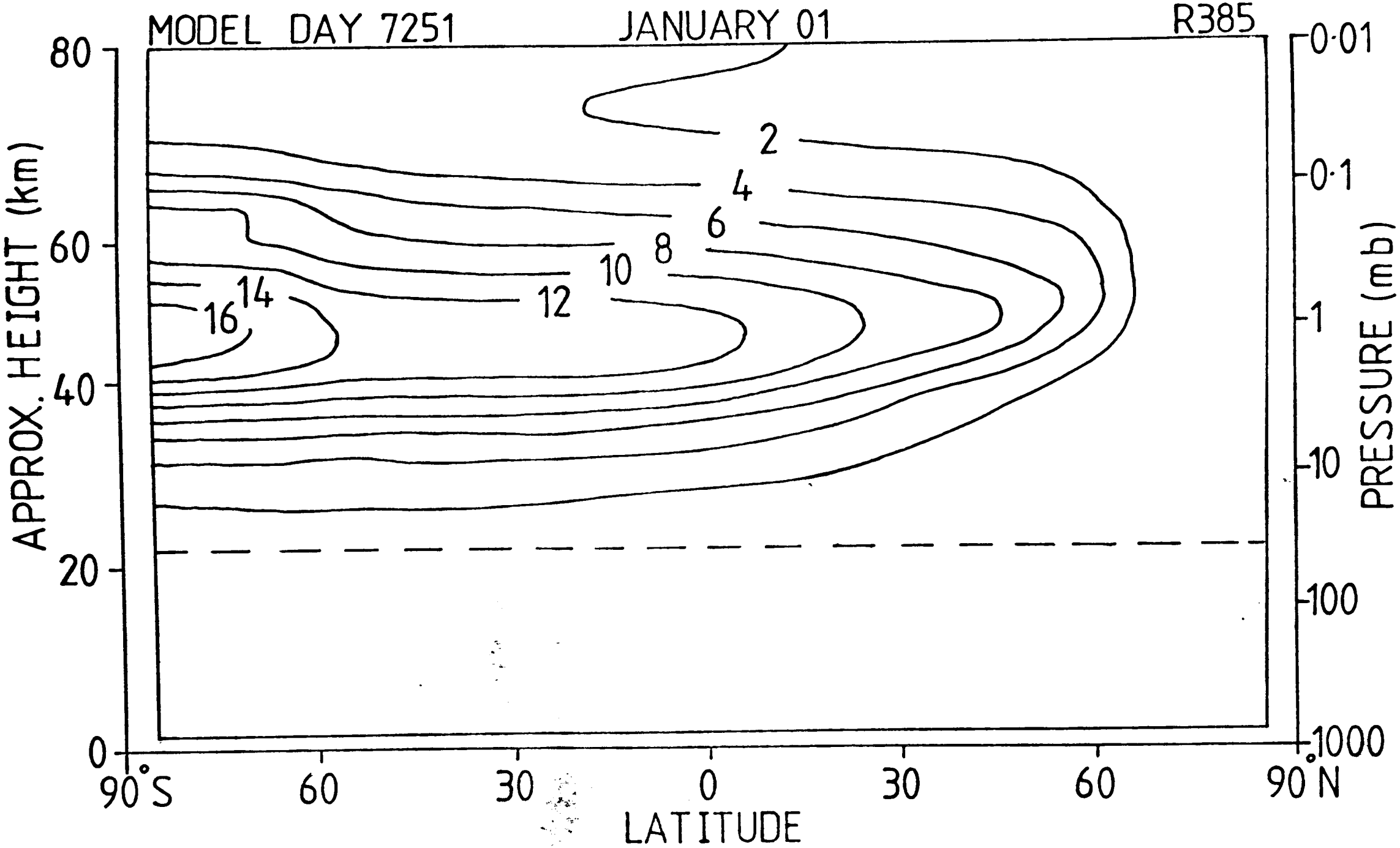

Fig.7.10(b) Solar heating rate (K / day) Run F

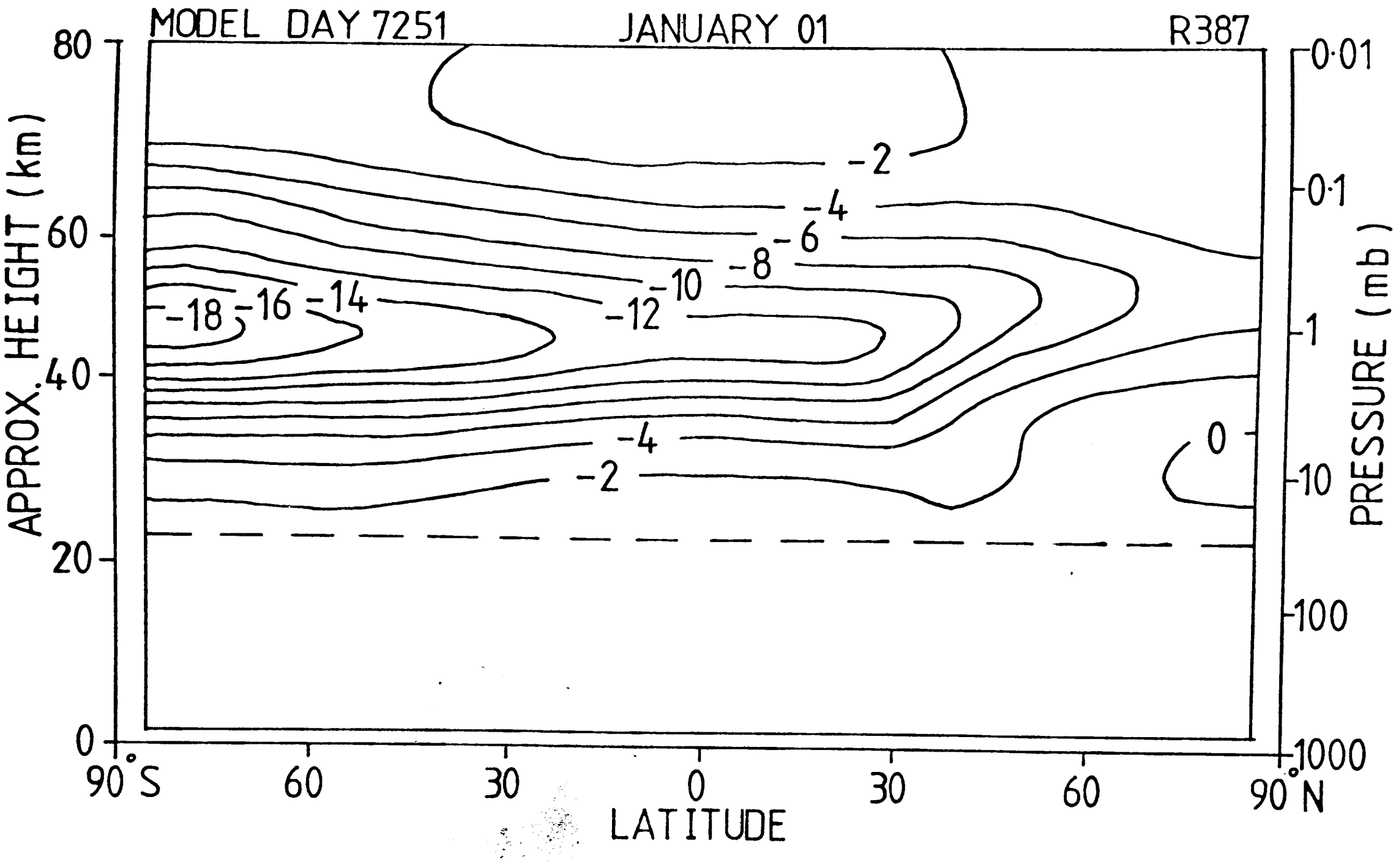

Fig.7.11(a) Heating rate - thermal radiation (K/day) Run H

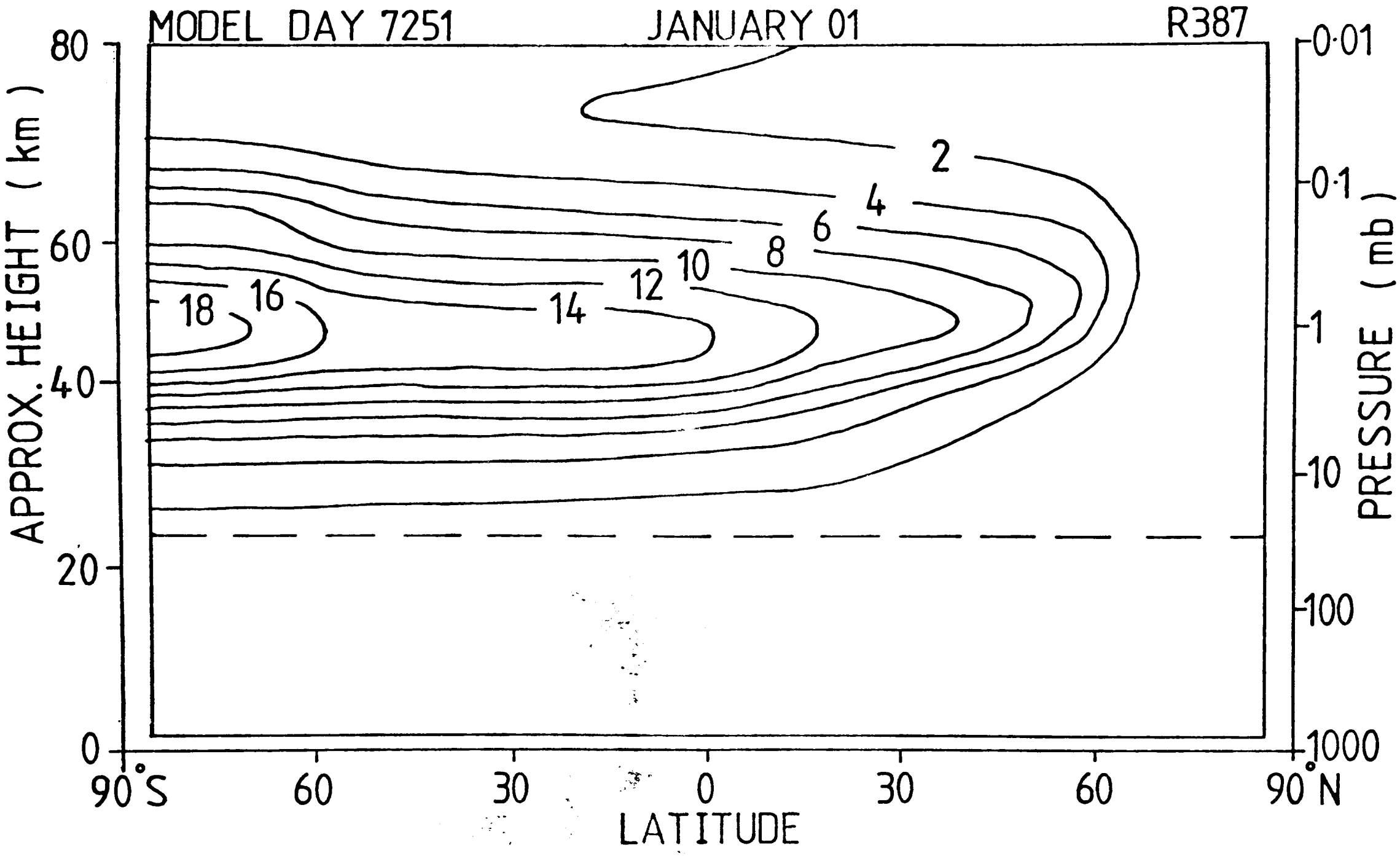

Fig.7.11(b) Solar heating rate (K/day) Run H

latitudes are not sufficient to balance the extra cooling and an annual cycle is produced in which temperature decreases are greater in summer than in winter.

Associated with the changes in temperature structure the strength of the jets in the middle stratosphere has been reduced with both easterly and westerly maxima decreased by about 10%. This is because, as discussed above, in the low and middle stratosphere the temperature decreases are greatest where the absolute temperatures are highest and thus the horizontal temperature gradients are reduced. Planetary waves are not explicitly included in this run but changes in the zonal wind field of the order described above could significantly affect their propagation and thus planetary wave eddy transport of heat, momentum and tracers. The effect of increased CO_2 on the meridional circulation is small with no uniform change : the greatest differences in heating rate due to advection by the mean motions occur in summer mid-latitudes where the heating by these means is small anyway. The magnitudes of the eddy heat fluxes have also changed very little.

The ozone concentration for day 7000 in Run F is shown in Fig. 7.12. The percentage difference in O_3 between Runs H and F is presented in Fig. 7.13 (this corresponds to the temperature changes of Fig. 7.9). An increase of 24 - 29% has occurred in the region of 42 km at all latitudes, this value is in good agreement with the result of Luther et al (1977) but slightly larger than that of Groves et al (1978), whose maximum increase was 22% at 45 km, and considerably larger than the 15% of Boughner (1978). The decrease observed in the lower stratosphere in some of the one-dimensional models is also seen in Fig. 7.13 but with considerable latitudinal variation. The peak decrease is nearly 10% at 24 km in low latitudes but in middle and high latitudes there is no decrease. At first this seems surprising; the increases in ozone which occur in the upper stratosphere should reduce the

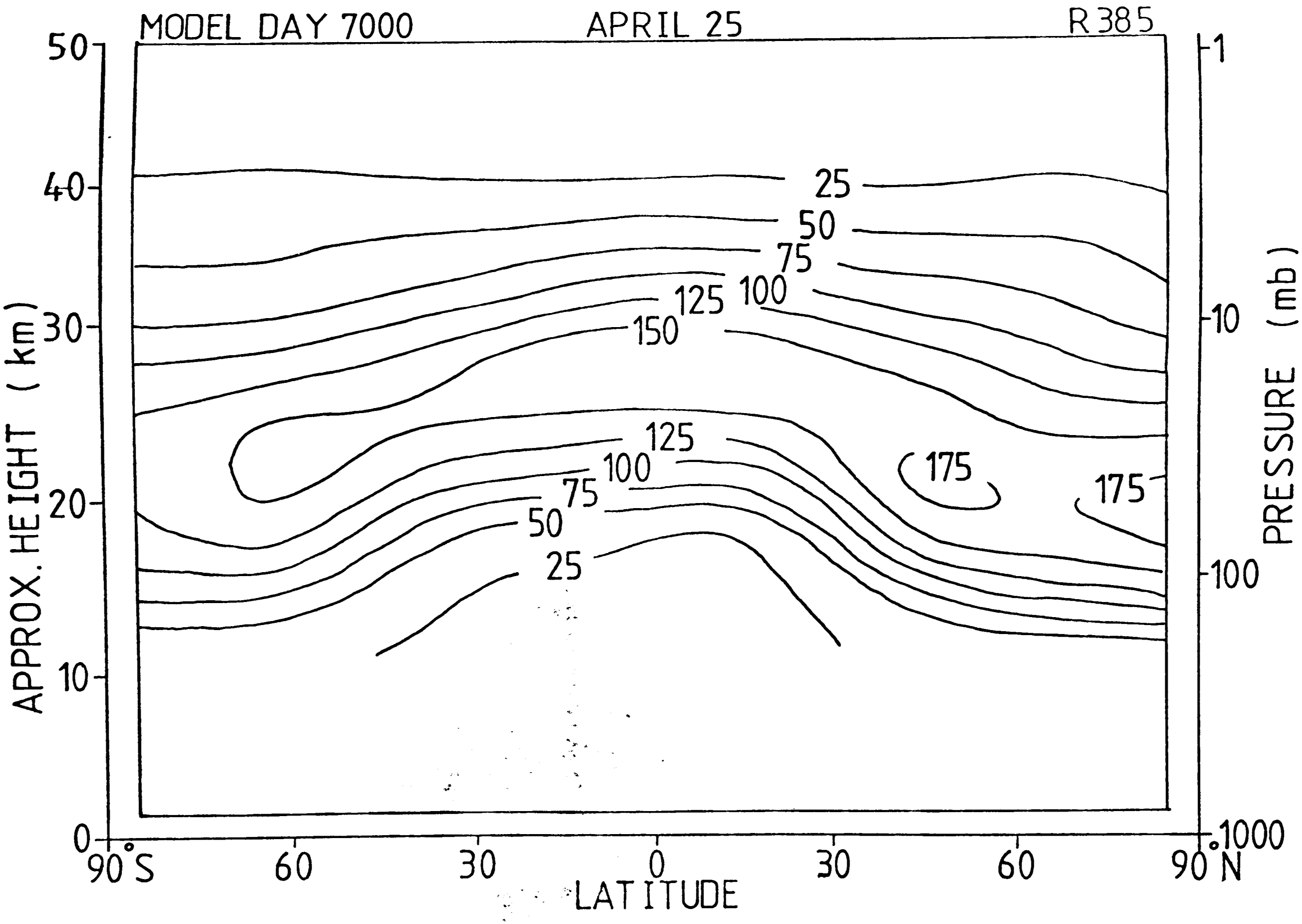

Fig.7.12 Ozone partial pressure (nb) Run F

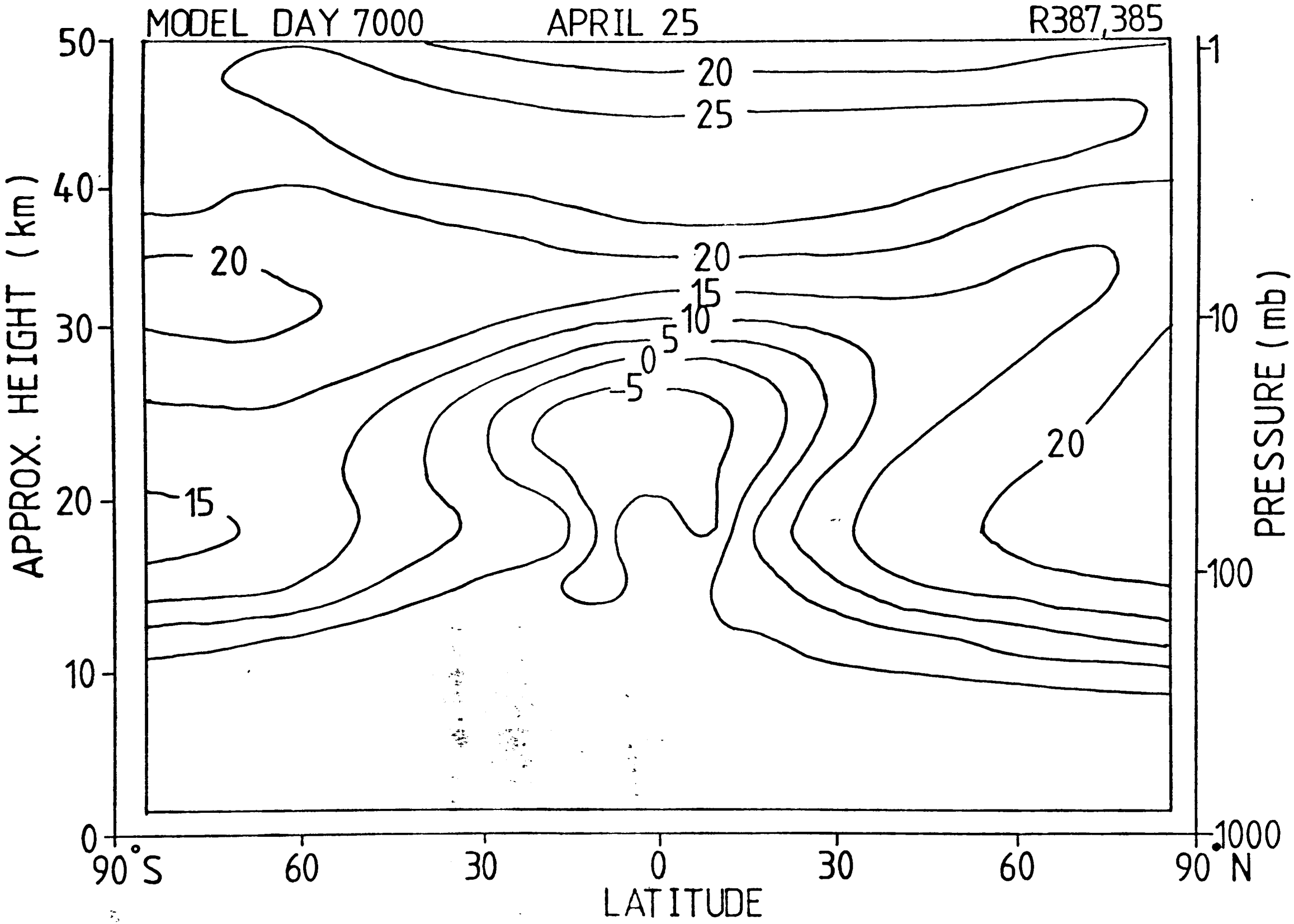

Fig. 7.13 Percentage increase in O_3 concentration Runs H, F

penetration of ultraviolet to lower levels at all latitudes. The cause of this lack of latitudinal symmetry may be inferred from Fig. 7.14 which shows for Runs F and H on day 7000 the rate of change of ozone at 24km due to:

(i) absorption of ultra-violet radiation and dissociation of O_2

(ii) other photochemical sources and dynamical effects

(iii) total = (i) + (ii).

In the perturbed case J_2, i.e. the production of O_3 due to (i), has indeed decreased at all latitudes however this has been offset by changes in the other photochemical contributions and the dynamical transports. Both NO_x and OH concentrations have been reduced (See Fig. 7.15) and in mid-latitudes in the southern hemisphere the changes in the chemistry over-compensate for the decrease in photochemical production. Thus there is a net increase in O_3 production here. As there is no uniform strengthening or weakening of the meridional circulation the increased production in mid-latitudes is reflected in an increased transport of O_3 from midlatitudes to the south pole where, as it is polar night, the ozone concentration is determined solely by dynamical effects. The result of all these factors is that the net production rate of ozone has decreased only in the summer hemisphere. The integrated result after several years is that the decrease in ozone concentration is only observed in the latitude range 30^oS - 30^oN where the input of solar radiation is high throughout the year.

The extent of the latitudinal asymmetry is revealed in Fig. 7.16 which shows the percentage increase in ozone column density as a function of latitude and time of year. There are large increases of about 20% near the north pole in summer and 14% in southern hemisphere high latitudes in spring. The difference between the hemispheres reflects the asymmetry in ozone distribution. In equatorial regions the increases vary between less than 2% and about 4% reflecting the 'reverse self-healing' effect in the lower stratosphere.

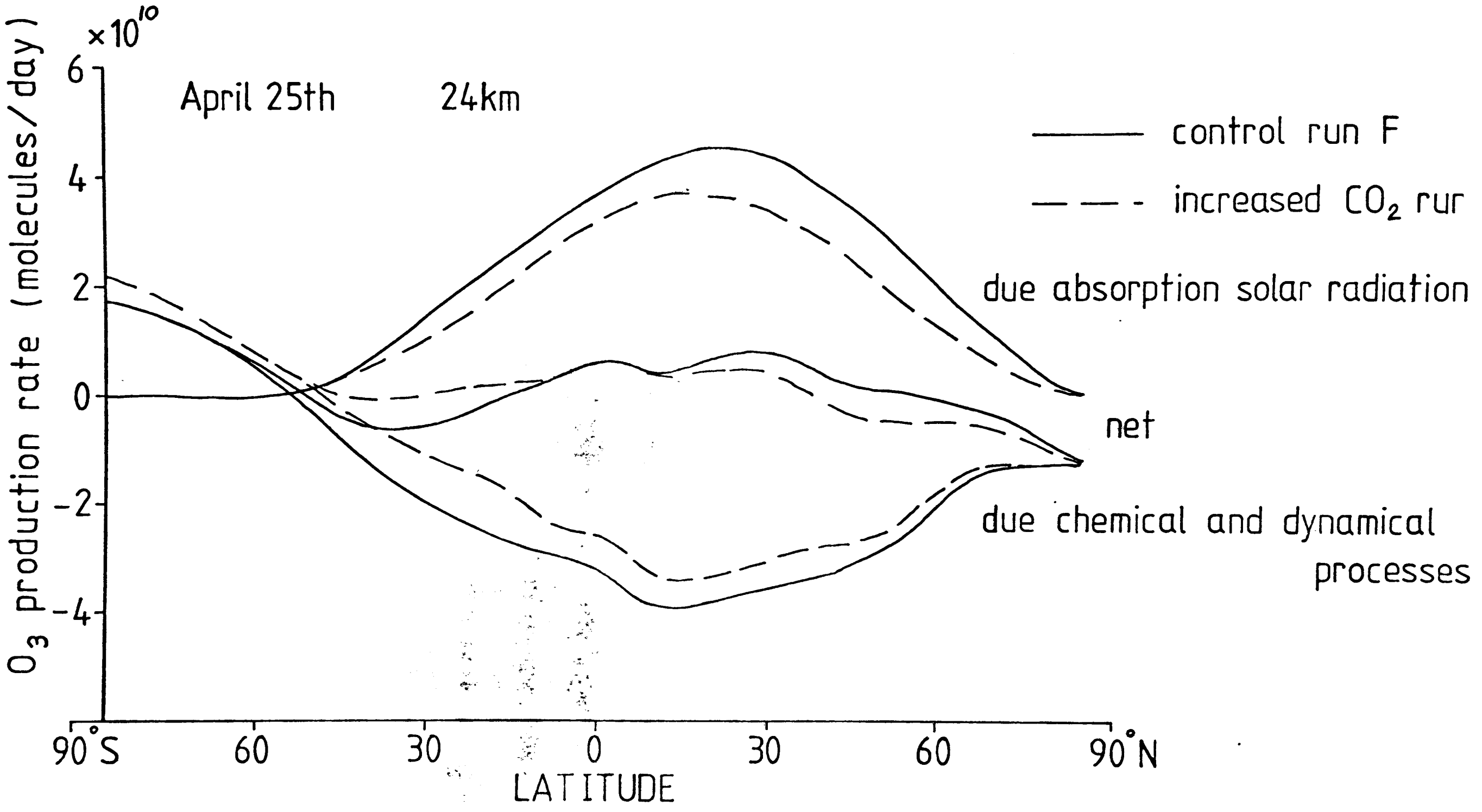
O_3 production rate (molecules/day)
×10^10
6
4
2
0
-2
-4
April 25th
24km
control run F
increased CO_2 rur
due absorption solar radiation
net
due chemical and dynamical processes
90°S
60
30
0
30
60
90°N
LATITUDE

Fig. 7.14

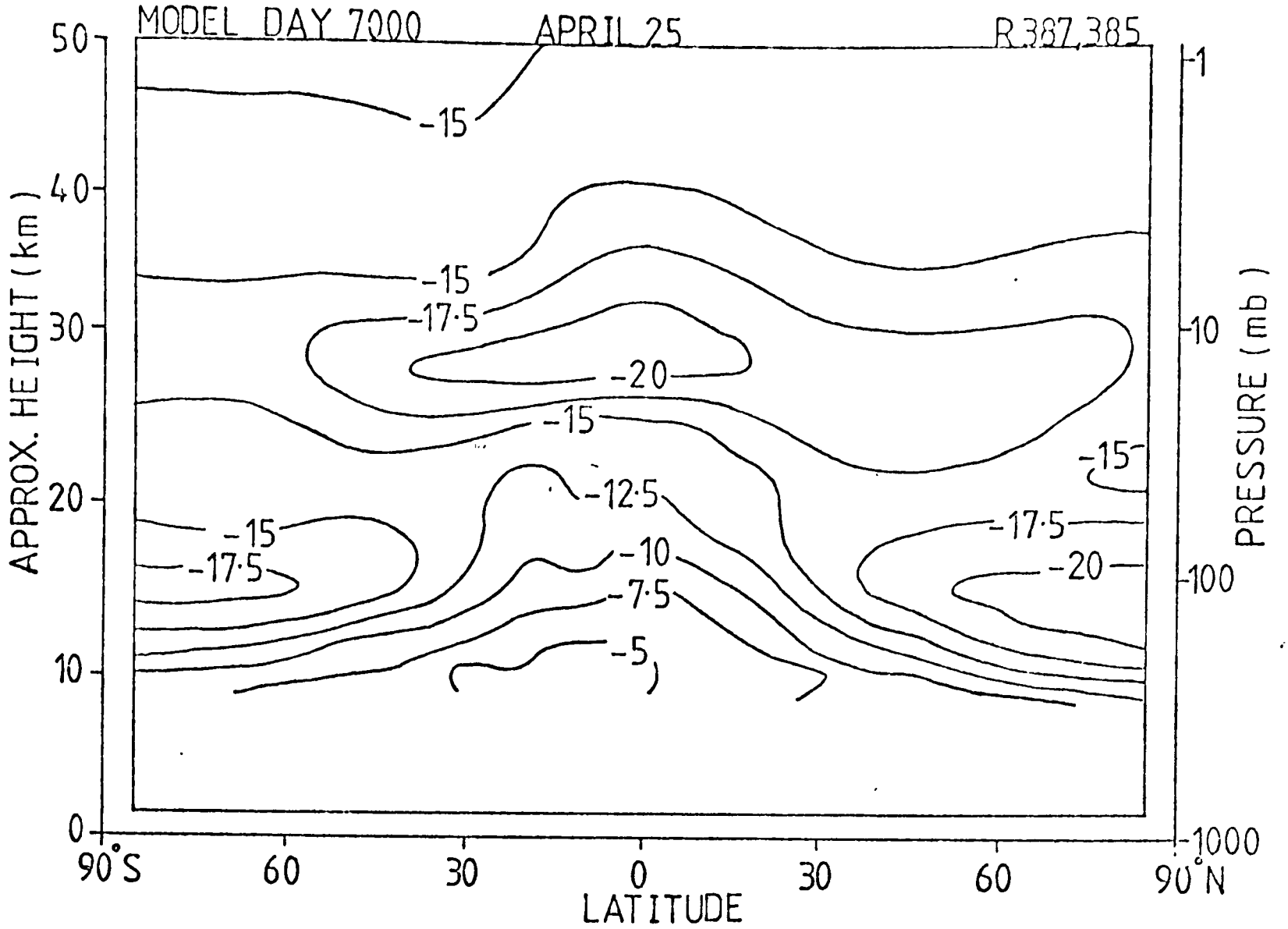

Fig.7.15(a) Percentage increase in NO_x concentration Runs H,F

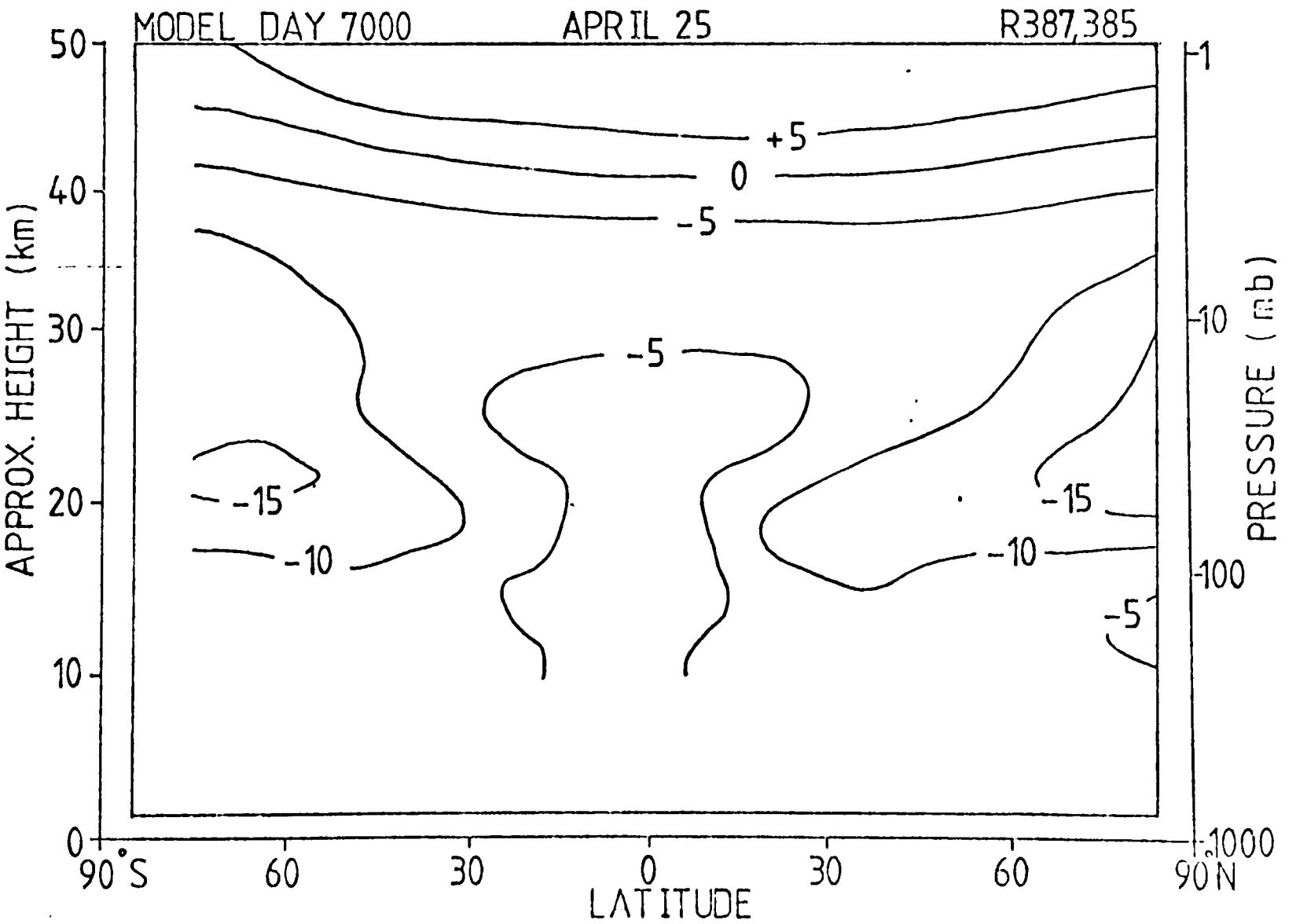

Fig.7.15(b) Percentage increase in OH concentration Runs H,F

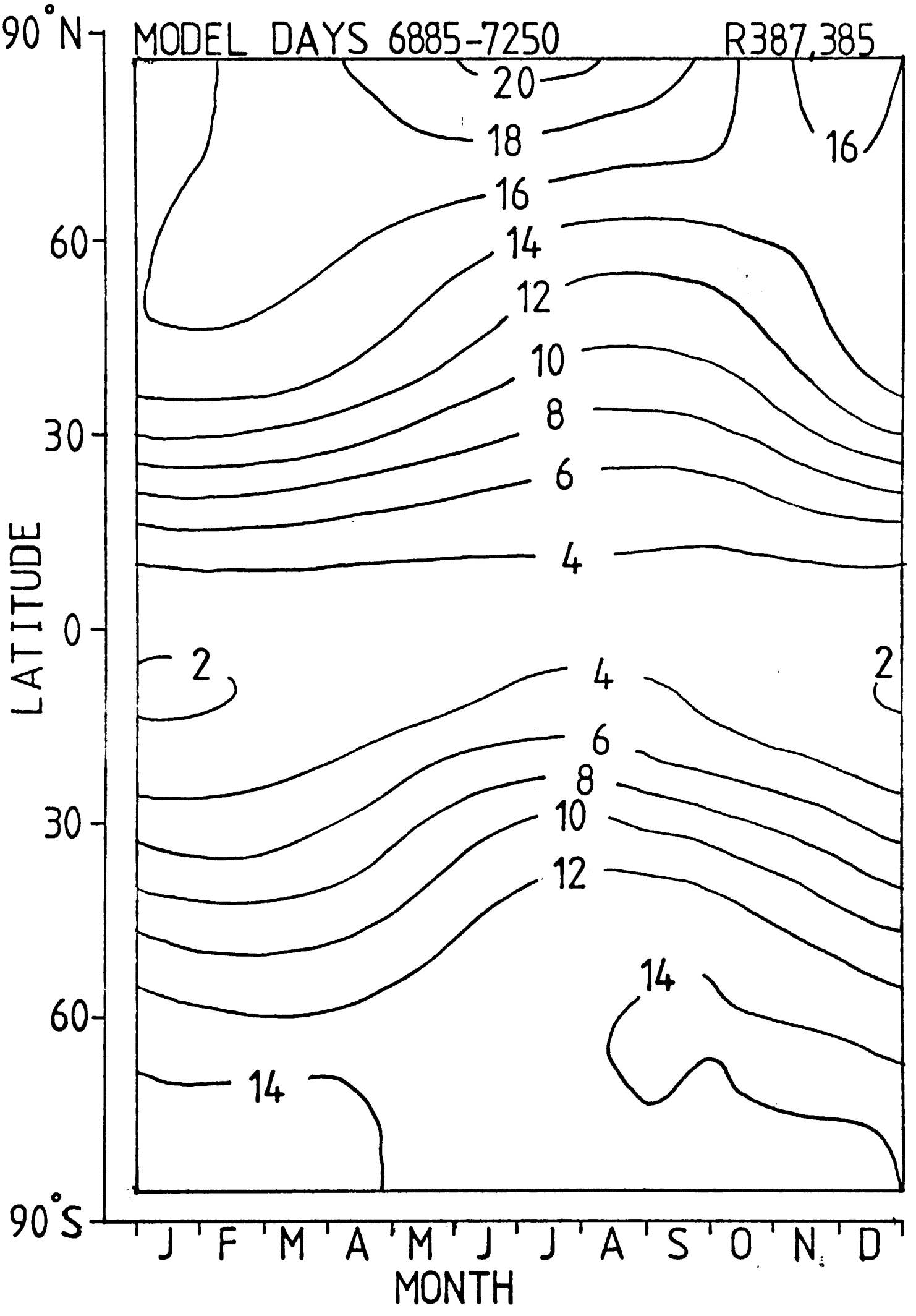

Fig.7.16 Percentage increase in O_3 column Runs H, F

The global increase in total ozone is around 9%. considerably larger than any of the values predicted by one-dimensional models (see Table 7.2). The changes in the upper stratosphere agree well with the results of Luther et al (1977) and Groves et al (1978) so that the discrepancies seem to be due to changes in the lower stratosphere. In this region ozone is predominantly dynamically controlled so a two-dimensional model should be more successful in predicting the ozone distribution. It is clear that photochemical, radiative and dynamical processes, and the feedback between them, are all important and should be included.

7.6 Variation of CO_2 with altitude

In all the above-mentioned calculations the CO_2 mixing ratio has been assumed constant with height. In the troposphere CO_2 released at ground level will be well mixed within a period of a few months but vertical transport in the lower stratosphere is slow and it is possible that there may be a decrease in CO_2 mixing ratio above the tropopause. Observational evidence of this is scarce. Volz et al (1977) give balloon measurements which show a drop from 327 ppm in the upper troposphere to 319 km at 20 km. Fig. 7.17 shows the CO_2 volume mixing ratio profile at $47^{o}N$ given by an experiment with the Model in which CO_2 was released at the surface uniformly between $30^{o}S$ and $60^{o}N$ at a rate equivalent to ten times the present release rate for a period of 7.3 model years. The initial mixing ratio was 300 ppm at all altitudes. This experiment was not intended to predict CO_2 mixing ratios but to give an indication of the trapping effect of the lower stratosphere. This is clearly demonstrated with a sharp decrease in mixing ratio between 12 and 20 km. Above 25 km the mixing ratio decreases only slowly with height and as all the radiation calculations discussed in this work are carried out only above 24 km

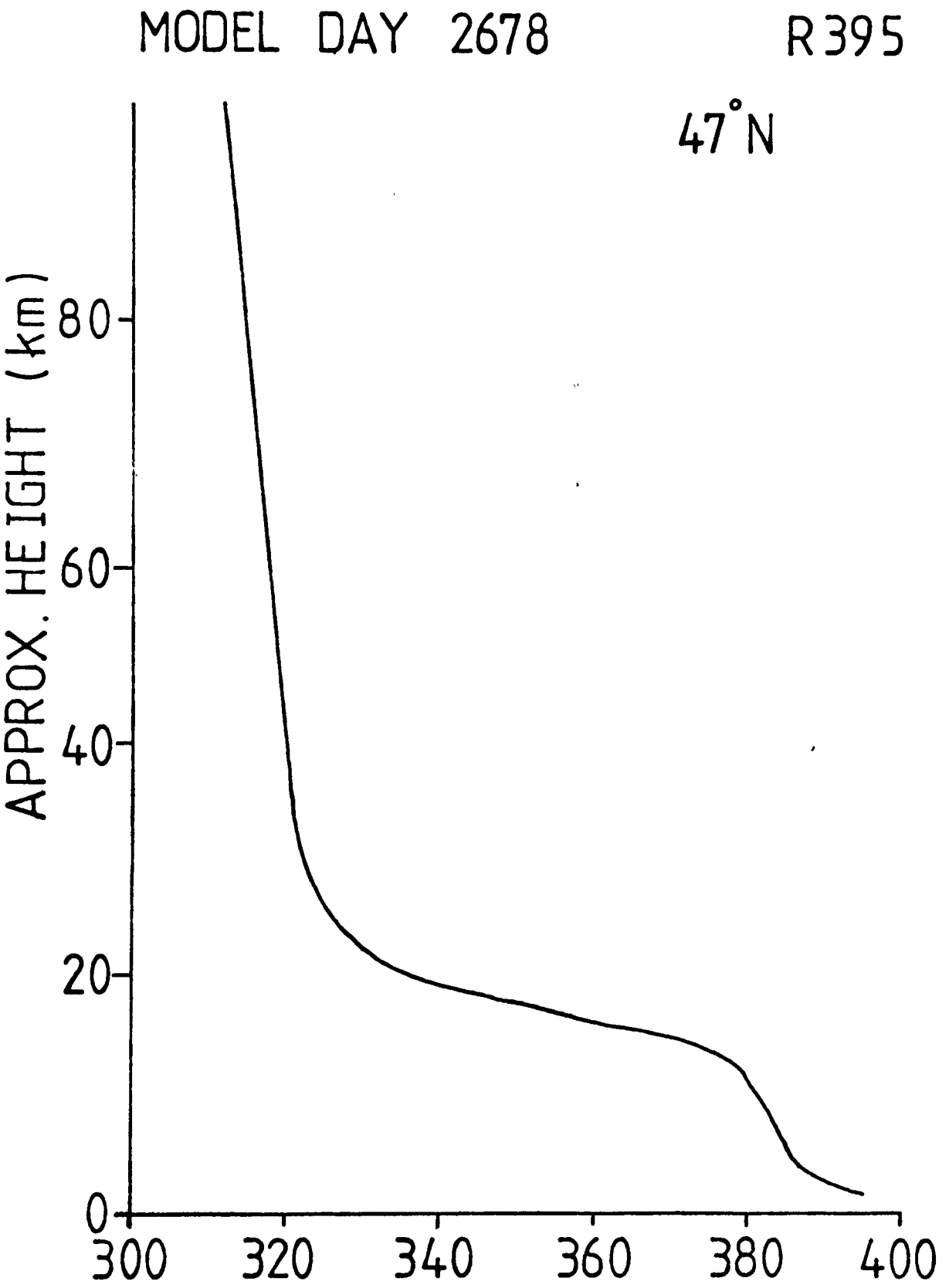

Fig.7.17 CO_2 volume mixing ratio (ppm)

the CO_2 gradient will not be important here. It should be remembered, however, that the CO_2 amounts stated refer to values in the stratosphere and mesosphere and not to those at the surface.

7.7 Chlorofluorocarbons and atmospheric ozone

Groves et al (1978) pointed out that the changes in ozone predicted due to increasing CO_2 concentrations were in exactly the opposite sense to those predicted due to fluorocarbons.

It has been remarked in previous sections of this chapter that ozone in the stratosphere may be sensitive to carbon dioxide amounts indirectly through the temperature-dependence of the reactions by which it is created and destroyed. It may also be directly affected by chemical reactions with pollutants. Various suggestions have been made as to anthropogenic activities which might be important in this respect e.g. the injection of NO_x by (i) high-flying aircraft (Johnson, 1971), (ii) the explosion of nuclear weapons (Foley and Ruderman, 1973) and (iii) the use of nitrogenous fertilisers (Crutzen, 1974). Investigation of these effects using the most recent measurement of the various reaction rates and including more reactions, however, has shown them to be small. Molina and Rowland (1974) suggested that the release of chlorofluorocarbons might endanger the ozone layer. The mechanism involved here is the transport of these chemicals, mainly $CFCl_3$ (called CFC11) and CF_2Cl_2 (called CFC12) which are used as propellants and refrigerants, from the troposphere, where they are stable, to the upper stratosphere where they are photodissociated by ultra-violet light releasing Cl and ClO. These latter species, collectively identified as ClO_x, act as catalysts in the destruction of odd oxygen in the same way as HO_x and NO_x in the cycles portrayed in Table 7.1 viz :

$$
\begin{array}{lll}
 & Cl + O_3 & \longrightarrow \quad ClO + O_2 \\
 & ClO + O & \longrightarrow \quad Cl + O_2 \\
\hline
\text{net} & O_3 + O & \longrightarrow \quad 2O_2 \\
\hline
\end{array}
$$

There are also reactions coupling the three cycles (see Table 2.1).

Since the proposition by Molina and Rowland many studies of possible ozone depletion have been made. Some of these are reviewed in reports by D.O.E. (1979), N.A.S. (1979) and N.A.S.A. (1979). Nearly all of the models used in these calculations are one-dimensional and therefore, although they can incorporate detailed chemical schemes, their representation of transport processes is poor and they are unable to include feedback between radiation and dynamics. Also most of these models do not allow feedback between the temperature and ozone fields. Ideally, a three-dimensional model including the chemical schemes would be used to study perturbations to the ozone layer. Such a model is, however, computationally very expensive and a compromise may be found in two-dimensional (zonal mean) models which can incorporate most of the important chemical and feedback processes and also investigate latitudinal and seasonal effects at less expense than their 3-D counterparts.

Pyle (1978, 1980) has described experiments with the Oxford two-dimensional model in which the effects of the release of CFC11 and CFC12 have been investigated. In these experiments, in order to reduce the computational expense, the fields of meridional wind and temperature were specified. Thus the feedback between the ozone concentration and the temperature and wind structure, via the absorption of solar radiation, was omitted. The results of a similar experiment in which the zonally-averaged fields of wind and temperature were calculated at each time-step will now be discussed.

The control run, Run F, has already been described; Run I includes a source of chlorine from CFCs. CFC11 and CFC12 were released into the bottom

model level uniformly between 30°N and 60°N. The total amount estimated to have been injected into the atmosphere before 1977 (i.e. 3.04 milliom tons CFC11 and 4.52 million tons of CFC12, McCarthy et al, 1977) was released in 2.5 model years and the subsequent release rate was at four times the average production rate between 1973 and 1976 (which is estimated at 1.34 million tons per year of CFC11 and 1.62 million tons per years of CFC12). Thus Run I simulates a situation of continuing and constant CFC release but a four times the estimated rate. It is therefore directly comparable with the CO_2 perturbation experiment Run H.

The latitude-time section of percentage change in ozone column density for one model year, corresponding roughly to the year 2045, is given in Fig. 7.18. The largest reductions (>20%) in each hemisphere occur in high latitudes in spring, reflecting the time of maximum ozone content. Near the equator, however, the changes vary between about -8 and -9%. Thus any attempt to estimate increased fluxes of ultraviolet radiation to the earth's surface following a depletion of ozone should include a dependence on latitude. Fig. 7.19 shows the cross-section of percentage change in ozone concentration on day 7000 (representing April in about 2045). The maximum depletions of 30 - 40% occur at 40 km while in the lower stratosphere there are increases of up to 5% in low latitudes. As in Run H this 'self-healing' accounts for the minimum change in O_3 column density in equatorial regions. Very few one-dimensional models have shown this increase. The reduction in global total O_3 predicted by Run I is 14%; a similar value to those given by I-D calculations. It is interesting to compare Figs. 7.18 and 7.19 respectively with Figs. 7.16 and 7.13 which show the corresponding fields for the increased CO_2 case (Run H). The structure of the changes is strikingly similar although, of course, in the opposite sense.

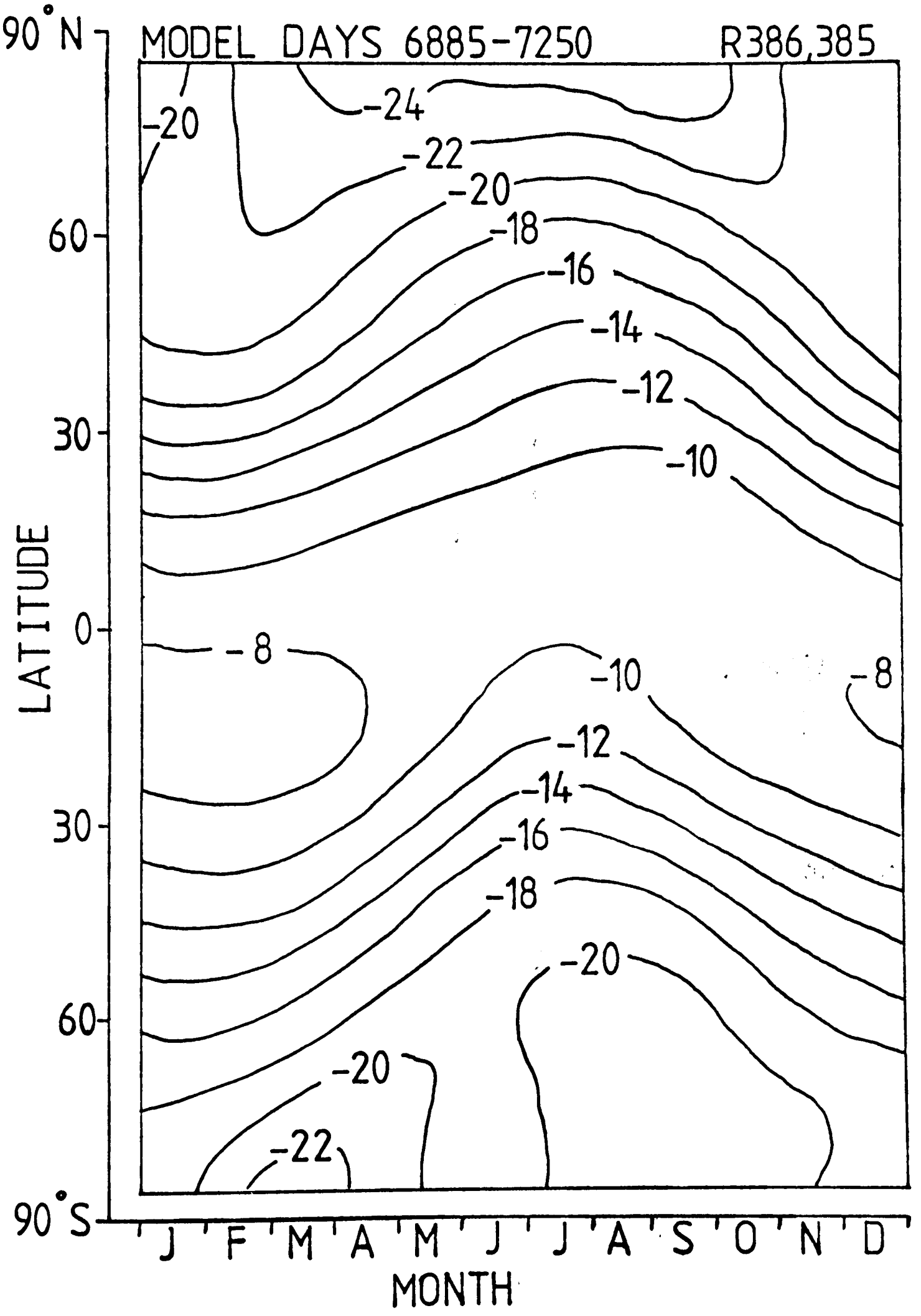

Fig.7.18 Percentage increase in O_3 column Runs I, F

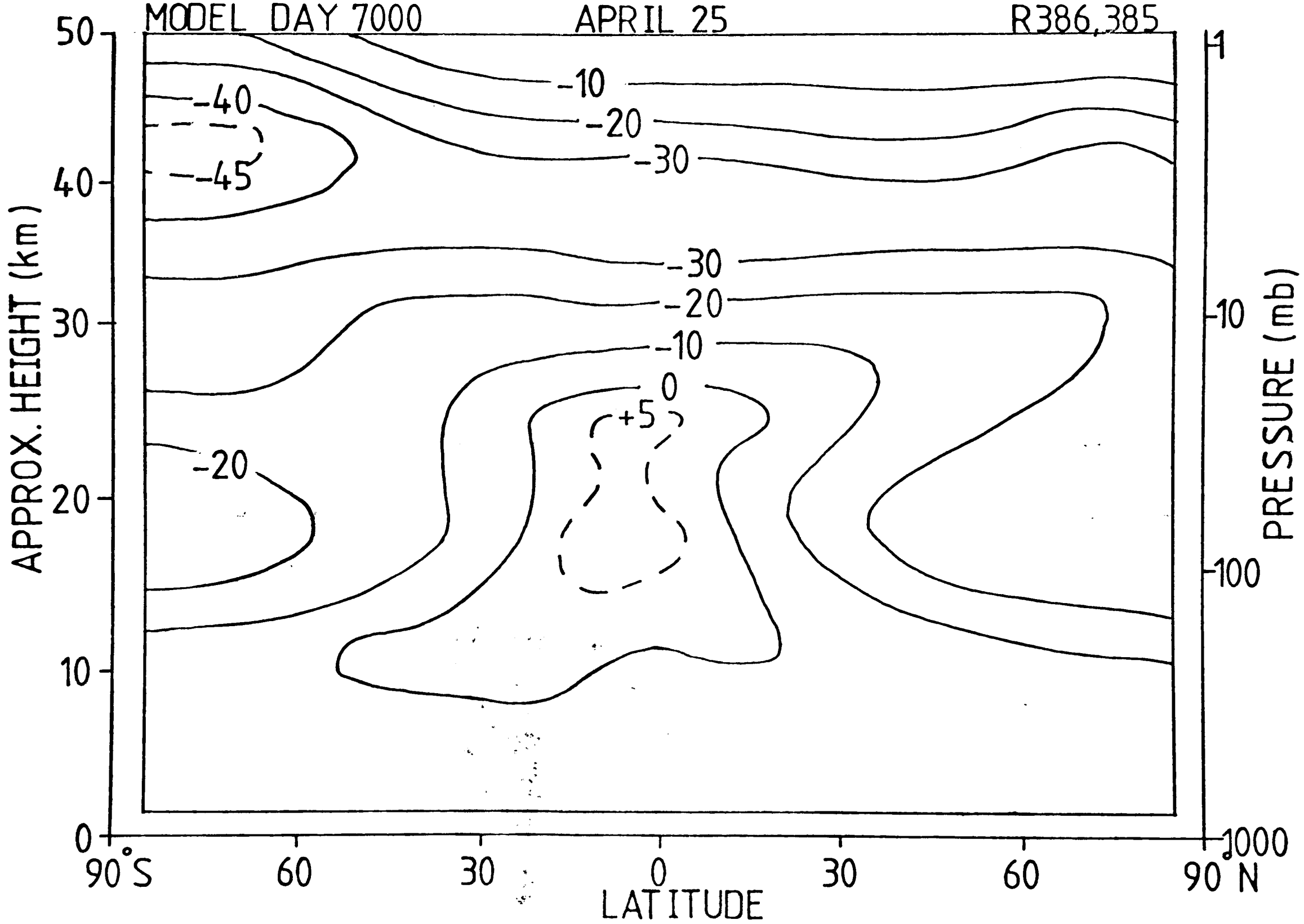

Fig. 7.19 Percentage increase in O_3 concentration Runs I, F

A reduction in ozone concentration results in decreased absorption of solar ultraviolet radiation and thus to lower temperatures. The temperature changes found in Run I relative to Run F are shown in Fig. 7.20; largest decreases, of about 10K, occur at 40 km in the northern hemisphere where temperatures are higher. Significant reductions are confined to an altitude range 30 - 50km; below this, in low latitudes, there is an area of slight (< 1K) increase corresponding to the region of increased ozone concentration and solar heating. Associated with the changes in temperature the strength of the zonal winds in the upper stratosphere has been reduced although the effect is smaller and more localised than in the increased CO_2 case (Run H). Again there is no significant or uniform change in the meridional circulation.

It appears, therefore, that the effects of CO_2 and CFCs on the ozone layer are of similar magnitude and in the opposite sense. It may not be assumed, however, that such perturbations are linearly additive (Tuck, 1977) and a further experiment has been carried out in order to assess their combined effect.

7.8 Simultaneous effects of CO_2 and CFCs on stratospheric ozone

7.8.1 One-dimensional calculations

Most assessments of possible changes in stratospheric ozone have focussed on the effects of a single perturbation while in the real atmosphere many changes occur at the same time. Some studies (e.g. Logan et al, 1978) have looked at simultaneous perturbations by species which react chemically with O_3 and found that they ineract ina non-linear fashion as expected given the coupling reactions in the $ClX - HO_x - NO_x$ photochemistry. (N.B. $ClX \equiv Cl + ClO + HCl + ClONO_2$). Increasing levels of CO_2 and CFCs have opposite effects on O_3 but both reduce upper stratospheric temperatures. Thus it might be expected that in a coupled run the larger temperature decreases would result in an amplification of the CO_2 effect.

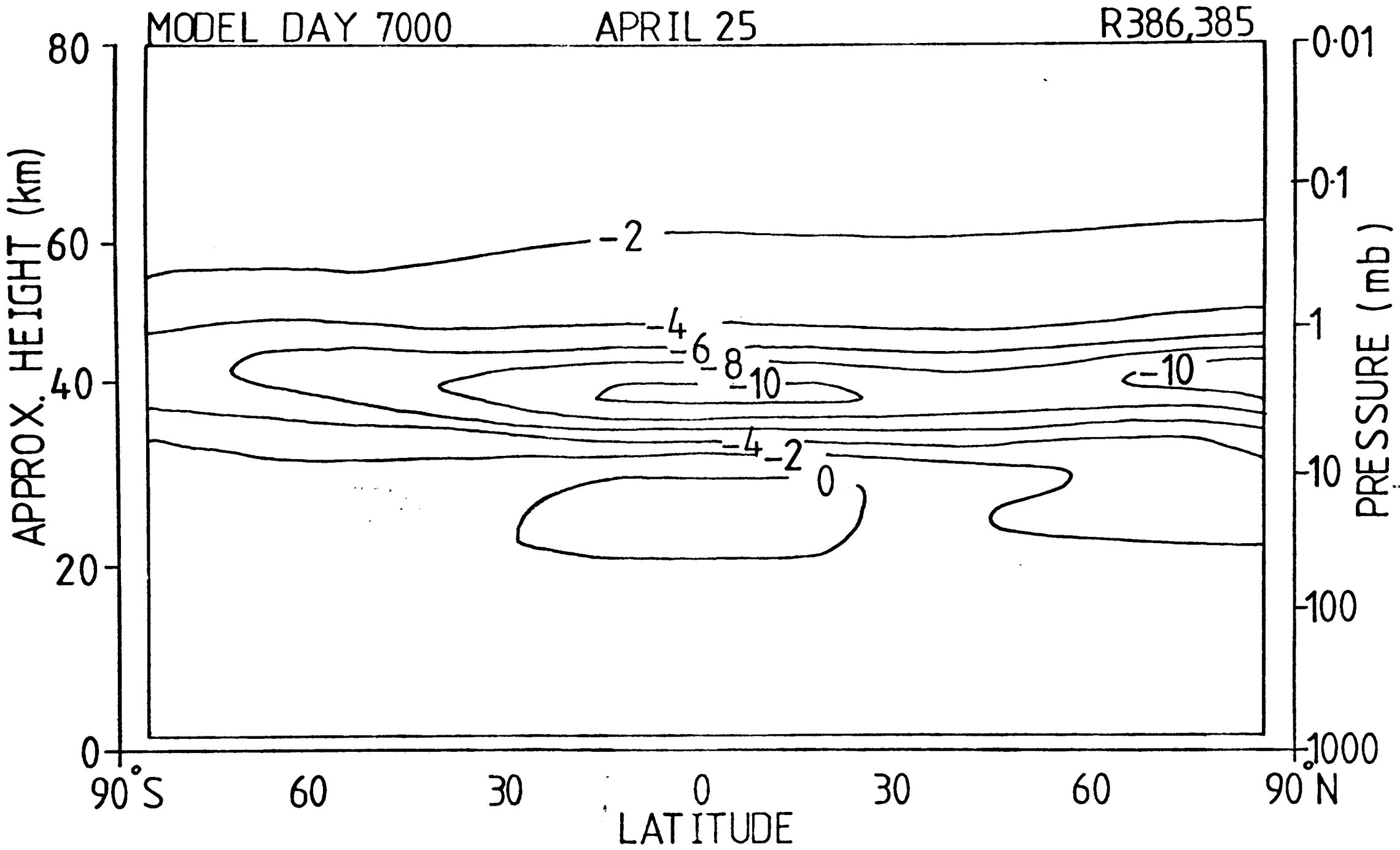

Fig.7.20 Change in temperature (K) Runs I,F

Groves and Tuck (1979, 1980b) investigated the simultaneous effects of CO_2 and CFCs on stratospheric ozone. Although they found that the inclusion of natural chlorine-containing species reduced the calculated ozone increase due to CO_2 doubling their results in the coupled experiment showed only a small departure from linearity. They concluded that increasing atmospheric CO_2 levels will substantially alleviate the reductions in O_3 caused by CFC release.

Isaksen et al (1980) came to a different conclusion. Using a one-dimensional photochemical model they calculated the effect on the ozone column of doubling the CO_2 concentration for several different, fixed, total chlorine amounts and found that the temperature (CO_2) effect decreased significantly as the chlorine content increased. Thus a CO_2 doubling produced a 5.1% increase in total ozone when there were no chlorine species included but only 2.8% when the ClX content was 4.4 ppb (the mixing ratio predicted for 2040 if CFC release continues at its 1975 value). This is ascribed to the decreased conversion at lower temperatures of active to inactive chlorine by the reaction

$$Cl + CH_4 \rightarrow HCl + CH_3 \qquad k = 7\times10^{-12}\, e^{-1269/T} \tag{7.2}$$

At higher total chlorine amounts the ClO_x cycle dominates the HO_x and NO_x cycles in ozone destruction and thus at lower temperatures, with more active chlorine present, the ozone increase due to CO_2 doubling is not as large. Isaksen et al concluded that the CO_2 effect would only slightly reduce the destruction of O_3 by the addition of CFCs. Their calculations are, however, likely to overestimate the CFC effect because they simulated the doubling of the CO_2 concentration by decreasing the model temperatures by a specified amount at each level and thus no feedback was allowed between ozone concentration and temperature.

Although Groves and Tuck (1979) and Isaksen et al (1980) come to different conclusions their results for the effect of CO_2 doubling in the presence of different ClX amounts are apparently quite similar. Table 7.3 shows their estimates (and some from the present work to be discussed in the next section). The main differences come in their assessments of the CFC effect. By 2040 the CFCs alone have caused a depletion of 13.9% in the model of Isaksen et al but by 2060 the depletion is only 8.6% in that of Groves and Tuck. The CO_2 effect is therefore considered to have more of an ameliorating effect in the latter work. The calculations of O_3 depletion due to CFCs by Isaksen et al are the more consistent with other one - dimensional models (see e.g. N.A.S.A. 1979) and the present work but few of these contain the diurnal variations included in the model of Groves and Tuck.

7.8.2. A two-dimensional calculation of the coupled perturbation

The simultaneous effects of increasing CO_2 and CFCs were investigated in the Oxford two-dimensional model. Run J was obtained from control Run F by including both the CO_2 increases as described in section 7.4 for Run H and the CFC11, CFC12 releases described in section 7.7 for Run I.

The percentage change in ozone concentration as a function of height at the equator is shown for April 2045 in Fig. 7.21 with the corresponding profiles from Runs H and I. There is a decrease in O_3 between 20 and 45 km, an increase above and a small region of 'self-healing' below. At nearly all altitudes, and especially at around 40 km where the depletion is greatest, the changes are more negative than would be estimated from summing the results of Runs H and I. This effect is reflected in the changes in column density at all latitudes, as shown in Fig. 7.22, and therefore in the changes in global total ozone, see Table 7.3.

Table 7.3

Results of coupled experiments

Percentage change in total O_3 for various CO_2 and ClX contents.

Groves and Tuck (1979) :

CO_2 content (ppm)	ClX content predicted for year		
	natural	2020	2060
275	0		-8.6
600	+3.2	-2.6	-6.3

Isaksen et al (1980) :

	natural	2000	2020	2040
300	0	-7.4	-11.1	-13.9
600	+4.3	-4.1	- 8.1	-11.1

present work :

	zero ClX	2000	2020	2040
320	0	-3.2	-8.3	-12.8
400	+3.0	-0.6		
500	+5.9		-4.1	
625	+8.8			-8.1

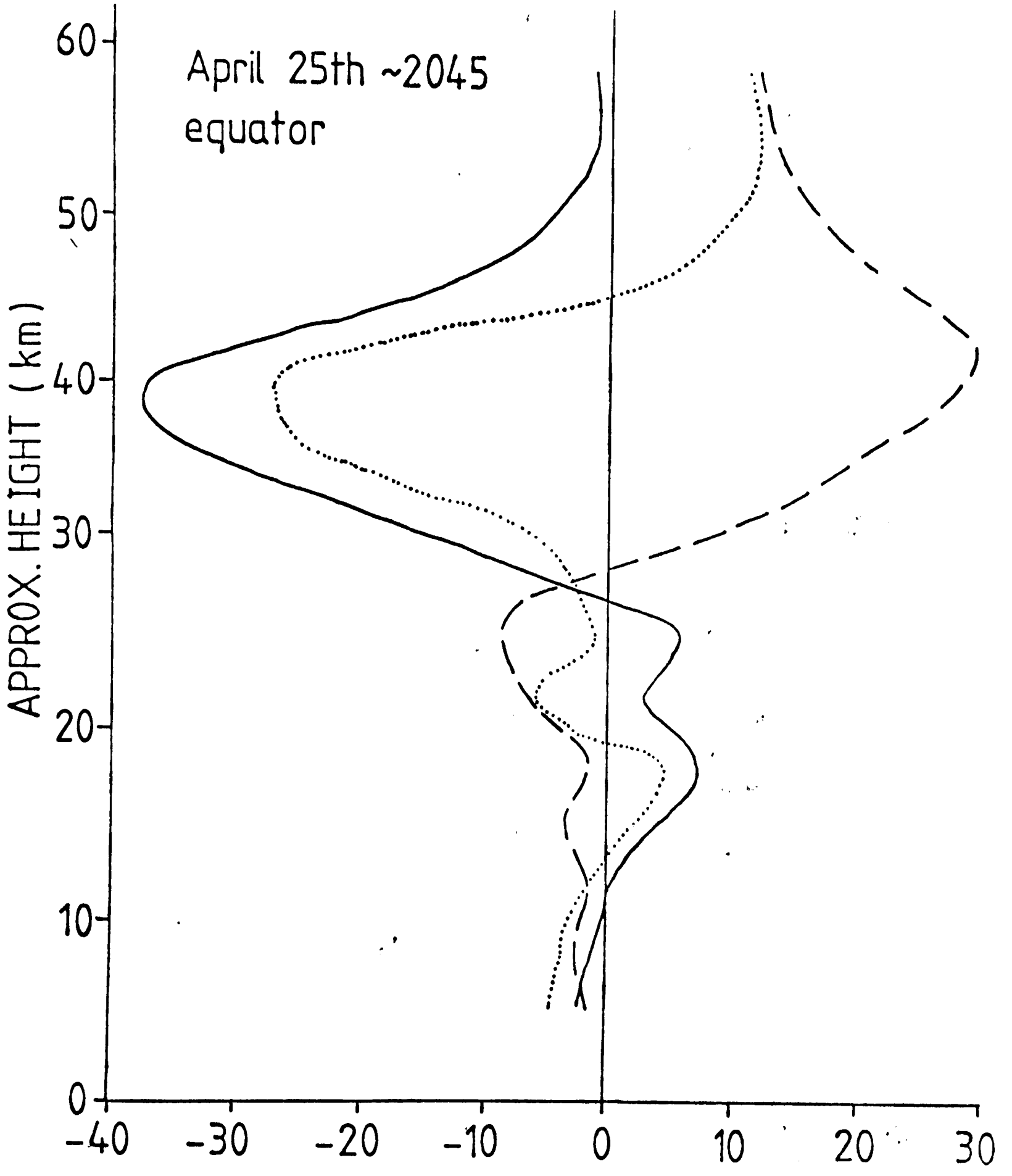

Fig.7.21 Percentage increase in O_3 concentration relative to Run F

— — — — Run H

———— Run I

..... Run J

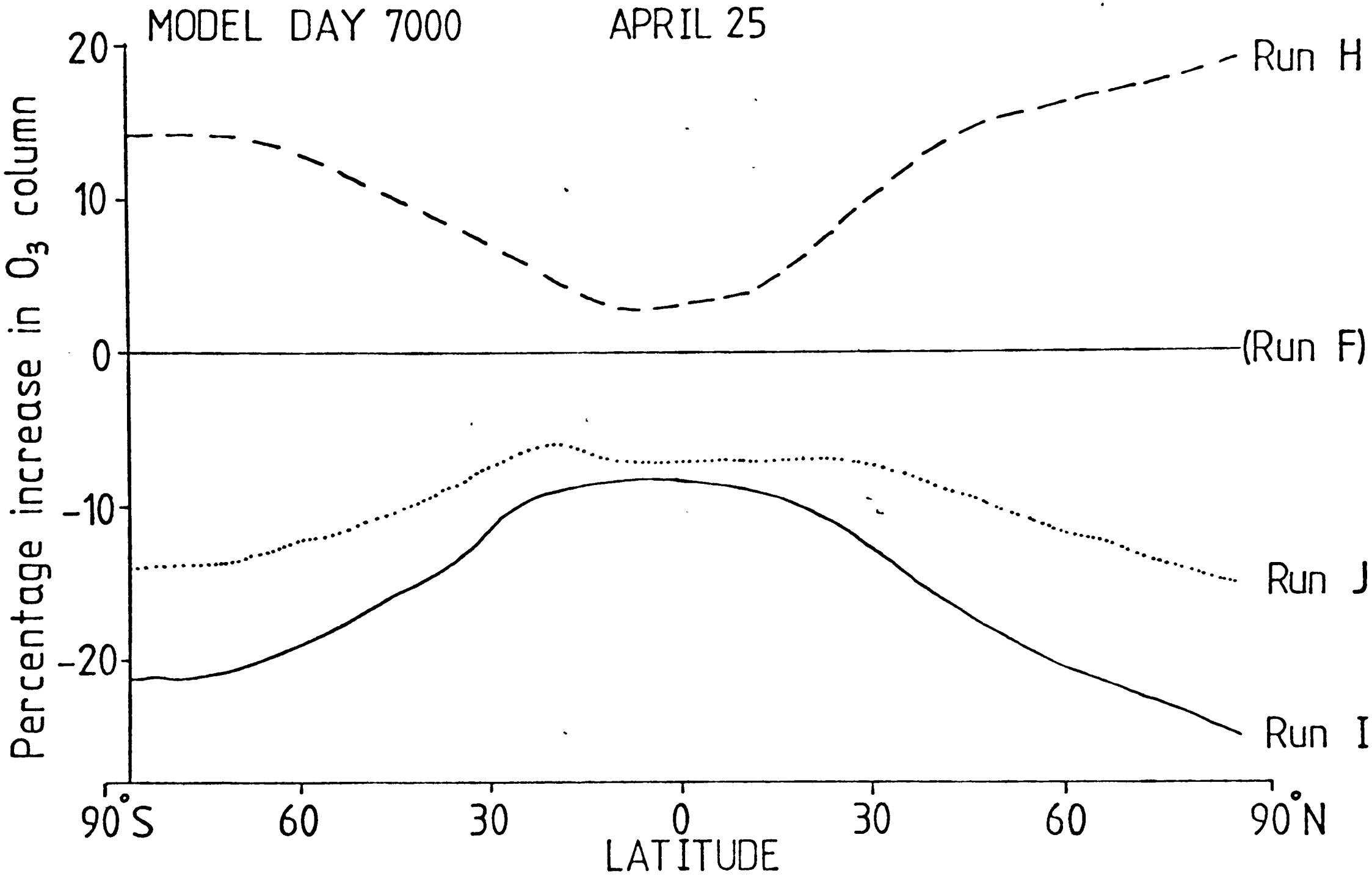
MODEL DAY 7000
APRIL 25
Run H
(Run F)
Run J
Run I
20
10
0
-10
-20
Percentage increase in O_3 column
90°S
60
30
0
30
60
90°N
LATITUDE

Fig.7.22

Thus the present work demonstrates the same effect found in the one-dimensional models discussed in section 7.8.1. i.e. that the influence of additional CO_2 declines as the chlorine content increases. In order to understand this it is necessary to look more closely at the temperature dependence of ozone. The destruction of ozone by ClO_x may be included by the addition of another term on the right hand side of Equation (7.1), assuming equilibrium between Cl and ClO. The equilibrium equation becomes :

$$J_2[O_2] = \frac{k_3}{k_2}\frac{J_3}{[O_2][M]}[O_3]^2 + \frac{k_8}{k_2}\frac{J_3}{[O_2][M]}[OH][O_3] + k_{17}[NO][O_3] + k_{50}[Cl][O_3]$$

which may be written :

$$S = \alpha A e^{-a/T}[O_3]^2 + \alpha B e^{-b/T}[O_3] + C e^{-c/T}[O_3] + D e^{-d/T}[O_3] \quad (7.3)$$

where S, A, B, C and D are independent of temperature, the exponential terms are the temperature-dependent contributions of the reaction rates and $\alpha \equiv J_3/J_2$. $[OH]$ and $[NO]$ have been assumed independent of temperature (this has been shown to be a fair assumption in previous model experiments); $[Cl]$ will be discussed shortly.

Differentiating Equation (7.3) with respect to T^{-1} and rearranging we obtain :

$$\frac{d\ln[O_3]}{dT^{-1}} = \frac{(a + bf_1 + cf_2 + df_3)}{(2 + f_1 + f_2 + f_3)} - \frac{(1 + f_1)}{(2 + f_1 + f_2 + f_3)}\frac{d\ln\alpha}{dT^{-1}} \quad (7.4)$$

Table 7.4

Percentage of total ozone destruction due to the various cycles at 40 km, equator, April ~2045.

Cycle	Run F	Run H	Run I	Run J
pure oxygen	26.3	24.4	6.6	4.5
HO_x (f_1)	17.9 (0.68)	19.6 (0.80)	9.5 (1.44)	8.7 (1.95)
NO_x (f_2)	55.8 (2.13)	56.0 (2.29)	30.0 (4.54)	25.9 (5.79)
ClO_x (f_3)	0 (0)	0 (0)	53.9 (8.17)	60.9 (13.59)

where f_1, f_2 and f_3 are the ratios of the rate of destruction of ozone by the HO_x , NO_x and ClO_x cycles, respectively, to the pure oxygen scheme. Assuming d $\ln \alpha / dT^{-1} = 0$ (this may introduce errors of about 15%, see Pyle, 1976) we see that the temperature dependence of ozone is an average of the four schemes, weighted according to their relative strengths.

Using the reaction rates given in Table 2.1 a = 2810, b = 510 and c = 1200. Contributions to d come from k_{5o} and from the temperature dependence of [Cl]. Considering k_{5o} alone d = 257. Cl , however, is strongly, and inversely, dependent on temperature through reaction (7.2) from which it might be assumed that $[Cl] \propto e^{126/T}$ and $k_{5o}[Cl] \propto e^{1000/T}$ giving d = -1000. For present considerations we take d = 0; this will only be used for the purposes of illustration and will not affect the conclusions later in this Chapter. Thus the ClO_x cycle is by far the least sensitive to temperature changes of the four destruction cycles.

The relative importance of each cycle at the equator near 40 km is shown for Runs F, H, I and J in Table 7.4. It demonstrates that for Runs F and H the oxygen and HO_x cycles are of similar importance while the NO_x cycle is about twice as large. In Runs I and J the destruction by ClO_x is clearly the most effective with the NO_x cycle contributing about half this amount and the HO_x and oxygen cycles less than 10% of the total. Also given in brackets in Table 7.4 are the values of f_1, f_2 and f_3 in each case.

Using the temperature factors and f-factors referred to above the temperature dependence of ozone was calculated from Equation (7.4) (neglecting the d $\ln \alpha$ / dT^{-1} term) for the four runs :

Run	$d \ln[O_3] / dT^{-1}$ (K)
F	1188
H	1172
I	557
J	461

In Runs I and J, which include chlorine chemistry, ozone shows much less dependence on temperature than in the cases without chlorine. Thus the CO_2 effect is less for an atmosphere containing chlorine.

The small difference between the value obtained for Run F and that for Run H, and the rather larger one between Runs I and J, can be ascribed to the fact that the temperatures appropriate to each Run are different and the temperature dependence of ozone itself depends slightly on temperature through the changing emphasis of the destruction cycles i.e. f_1, f_2 and f_3. Thus the ClO_x cycle is responsible for 61% of the O_3 destruction in Run J and only 54% in Run I. In the work of Isaksen et al (1980) it is this effect which is used to explain the non-linearity of the simultaneous CO_2 and CFC injections. The present work, however, shows that it is the temperature dependence of the ClO_x destruction cycle which is of importance and not, to a first approximation, the temperature dependence of the chlorine species themselves.

In Fig. 7.23 $\log_{10}[O_3]$ is plotted versus T^{-1} using values obtained from the Model. The slope is much steeper for Runs F and H than for Runs I and J, as expected from the simple photochemistry discussed above. The temperatures at the equator near 40 km on day 7000 for Runs F and H were 253 and 242 K respectively and $d \ln [O_3] / dT^{-1}$ at an intermediate temperature for these Runs is about 1550K. At the same place and date the temperatures in Runs I and J were 242 and 230K respectively, the slope of the appropriate

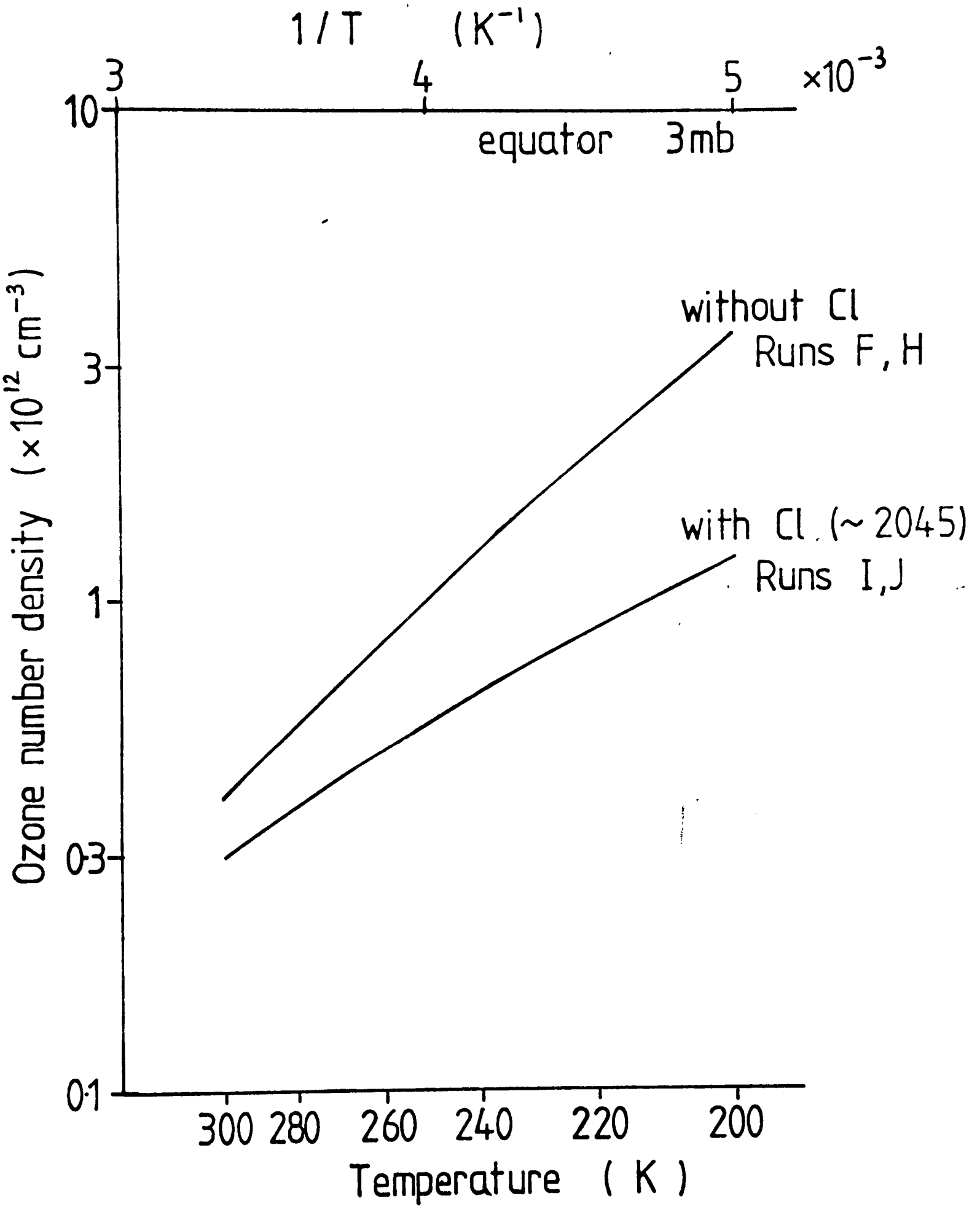
1/T (K⁻¹)
3
4
5
×10⁻³
10
equator 3mb
Ozone number density (×10¹² cm⁻³)
3
1
0·3
0·1
without Cl
Runs F, H
with Cl (~2045)
Runs I, J
300 280 260 240 220 200
Temperature (K)

Fig. 7.23

graph in Fig. 7.23 gives d ln $[O_3]$ / $dT^{-1} \simeq$ 800 K. Both these values are higher than those obtained by the rough photochemical calculations; the difference is due to the neglect of d ln α / dT^{-1} (which is, in fact, negative) in Equation (7.4) and of the temperature dependence of $[O_2]$, $[M]$ and, to a lesser extent, $[NO]$ and $[OH]$ in a, b and c and also to the approximate assumption of a value for d.

The non-linearity of the simultaneous effects of CO_2 and CFCs may now be investigated further. The decrease in temperature of Run H relative to Run F at the equator near 40 km on day 7000 will cause an increase in ozone concentration :

$$\frac{\Delta [O_3]}{[O_3]} = 1550\ \Delta(T^{-1}) = \frac{1550.11}{253.242} = 0.28$$

A 28% increase may be observed in Figs. 7.13 and 7.21.

The difference between Runs I and J will be :

$$\frac{\Delta [O_3]}{[O_3]} = 800\ \Delta(T^{-1}) = \frac{800.12}{242.230} = 0.17$$

From Fig. 7.21 the ozone concentration at 40 km in Run I is 63% of that of Run F so the concentration of Run J should be 1.17 x 63% = 74% of Run F. This is in good agreement with the 73% shown in Fig. 7.21.

7.9 Conclusions

In this Chapter the effects of increasing CO_2 on the temperature and ozone structure of the atmosphere have been investigated. This included the first calculation of the latitudinal variations of the changes up to the stratopause. There were large increases in ozone in the upper stratosphere but a striking latitudinal dependence in the lower stratosphere with decreased ozone in low latitudes. The work of Pyle (1980) in calculating ozone depletion

due to CFCs was extended in that feedback between the ozone, temperature and wind fields was allowed. The changes in O_3 due to CFCs were of similar magnitude and in exactly the opposite sense to those predicted for CO_2. An experiment including simultaneous perturbation by CO_2 and CFCs showed that the CO_2 effect does not reduce the CFC effect by as much as would be expected from a linear addition of the changes predicted in the separate experiments. A simple photochemical theory was used to show how the temperature dependence of O_3 is decreased in the presence of chlorine-containing species and values of $d \ln[O_3] / dT^{-1}$ from the model introduced to explain the non-linearity. The effect on ozone of increased CO_2 is lessened at higher atmospheric ClX levels because the destruction of O_3 in the ClO_x cycle is significantly less dependent on temperature than its destruction in the other cycles.

Thus the effects of various pollutants may not be assumed to be linearly additive. A perfect experiment would include all possible feedbacks and allow for all possible combinations of pollutants. As such a model does not, as yet, exist the experimenter must be aware of the limitations of the model she uses.

CHAPTER 8

The general circulation of the stratosphere and mesosphere

8.1 Introduction

The general circulation of the stratosphere and mesosphere depends on many physical processes and in order to understand the circulation each process must be identified and its relative importance assessed. Any theories resulting must be able to explain not only the mean state of the atmosphere but also interannual variability, hemispheric asymmetry and seasonal fluctuations.

The mean zonal wind and temperature fields for solstice conditions up to 75 km were portrayed in Figs. 1.2 and 1.1 respectively and in Chapter 6 the ability of the Model to reproduce the features of these fields was discussed. It was found to be quite successful at altitudes lower than about 65 km but unsatisfactory above as the cold summer mesopause and closure of the stratospheric jets were not reproduced. In this chapter the heat and momentum budgets of the stratosphere and mesosphere will be reviewed and the influence of planetary waves on the mean circulation investigated using the Model.

8.2 Heat and momentum budgets and the mean meridional circulation

The zonally averaged zonal momentum and thermodynamic equations in a spherical coordinate system may be written (e.g. Holton, 1975) :

$$\frac{\partial \bar{u}}{\partial t} = -\frac{\bar{v}}{a\cos\phi}\frac{\partial}{\partial\phi}(\bar{u}\cos\phi) - \bar{w}\frac{\partial \bar{u}}{\partial \xi} + f\bar{v}$$

$$-\frac{1}{a\cos^2\phi}\frac{\partial}{\partial\phi}(\overline{u'v'}\cos^2\phi) - \frac{\partial}{\partial\xi}(\overline{u'w'}) + (\overline{u'w'}) \qquad (8.1)$$

$$\frac{\partial \bar{T}}{\partial t} = -\frac{\bar{v}}{a}\frac{\partial \bar{T}}{\partial \phi} - \bar{w}\frac{\partial T}{\partial \xi} - \bar{w}\frac{RT}{c_p} + \frac{\overline{Q}}{c_p}$$

$$- \frac{1}{a\cos\phi}\frac{\partial}{\partial \phi}(\overline{v'T'}\cos\phi) - \frac{\partial}{\partial \xi}(\overline{w'T'}) + \overline{w'T'}\left(1 - \frac{R}{c_p}\right) \quad (8.2)$$

where $\xi = \ln(p_s/p)$, $w = d\xi/dt$, ϕ = latitude, a = radius of Earth, Q = diabatic heating, f = Coriolis parameter, R = gas constant and c_p = specific heat of air at constant pressure. Equation (8.1) demonstrates that the rate of change of zonal mean zonal momentum is determined by advection of momentum by the mean circulation, by the Coriolis acceleration of the meridional circulation and by the divergence of eddy fluxes of momentum. Similarly Equation (8.2) shows that the local rate of change of zonal mean temperature depends on heat advected by the mean circulation, adiabatic heating/cooling on descent/ascent, diabatic sources and the divergence of eddy heat fluxes. An analysis of the budget requires an estimate of each of these factors.

The structure of the lower stratosphere is predominantly dynamically controlled with eddy transport of heat up the horizontal gradient of zonal mean temperature. Using eddy momentum and heat flux values derived from satellite observations of wave activity Vincent (1968) and Adler (1975) have calculated the mean circulation in the region 100 - 10 mb. They show that poleward eddy fluxes of heat and momentum in winter high latitudes cause a thermally indirect cell with ascent near the winter pole and descent near 50^{o}. The disturbances important at these altitudes include planetary-scale eddies and vertical extensions of baroclinically unstable synoptic-scale eddies while small scale turbulence appears to be relatively unimportant (Lilly et al, 1974).

Synoptic-scale eddies do not penetrate into the upper stratosphere so eddy activity is dominated by planetary-scale waves and also, possibly, small scale turbulence. In the upper stratosphere and mesosphere radiative forcing of the mean circulation is considerably more important than it is in the lower stratosphere. In the first calculation of the mesospheric circulation Murgatroyd and Singleton (1961) estimated the meridional overturning required to maintain the observed temperature structure against the effects of radiative heating and cooling in the absence of any eddy transports. The resulting circulation was a global cell with ascent at the summer pole, descent near the winter pole and strong flow from the summer to the winter hemisphere in the upper mesosphere. This calculation, however, gave rise to zonal flow accelerations of several tens of m s^{-1} day^{-1}. They concluded that eddy momentum transports would be required to offset these accelerations and that such transports would presumably be accompanied by heat transports which would influence the thermal balance.

In a zonal mean dynamical model Leovy (1964) parameterised the eddy flux divergences of momentum and heat in terms of a linear relaxation back to mean zonal wind and temperature fields (i.e. Rayleigh friction and Newtonian cooling). The resulting meridional circulation was identical in structure to that of Murgatroyd and Singleton but reduced in strength so that the Coriolis torques gave rise to a zonal wind field similar to that observed. Schoeberl and Strobel (1978) included the effects of vertically propagating planetary waves, of wavenumbers one and two, in a model similar to that of Leovy. They concluded that the momentum fluxes associated with planetary wavenumber two have a negligible effect on the mean circulation and they were unable to find a stable solution for the wavenumber one case. Thus their model could not assess the importance of planetary wave propagation and their

results were very sensitive to the choice of damping coefficient. Like the model of Leovy that of Holton and Wehrbein (1980) does not include any eddy transport and cannot, therefore, reproduce the indirect cell in high latitudes of the winter stratosphere (see section 8.3). Also, as in the model of Schoeberl and Strobel, the predicted circulations are strongly dependent on the damping parameter used. All these authors contend that the inclusion of eddy fluxes of momentum and heat are not important to the wind and temperature fields produced in their models. As the Coriolis term acts to balance the eddy term in the momentum equation (non-interaction theorem, see section 8.3) the acceleration of the zonal wind is unaffected by the presence of eddies. Thus the zonal mean zonal wind and temperature fields, which are of concern to the authors mentioned above, are relatively insensitive to the presence of eddies whereas eddies are of vital importance to the Eulerian mean meridional circulation.

The heat and momentum budget of the Oxford model as specified in Run E will now be investigated. Fig. 8.1 shows the rate of change of temperature on December 31st due to (a) the radiative sources and sinks, (b) heat transport by the mean circulation and (c) heat transport by eddies. In the summer hemisphere there is very little eddy activity and the diabatic heating in the upper stratosphere and mesosphere is offset by a removal of heat by the mean circulation. The zonal mean meridional vertical velocity fields for this day are shown in Figs. 8.2(a) and (b). They indicate ascent in the summer hemisphere and motion across the equator into the winter hemisphere throughout the upper stratosphere and mesosphere. Descent occurs in middle to high latitudes in the mesosphere while in the stratosphere it is strongest in mid-latitudes forming a reverse cell in high latitudes with rising motion near the winter pole.

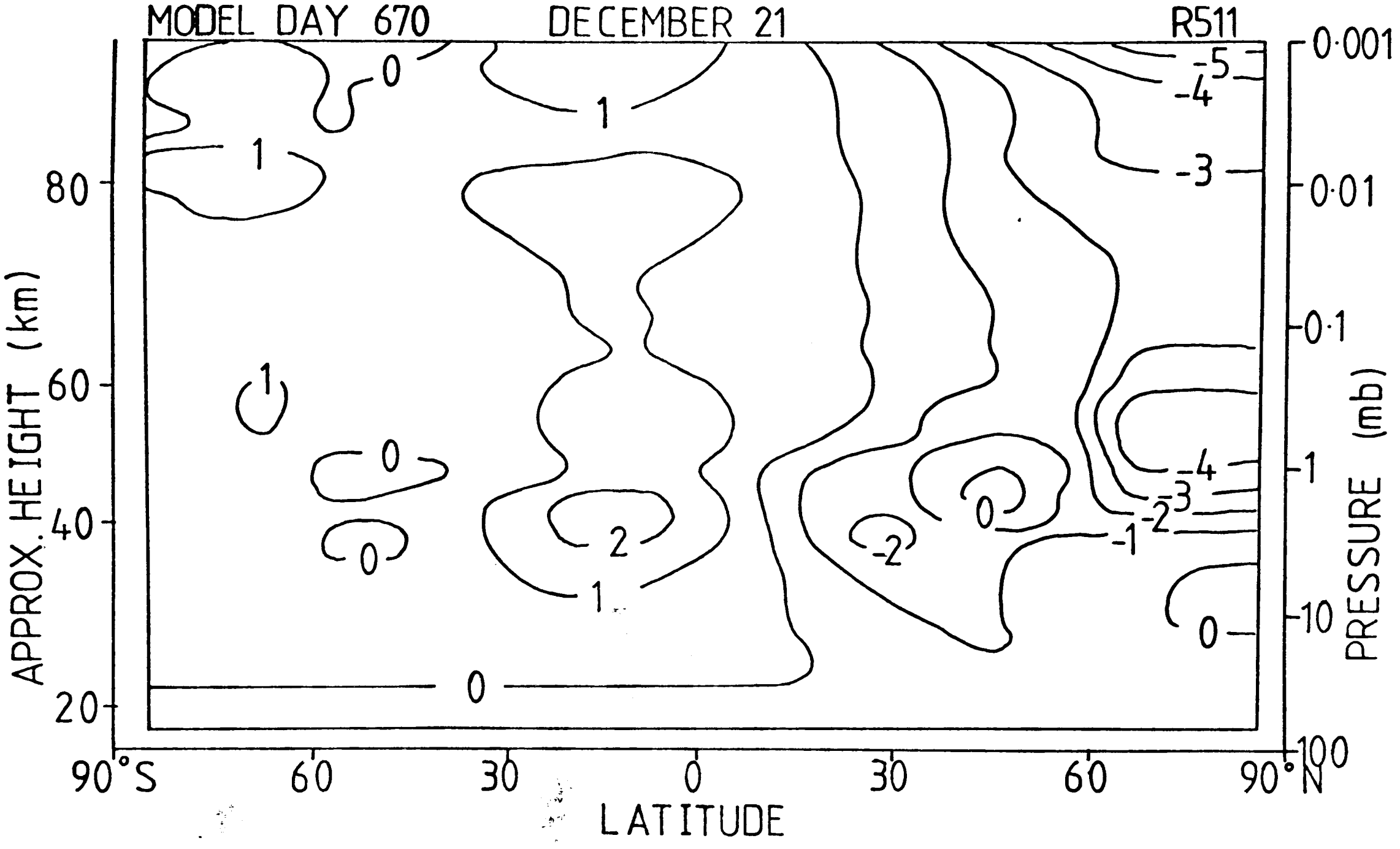

Fig. 8.1(a) Net diabatic heating (K/day) Run E

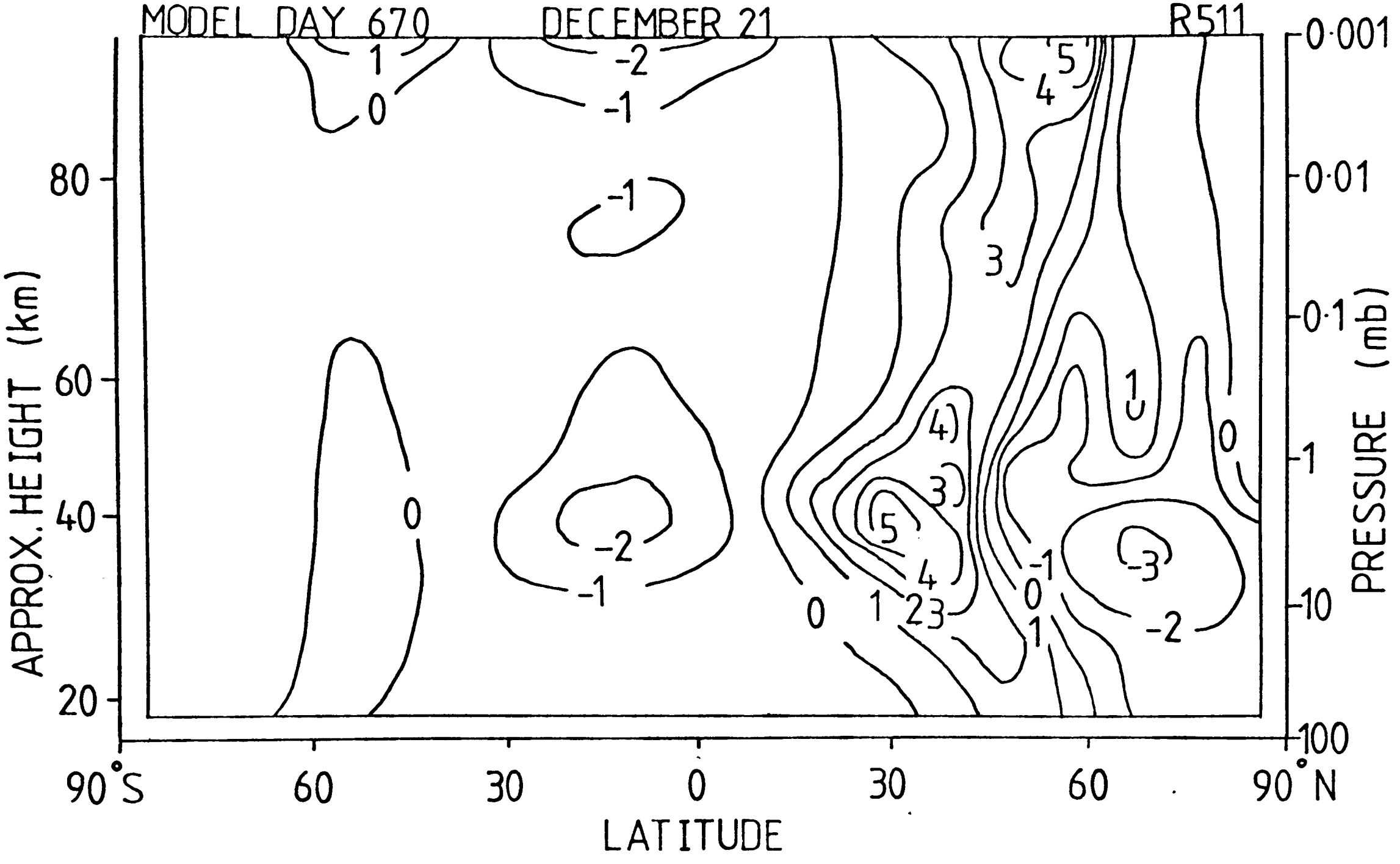

Fig. 8.1(b) $\partial \bar{T} / \partial t$ due to mean circulation (K/day) Run E

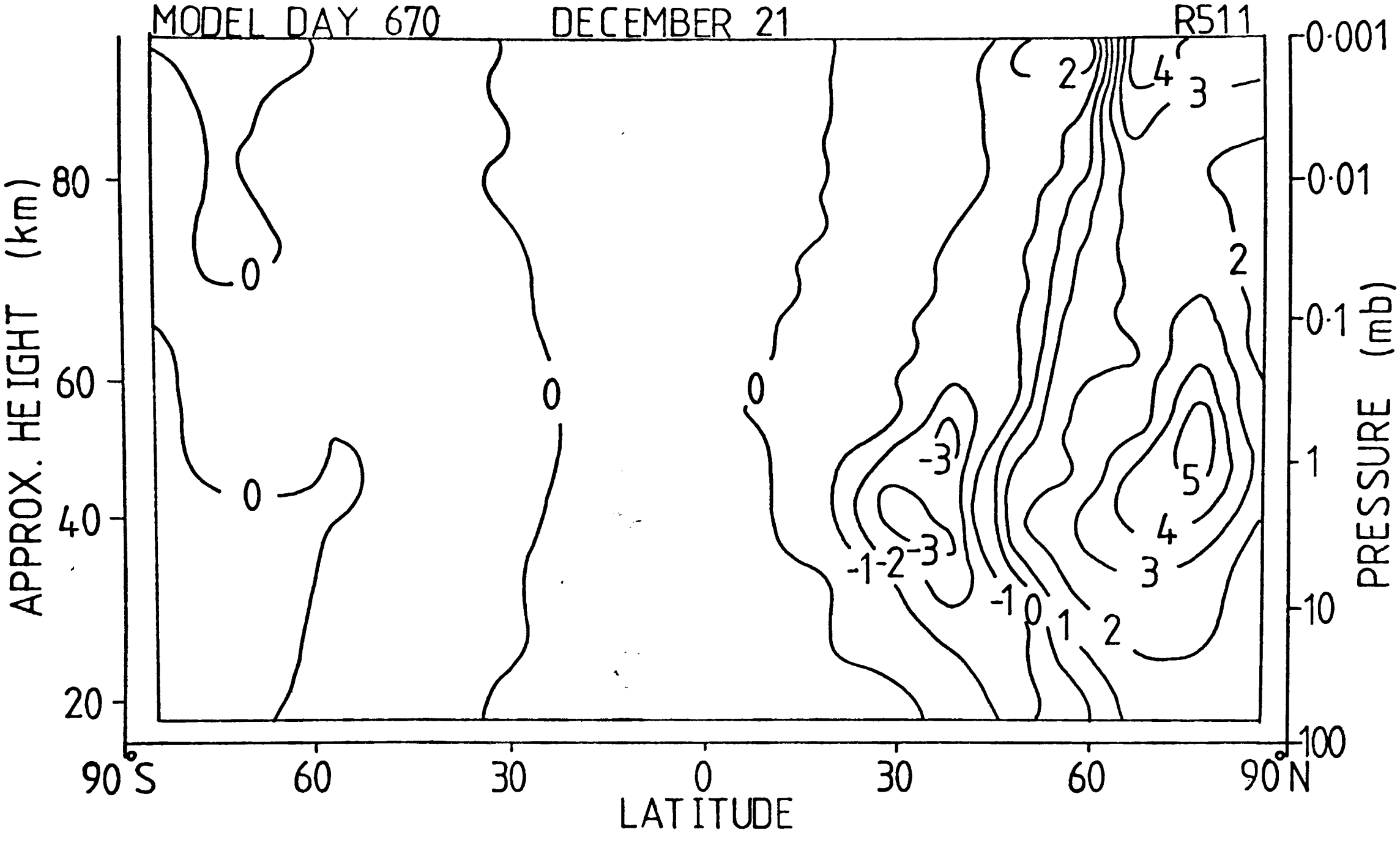

Fig.8.1(c) $\partial\bar{T}/\partial t$ due to horiz. eddy heat fluxes (K/day) Run E

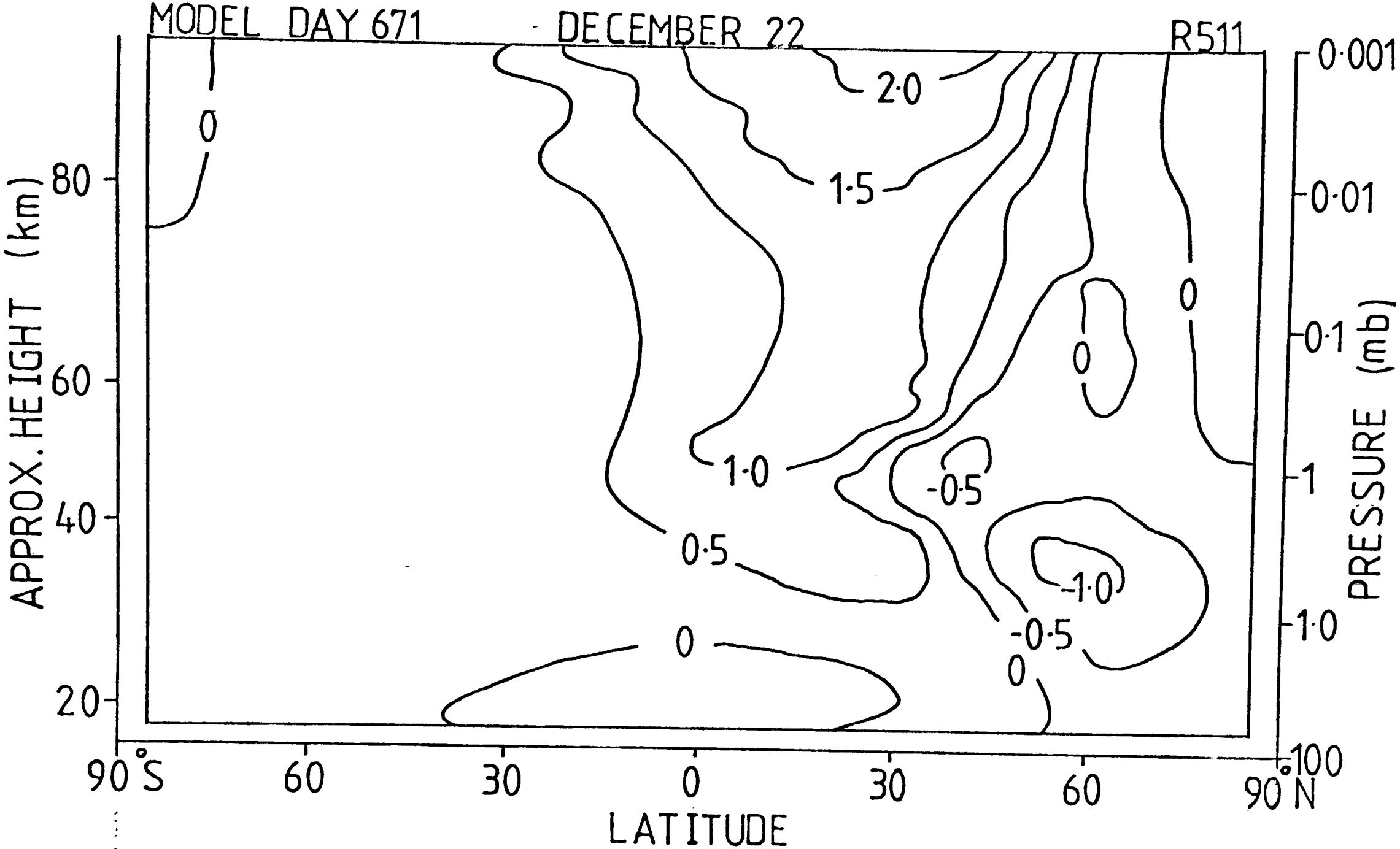

Fig. 8.2(a) Meridional wind (m/s) Run E

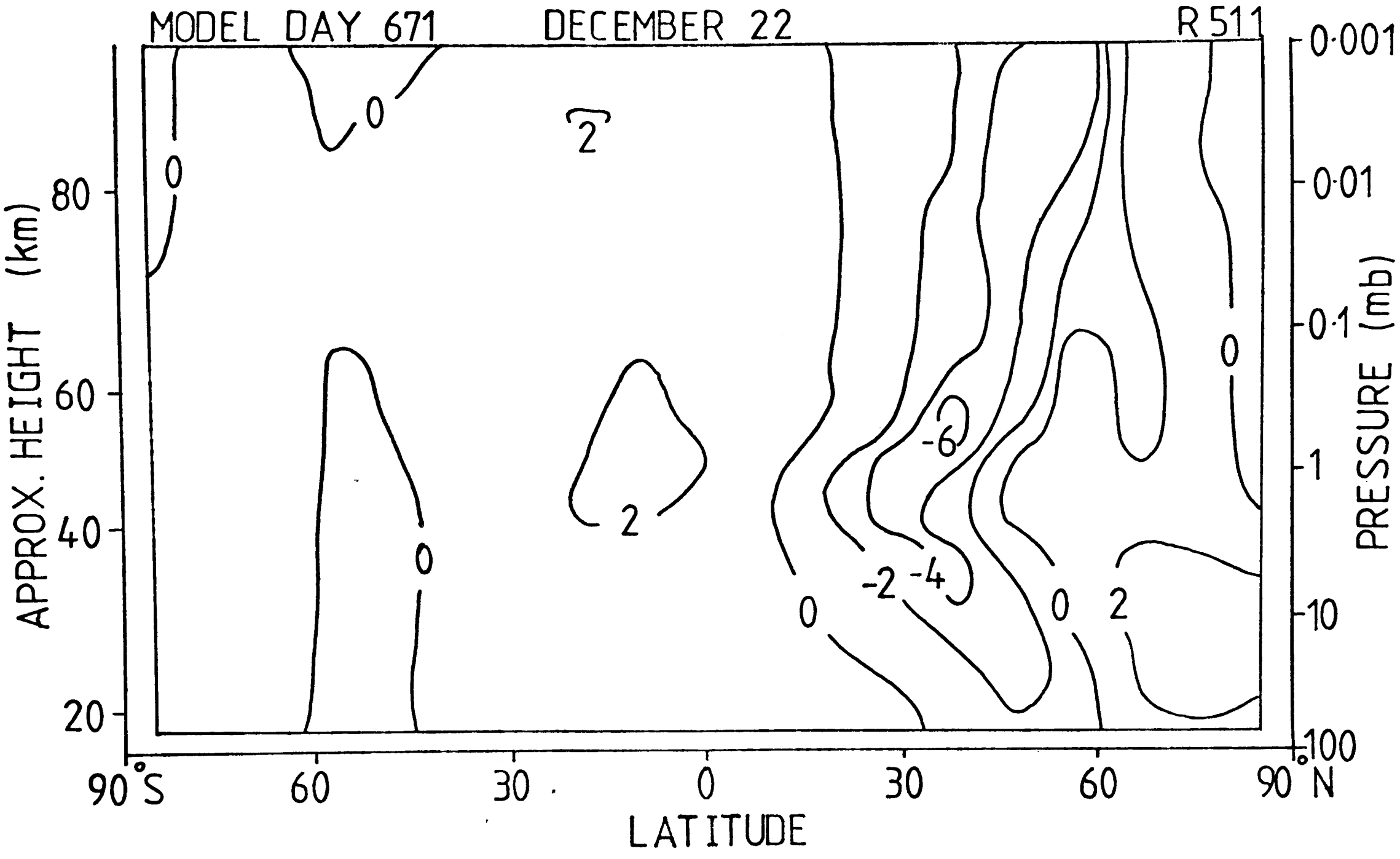

Fig. 8.2(b) Vertical wind (mm/s) Run E

In winter eddy heat transport is important and in the lower stratosphere the temperature structure is dynamically controlled with a near balance between the contributions of themean motions and the addies. Near the stratopause in high latitudes radiative cooling becomes significant and is largely countered by eddy heat fluxes. In the mesosphere all three components contribute while in the lower thermosphere the diabatic contribution is dominant.

Fig. 8.3 shows contributions to the momentum budget from (a) Coriolis acceleration of the meridional velocity, (b) horizontal advection, (c) vertical advection and (d) horizontal eddy flux divergences. Planetary scale vertical eddy fluxes are not included as they are very small in the stratosphere and mesosphere. In the winter upper stratosphere the eddies transfer momentum out of mid-latitudes and into high latitudes (Fig. 8.3 (d)): this results in a meridional circulation which causes transfer in the opposite sense due to both advection (Figs. 8.3 (b) and (c)) and the Coriolis term (Fig. 8.3 (a)). This is the only region in which eddy fluxes play a significant role: in the mesosphere and lower thermosphere the zonal acceleration is determined by a balance between the horizontal advection of momentum and the Coriolis term. It is interesting to note that the sum of these components of the momentum equation gives a net du/dt of greater than 1 m s^{-1} day^{-1} throughout most of the northern hemisphere mesosphere and around - 1 m s^{-1} day^{-1} in the southern hemisphere mesosphere. These accelerations lead to the very strong westerly and easterly jets illustrated in Fig. 6.24.

It is obvious that the heat and momentum budgets depend on the wind fields and, conversely, that the circulations depend on the transport of heat and momentum. The latter dependence is expressed by the stream function equation (Equation 2.16) which may be rewritten in the form :

$$\mathcal{L}(\psi) = \{H\} + \{Q\} + \{q\}$$

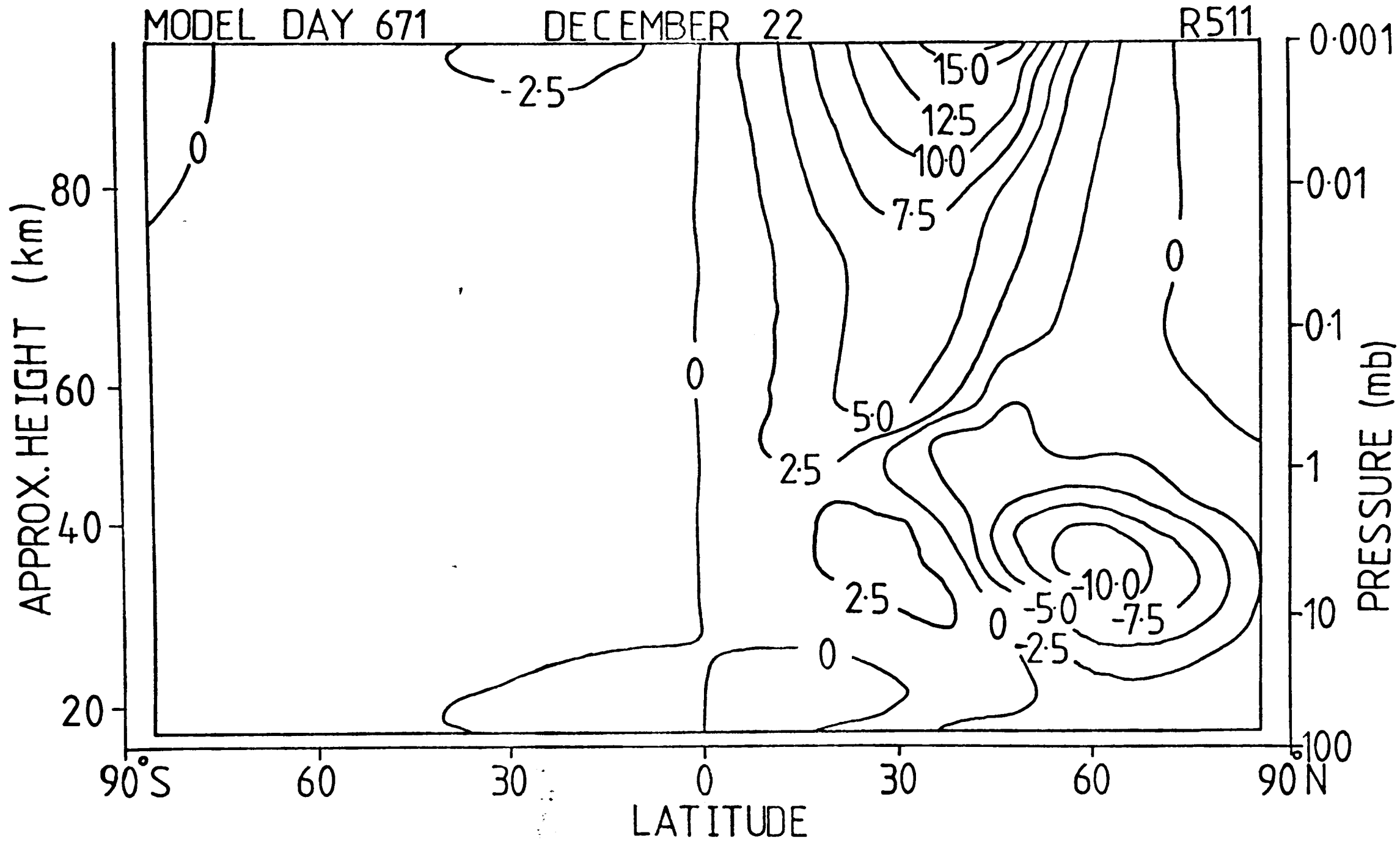

Fig.8.3(a) fv (m/s/day) Run E

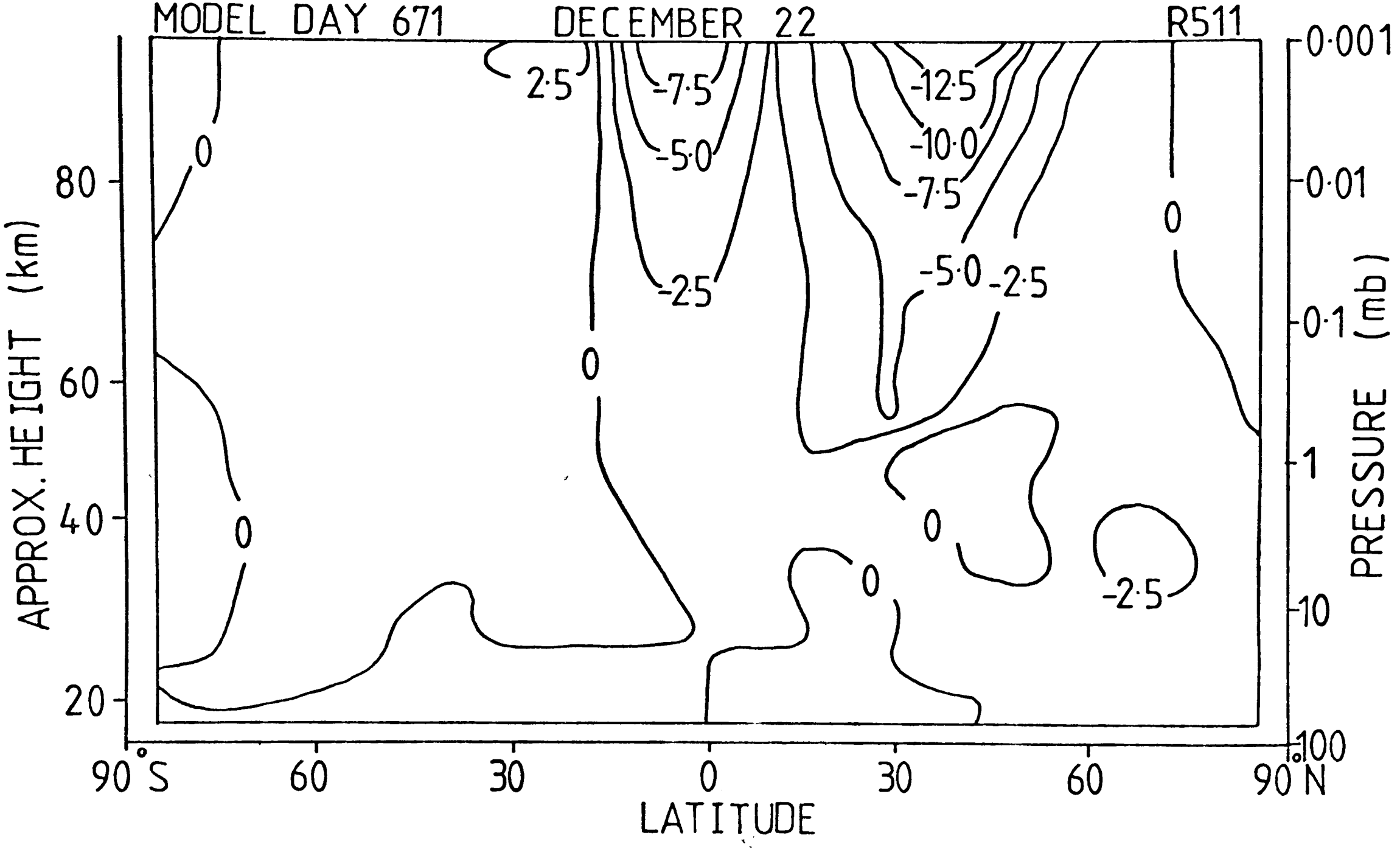

Fig. 8.3(b) $\frac{-v}{a\cos\phi}\frac{\partial}{\partial\phi}(u\cos\phi)$ (m/s/day) Run E

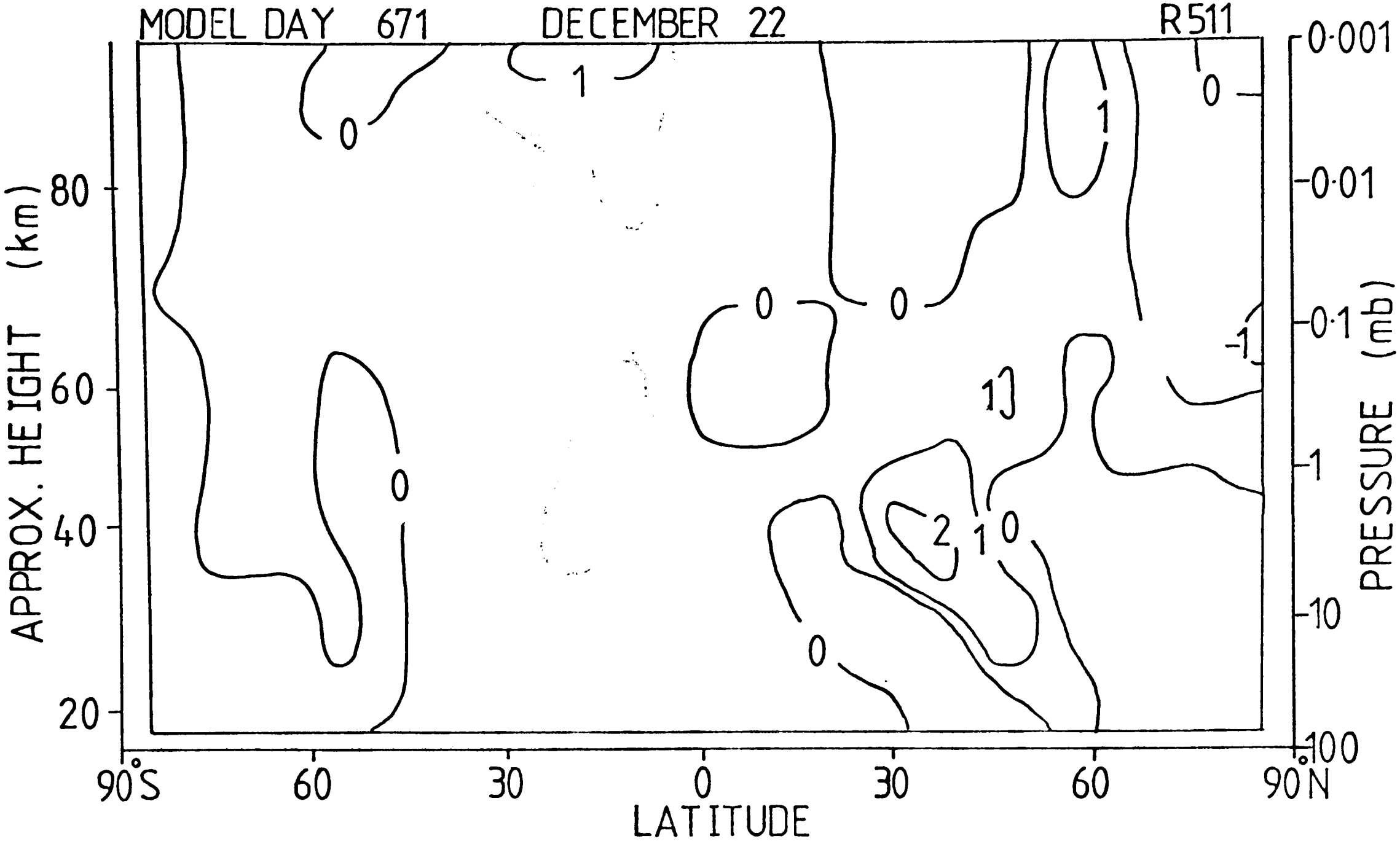

Fig. 8.3(c) $-w\frac{\partial u}{\partial \xi}$ (m/s/day) Run E

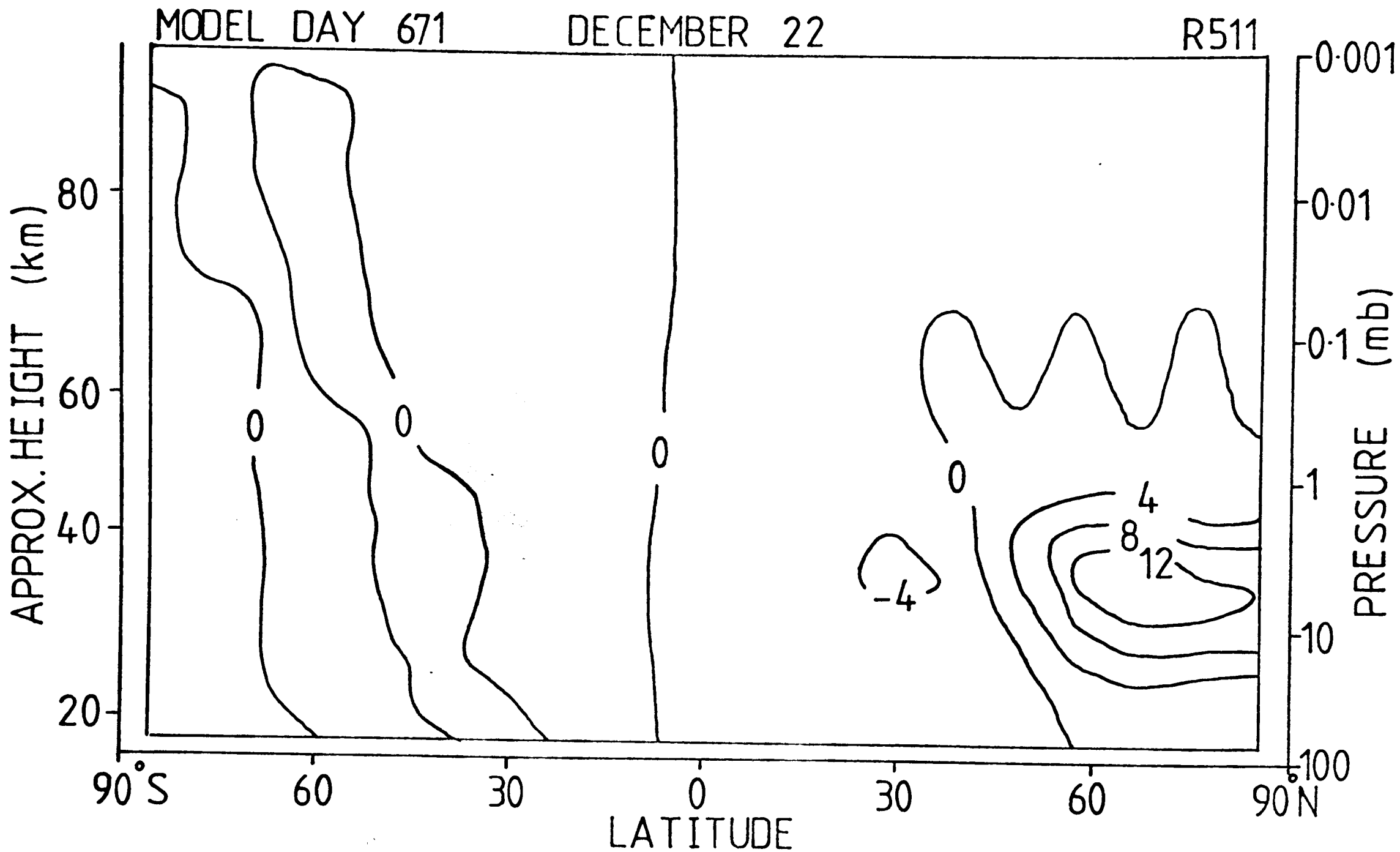

Fig. 8.3(d) horiz. divergence of eddy momentum fluxes (m/s/day) Run E

where $\mathcal{L}$ is a linear, second order, elliptic differential operator, $\{H\}$ is a term which involves only the vertical gradients of the eddy momentum flux convergences, $\{Q\}$ involves only horizontal gradients of the eddy flux convergences of potential temperature and $\{q\}$ involves only the horizontal gradients of diabatic heating. Since $\mathcal{L}$ is linear it is possible to separate Ψ, and thus v and w, into parts due to $\{H\}$, $\{Q\}$ and $\{q\}$. (This partitioning is not absolute, however, as the coefficients of Ψ involve zonal mean temperatures and zonal winds which have evolved in a non-linear manner from H, Q and q).

Fig. 8.4 presents the meridional velocity field due to (a) eddy momentum flux convergence, (b) eddy heat flux convergence and (c) the diabatic heating. Comparison of these cross-sections with Fig. 8.2(a) which shows total meridional velocity, reveals that the eddy momentum flux convergence is the most important component in the stratosphere causing flow from summer to winter hemispheres and a reverse flow in winter high latitudes. There is also a contribution to the northward flow from the diabatic heating and to the indirect cell from the eddy heat fluxes. Above the stratopause the eddy momentum fluxes play only a minor part. The diabatic heating causes a strong flow, which increases with altitude, from the summer to the winter hemisphere. The eddy heat fluxes assist this in low latitudes but cause a flow in the opposite direction in high latitudes which counters the effect of the diabatic heating. The main driving force of the meridional circulation in the mesosphere in Run E is obviously the radiative heating.

It would appear, therefore, that momentum fluxes due to planetary scale waves are not important in the mesosphere. This analysis, however, was based on momentum fluxes from satellite data extrapolated above 50 km (see Section 8.5) and for a greater understanding of the meridional circulation an assessment of the role played by planetary waves in transporting heat and

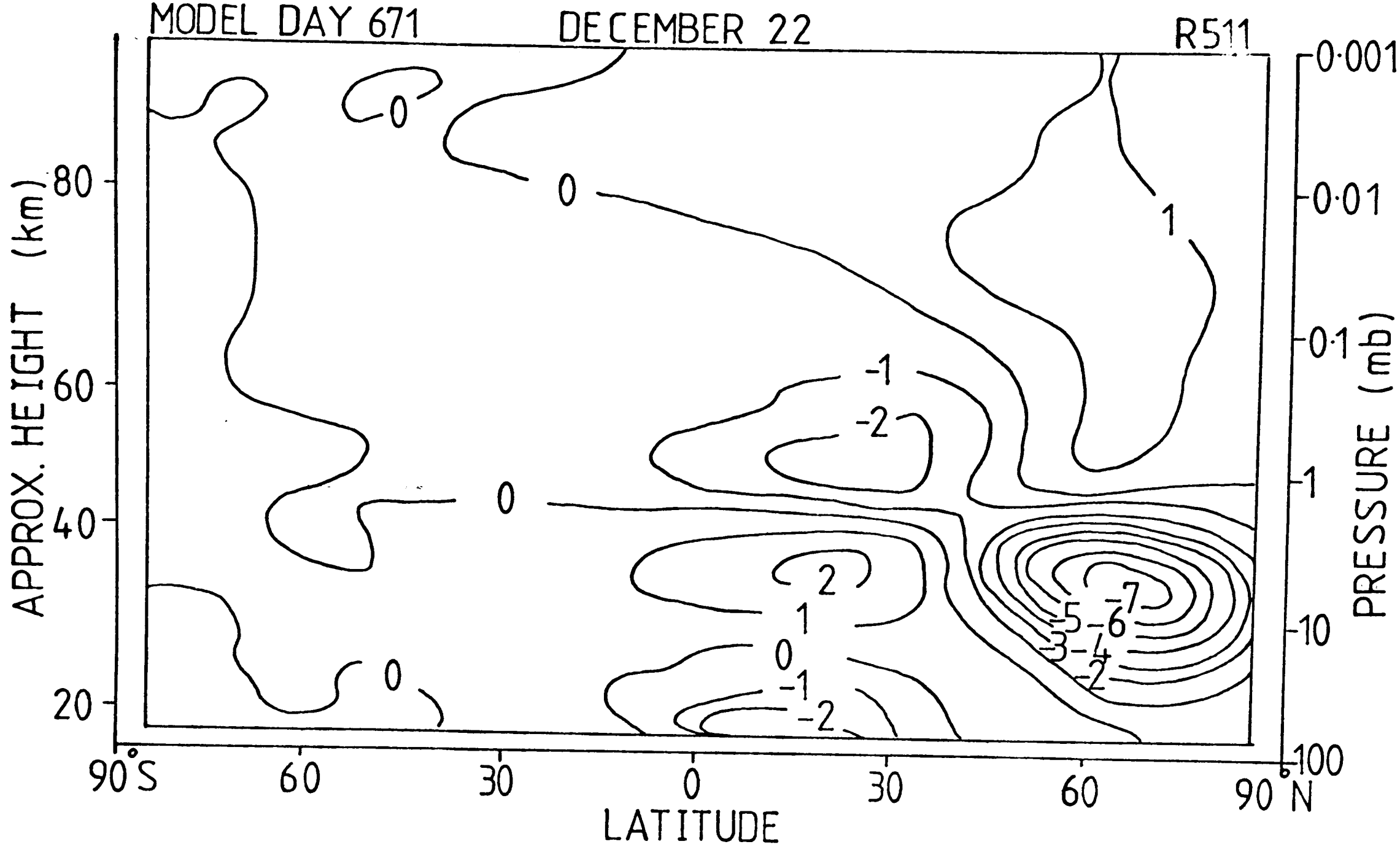

Fig. 8.4(a) v due to eddy momentum fluxes(0.1m/s) Run E

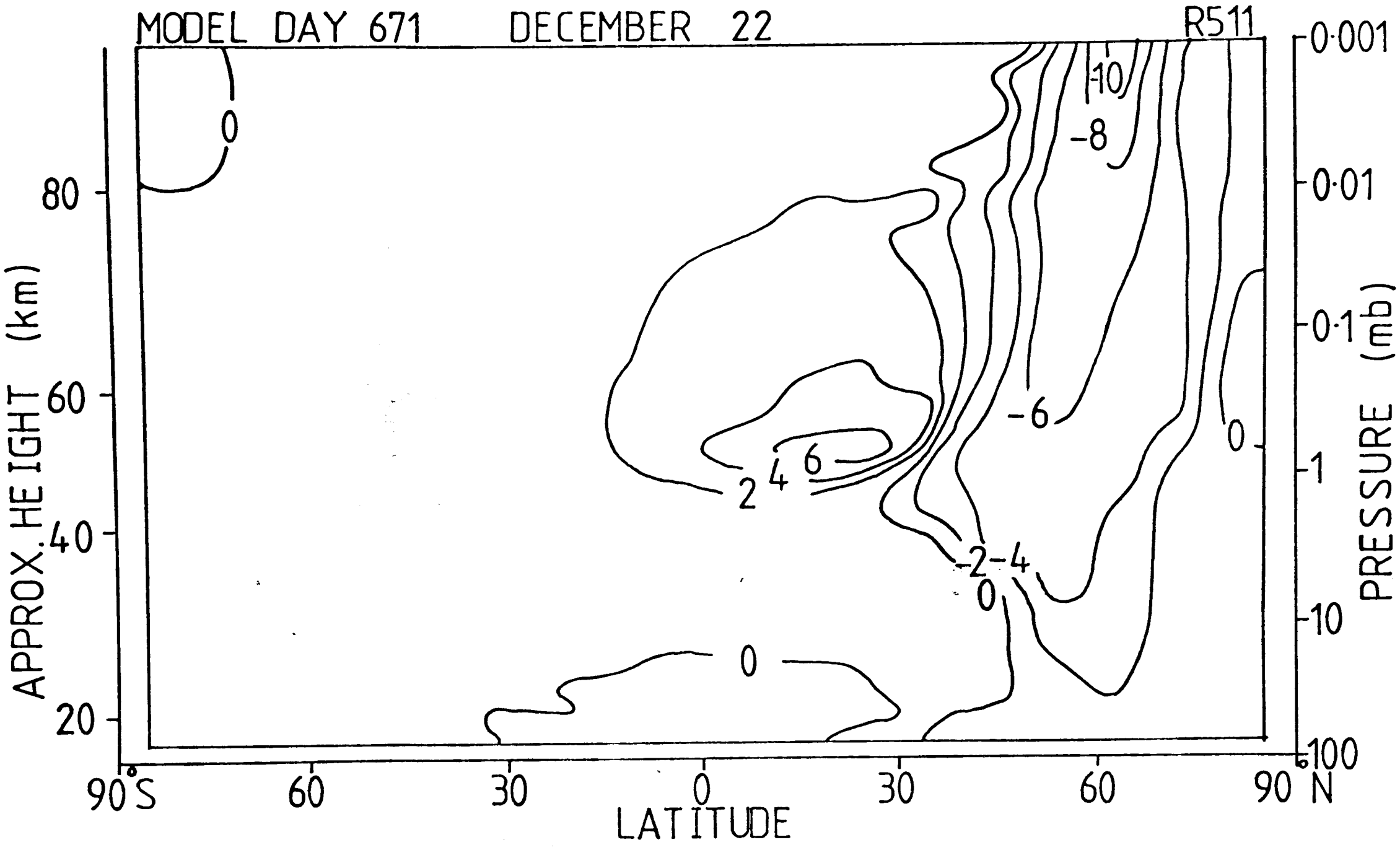

Fig. 8.4(b) v due to eddy heat fluxes (0·1m/s) Run E

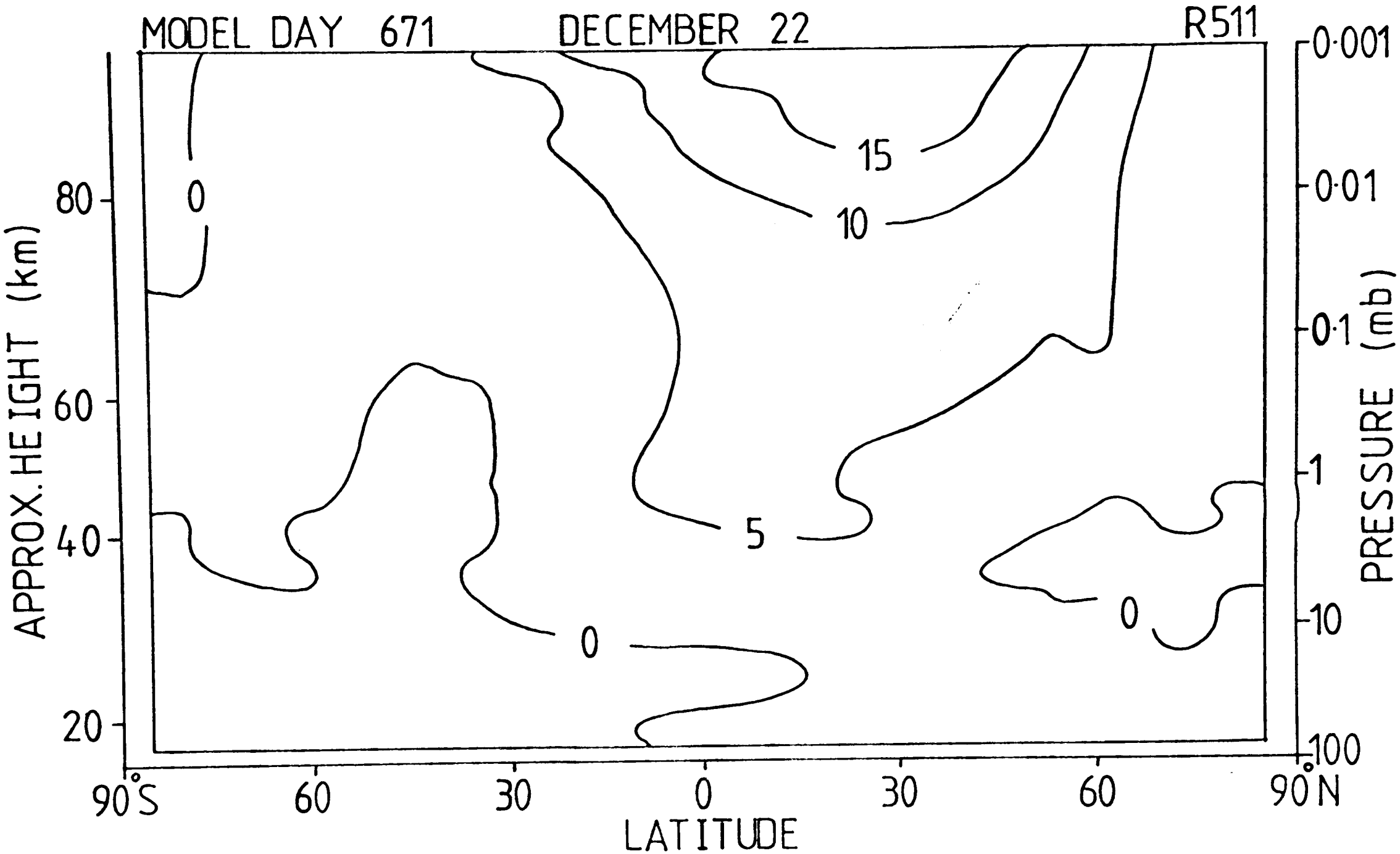

Fig. 8.4(c) v due to radiative heating (0·1 m/s) Run E

momentum is needed. An experiment to this effect will be described later in this chapter. First, however, a short discussion of mass motions will be included.

8.3 Mean meridional mass motions

Because of the discrepancies in the angular momentum budget of the circulation calculated by Murgatroyd and Singleton their results were treated with some reserve. Their study of particle trajectories, however, showed a mass transport which agreed closely with the Brewer-Dobson circulation (Brewer, 1949 ; Dobson, 1956) derived from observations of tracers. It would appear possible that whilst a knowledge of the eddy fluxes is required for deduction of the mean meridional circulation it is not needed for studies of mass transport.

This apparent paradox was explained by Dunkerton (1978) who showed that the transport of matter is determined by the Lagrangian-mean circulation (Andrews and M^{c}Intyre, 1976) which, in the absence of wave transience or dissipation, is determined by the diabatic heating and static stability alone. This theory is an extended application of the "non-interaction theorem" (see e.g. Holton, 1974) which states that steady, conservative waves will induce a mean meridional cell which acts to identically cancel the eddy fluxes of the waves themselves. Thus the indirect cell deduced by Vincent and Adler for the lower stratosphere winter high latitudes has little relevance to mass transport as it exists to cancel the poleward fluxes due to the eddies.

A model formulated in a Lagrangian-mean framework would not, therefore, require any knowledge of eddy fluxes. Such a model, however, poses serious mathematical difficulties and hasnot yet been constructed. Meanwhile the K-theory parameterisation of eddy fluxes used in Eulerian-mean models is being

put on a stronger physical basis (see next section) and these models continue to be useful tools without the conceptual difficulties involved in Lagrangian dynamics.

8.4 K-theory

As mentioned in Section 2.4.3 the eddy fluxes of heat and tracers (but not momentum) are parameterised in the Oxford Model by the K-theory approach of Reed and German (1965) i.e. the northward and upward fluxes of a substance s are given by :

$$\overline{v's'} = -\left(K_{yy}\frac{\partial\bar{s}}{\partial y} + K_{y\xi}\frac{\partial\bar{s}}{\partial\xi}\right)$$

$$\overline{w's'} = -\left(K_{\xi y}\frac{\partial\bar{s}}{\partial y} + K_{\xi\xi}\frac{\partial\bar{s}}{\partial\xi}\right)$$

According to Reed and German, whose theory was based on mixing-length arguments, both K_{yy} and $K_{\xi\xi}$ must be positive and $K_{y\xi} = K_{\xi y}$. It was assumed that a set of K=factors estimated from observations of one quasi-conservative tracer (e.g. potential temperature) would apply in the calculations of the fluxes of all other substances. The values used in the model are those of Luther (1973) which were specified monthly up to 60 km based on observatinn of fluxes of potential temperature. Above 60 km the values were usually kept constant at their value at this altitude for lack of other information. In an attempt to improve the Model's temperature structure in the upper mesosphere various experiments were carried out in which fairly arbitrary changes were made to the K-factors above 60 km. It was found that by sharply increasing $K_{\xi\xi}$ in winter high latitudes a slight improvement could be achieved but of insufficient magnitude to reverse the temperature gradient. This form of experiment was rather unsatisfactory from a scientific point of view, as the physical basis was tenuous, and thus the K-factors are generally kept constant in the mesosphere.

Pyle and Rogers (1980) have studied the transport of reactive trace gases by stationary planetary scale waves and have shown that K-theory fields, as introduced by Reed and German, may be defined. They indicate, however, that for an inert tracer $K_{yy} = K_{zz} = 0$ and $K_{yz} = -K_{zy}$, in contradication with the result of Reed and German, and for a reactive species the fluxes depend not only on the gradients of the species itself but also on the gradients of the other chemicals with which it reacts. These results also raise serious questions as to the validity of the K-theory approach used in one-dimensional models. Currently Pyle and Rogers are aiming to incorporate a calculation of planetary wave propagation within the Oxford two-dimensional model. This scheme will enable the fluxes of heat, momentum and tracers to be calculated in a model-dependent manner and will greatly improve the model's dynamical formulation, especially for experiments in which transport is particularly important (e.g. pollution studies).

8.5 Eddy fluxes of angular momentum

Because angular momentum is not conserved by fluid particles eddy fluxes of momentum may not be calculated by K-theory. This problem is circumvented in the Model by the specification of planetary wave fluxes estimated from satellite observations.

Dr. A.J.Crane has calculated two sets of momentum fluxes : one set, up to about 50 km, from Nimbus 5 selective chopper radiometer data for 1973 and another, up to about 80 km in the northern hemisphere, from Nimbus 6 pressure modulator radiometer data for 1976. Details of the retrieval method are given by Crane et al (1980). In both sets fluxes due to the first four zonal harmonics, were calculated as monthly means. For use in the Model the 1973 values were extrapolated above 50 km to zero at 80 km and it is this set that was used in the model runs described so far in this thesis. As has

been noted (see e.g. Fig. 6.24) these eddy fluxes are not sufficient to close the polar night westerly jet or the summer easterly jet in the mesosphere. As the values used in the mesosphere were extrapolated rather than measured, however, the role played by planetary waves here could not be accurately assessed.

In Run K the basic model specification of Run E (better radiation, simple photochemistry) was used but with the 1976 eddy momentum flux values replacing the 1973 set in the northern hemisphere. The eddy flux divergence in December is illustrated in Fig. 8.5. Comparison with Fig. 8.3(d) (which shows the same for Run E) indicates that the maximum momentum deposition in winter high latitudes has increased by about 10% and occurs at around 55 km rather than 35 km. Fig. 8.6 shows the zonal field for model day 1040 (Dec. 26th) in Run K. Comparison with Fig. 6.24 (Run E) reveals the effect of changing the momentum fluxes. This is to weaken slightly the polar night jet in the stratosphere and strengthen it slightly in the mesosphere. There is no sign of the jets closing. Inclusion of the 1976 eddy fluxes also removes the small subsidiary easterly jet apparent in Run E at 35 km. The changes are more dramatic in the meridional circulation: Fig. 8.7 shows (a) the meridional and (b) the vertical velocity fields for Run K in December. These may be compared with Figs. 8.2(a) and (b) for Run E. Both runs clearly demonstrate flow from the summer to the winter hemisphere in the stratosphere, sinking in mid-latitudes and the eddy-induced indirect cell in high latitudes. In Run K, however, these circulations have intensified considerably and the maximum velocities occur at slightly higher altitudes, corresponding to the changes in the eddy momentum fluxes.

These results indicate that planetary wave momentum fluxes are incapable of producing the necessary momentum redistribution in the mesosphere but that they play a profound role in determining the stratospheric circulation.

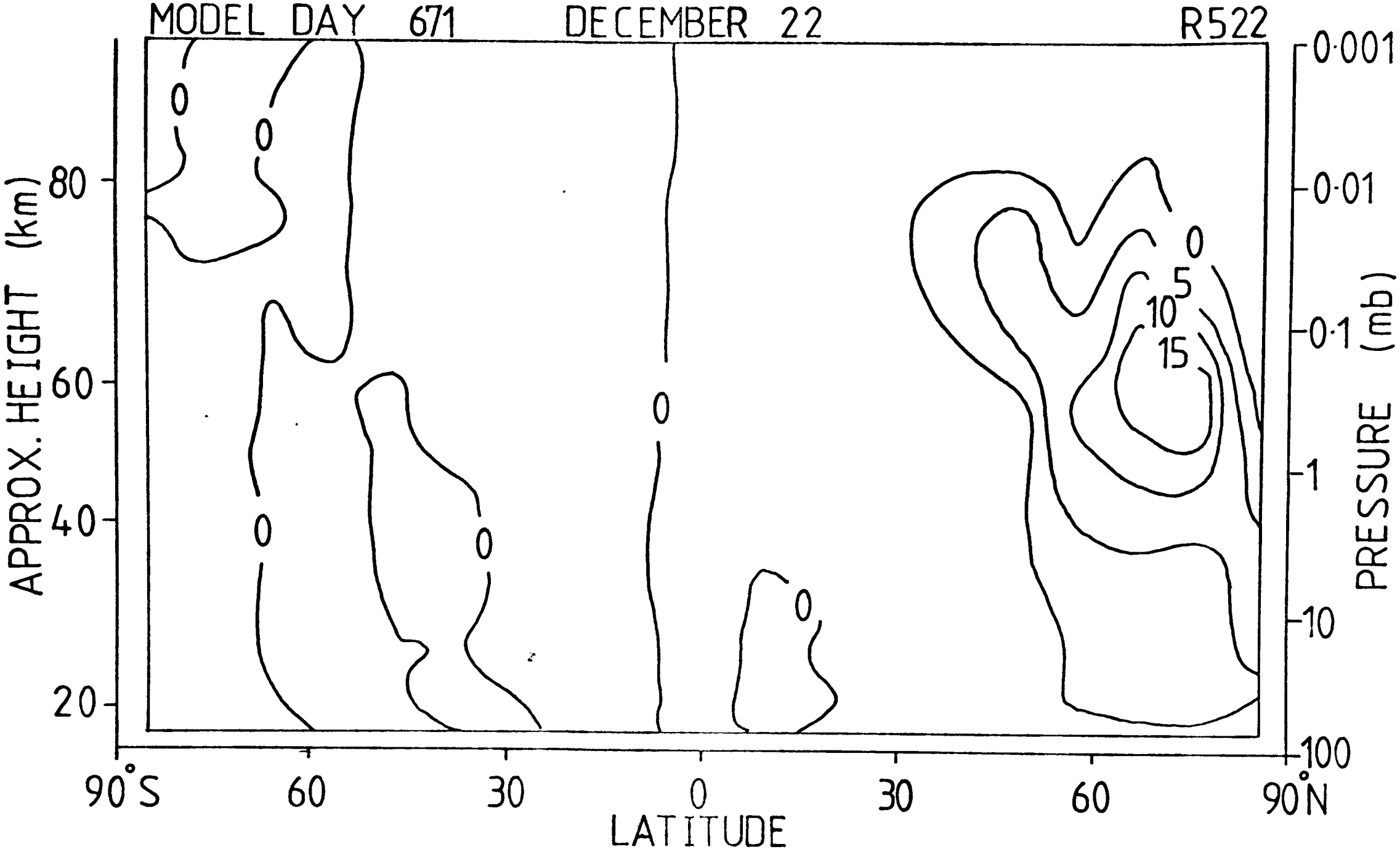

Fig. 8.5 horiz. divergence of eddy momentum fluxes (m/s/day) Run K

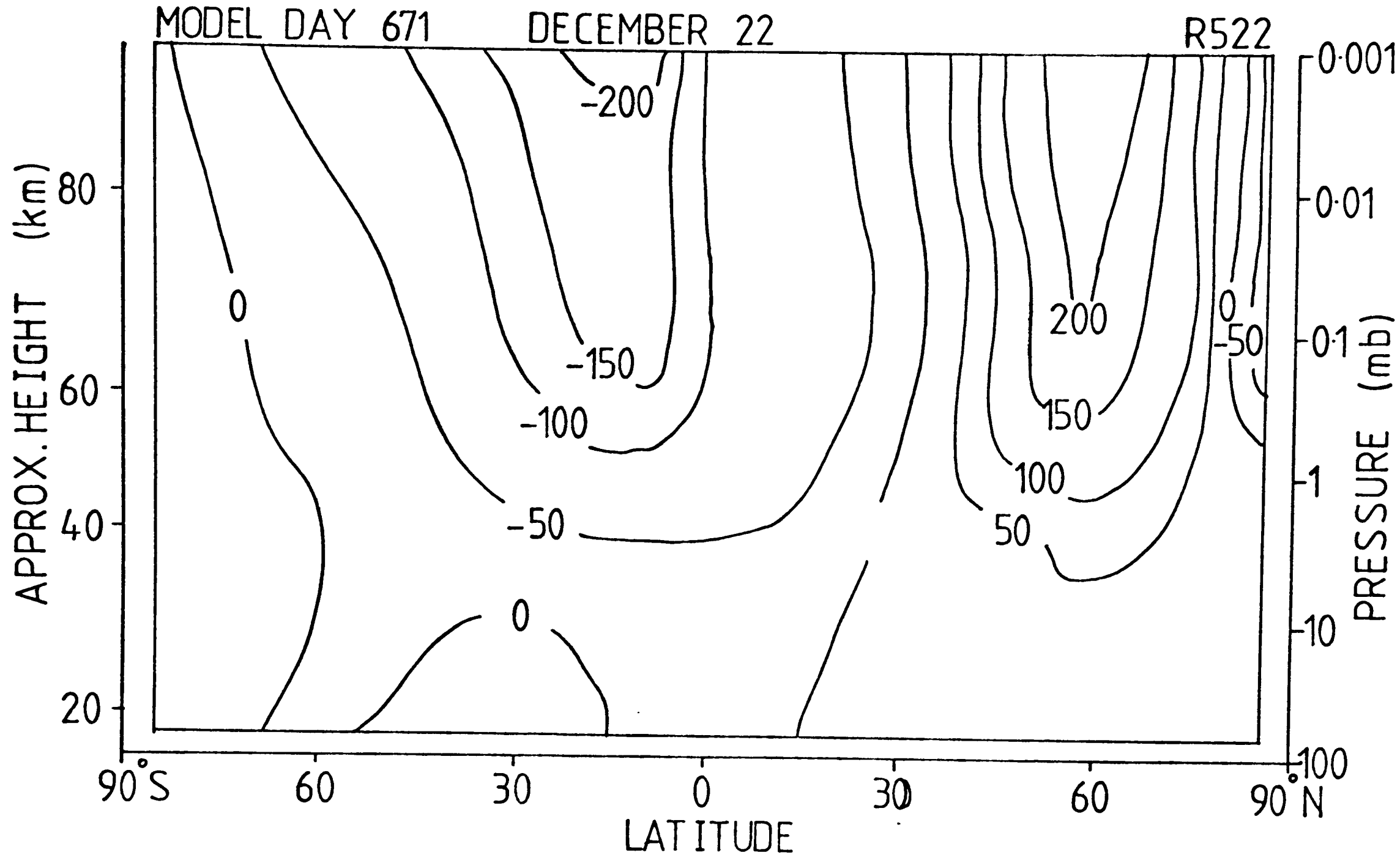

Fig.8.6 Zonal wind (m/s) Run K

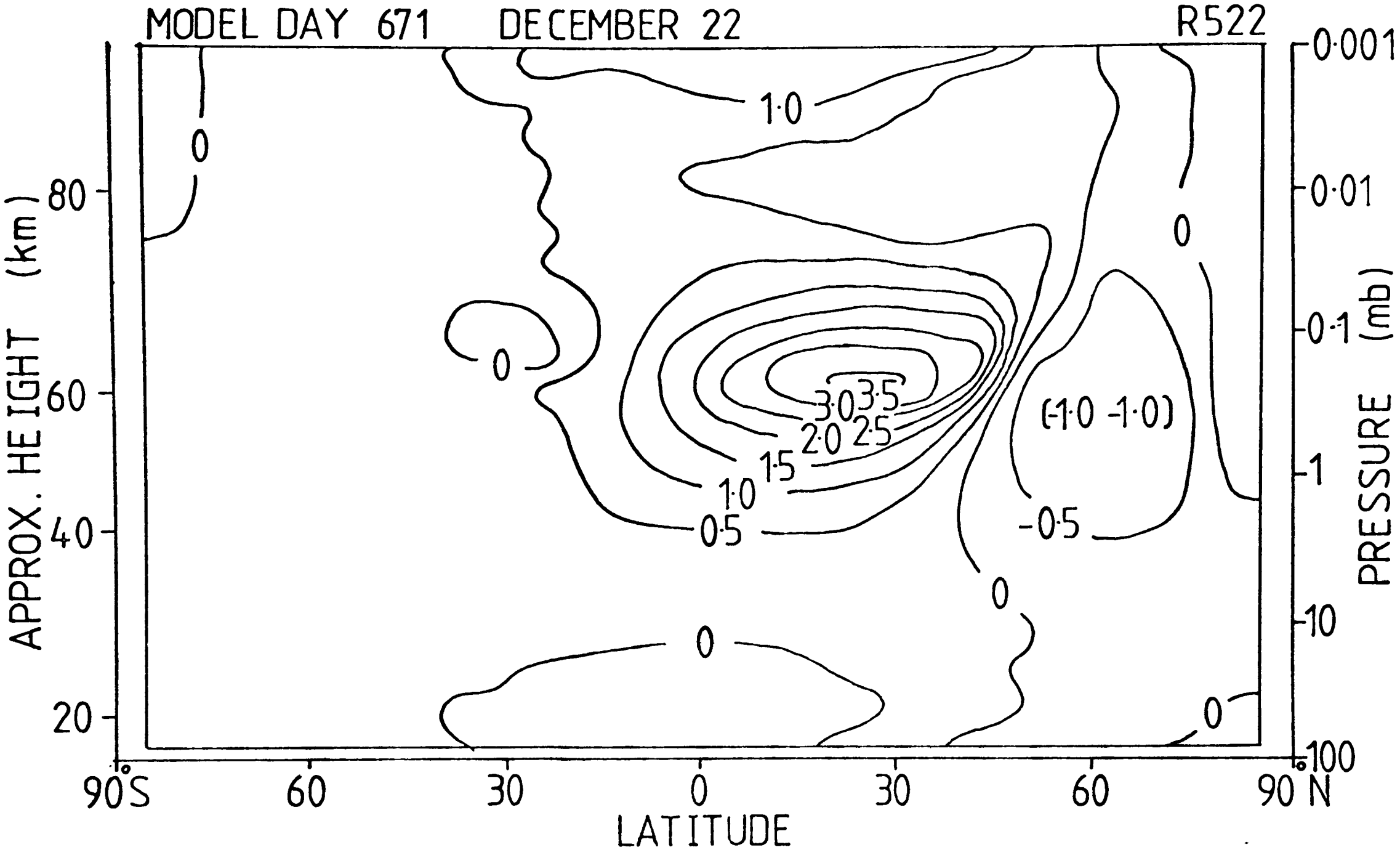

Fig. 8.7(a) Meridional wind (m/s) Run K

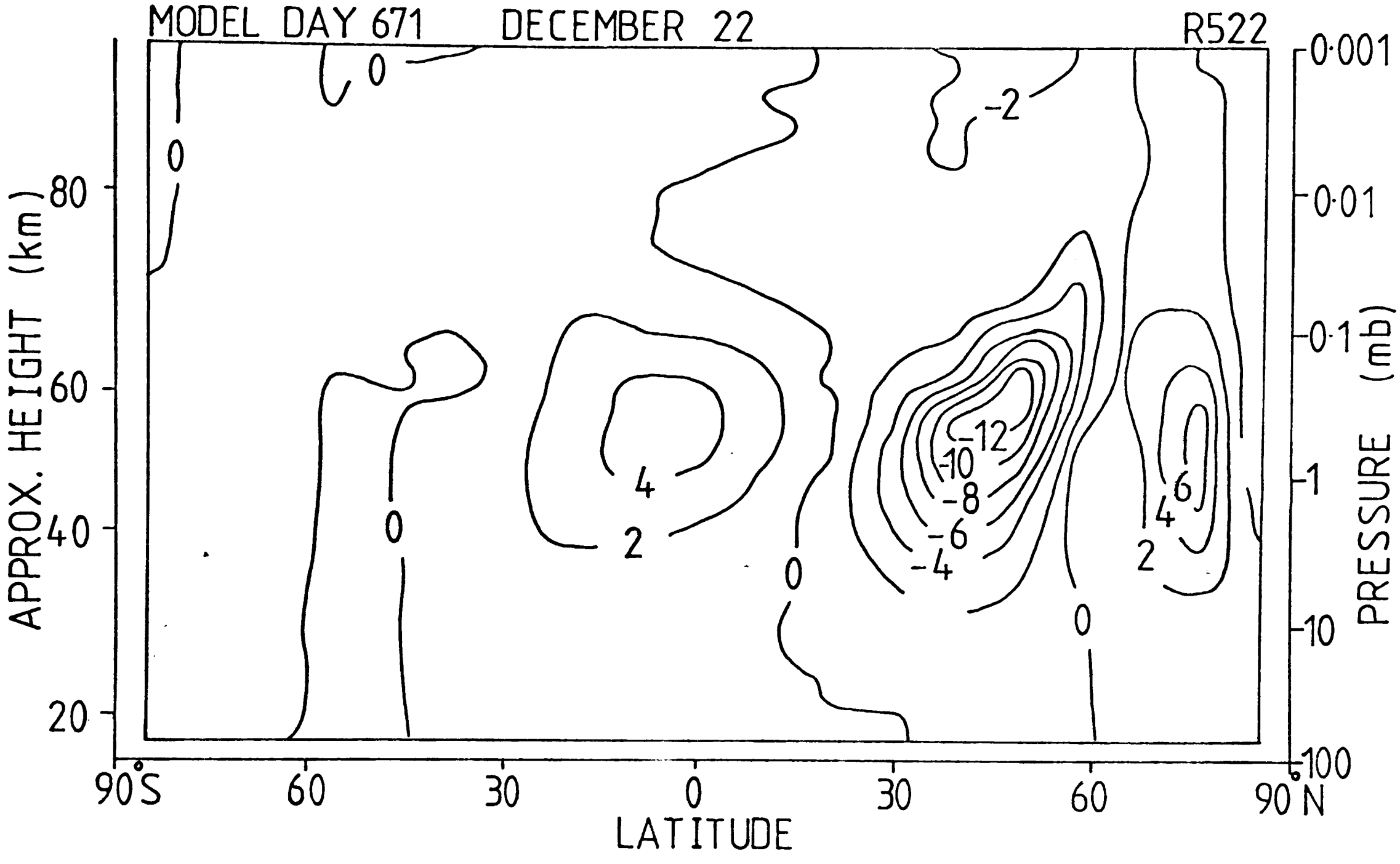

Fig. 8.7 (b) Vertical wind (mm/s) Run K

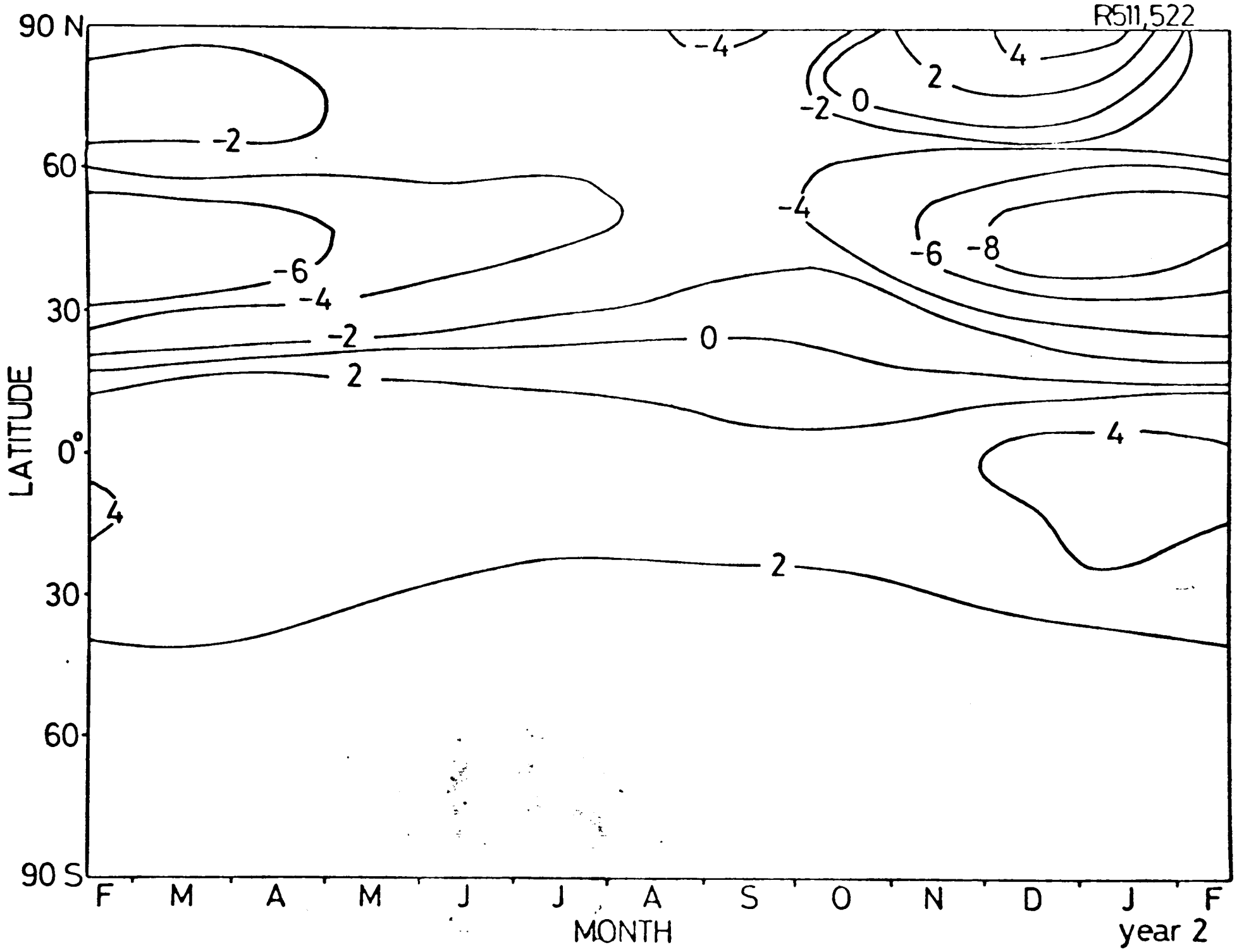

Fig.8.8 % difference in total ozone with $\overline{u'v'}$ from 1973 and 1976 in N.Hemisphere only.

The changes in the circulation of the stratosphere induce changes in the ozone distribution. Fig. 8.8 shows the percentage increase in ozone column density between the two runs during the second model year. There are decreases of over 8% in winter mid-latitudes corresponding to the increased eddy fluxes out of this region. That the ozone column density might vary by this amount, or more, from year to year is quite significant in the context of the effects predicted due to anthropogenic perturbations such as those discussed in Chapter 7.

8.6 Balancing the equations

Models which do not include eddy heat transport, such as those of Leovy (1964), Schoeberl and Strobel (1978) and Holton and Wehrbein (1980), require a stress term in the momentum equation of magnitude equivalent to an eddy diffusion coefficient of 1000 $m^2 s^{-1}$ to balance the meridional circulation (Green ,1972). Hines (1972a) claims, on the basis of observations of turbulence in the lower ionosphere, that an eddy diffusion coefficient could lie in the range 100 - 1000 $m^2 s^{-1}$. Green, however, suggests that such small scale eddies would be unable to detect, and therefore diffuse, the variations of velocity on the larger scale of the mean circulation and that eddy transport must be carried out by planetary waves.

It has been shown that planetary wave fluxes of angular momentum were insufficient to balance the momentum budget in the Oxford Model. Dr. A. J. Crane also calculated monthly mean eddy heat fluxes from the satellite data (Crane et al, 1980) and in Run L the Model's K-theory approach to heat fluxes was replaced by a scheme in which the fluxes were specified monthly up to 80 km in the northern hemisphere. Crane's heat fluxes included large areas of high values (poleward fluxes of over 100 K m s^{-1}) in the winter high latitudes near the stratopause and their inclusion in the Model resulted in a

very strong indirect meridional circulation in the winter stratosphere and, through the Coriolis acceleration on this cell, a vigorous easterly jet near the pole. The polar night (Westerly) jet was not improved from previous runs. In Section 8.2 it was shown that eddy heat fluxes play a major part in determining the mean circulation in the stratosphere so it is not surprising that the circulation of Run L should have reacted so sensitively to the strong heat flux values. It is possible that these heat fluxes are larger than average because of the unusually intense wave activity that occurred in the winter of 1976 or it may be that the climatological net heating rates used in their calculation were inappropriate for 1976 and thus the eddy fluxes were overestimated. Furthermore, the heat fluxes could not respond to changes in the atmospheric state. Eddy heat fluxes were calculated by K-theory in all successive runs.

In order to determine the momentum convergences necessary to close the mesospheric jets Rayleigh frictional damping of the zonal flow was introduced into the Model i.e. an additional term -ku was added to the right hand side of Equation (8.1). k is knows as the Rayleigh friction coefficient; as it is not based on any complete physical theory and is included only to enable the model to reproduce the observed zonal wind and temperature fields its specification, as a function of height, latitude or season, is left open to the modeller.

The inclusion of Rayleigh frictional damping has been adopted in most zonal mean models of the middle atmosphere and various choices of k have been made. Leovy (1964) used a constant value of $k = 0.1\ day^{-1}$ throughout. Schoeberl and Strobel (1978) experimented with various constant factors and concluded that a factor of $k \geqslant 0.1\ day^{-1}$ is required above the stratopause to produce the observed zonal wind and temperature structure but that smaller

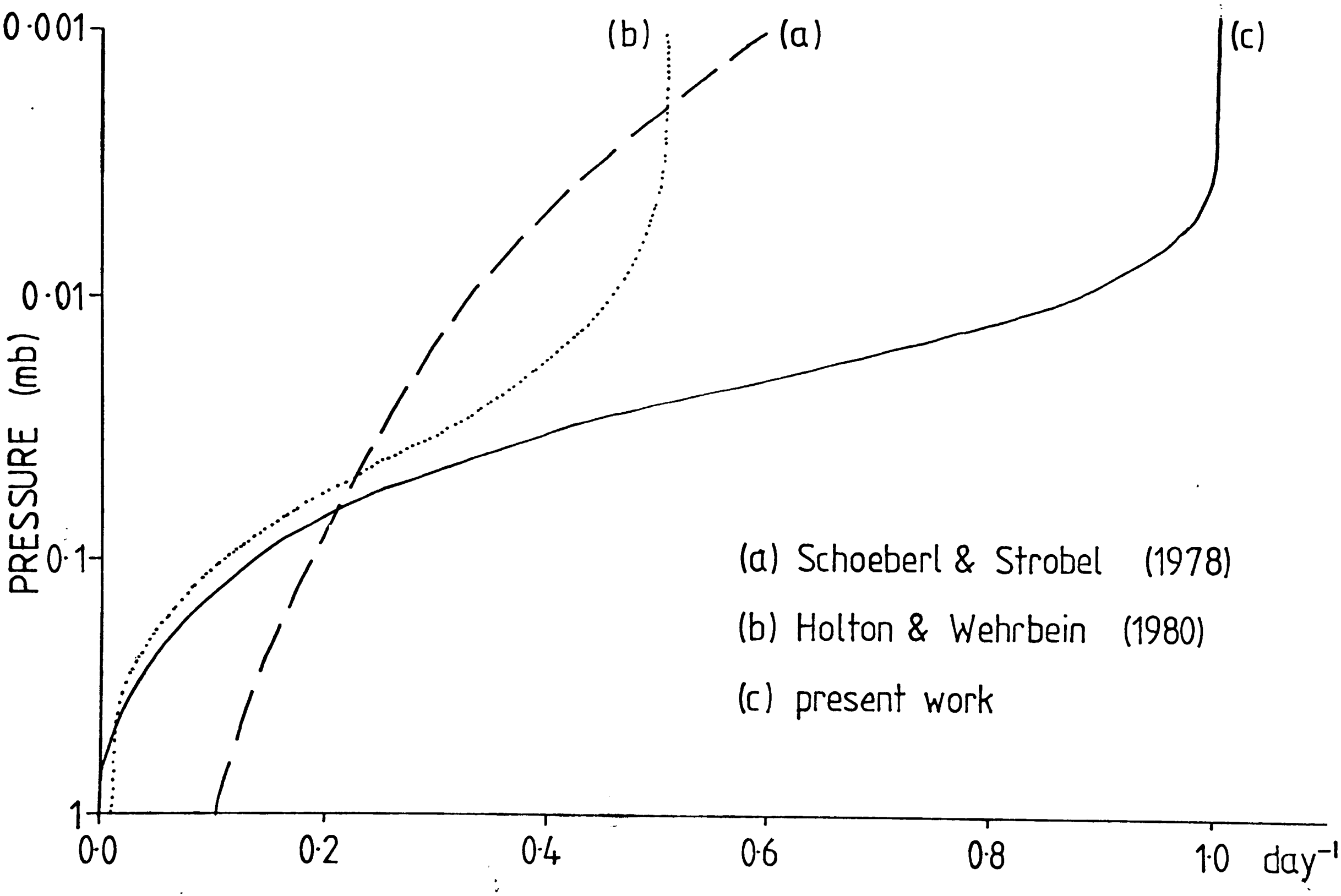

Fig. 8.9 Rayleigh friction coefficient.

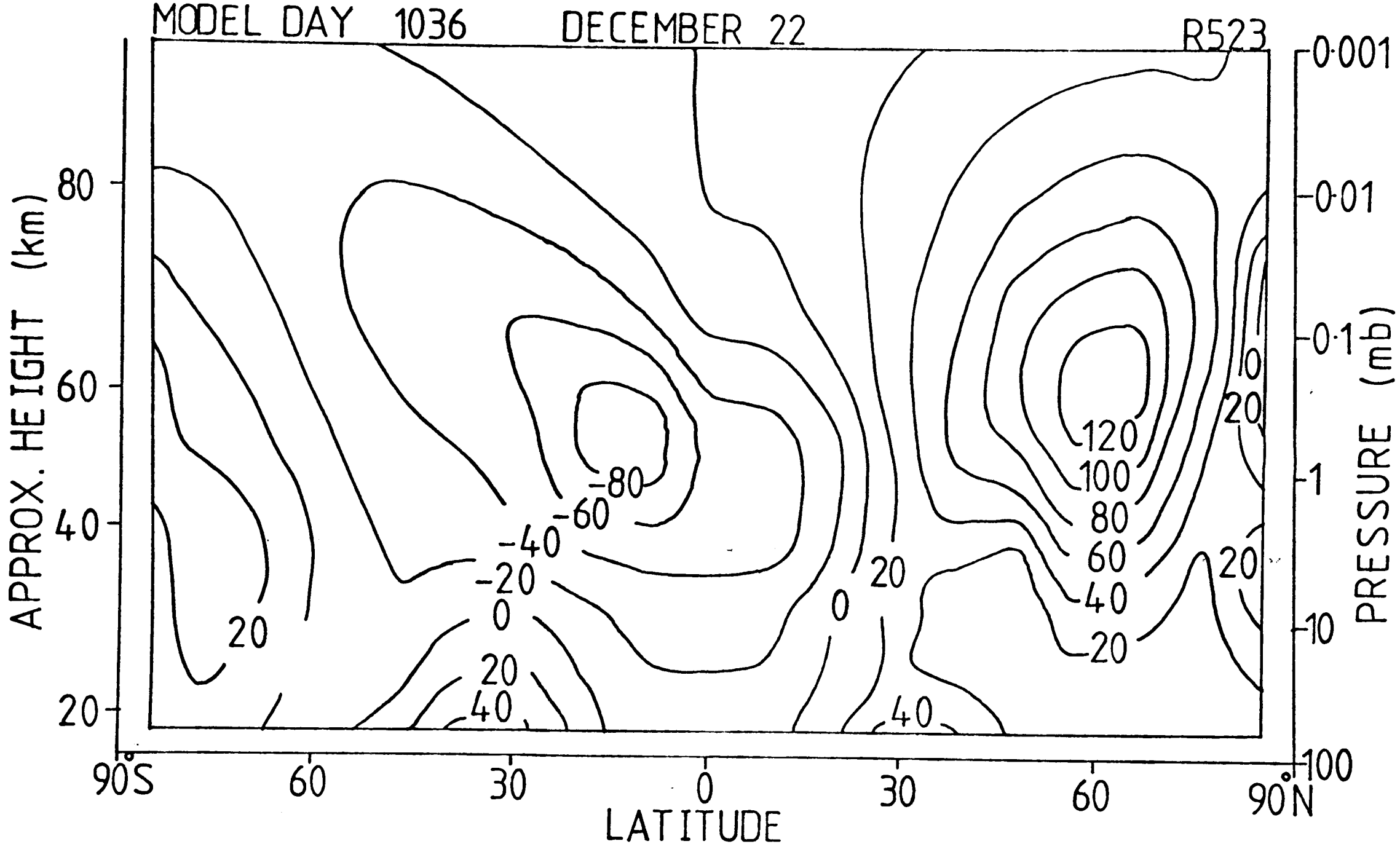

Fig. 8.10 Zonal wind (m/s) Run M

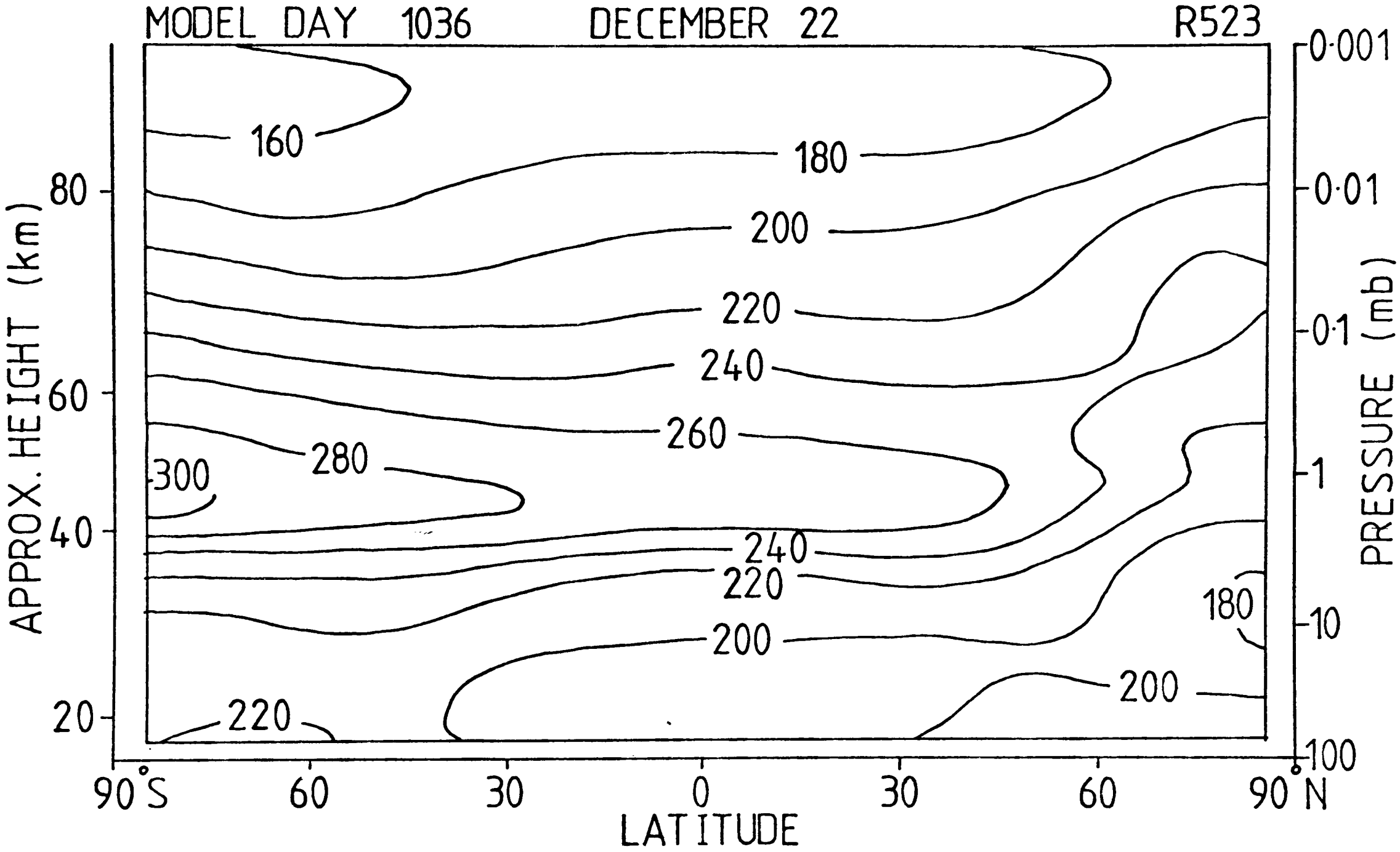

Fig. 8.11 Temperature (K) Run M

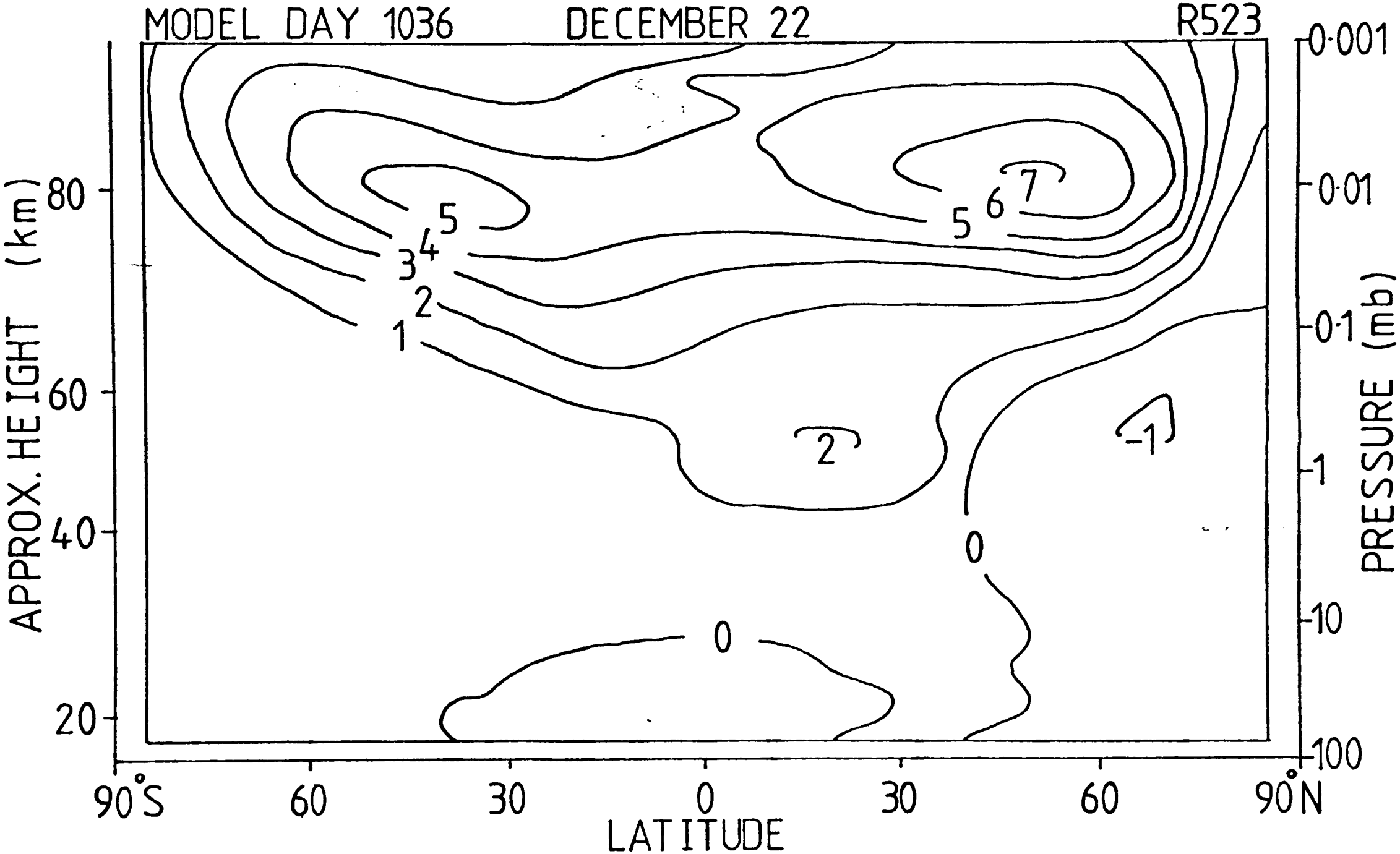

Fig. 8.12 (a) Meridional wind (m/s) Run M

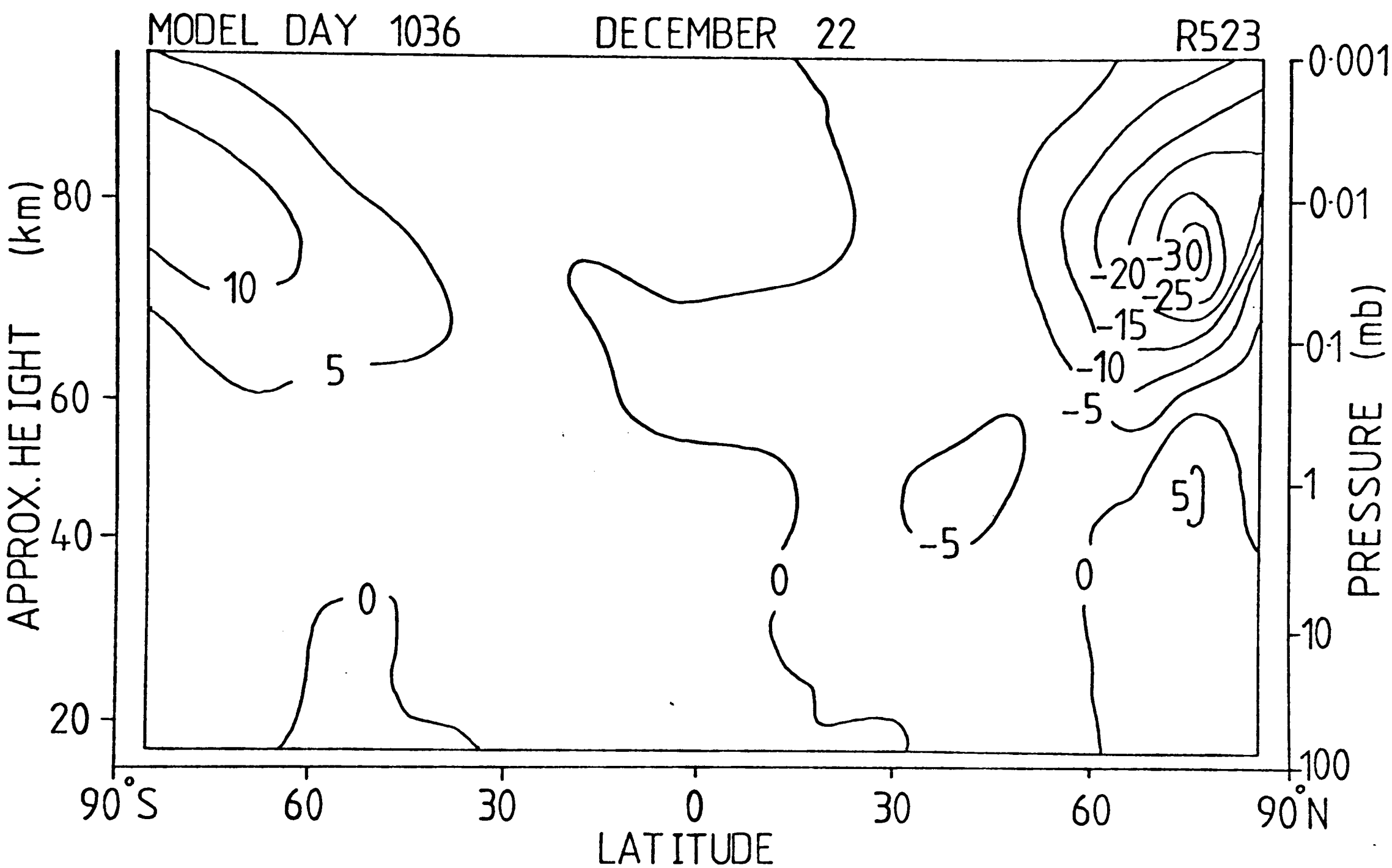

Fig. 8.12 (b) Vertical wind (mm/s) Run M

values ($k \sim 0.025$ day^{-1}) should be used in the lower stratosphere in order to avoid damping features such as the quasibiennial oscillation. They decided on a coefficient which increased exponentially with altitude and were able to produce zonal wind and temperature fields of reasonable shape and magnitude.

In the Oxford Model the Rayleigh friction coefficient is given the form of a smoothed step-function. Fig. 8.9 shows the values used along with the profiles of (a) Schoeberl and Strobel and (b) Holton and Wehrbein. The latter has, coincidentally, the same form as that used in this work although it has somewhat less damping above the mesospause. Run M was specified as Run E but included the frictional damping and also the 1976 planetary wave momentum fluxes. The zonal wind and temperature fields for Run M are shown in Figs. 8.10 and 8.11 respectively. The zonal wind jets close and the horizontal temperature gradient reverses in the upper mesosphere. The strength of the jets is somewhat high, associated with the exaggerated temperature gradient at the stratopause, but the improvement in general structure is obvious. The meridional and vertical winds are shown in Fig. 8.12; the major difference from the mean meridional circulation of Run E (Fig. 8.2) is the strong flow upwards in the summer high latitude mesosphere across to winter high latitudes and sinking there. This is now a thermally indirect cell, as the winter mesospause temperatures are higher than those of the summer mesopause, and, as shall be discussed below, is driven by the frictional damping such that the Coriolis acceleration on the meridional velocity acts to balance the Rayleigh friction term in the momentum equation.

In Fig. 8.3 the components of the zonal mean momentum equation were portrayed for Run E. Fig. 8.13 shows the same for Run M including the friction term $-ku$. The major differences between the two runs occur in the mesosphere and lower thermosphere. At 80 km the equation is dominated by a balance between the Rayleigh friction and Coriolis terms. The mean circulation components

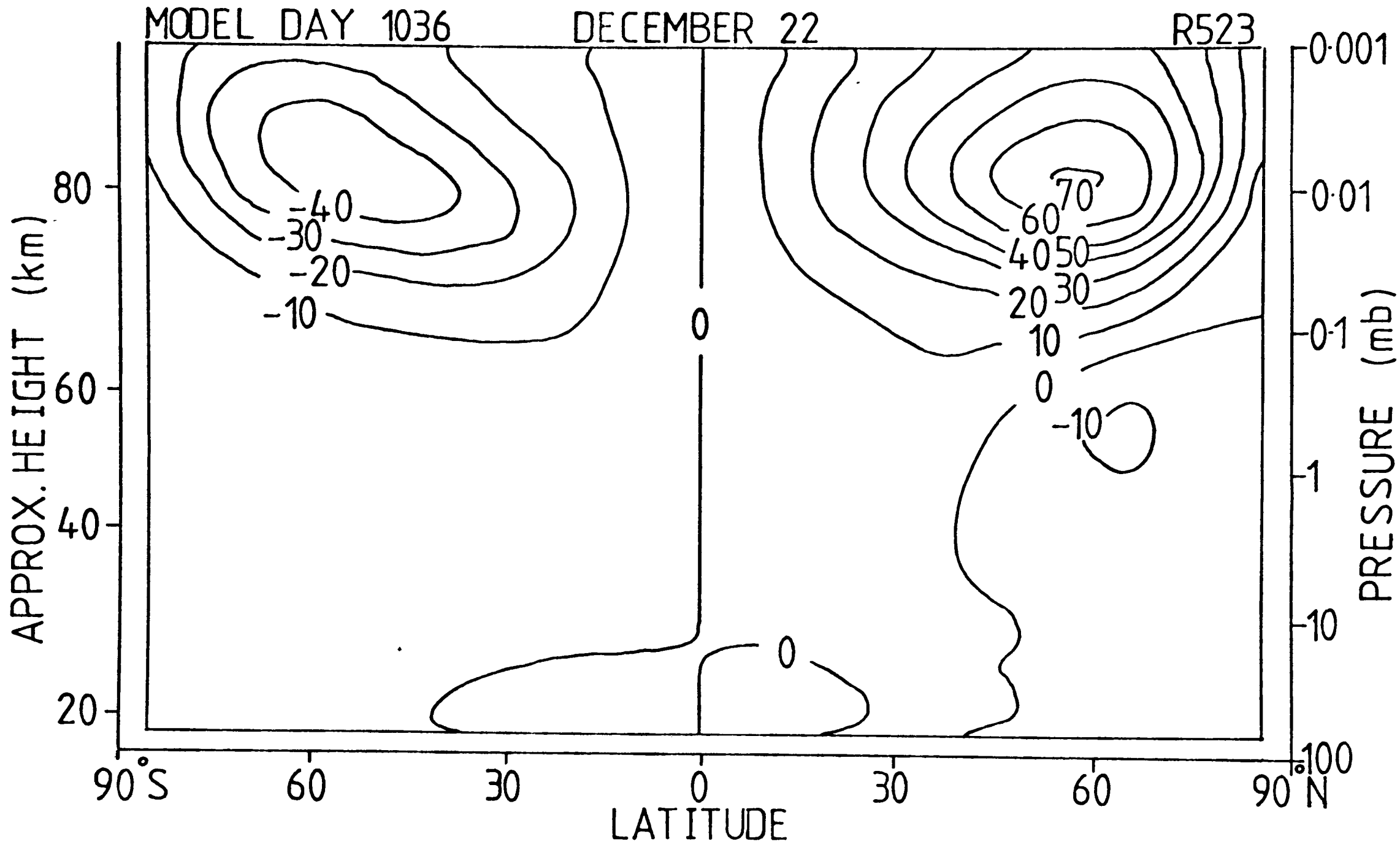

Fig. 8.13(a) fv (m/s/day) Run M

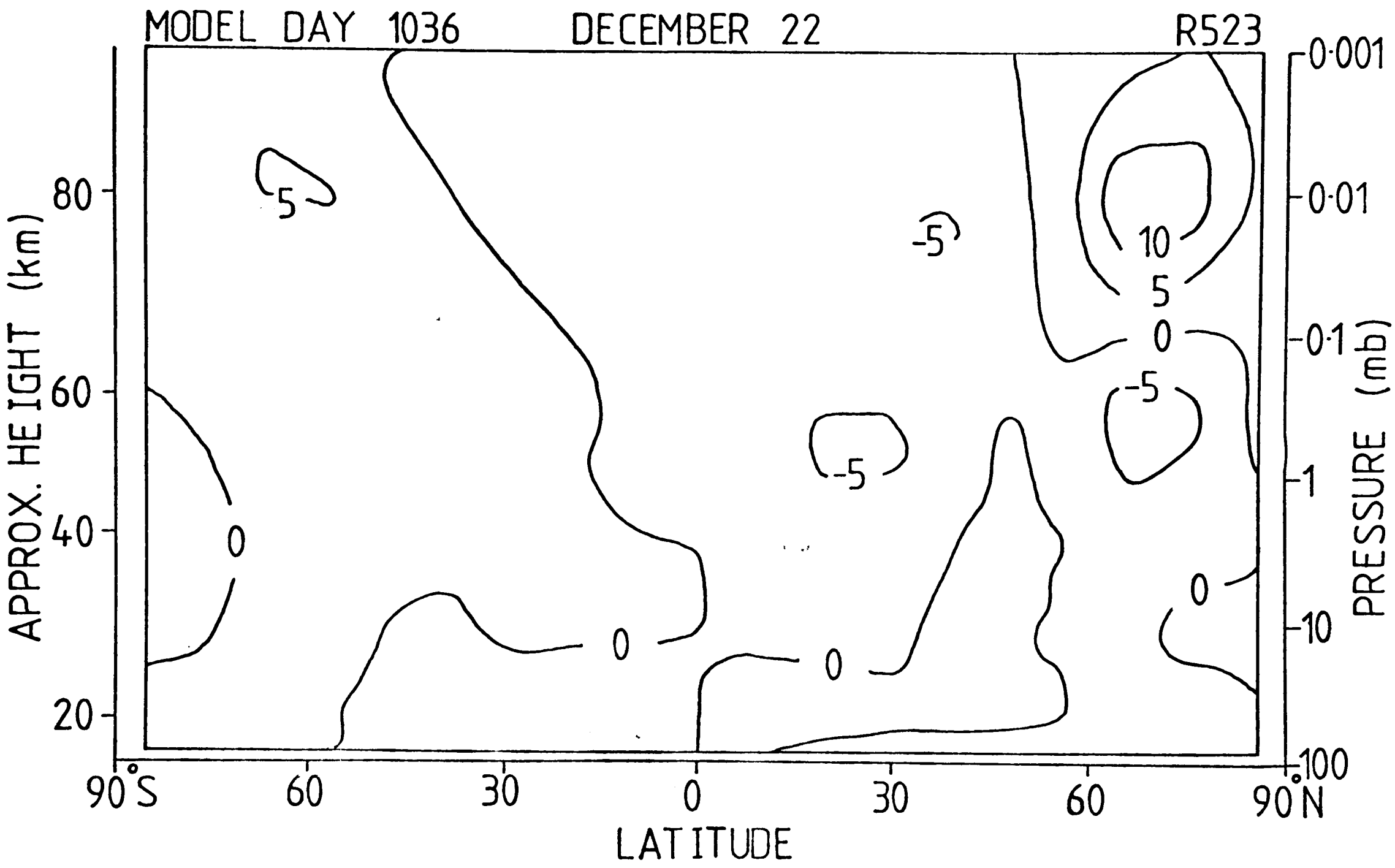

Fig. 8.13 (b) $-\frac{v}{a\cos\phi}\frac{\partial}{\partial\phi}(u\cos\phi)$ (m/s/day) Run M

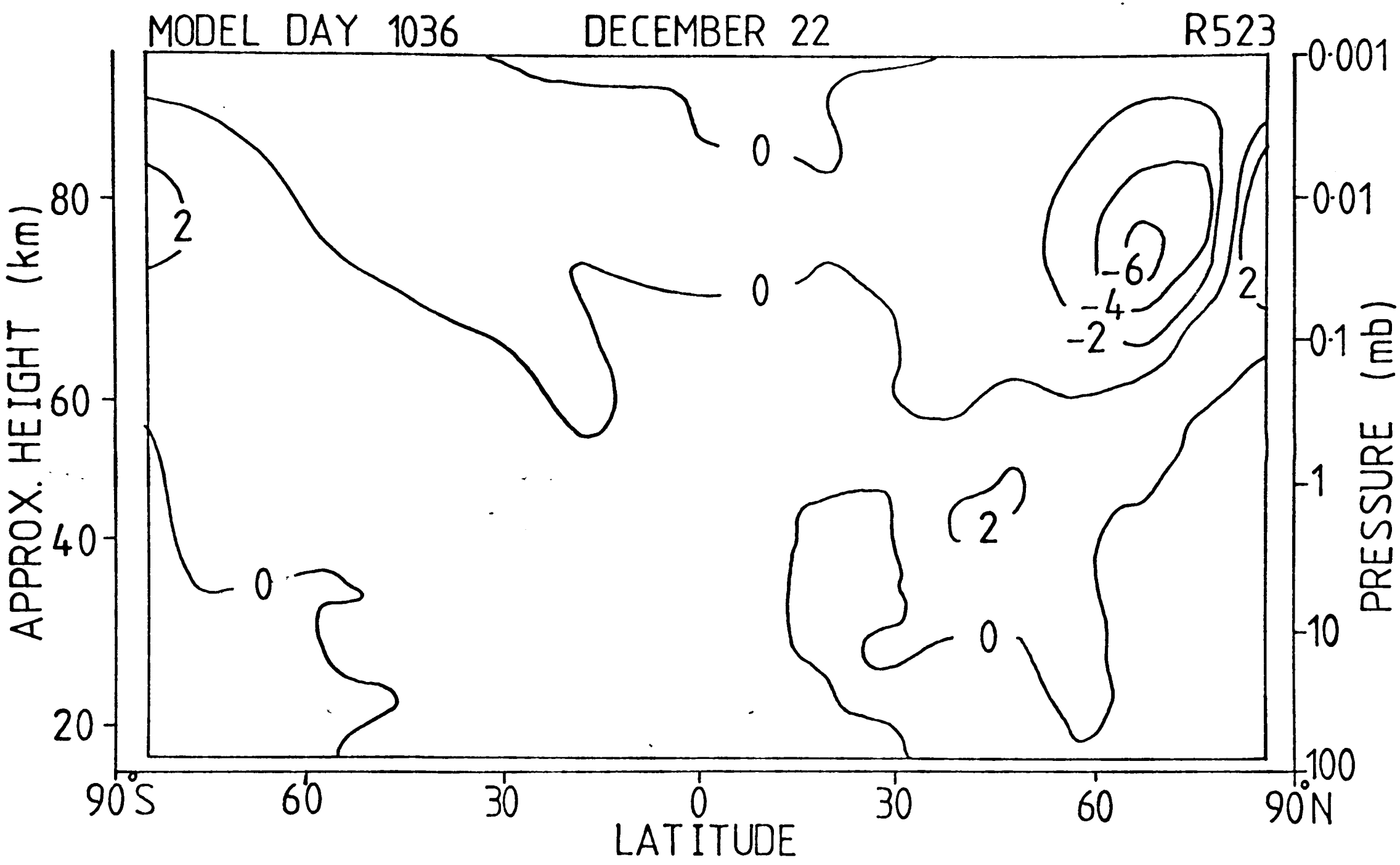

Fig. 8.13(c) $-w\,\frac{\partial u}{\partial \xi}$ (m/s/day) Run M

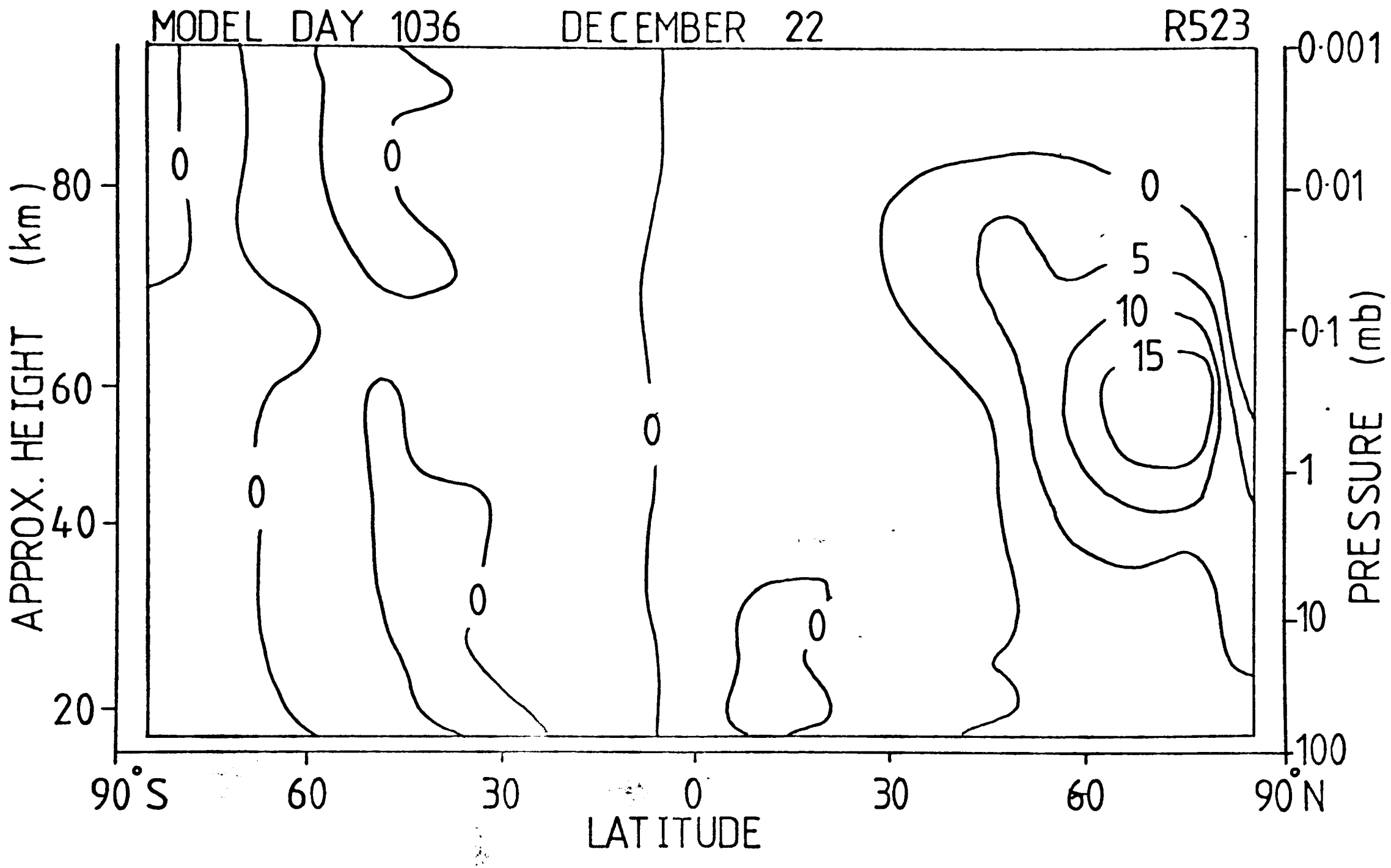

Fig. 6.13(d) horiz. divergence of eddy momentum fluxes (m/s/day) Run M

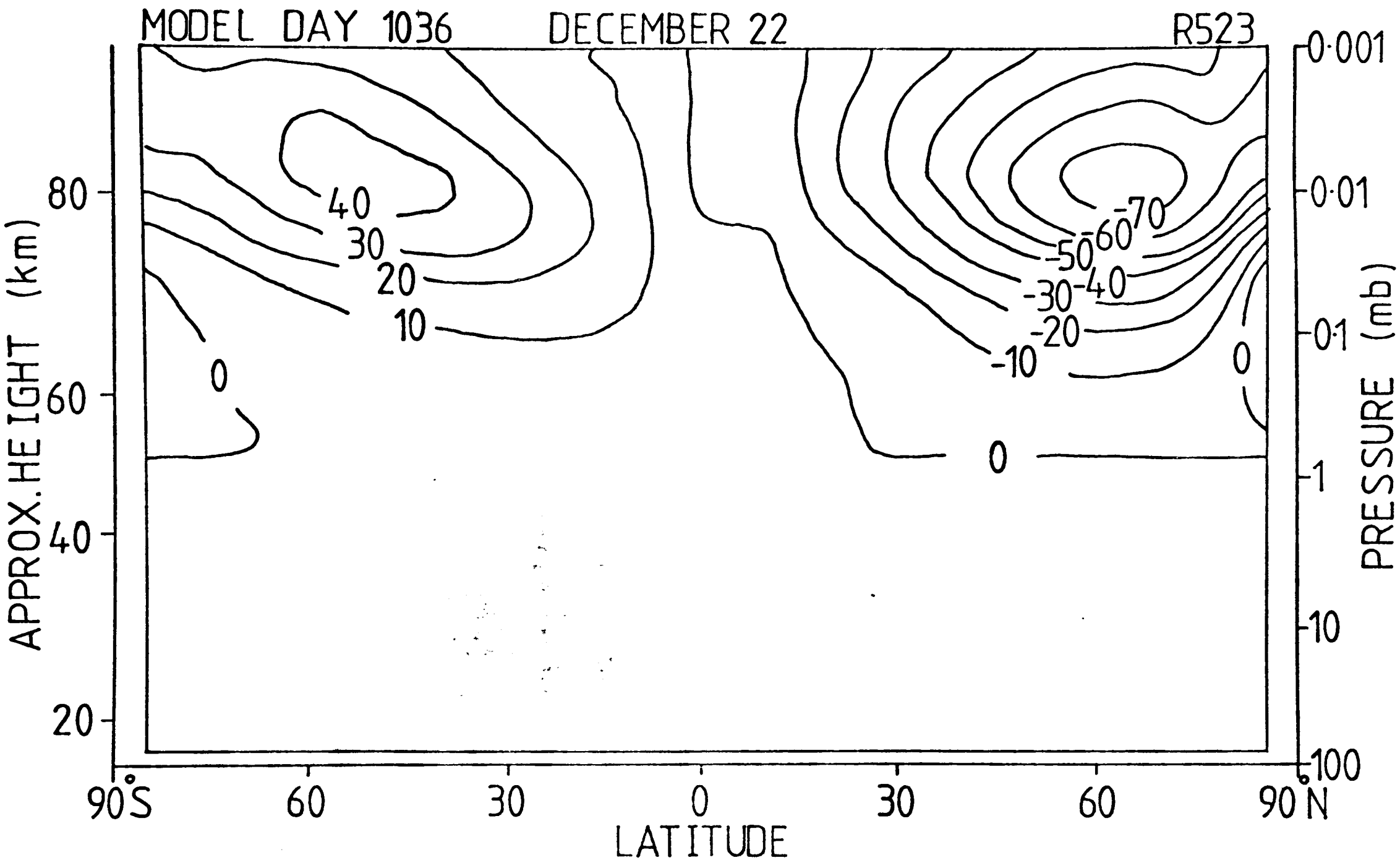

Fig. 8.13(e) — ku (m/s/day) Run M

also have maximum values at this level although they are of much smaller magnitude. The individual components at 50 km for Runs E and M are revealed in more detail in Figs. 8.14 (c) and (d). There is no frictional damping at this altitude and the difference between the two Runs is due to the use of the 1976 horizontal eddy momentum fluxes in Run M, as discussed in Section 8.5. The importance of planetary wave momentum fluxes at 50 km may be emphasised from these diagrams but although the magnitudes of the terms differ, the two runs are qualitatively very similar at this altitude. This is not the case at 80 km as shown by Figs. 8.14 (a) and (b) (note different vertical scale in Fig. 8.14 (b)). While transport by the mean circulation plays an important role in low and middle latitudes in Run E, Run M is dominated by the Rayleigh friction term with the mean circulation, and thus the Coriolis acceleration, adjusting accordingly.

It is interesting to study the relative importance of each driving force for the mean meridional circulation, as was done for Run E in Section 8.2. Fig. 8.15 shows the meridional velocity due to (a) Rayleigh frictional damping, (b) planetary wave momentum fluxes, (c) eddy heat fluxes and (d) radiative heating and cooling. The total meridional velocity was shown in Fig. 8.12 (a). The dominant driving force is that due to the frictional damping of the zonal wind; previously it has been assumed that diabatic heating and cooling were responsible for the circulation but in this work the radiative sources only become important at the highest altitudes considered. Planetary scale eddy fluxes of momentum and heat play only minor parts in driving the circulation in the mesosphere. To explore this result further an experiment, Run N, was conducted in which the net radiative heating was set to zero above the stratopause throughout the run but in which the Rayleigh frictional damping was maintained. Themodel fields of Run N showed all the gross features of Run M (the zonal wind jets closed, the horizontal temperature

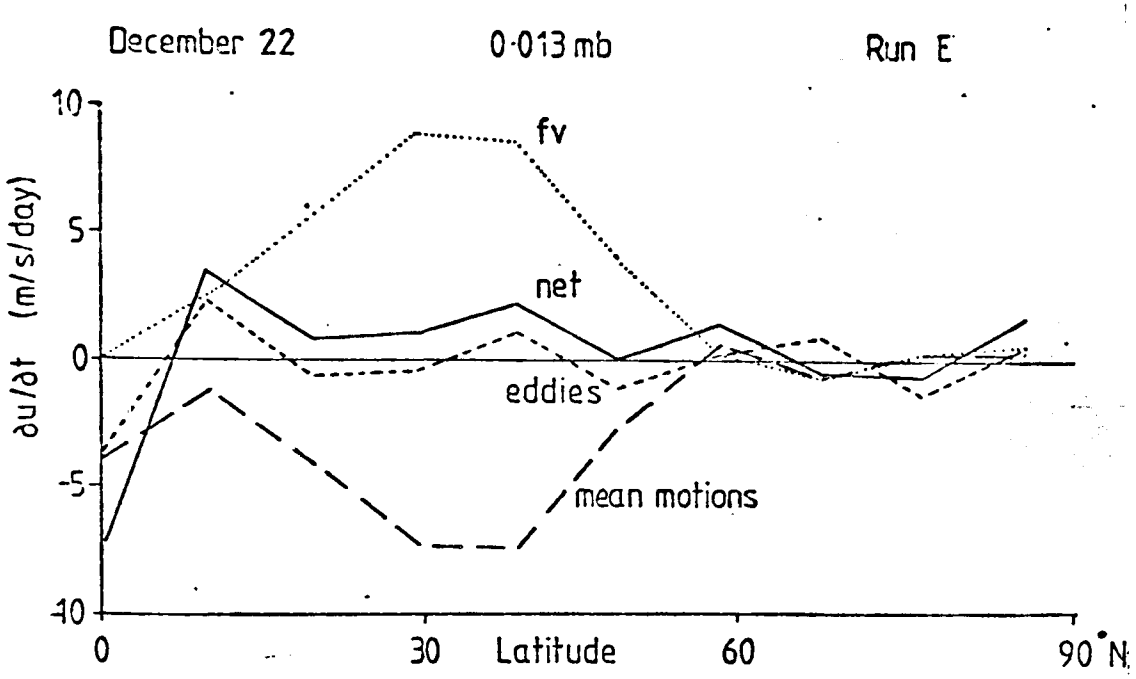

Fig. 8.14(a)

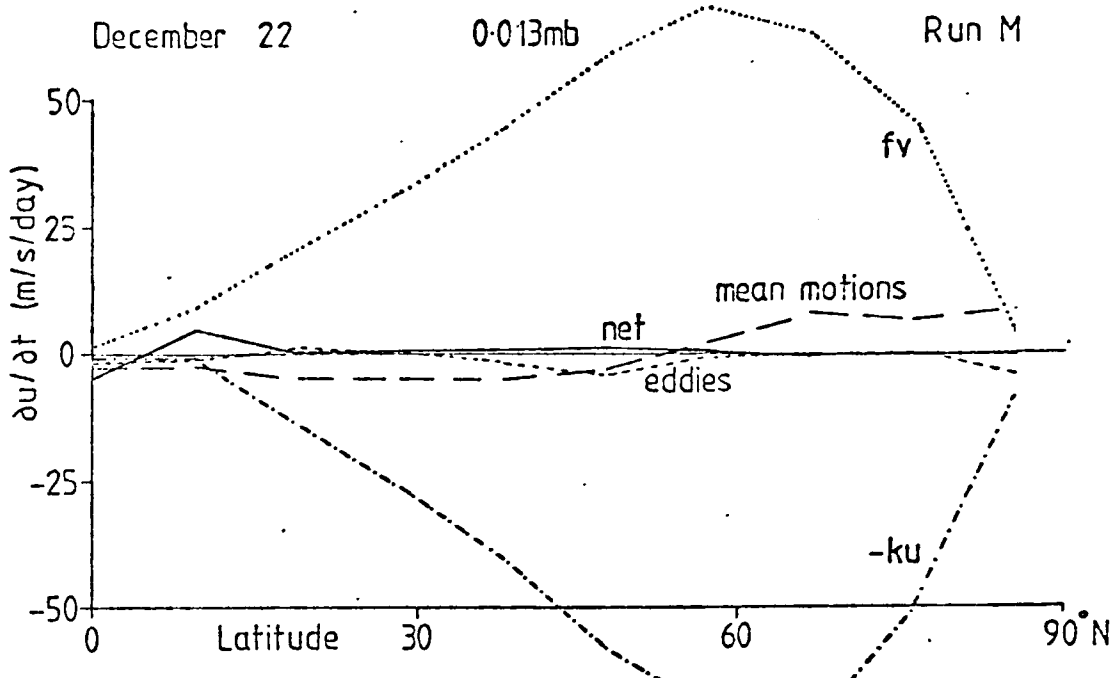

Fig. 8.14(b)

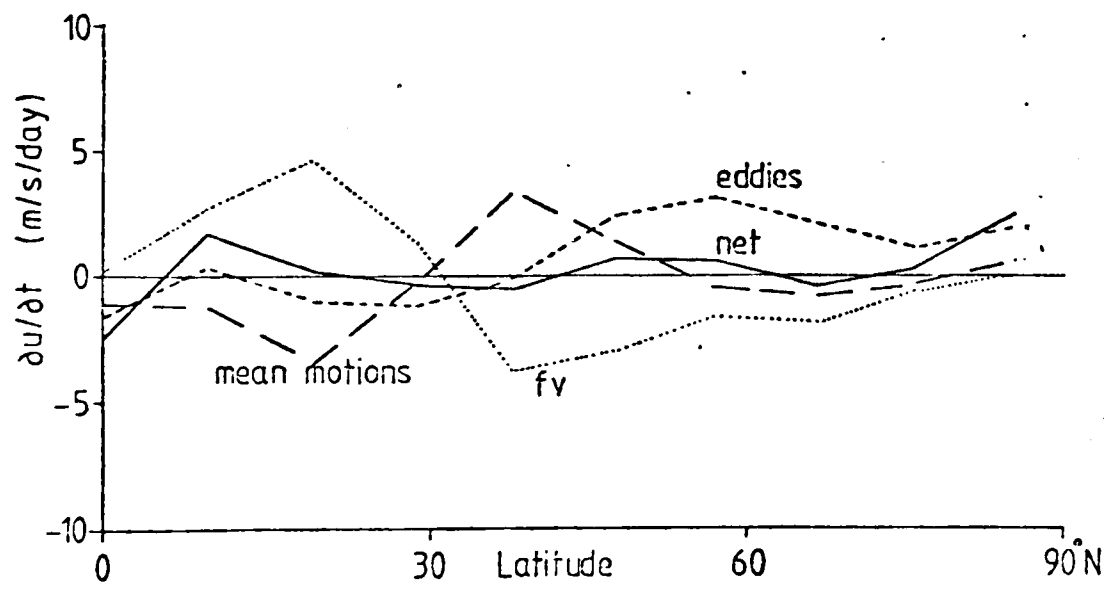

Fig. 8.14(c)

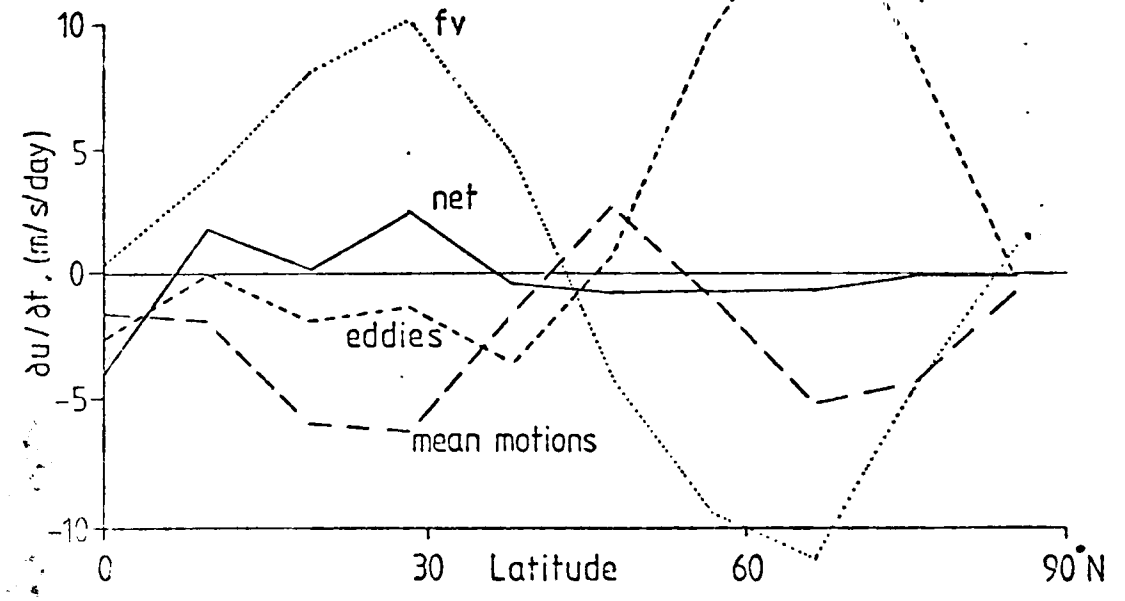

Fig. 8.14(d)

gradient reversed and the mean meridional circulation was still the huge pole to pole cell) although the absolute temperatures in the upper mesosphere were considerably reduced. Apparently the processes reporesented by the Rayleigh friction play a crucial role in the maintenance of the mesospheric circulation and an understanding of what these processes are is desirable.

8.7 Momentum deposition by tides and gravity waves

As discussed above it is necessary to include an extra term in the momentum equation to represent eddy frictional damping if the heat and momentum budgets are to be satisfied simultaneously. The source of this damping, however, is not clear. It has been shown that planetary waves cannot supply large enough eddy momentum fluxes and it is possible that the damping is a result of turbulent mixing due to the breakdown of atmospheric tides and vertically propagating gravity waves. In the absence of dissipation or critical levels the vertical momentum flux due to internal gravity waves, $\rho\overline{u'w'}$, is constant with height (Eliassen and Palm, 1960) but at a critial level, i.e. where the wave phase speed equals the mean wind speed, most of the waves' momentum is lost (Booker and Bretherton, 1967). As the atmospheric density decreases exponentially with height the wave amplitude must increase if the momentum flux is to remain constant and it is possible that as their amplitudes become large the waves become unstable and above a certain height the amplitudes remain constant (Lindzen, 1968). Thus, even in the absence of a critical level, momentum may be deposited. The shape of the profile for the Rayleigh friction parameter chosen in this work and by Holton and Wehrbein (1980) is consistent with the idea of the waves becoming unstable in a certain altitude region and maintaining a constant amplitude above.

The two most prominent of the atmospheric tides are the diurnal and

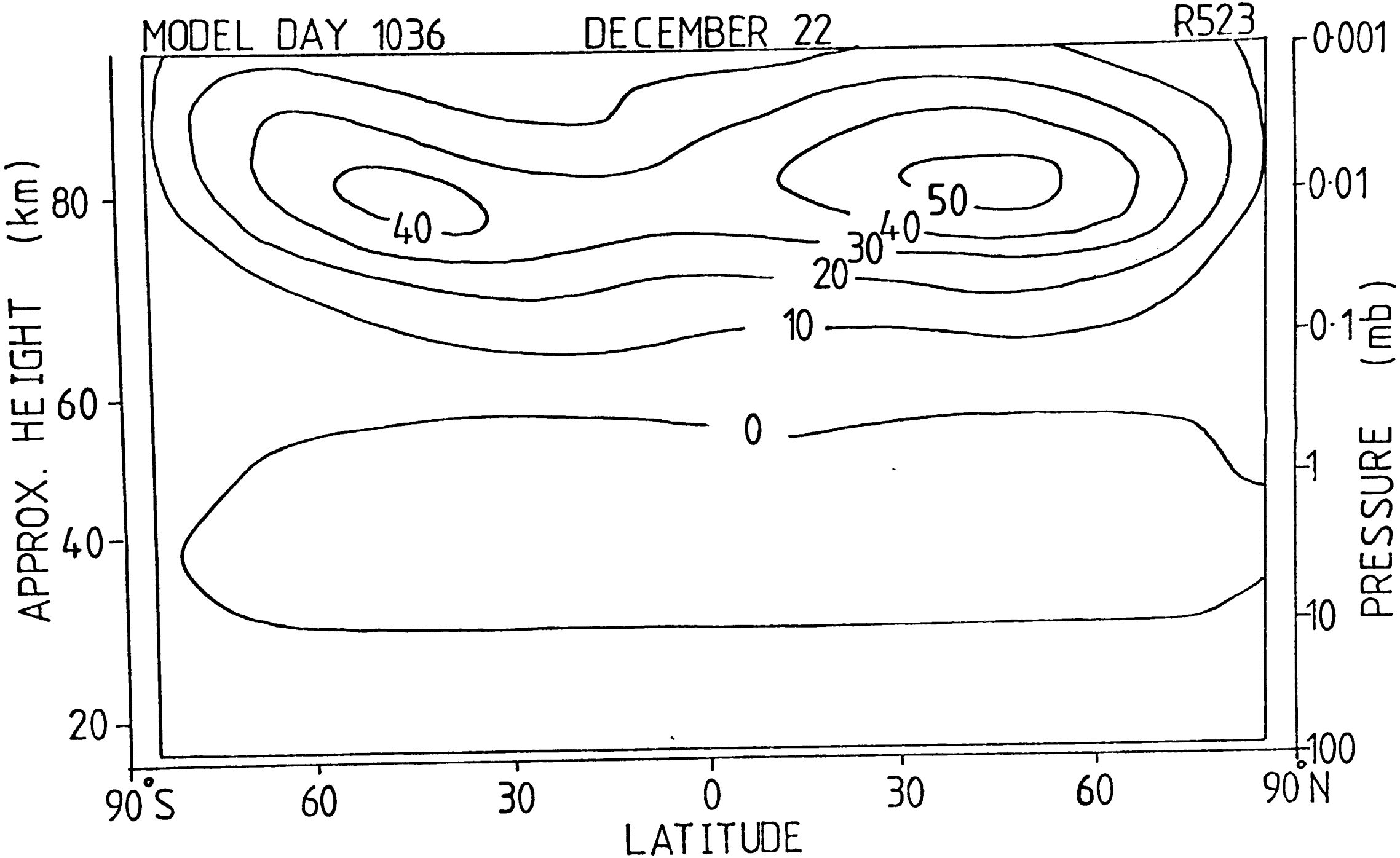

Fig. 8.15(a) v due to Rayleigh friction (0·1m/s) Run M

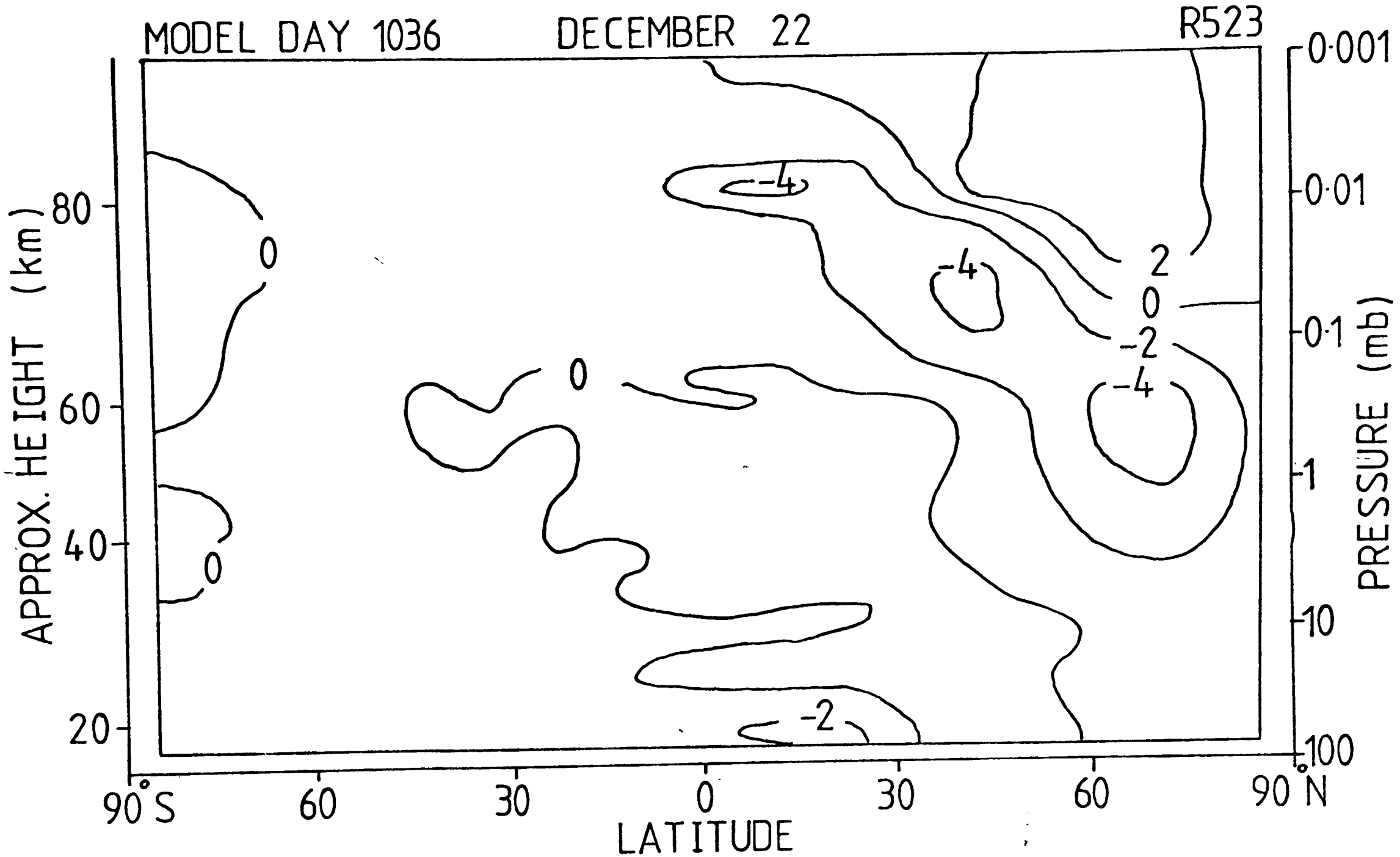

Fig. 8.15 (b) v due to eddy momentum fluxes (0·1m/s) Run M

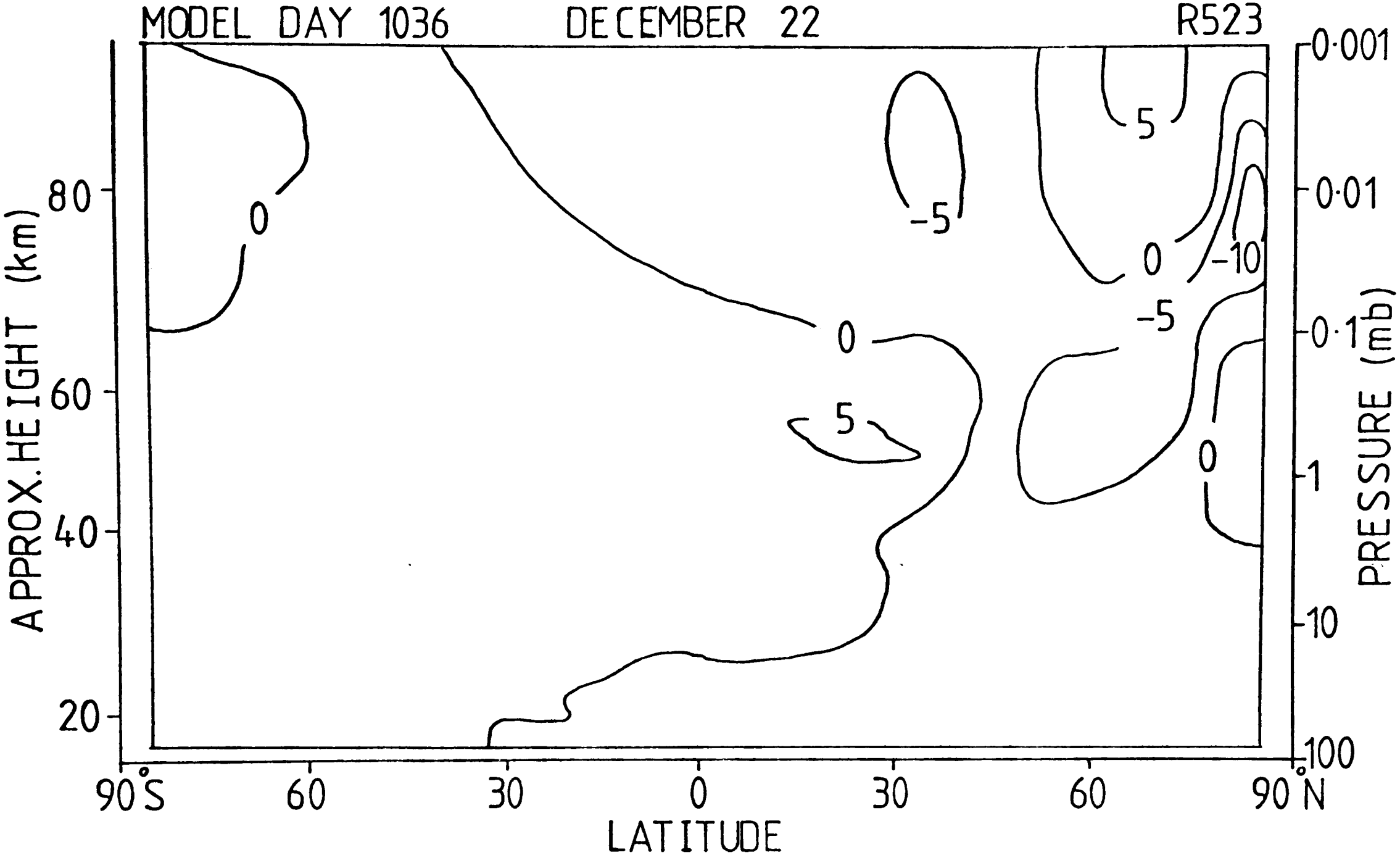

Fig.8.15(c) v due to eddy heat fluxes (0·1m/s) Run M

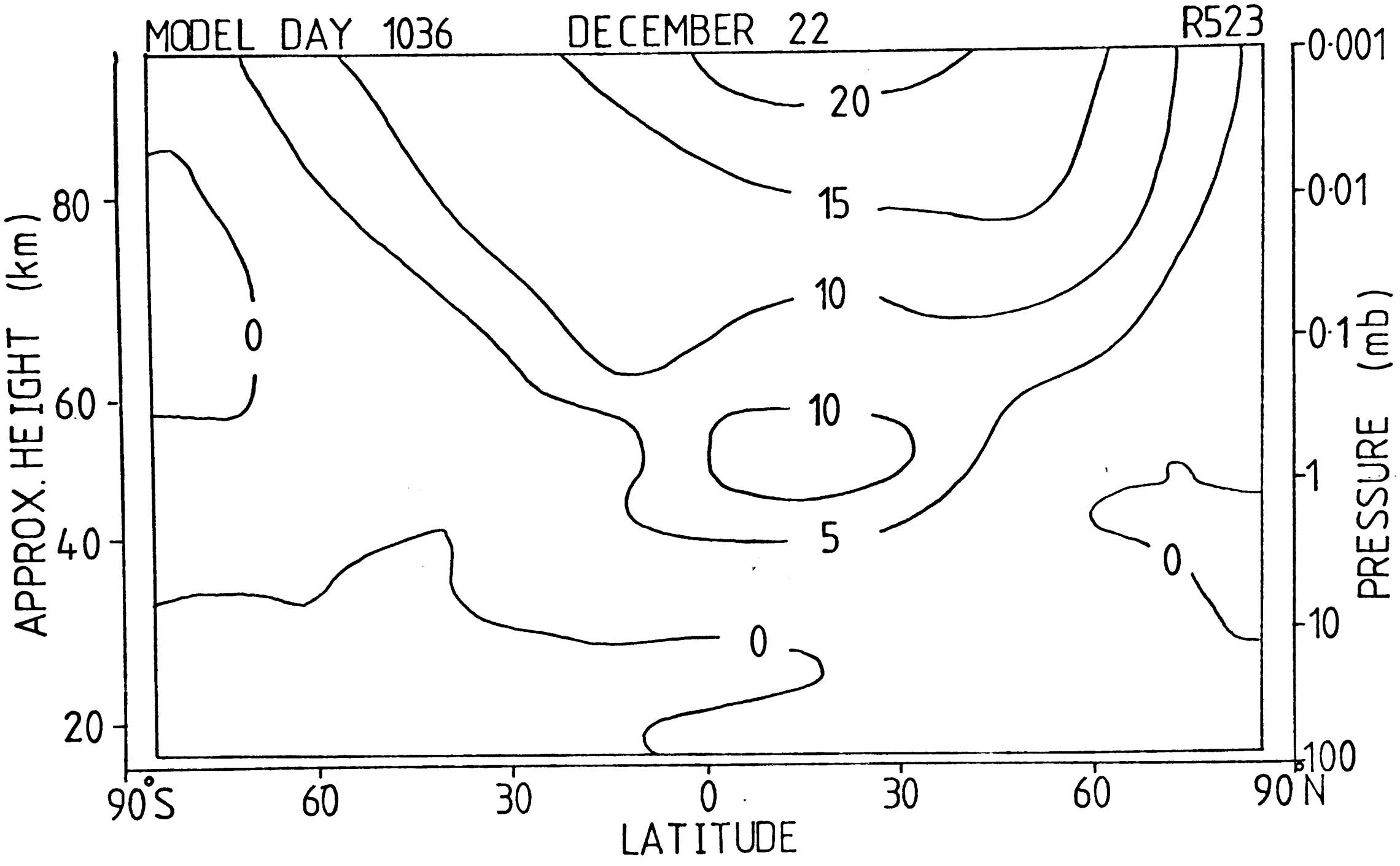

Fig. 8.15(d) v due to radiative heating (0·1m/s) Run M

semi-diurnal tides driven by thermal forcing due to the absorption of solar radiation by water vapour and ozone. Above 70 km the energy in tidal motions is comparable to that of the large scale winds but because of the magnitude of tidal phase speeds critical level interactions cannot occur and interaction with the mean flow will only happen in regions of strong dissipation. Hines (1972b), using estimates of the amplitude of the propagating diurnal mode made by Lindzen (1967), calculated that at 85 km in low latitudes the convergence of the vertical flux of westward momentum would lead to an acceleration of about 20 m s^{-1} day^{-1} if the wave amplitude remained constant. This is of significant magnitude with respect to the values estimated for the Rayleigh friction term in Run M (see Fig. 8.15 (a)). However Elford (1978) has analysed a series of meteor wind observations at 35°S and found that the maximum contribution from diurnal and semi-diurnal winds to a change in the zonal flow at 90 km is about 7 m s^{-1} day^{-1}. At higher latitudes Hines (1972b) estimates a deposition of eastward momentum but at greater altitudes.

Gravity waves are generated in stably stratified layers by flow over topographic barriers or by other perturbations of the background flow. Their periods typically range from several minutes to a few hours and their wave lengths are of the order of 100 km in the horizontal and 1 km in the vertical. Hodges (1969) and Hines (1970) have discussed gravity waves as a major source of turbulence near the mesopause.

The observations of winds in the region 60 - 118 km at 52°N made by Manson et al (1979) shows that throughout 1976 in this region the energy density of gravity waves was higher than that of tides or planetary waves and that it decreased with height. If the dissipated energy goes into the background flow in a layer of thickness H the acceleration of the mean flow is given, approximately, by

$$\dot{u} = \Delta(\overline{\rho v^2}) \frac{\tau_g}{\tau H \bar{\rho}}$$ Hines (1972b)

where $\Delta(\overline{\rho v^2})$ is the change in energy density over layer H,

τ is the wave period,

τ_g is the Brunt-Vaisala period,

and $\bar{\rho}$ is the density at the centre of H.

Using the data ofManson et al (1979) it is found that at 90 km $\dot{u}$= 12 -48 m s^{-1} day^{-1}. This acceleration is only realisable if a significant portion of the internal gravity waves is polarised in some direction. Even a small coherence, however, could modify the prevailing wind considerably and Mansen et al found some evidence of correlation between variance and direction.

Although the correspondence between the dissipation of tides and gravity waves and the strong damping required in the two-dimensional numerical models described above has not been firmly established it appears to be energetically possible. Further observations of upper atmospheric winds are needed to give more detailed information on the amplitude and direction of propagation of gravity waves together with their latitudinal and seasonal variations before this hypothesis becomes acceptable.

CHAPTER 9

Conclusions and suggestions for future work

9.1 Conclusions

This thesis has described experiments with a two-dimensional model of the general circulation already established at Oxford University. A major part of the work has been the replacement of the schemes to calculate solar heating and long-wave cooling rates by more accurate methods which extend up to the top of the model domain (~ 95 km). A Curtis matrix approach was found to be suitable for calculating radiative cooling in the carbon dioxide 15μm band. This method incorporates the transfer of radiation between atmospheric layers and non-L.T.E. effects. The use of one matrix provides a suitable accuracy for all reasonable temperature profiles.

Calculations of the deviation from L.T.E. require a knowledge of the collisional relaxation time, τ. The effects of using recent, temperature-dependent measurements of τ for the relaxation of CO_2 (ν_2) by N_2 and O_2 were assessed. The new values show less temperature dependence at atmospheric temperatures than values extrapolated from previous higher temperature measurements and they had significant effect on the cooling rates above about 75 km; this is particularly important in winter when cooling rates are larger and there is little solar heating. Using the new τ values a radiative relaxation time for the atmosphere at 85 km was estimated at 2 days implying some form of continual forcing for the 7 - 12 day waves observed at this altitude during the Winter Anomaly Campaign. A method for calculating a Curtis matrix for a species with altitude-dependent mixing ratio was developed and an attempt was made to evalute τ for the de-excitation of CO_2 (ν_2) by atomic oxygen by comparison of calculated and observed values of radiative flux up to 140 km. The correspondence between theory and measurement was good but a value could not be fixed for τ because of a lack of information on other

atmospheric parameters appropriate to the time of the observations.

The inclusion of the Curtis matrix in the model improved the temperature structure of the stratosphere and lower mesosphere. The stratopause temperature was reduced to a realistic value in summer but a rather low value in winter. The altitude of the stratopause was unaffected and still too low. The summer high latitude stratopause was found to be in approximate radiative equilibrium for both methods. The heat budget of the stratosphere was discussed and the balance between heat transport by eddies and the mean circulation observed in winter high latitudes.

A scheme for calculating the heating of the atmosphere by the absorption of solar radiation by O_3 and also O_2 has been developed. It is 'exact' in that it uses recent solar flux data and absorption cross-section measurements in small wavelength bands but approximate in that it neglects wavelength regions which are of minor importance at various altitudes. When used in the Model the improved scheme made only a small difference with temperatures in the middle stratosphere increasing slightly.

The inclusion of the new schemes for both thermal and solar radiation enabled the calculated of the net heating rate up to the top level of the model at 95 km. Other diabatic sources of heating near the mesopause have been discussed. The inclusion of a representative airglow cooling caused instability in the model's relaxation scheme so an empirical factor was introduced which did not affect the results below the mesopause. Because of the strong O_2 absorption in the summer high latitude upper mesosphere the temperatures here increased giving a horizontal temperature gradient in the opposite sense to that observed and a zonal wind structure with no indication of a decrease in strength of either easterly or westerly jets above 65 km.

The new radiation schemes did not induce significant changes in the ozone field. The use of the more complete photochemical scheme, however,

improved the latitudinal and temporal distribution of ozone and raised the altitude of the stratopause. Thus the inclusion of the new radiation schemes together with the new photochemical scheme produced a good representation of the temperature, wind and ozone structure of the stratosphere and lower mesosphere. The success of the model may be attributed not only to the inclusion of realistic representations of dynamics, photochemistry and radiation but also, and just as important, to the fact that these schemes are coupled so that feedbacks between the various fields are allowed. An experiment in which the radiative equilibrium in the lower stratosphere was replaced by climatological net heating rates showed the extreme sensitivity of temperature and ozone to the diabatic heating there.

The Curtis matrix may be calculated for any specified CO_2 mixing ratio and an experiment was conducted in which the concentration was increased at four times the estimated rate. By a date equivalent to the year 2040 the temperature of the middle and upper stratosphere had decreased by about 10K. The changes in ozone showed increases of about 25% at 40 km at all latitudes and in the lower stratosphere a reverse 'self-healing' effect (i.e. decreases of O_3) in low latitudes. The changes in ozone column density emphasised this with large increases in high latitudes and smaller effects in the tropics. No other calculation has been able to show this latitudinal variation.

It was noticed that the effect of increasing CO_2 on O_3 was in exactly the opposite sense to that predicted for the effect of an increasing atmospheric content of chlorofluorocarbons (CFCs). An experiment was conducted in which CFCs were introduced at four times the estimated rate. By the simulated year 2040 decreases of about 35% were apparent at 45 km and a 'self-healing' effect obvious in the lower stratosphere low latitudes. Again the ozone column density showed largest changes in high latitudes. Unlike previous experiment with CFCs in the Model (Pyle, 1980) the feedback between ozone and

temperature was permitted and the changes in temperature showed a band of temperature decrease in the upper stratosphere. Thus the CFCs showed an opposite effect to CO_2 on the ozone concentration but a similar one on the temperature.

A run in which both CO_2 and CFCs were introduced was carried out. The change in ozone was not a linear addition of the changes due to the two perturbers introduced separately. The non-linearity was particularly clear in O_3 concentration at 40 km and in O_3 column density at all latitudes. A simple photochemical theory was used to show that O_3 has a different temperature dependence in the presence of ClO_x and values of $d \ln [O_3] / dT^{-1}$ produced by the Model were used to explain the non-linearity of the two effects. Because the catalytic destruction of O_3 in the ClO_x cycle is less dependent on temperature than in the other cycles the effect of increasing CO_2 is lessened at higher atmospheric chlorine contents.

The heat and momentum budgets and the mean meridional circulation of the upper stratosphere and mesosphere have been investigated using the Model. Eddy momentum fluxes derived from satellite observations of planetary waves, of wavenumber four and less, up to 80 km were incorporated in the Model. The use of data from different years was shown to have a significant effect on the circulation and transport properties of the stratosphere. The planetary wave eddy momentum fluxes were, however, incapable of producing the necessary momentum redistribution in the mesosphere and had no significant effect on the zonalwind structure at these altitudes.

In order to reproduce the observed zonal wind fields a Rayleigh friction term was introduced into the momentum equation in the mesosphere. The temperature structure is also improved through the thermal wind relationship. The meridional circulation consists of ascent at the summer pole, horizontal motion to the winter pole and descent there. This is a result of the Coriolis term balancing the friction term in the momentum equation.

The relative importance of frictional damping, eddy momentum fluxes, eddy heat fluxes and diabatic heating in driving the mean meridional circulation were assessed. The diabatic sources were found to be of secondary importance to the friction term in maintaining the circulation. Momentum deposition due to the breakdown of vertically propagating gravity waves was discussed as a process possibly represented by the Rayleigh friction parameterisation and found, on the basis of wind observations, to be energetically possible.

9.2 Future work

The Model as presently established is a useful tool for studying atmospheric structure, composition and behaviour and it incorporates many of the feedback mechanisms that exist between dynamics, radiation and photochemistry. The major scope for improvement lies in the regions in which quantities are specified independent of the model state and in which, therefore, the feedbacks are not present.

One example of this is the radiative heating and latent heat release in the troposphere and lower stratosphere. To incorporate these in a model-dependent fashion a scheme is needed which includes the absorption of radiation by water vapour, a hydrologic cycle, modelled sea-surface temperatures, clouds and scattering by air molecules and in clouds. Also desirable is a method which calculates cooling in the 9.6μm band of ozone in a manner dependent on local O_3 mixing ratio. The calculation of the Curtis matrix could be improved with the use of more recent line strength data and temperature-dependent Lorentz widths. If the Curtis matrix method were to be used in the lower stratosphere a different band model would be needed. A decrease in the computing time required would be achieved by the amalgamation of the photochemical and solar heating schemes.

Another area for future research is the eddy transport of momentum, heat and tracers. A method currently being investigated (Pyle and Rogers, 1980) involves a linearised scheme for the calculation of planetary wave propagation with appropriate assumptions as to the forcing at the lower boundary. If this can be incorporated into the Model it will provide eddy fluxes calculated in a manner more sensitive to the Model state and therefore more reliable, especially in perturbation studies where the modelled fields deviate markedly from their unperturbed values.

The heat and momentum balance of the mesopause region needs to be investigated in more detail. Heating due to chemical reactions and quenching could be incorporated if a combined solar heating-photochemistry scheme were introduced up to the top level of the Model. Heat and momentum deposition by gravity waves might be included if more data on the wavelength spectrum, amplitudes and frequency of occurrence of gravity waves become available.

Appendix A

Details of the finite difference equation for the stream function.

$$D_1(L,M) = \{[-\bar{\tau}(L-1,m+1) + \bar{\tau}(L+1,m+3)]F_1(L) + [\bar{\tau}(L+1,m+1) - \bar{\tau}(L-1,m+3)]F_3(L) + G_1(L,m)[-\bar{\theta}(L-1,m+1) + \bar{\theta}(L+1,m+3)]F_1(L) - [\bar{\theta}(L+1,m+1) - \bar{\theta}(L-1,m+3)]F_3(L)\}\beta^{-1}$$

$$D_2(L,M) = \{[\bar{\tau}(L+3,m+1) - \bar{\tau}(L+1,m+3)]F_1(L) + G_1(L,m)[\bar{\theta}(L+3,m+1) - \bar{\theta}(L+1,m+3)]F_1(L)\}\beta^{-1}$$

$$D_3(L,M) = \{[-\bar{\tau}(L+3,m+1) + \bar{\tau}(L+1,m-1)]F_1(L) - [\bar{\tau}(L+3,M-1) - \bar{\tau}(L+1,m+1)]F_2(L) + G(L,m)[-\bar{\theta}(L+3,m+1) + \bar{\theta}(L+1,m-1)]F_1(L) + [\bar{\theta}(L+3,m-1) - \bar{\theta}(L+1,m+1)]F_2(L)\}\beta^{-1}$$

$$D_4(L,M) = \{[\bar{\tau}(L+3,m-1) - \bar{\tau}(L+1,m-3)]F_2(L) + [-\bar{\theta}(L+3,m-1) + \bar{\theta}(L+1,m-3)]F_2(L)G(L,m)\}\beta^{-1}$$

$$D_5(L,M) = \{[-\bar{\tau}(L+1,m-1) + \bar{\tau}(L+1,m-3)]F_2(L) + [\bar{\tau}(L+1,m-1) - \bar{\tau}(L-1,m-3)]F_4(L) + G(L,m)[\bar{\theta}(L-1,m-1) - \bar{\theta}(L+1,m-3)]F_2(L) + [\bar{\theta}(L+1,m-1) - \bar{\theta}(L-1,m-3)]F_4(L)\}\beta^{-1}$$

$$D_6(L,M) = \{-\bar{\tau}(L-3,m-1) + \bar{\tau}(L-1,m-3) + G(L,m)[\bar{\theta}(L-3,m-1) + \bar{\theta}(L-1,m-3)]\}F_4(L)\beta^{-1}$$

$$D_7(L,M) = \{[\bar{\tau}(L-3,m+1) - \bar{\tau}(L-1,m-1)]F_3(L) + [-\bar{\tau}(L-3,m-1) - \bar{\tau}(L-1,m+1)]F_4(L) + G(L,m)[-\bar{\theta}(L-3,m+1) + \bar{\theta}(L-1,m-1)]F_3(L) + [\bar{\theta}(L-3,m-1) - \bar{\theta}(L-1,m+1)]F_4(L)\}\beta^{-1}$$

$$D_8(L,M) = \{-\bar{\tau}(L-3,m+1) + \bar{\tau}(L-1,m+3) + G(L,m)[\bar{\theta}(L-3,m+1) - \bar{\theta}(L-1,m+3)]\}F_3(L)\beta^{-1}$$

$$RHS(L,M) = \{-H(L+1,m+1)F_1(L) - H(L-1,m+1)F_3(L) + H(L+1,m-1)F_2(L) + H(L-1,m-1)F_4(L) + G(L,m)E(m)[-q(L+1,m+1) - q(L+1,m-1) + q(L-1,m+1) + q(L-1,m-1)] + G(L,m)[-Q(L+1,m+1)F_1(L) - Q(L+1,m-1)F_2(L) + Q(L-1,m+1)F_3(L) + Q(L-1,m-1)F_4(L)]\}f\beta^{-1}$$

where $F_1(L) = \exp(1/4)/C_0(L+1)$ $\quad F_2(L) = \exp(-1/4)/C_0(L+1)$

$F_3(L) = \exp(1/4)/C_0(L-1)$ $\quad F_4(L) = \exp(-1/4)/C_0(L-1)$

$f = 2hk$

and $B = \{[\bar{\tau}(L-1,m+1) - \bar{\tau}(L+1,m-1)]F_1(L) + [-\bar{\tau}(L+1,m+1) + \bar{\tau}(L-1,m-1)]F_3(L) + [\bar{\tau}(L-1,m-1) - \gamma(L+1,m+1)]F_2(L) + [-\bar{\tau}(L+1,m-1) + \bar{\tau}(L-1,m-1)]F_4(L) + G(L,m)[\bar{\theta}(L-1,m+1) - \bar{\theta}(L+1,m-1)]F_1(L) + [\bar{\theta}(L+1,m+1) - \bar{\theta}(L-1,m-1)]F_3(L) + [-\bar{\theta}(L-1,m-1) + \bar{\theta}(L+1,m+1)]F_2(L) + [-\bar{\theta}(L+1,m-1) + \bar{\theta}(L-1,m+1)]F_4(L)\}$

Appendix B

Solar flux and absorption cross-section data.

From Ackerman (1971).

No.	$\Delta\lambda$(Å)	$\Delta\nu$(cm^{-1})	q(cm^{-2} s^{-1})	$\sigma(O_2)$ (cm^2)	$\sigma(O_3)$ (cm^2)
1	Ly α 1.215,67	82.259	3.00×10^{11}	1.00×10^{-20}	2.32×10^{-17}
2	1.170–1.163	85.500–86.000	1.03×10^{8}	2.00×10^{-20}	7.80×10^{-18}
3	1.176–1.170	85.000–85.500	2.66	1.25×10^{-18}	7.97
4	1.183–1.176	84.500–85.000	1.12	2.55×10^{-19}	8.66
5	1.190–1.183	84.000–84.500	1.24	3.00×10^{-20}	9.51
6	1.198–1.190	83.500–84.000	1.82	3.75×10^{-19}	1.25×10^{-17}
7	1.205–1.198	83.000–83.500	1.90	4.45×10^{-18}	1.84
8	1.212–1.205	82.500–83.000	7.40	8.35	2.19
9	1.220–1.212	82.000–82.500	2.28×10^{9}	6.00×10^{-19}	2.30
10	1.227–1.220	81.500–82.000	3.67	2.35	2.26
11	1.235–1.227	81.000–81.500	1.36	4.50	2.06
12	1.242–1.235	80.500–81.000	1.61	3.35	1.30
13	1.250–1.242	80.000–80.500	1.32	1.75×10^{-17}	8.91×10^{-18}
14	1.258–1.250	79.500–80.000	1.41	8.95×10^{-19}	7.24
15	1.266–1.258	79.000–79.500	3.11	4.30	6.09
16	1.274–1.266	78.500–79.000	1.06	1.10	5.66
17	1.282–1.274	78.000–78.500	1.37	2.05	5.87
18	1.290–1.282	77.500–78.000	1.02	4.43	6.47
19	1.299–1.290	77.000–77.500	1.14	5.55	8.14
20	1.307–1.299	76.500–77.000	7.29	4.20	1.24×10^{-17}
21	1.316–1.307	76.000–76.500	2.20	6.85	1.52
22	1.324–1.316	75.500–76.000	1.59	1.45×10^{-18}	1.47
23	1.333–1.324	75.000–75.500	2.21	2.25	1.51
24	1.342–1.333	74.500–75.000	1.24×10^{10}	2.30×10^{-18}	1.51×10^{-17}
25	1.351–1.342	74.000–74.500	1.99×10^{9}	4.55	1.65
26	1.360–1.351	73.500–74.000	3.09	7.23	1.54
27	1.370–1.360	73.000–73.500	2.57	9.50	1.35
28	1.379–1.370	72.500–73.000	2.74	1.23×10^{-17}	1.05
29	1.389–1.379	72.000–72.500	3.10	1.32	7.97×10^{-18}
30	1.408–1.389	71.000–72.000	7.60	1.36	7.17
31	1.428–1.408	70.000–71.000	1.01×10^{10}	1.40	6.28
32	1.449–1.428	69.000–70.000	1.30	1.48	5.66
33	1.470–1.449	68.000–69.000	1.82	1.41	5.23
34	1.492–1.470	67.000–68.000	2.33	1.29	4.47
35	1.515–1.492	66.000–67.000	2.66	1.15	3.69
36	1.538–1.515	65.000–66.000	2.90	9.91×10^{-18}	2.93
37	1.562–1.538	64.000–65.000	3.60	8.24	2.19
38	1.587–1.562	63.000–64.000	4.75	6.58	1.63
39	1.613–1.587	62.000–63.000	6.40	4.97	1.20
40	1.639–1.613	61.000–62.000	5.49	3.45	9.77×10^{-19}
41	1.667–1.639	60.000–61.000	1.19×10^{11}	2.08	8.66
42	1.695–1.667	59.000–60.000	1.76	1.23	8.14
43	1.724–1.695	58.000–59.000	2.32	7.22×10^{-19}	8.17
44	1.739–1.724	57.500–58.000	1.44	4.58	8.57
45	1.754–1.739	57.000–57.500	1.83	2.74	8.40
46	1.770–1.754	56.500–57.000	2.34	a	8.11
47	1.786–1.770	56.000–56.500	2.62	a	7.99
48	1.802–1.786	55.500–56.000	2.88×10^{11}	a	7.86×10^{-19}
49	1.818–1.802	55.000–55.500	3.14	a	7.63
50	1.835–1.818	54.500–55.000	3.81×10^{11}	a	7.29×10^{-19}
51	1.852–1.835	54.000–54.500	4.43	a	6.88
52	1.869–1.852	53.500–54.000	4.95	a	6.40
53	1.887–1.869	53.000–53.500	5.94	a	5.88
54	1.905–1.887	52.500–53.000	6.59	a	5.31
55	1.923–1.905	52.000–52.500	7.26	a	4.80
56	1.942–1.923	51.500–52.000	9.85	a	4.38
57	1.961–1.942	51.000–51.500	1.27×10^{12}	a	4.11
58	1.980–1.961	50.500–51.000	1.39	a	3.69
59	2.000–1.980	50.000–50.500	1.53	a	3.30
60	2.020–2.000	49.500–50.000	1.60	a	3.26

a temperature-dependent $\sigma(O_2)$, see Kockarts (1971)

No.	$\Delta\lambda$(Å)	$\Delta\nu$(cm^{-1})	q(cm^{-2} s^{-1})	$\sigma(O_2)$ (cm^2)	$\sigma(O_3)$ (cm^2)
61	2.041–2.020	49.000–49.500	1.74	1.14×10^{-23}	3.26
62	2.062–2.041	48.500–49.000	2.31	1.05	3.51
63	2.083–2.062	48.000–48.500	4.20	1.00	4.11
64	2.105–2.083	47.500–48.000	7.30	9.55×10^{-24}	4.84
65	2.128–2.105	47.000–47.500	9.42	8.93	6.26
66	2.150–2.128	46.500–47.000	1.06×10^{13}	8.28	8.57
67	2.174–2.150	46.000–46.500	1.34	7.60	1.17×10^{-18}
68	2.198–2.174	45.500–46.000	1.32	6.92	1.52
69	2.222–2.198	45.000–45.500	1.73	6.28	1.97
70	2.247–2.222	44.500–45.000	1.80	5.65	2.55
71	2.273–2.247	44.000–44.500	1.82	5.03	3.24
72	2.299–2.273	43.500–44.000	2.26	4.40	4.00
73	2.326–2.299	43.000–43.500	2.40	3.76	4.83
74	2.353–2.326	42.500–43.000	2.25	3.09	5.79
75	2.381–2.353	42.000–42.500	2.21	2.44	6.86
76	2.410–2.381	41.500–42.000	2.32	1.75	7.97
77	2.439–2.410	41.000–41.500	2.50	6.74×10^{-25}	9.00
78	2.469–2.439	40.500–41.000	2.73		1.00×10^{-17}
79	2.500–2.469	40.000–40.500	2.88		1.07
80	2.532–2.500	39.500–40.000	3.02		1.11
81	2.564–2.532	39.000–39.500	3.97		1.12
82	2.597–2.564	38.500–39.000	7.13		1.11
83	2.632–2.597	38.000–38.500	4.37		1.03
84	2.667–2.632	37.500–38.000	1.12×10^{14}		9.43×10^{-18}
85	2.703–2.667	37.000–37.500	1.25		8.23
86	2.740–2.703	36.500–37.000	1.16		6.81
87	2.778–2.740	36.000–36.500	1.19		5.31
88	2.817–2.778	35.500–36.000	1.38		3.99
89	2.857–2.817	35.000–35.500	1.70		2.84
90	2.899–2.857	34.500–35.000	2.46		1.92
91	2.941–2.899	34.000–34.500	3.90		1.14
92	2.985–2.941	33.500–34.000	3.99		6.60×10^{-19}
93	3.030–2.985	33.000–33.500	3.86		3.69
94	3.077–3.030	32.500–33.000	5.08		1.97
95	3.100 (±25)	32.520–32.000	5.92		1.05
96	3.150	32.000–31.496	6.05		5.23×10^{-20}
97	3.200	31.496–31.008	6.94		2.91
98	3.250	31.008–30.534	8.12		1.50
99	3.300	30.534–30.075	9.71		7.78×10^{-21}
100	3.350	30.075–29.630	8.97		3.72
101	3.400 (±25)	29.630–29.197	9.44×10^{14}		1.71×10^{-21}
102	3.450	29.197–28.777	1.01×10^{15}		7.46×10^{-22}
103	3.500	28.777–28.369	1.03		2.66
104	3.550	28.369–27.972	1.03		1.09
105	3.600	27.972–27.586	1.04		5.49×10^{-23}
106	3.650	27.586–27.211	1.18		–
107	3.700	27.211–26.846	1.23		–
108	3.750	26.846–26.490	1.24		–
109	3.800	26.490–26.144	1.17		–
110	3.850	26.144–25.806	1.11		–
111	3.900	25.806–25.478	1.09		–
112	3.950	25.478–25.157	1.19		–
113	4.000	25.157–24.845	1.54		–
114	4.050	24.845–24.540	1.90		–
115	4.100	24.540–24.242	1.99		2.91
116	4.150	24.242–23.952	1.99		3.14
117	4.200	23.952–23.669	2.02		3.99
118	4.250	23.669–23.392	2.01		6.54
119	4.300	23.392–23.121	1.94		6.83
120	4.350	23.121–22.851	1.98		8.66

No.	$\Delta\lambda$(Å)	$\Delta\nu$(cm^{-1})	q(cm^{-2} s^{-1})	$\sigma(O_2)$ (cm^2)	$\sigma(O_3)$ (cm^2)
121	4.400	22.851–22.599	2.25		1.25×10^{-22}
122	4.450	22.599–22.346	2.39		1.49
123	4.500	22.346–22.099	2.48		1.71
124	4.550	22.099–21.858	2.49		2.12
125	4.600	21.858–21.622	2.48		3.57
126	4.650	21.622–21.390	2.50		3.68
127	4.700	21.390–21.164	2.55		4.06
128	4.750	21.164–20.942	2.61		4.89
129	4.800	20.942–20.725	2.59		7.11
130	4.850	20.725–20.513	2.46		8.43
131	4.900	20.513–20.504	2.44		8.28
132	4.950	20.504–20.100	2.53		9.09
133	5.000	20.100–19.900	2.48		1.22×10^{-21}
134	5.050	19.900–19.704	2.49		1.62
135	5.100	19.704–19.512	2.50		1.58
136	5.150	19.512–19.324	2.43		1.60
137	5.200	19.324–19.139	2.43		1.78
138	5.250	19.139–18.957	2.52		2.07
139	5.300	18.957–18.779	2.58		2.55
140	5.350	18.779–18.605	2.64		2.74
141	5.400	18.605–18.433	2.67		2.88
142	5.450	18.433–18.265	2.70		3.07
143	5.500	18.265–18.100	2.68		3.17
144	5.550	18.100–17.937	2.66		3.36
145	5.600	17.937–17.778	2.66		3.88
146	5.650	17.778–17.621	2.67		4.31
147	5.700	17.621–17.467	2.67		4.67
148	5.750	17.467–17.316	2.69		4.75
149	5.800	17.316–17.667	2.71		4.55
150	5.850	17.667–17.021	2.71		4.35
151	5.900	17.021–16.878	2.71		4.42
152	5.950	16.878–16.736	2.72		4.61
153	6.000 (±25)	16.736–16.598	2.72×10^{15}		4.89×10^{-21}
154	6.050	16.598–16.461	2.71		4.84
155	6.100	16.461–16.326	2.70		4.54
156	6.150	16.326–16.194	2.70		4.24
157	6.200	16.194–16.064	2.70		3.90
158	6.250	16.064–15.936	2.69		3.60
159	6.300	15.936–15.810	2.68		3.43
160	6.350	15.810–15.686	2.67		3.17
161	6.400	15.686–15.564	2.66		2.74
162	6.450	15.564–15.444	2.65		2.61
163	6.500 (±50)	15.384–15.265	3.95		2.40
164	6.600	15.265–15.038	5.22		2.07
165	6.700	15.038–14.815	5.18		1.72
166	6.800	14.815–14.598	5.14		1.37
167	6.900	14.598–14.388	5.09		1.11
168	7.000	14.388–14.184	5.04		9.13×10^{-22}
169	7.100	14.184–13.986	4.99		7.93
170	7.200	13.986–13.793	4.94		6.40
171	7.300	13.793–13.605	4.90		5.14

Appendix C

Model Runs described in this thesis

Run	Specifications
A	As described in Chapter 2 with the linear photochemical scheme.
B	Run A with the thermal radiation scheme for CO_2 replaced by the Curtis matrix method.
C	Run A with the solar heating scheme replaced by the 'almost exact' method.
D	Run A with both new radiation schemes and an airglow array.
E	Run D with modified 'airglow'.
F	Run E with the more complete photochemical scheme.
G	Run F with climatological heating rates in the lower stratosphere.
H	Run F with increasing CO_2 mixing ratio.
I	Run F with increasing CFC amounts.
J	Run F with increasing CO_2 and CFCs.
K	Run E with 1976 eddy momentum fluxes.
L	Run K with eddy heat fluxes from satellite data.
M	Run K with Rayleigh friction.
N	Run M with no radiative heating in the mesosphere.

References

Ackerman M. (1971). 'Ultraviolet solar radiation related to mesospheric processes'. Mesospheric models and related experiments, ed. Fiocco D.Reidel Publ Co., Dordrecht. 149-159.

Ackerman M., Biaume F. and Kockarts G. (1970). 'Absorption cross-sections of the Schumann-Runge bands of molecular oxygen. Planet. Space Sci., 18, 1639-1651.

Ackerman M., Frimout D. and Pastiels R. (1971). 'New ultraviolet solar flux measurements at 2000Å using a balloon borne instrument'. New techniques in Space Aeronomy, ed Labuhn and Lust, D.Reidel, Publ. Co., Dordrecht, 251-

Ackerman M. and Simon P.C. (1973). 'Rocket measurements of solar fluxes at 1216Å, 1450Å and 1710Å'. Solar Phys., 30, 345-350.

Adler R.F. (1975). 'Mean meridional circulation in the Southern Hemisphere stratosphere based on satellite information'. J.Atmos. Sci., 32, 893-898.

Allen D.C. (1979). D. Phil. thesis, University of Oxford.

Allen D.C., Haigh J.D., Houghton J.T. and Simpson C.J.S.M. (1979). 'Radiative cooling near the mesopause'. Nature, 281, 660-661.

Allen D.C., Price T.J. and Simpson C.J.S.M. (1977). 'Vibrational deactivation of the bending mode of CO_2 measured between 1500K and 150K'. Chem. Phys. Lett., 45, 183-187.

Andrews D.G. and M^{c}Intyre M.E. (1976). 'Planetary waves in horizontal and vertical shear: The generalised Eliassen-Palm relation and the mean zonal acceleration'. J.Atmos. Sci., 33, 2031-2048.

Arrhenius S. (1896). 'The influence of the carbonic acid in the air upon the temperature of the ground'. Phil. Mag., 41, 237-276.

Bacastow R. and Keeling C.D. (1973). 'Atmospheric carbon dioxide and radio carbon in the natrual carbon cycle: II Changes from A.D. 1700 to 2070 as deduced from a geochemical model'. Carbon and the Biosphere, ed. Woodwell and Pecan, 86-135.

Barnett J.J., Houghton J.T. and Pyle J.A. (1975). 'The temperature dependence of the ozone concentration near the stratopause'. Quart. J. Roy. Meteorol. Soc., 101, 245-257.

Bass H.E. (1973). 'Vibrational relaxation in CO_2/O_2 mixtures'. J. Chem. Phys., 58, 4783-4786.

Bates J.R. (1977). 'Dynamics of stationary ultra-long waves in middle latitudes' Quart. J. Roy. Meteorol. Soc., 103, 397-430.

Bischof W. (1977). 'Comparability of CO_2 measurements'. Tellus, 29, 435-444.

Bolin B. (1970). 'The carbon cycle'. Scientific American, 223, 136-146.

Bolin B. (1977). 'Changes of land biota and their importance for the carbon cycle'. Science, 196, 613-615.

Bolin B. and Keeling C.D. (1963). 'Large scale atmospheric mixing as deduced from the seasonal and meridional variations of carbon dioxide'. J. Geophys. Res., 68, 3899-3920.

Booker J.R. and Bretherton F.P. (1967). 'The critical layer for internal gravity waves in a shear flow'. J. Fluid. Mech., 27, 513-539.

Boughner R.E. (1978). 'The effect of increased carbon dioxide concentrations on stratospheric ozone'. J. Geophys. Res., 83, 1326-1332.

Brewer A.W. (1949). 'Evidence for a world circulation provided by the measurements of helium and water vapour distribution in the stratosphere'. Quart. J. Roy. Meteorol. Soc., 75, 351-363.

Broadfoot A.L. (1972). 'The solar sprectrum 2100-3200 Å'. Astrophys. J. 173, 681-689.

Broecker W.S. (1975). 'Climatic change: Are we on the brink of a pronounced global warming?'. Science, 189, 460-463.

Broecker W.S., Takahashi T., Simpson H.J. and Peng T.H. (1979). 'Fate of fossil fuel carbon dioxide and the global carbon budget'. Science, 206, 409-418.

Brueckner G.E., Bartoe J.D.F., Moe O.K. and Von Hoosier M.E. (1976). 'Absolute solar ultraviolet intensities and their variations with solar activity. I. The wavelength region 1750-2100Å'. Astrophys. J., 209, 935-944.

Buchwald M.I. and Wolga G.J. (1975). 'Vibrational relaxation of CO_2 (001) by atoms'. J. Chem. Phys., 62, 2828-2832.

Cadle R.D. (1977). 'The structure composition and distribution of stratospheric aerosol particles and their radiative properties and importance for the radiation budget'. Proceedings of the symposium on radiation in the atmosphere, ed. Bolle H. -J., 116-120.

Cadle R.D. and Grams G.W. (1975), 'Stratospheric aerosol particles and their optical properties'. J. Geophys. Red., 13, 475-501.

Callendar G.S. (1938). 'The artificial production of carbon dioxide and its influence on temperature'. Quart. J. Roy. Meteorol. Soc., 64, 223-240.

Cannemeyer F. and de Vries A.E. (1974). 'Vibrational relaxation of CO_2 in CO_2 - N_2 and CO_2 - O_2 mixtures'. Physica, 74, 196-204.

Chamberlin T.C. (1899). 'An attempt to frame a working hypothesis of the cause of glacial periods on an atmospheric basis'. J. Geol., 7, 545-584, 667-685.

Chapman S. (1930). 'On ozone and atomic oxygen in the upper atmosphere'. Phil. Mag., 10, 369-383.

Charney J.G. and Drazin P.G. (1961). 'Propagation of planetary-scale disturbances from the lower into the upper atmosphere.' J. Geophys. Res., 66, 83-109.

C.I.R.A. (1972). COSPAR International Reference Atmosphere. North Holland Publishing Company, Amsterdam.

Clarke R.H. (1970). 'Recommended methods for the treatment of the boundary layer in numerical models'. Am. Met. Mag, 18, 51-71.

Cottrell T.L. and M^{c}Coubrey J.C. (1961). Molecular energy transfer in gases, Butterworths, London.

Craig R.A. (1951), 'Radiative temperature changes in the ozone layer'. Compendum of Meteorology, ed. Malone T.F., Boston, Amer. Meteor. Soc. 292-302.

Cramp J.H.W. and Lambert J.D. (1973). 'Vibrational relaxation of $CO_2(\nu_3)$ by O atoms'. Chem. Phys. Lett., 22, 146-149.

Crane A.J., Haigh J.D., Pyle J.A. and Rogers C.F. (1980). 'Mean meridional circulations of the stratosphere and mesosphere'. Pure Appl. Geophys., 118, 307-328.

Crutzen P.J. (1970). Comment on the paper 'Absorption and emission by carbon dioxide in the mesosphere' by J.T.Houghton. Quart. J.Roy.Meteorol. Soc., 96, 767-769.

Crutzen P.J. (1971). 'Energy conversions and mean vertical motions in the high latitude summer mesosphere and lower thermosphere'. Mesospheric Models and related experiments, D. Reidel Publ. Co., Dordrecht. 78-88.

Crutzen P.J. (1974). 'Estimates of possible variations in total ozone due to natural causes and human activities'. Ambio, 3, 201-210.

Curtis A.R. (1956). 'The computation of radiative heating rates in the atmosphere'. Proc. Roy. Soc. London, A236, 156-159.

Curtis A.R. and Goody R.M. (1956). 'Thermal radiation in the upper atmosphere'. Proc. Roy. Soc. London, A236, 193-206.

Dave J.V. and Furukawa P.M. (1967). 'The effects of scattering and ground reflection on the solar energy absorbed by ozone in a Rayleigh atmosphere'. J. Atmos, Sci., 24, 175-181.

Degges T.C. (1974). 'A high altitude radiance model'. AFCRL-74-0606, Visidyne Corp., Burlington, Mass.

Delaboudinière J.P., Donnelly R.F., Hinteregger H.E., Schmidtke G., and Simon P.C. (1978). 'Intercomparison/compilation of relevent solar flux data related to aeronomy'. COSPAR manual no 7.

Detweiler C.R., Garrett D.L., Purcell J.D. and Tousey R. (1961). 'The intensity distribution in the unltraviolet solar spectrum'. Ann. Geophys., 17, 263-272.

Dickinson R.E. (1973). 'Method of parameterisation for infrared cooling between altitudes of 30 and 70 kilometers'. J.Geophys. Res., 78, 4451-4457.

Dobson G.M.B. (1956). 'Origin and distribution of polyatomic molecules in the atmosphere'. Proc. Roy. Soc. London, A236, 187-193.

D.O.E. (1979). 'Chlorofluorocarbons and their effect on stratospheric ozone'. Pollution Paper no 15, H.M.S.O., 236pp.

Drayson S.R. (1967). 'The calculation of long-wave radiative transfer in planetary atmospheres'. University of Michigan College of Engineering, Technical Report 07584-1-T.

Drayson S.R. (1976). 'Rapid Computation of the Voigt profile'. J Quant. Spectrosc. Radiat. Transfer, 16, 611-614.

Drayson S.R. and Young (1967). 'The frequencies and intensities of carbon dioxide absorption lines between 12 and 18μ'. University of Michigan College of Engineering, Technical Report 08183-1-T.

Dunkerton T. (1978). 'On the mean meridional mass motions of the stratosphere and mesosphere'. J.Atmos. Sci., 35, 2325-2333.

Dütsch H.U. (1968). 'The photochemistry of stratospheric ozone'. Quart. J. Roy. Meteorol. Soc., 94, 483-497.

Dütsch H.U. (1971). 'Photochemistry of atmospheric ozone'. Adv. in Geophys. 15, 219-322.

Eckdahl C.A. and Keeling C.D. (1973). 'Atmospheric carbon dioxide and radiocarbon in the natural carbon cycle: I. Quantitative deductions from records at Mauna Loa Observatory and at the South Pole'. Carbon and the biosphere, ed. Woodwell and Pecan, 51-85.

Edwards D.P. (1970). D. Phil. thesis, University of Oxford.

Elford W.G. (1978). 'Momentum transport due to atmospheric tides'. Presented at solar-terrestial physics symposium, Innsbruck.

Eliassen A.N. and Palm E. (1960). 'On the transfer of energy in stationary mountain waves'. Geophys. Publ., 22, no 3, 22pp.

Foley H.M. and Ruderman M.A. (1973). 'Stratospheric NO production from past nuclean explosions'. J. Geophys. Res., 78, 4441-4450.

Fonselius S., Koroleff F. and Warme K. -E. (1956). 'Carbon dioxide variations in the atmosphere'. Tellus, 8, 176-183.

Fukuyama K. (1974). 'Latitudinal distributions of photochemical heating rates in the winter mesosphere and lower thermosphere'. J. Atmos. Terr. Phys., 36, 1321-1334.

Goody R.M. (1964). Atmospheric Radiation. I Theoretical Basis. Oxford University Press. 436 pp.

Gordiets B.F., Markov M.N. and Shelepin L.A. (1978). 'I.R. radiation of the upper atmosphere'. Planet. Space Sci., 26, 933-948.

Green J.S.A. (1972). 'Large-scale motion in the upper stratosphere and mesosphere: An evaluation of data and theories'. Phil. Trans. Roy. Soc. London, A271, 577-583.

Groves G.V. (1970). 'Seasonal and latitudinal models of atmospheric temperature, pressure and density, 25-110km'. Air Force Cambridge Research Laboratories, Massachusetts.

Groves K.S., Mattingly S.R. and Tuck A.F. (1978). 'Increased atmospheric carbon dioxide and stratospheric ozone'. Nature, 273, 711-715.

Groves K.S. and Tuck A.F. (1979). 'Simultaneous effects of CO_2 and chlorofluoromethanes on stratospheric ozone'. Nature, 280, 127-129.

Groves K.S. and Tuck A.F. (1980a). 'Stratospheric O_3 - CO_2 coupling in a photochemical-radiative column model. I: without chlorine chemistry'. Quart. J. Roy. Meteorol. Soc. 106, 125-140.

Groves K.S. and Tuck A.F. (1980b). 'Stratospheric O_3 -CO_2 coupling in a photochemical-radiative column model. II: with chlorine chemistry'. Quart. J. Roy. Meteorol. Soc., 106, 141-157.

Haigh J.D. and Pyle J.A. (1979). 'A two-dimensional calculation including atmospheric carbon dioxide and stratospheric ozone.' Nature, 279, 222-224.

Haltiner G.J. (1971). Numerical Weather Prediction, John Wiley and Sons, New York, 317pp.

Harwood R.S. and Pyle J.A. (1973). 'A two-dimensional mean circulation model for the atmosphere below 80km'. Meteorological Research Committee, Ministry of Defence (Air Force Dept.), MRCP 344.

Harwood R.S. and Pyle J.A. (1975). 'A two-dimensional mean circulation model for the atmosphere below 80km. Quart. J. Roy. Meteorol. Soc., 101, 723-748.

Harwood R.S. and Pyle J.A. (1977). 'Studies of the ozone budget using a zonal mean circulation model and linearised photochemistry'. Quart. J. Roy. Meteorol. Soc., 103, 319-343.

Harwood R.S. and Pyle J.A. (1980). 'The dynamical behaviour of a two-dimensional model of the stratosphere'. Quart. J. Roy. Meteorol. Soc. 106, 395-420.

Harwood R.S., Pyle J.A. and Rendel D.D. (1972). 'A mean circulation model for the atmosphere up to 80km'. Oxford University Department of Atmospheric Physics Report No. 10/72.

Heath D.F. (1973). 'Space observations of the variability of solar irradiance in the near and far ultraviolet'. J. Geophys. Res., 78, 2779-2792.

Heroux L. and Swirbalus R.A. (1976). 'Full-disk solar fluxes between 1230 and 1940 Å'. J. Geophys. Res., 81, 436-440.

Hesstvedt E. (1971). 'A meridional model of the oxygen-hydrogen atmosphere'. Mesospheric models and related experiments, ed. Fiocco, D.Reidel Publ. Co., Dordrecht, 52-64.

Hines C.O. (1963). 'The upper atmosphere in motion'. Quart. J. Roy. Meteorol. Soc., 89, 1-42.

Hines C.O. (1965). 'Dynamical heating of the upper atmosphere'. J. Geophys. Res., 70, 177-183.

Hines C.O. (1970). Comments on paper by E.E.Gossard, J.M.Richter and D.Atlas, 'Internal waves in the atmosphere from high resolution radar measurements'. J. Geophys. Res., 75, 5956-5959.

Hines C.O. (1972a). 'Motions in the ionospheric D and E regions'. Phil. Trans. Roy. Soc. London., A271, 457-471.

Hines C.O. (1972b). 'Momentum deposition by atmospheric waves and its effects on the thermospheric circulation'. Space Res., 12, 1157-1161.

Hodges R.R. (1969). 'Eddy diffusion coefficients due to instabilities in internal gravity waves'. J. Geophys. Res., 74, 4086-4090.

Hoffert M.I. (1974). 'Global distribution of atmospheric CO_2 in the fossil fuel era : a projection'. Atmos. Envir., 8, 1225-1249.

Holton J.R. (1974). 'Forcing of mean flows by stationary waves'. J.Atmos. Sci., 31, 942-945.

Holton J.R. (1975). 'The dynamic meteorology of the stratosphere and mesosphere'. Meteorol. Monog., 15, no 37, 216 pp.

Holton J.R. and Wehrbein W.M. (1980). 'A numerical model of the zonal mean circulation of the middle atmosphere'. Pure Appl. Geophys., 118. 284-306.

Houghton J.T. (1963). 'The absorption of solar infra-red radiation by the lower stratosphere'. Quart. J. Roy. Meteorol. Soc., 89, 319-331.

Houghton J.T. (1965). 'Infrared emission from the stratosphere and mesosphere'. Proc. Roy. Soc. London. A288, 545-555.

Houghton J.T. (1969). 'Absorption and emission by carbon-dioxide in the mesosphere'. Quart. J. Roy. Meteorol. Soc., 95, 1.20.

Houghton J.T. (1977). The physics of atmospheres. C.U.P. 203pp.

Houghton J.T. (1978). 'The stratosphere and mesosphere'. Quart J. Roy. Meteorol. Soc., 104, 1-29.

Howard J.N., King J.I.F. and Gast P.R. (1961). 'Thermal radiation'. Handbook of Geophysics, New York, MacMillan, Chap. 16.

Hoyt D.V. (1979). 'An empirical determination of the heating of the earth by the carbon dioxide greenhouse effect'. Nature, 282, 388-390.

Hunt B.G. (1972). 'Photochemical heating of the mesosphere and lower thermosphere'. Tellus, 24, 47-55.

Inn E.C.Y. and Tanaka Y. (1956). 'Comparison of recently recorded ozone absorption coefficients in the visible and ultra-violet regions.' Conference on Ozone, Armour Research Foundation, 263-268.

Isaksen I.S.A., Hesstvedt E. and Stordal F. (1980) 'Influence of stratospheric cooling from CO_2 on the ozone layer'. Nature, 283, 189-191.

James T.C. and Kumer J.B. (1974). 'Approximate CO_2 15μm zenith radiance calculations'. Trans. Am. Geophys. Union. 55, 375 (abstract).

Johnson F.S. (1954). 'The solar constant'. J. Meteorol., 11, 431-439.

Johnston H.S. (1971). 'Reduction of stratospheric ozone by nitrogen oxide catalysts from supersonic transport exhaust.' Science, 173, 517-522.

Justus C.G. (1967). 'Eddy diffusivities, energy balance parameters and heating rates of upper atmospheric turbulence'. J. Geophys. Res., 72, 1035-1039.

Justus C.G. (1969). 'Dissipation and diffusion by turbulence and irregular winds near 100km'. J. Atmos. Sci., 26, 1137-1141.

Kaplan L.D. (1960). 'The influence of carbon dioxide variation on the atmospheric heat balance'. Tellus, 12, 204-208.

Keeling C.D. (1973). 'Industrial production of carbon dioxide from fossil fuels and limestone'. Tellus, 25, 174-198.

Keeling C.D. and Bacastow R.B. (1978). 'Impact of industrial gases on climate'. Energy and climate, National Academy of Sciences, Was ington D.C., 72-95.

Kellogg W.W. (1961). 'Chemical heating above the polar mesopause in winter'. J. Meteorol., 18, 373-381.

Kellogg W.W., Coakley J.A. and Grams G.W. (1975). 'Effect of anthropogenic aerosols on the global climate'. Proc. WMO/IAMAP Symp. on Long Term Climatic Fluctuations (Norwich, U.K.) WMO Document 421, Geneva, 320-330.

Kennedy J.S. (1964). 'Energy generation through radiative processes in the lower stratosphere'. M.I.T. Report no. 11, December 1964, Contract no. AT(30-1) 2241, 116 pp.

Kochanski A. (1964). 'Atmospheric motions from sodium cloud drifts'. J. Geophys. Res., 69, 3651-3662.

Kockarts G. (1971). 'Penetration of solar radiation in the Schumann-Runge bands of molecular oxygen'. Mesospheric models and related experiments, ed. Fiocco, D.Reidel Publ. Co., Dordrecht, 160-176.

Kockarts G. (1976). 'Absorption and photodissociation in the Schumann-Runge bands of molecular oxygen in the terrestial atmosphere'. Planet. Space Sci., 24, 589-604.

Kubik R.N. (1965). 'Algorithm 257, Havie integrator'. Communciations of the Association for Computing Machinery, 8, 381.

Kukn W.R. and London J. (1969). 'Infrared radiative cooling in the middle atmosphere (30-110km)'. J. Atmos. Sci., 26, 189-204.

Labs D. and Neckel H. (1968). 'The radiation of the solar photosphere from 2000Å to 100μ'. Z. Astrophys., 69, 1-73.

Labs D. and Neckel H. (1973). 'Intensity of the solar disk in the spectral region 0.33 to 1.25 m measured from high mountain station'. Proc. Symp. on solar radiation, ed Klein and Hickey, 269-

Lacis A.A. and Hansen J.E. (1974). 'A parameterisation for the absorption of solar radiation in the earth's atmosphere'. J. Atmos. Sci., 31, 118-133.

Lambert J.D. (1977). Vibrational and rotational relaxation in gases. Clarendon Press, Oxford, 142 pp.

Landau L. and Teller E. (1936) 'Zur theorie der schalldispersion'. Phys Z. Sowj. Un., 10, 34-43.

Leovy C.B. (1964). 'Simple models of thermally driven mesospheric circulations'. J. Atmos. Sci., 21, 327-341.

Lilly D.R., Waco D.E. and Adelfang S.I. (1974). 'Stratospheric mixing estimated from high-altitude turbulence measurements'. J. Appl. Meteorol, 13. 488-493.

Lindzen R.S. (1967). 'Thermally driven diurnal tide in the atmosphere'. Quart. J. Roy. Meteorol. Soc., 93, 18-42.

Lindzen R.S. (1968). 'The application of classical atmospheric tidal theory'. Proc. Roy. Soc. London, A303, 299-316.

Lindzen R.S. and Blake D. (1970). 'Mean heating of the thermosphere by tides'. J. Geophys. Res., 75, 6868-6871.

Lindzen R.S. and Will D.I. (1973). 'An analytic formula for heating rate due to ozone absorption'. J. Atmos. Sci., 30, 513-515.

Logan J.A., Prather M., Wofsy S. and McElroy M.B. (1978). 'Atmospheric chemistry : response to human influence'. Phil. Trans. Roy. Soc. London, A290, 187-234.

Luther F.M. (1973). 'Monthly mean values of eddy diffustion coefficients in the lower stratosphere'. AIAA paper 73-498, AIAA/AMA conference, Denver.

Luther F.M., Wuebbles D.J. and Chang J.S. (1977). 'Temperature feedback in a stratospheric model'. J. Geophys. Res., 82, 4935-4942.

Machta L. (1973). 'Predictions of CO_2 in the atmosphere'. Carbon and the biosphere, ed. Woodwell and Pecan, 21-31.

Manabe S. and Stouffer R.J. (1979). 'A CO_2 -climate sensitivity study with a mathematical model of the global climate. Nature, 282, 491-493.

Manabe S. and Wetherald R.T. (1967). 'Thermal equilibrium of the atmosphere with a given distribution of relative humidity'. J. Atmos. Sci., 24, 241-259.

Manabe S. and Wetherald R.T. (1975). 'The effects of doubling the CO_2 concentration on the climate of a General Circulation Model'. J. Atmos. Sci., 32, 3-15.

Manabe S. and Wetherald R.T. (1980). 'On the distribution of climatic change resulting from an increase in CO_2 content of the atmosphere'. J. Atmos. Sci., 37, 99-118.

Manson A.H., Meek C.E. and Stening R.J. (1979). 'The role of atmospheric waves (1.5h-10 days) in the dynamics of the mesophere and lower thermosphere at Saskatoon (52°N, 107°W) during the four seasons of 1976'. J. Atmos, Terr. Phys., 41, 325-335.

McCarthy R.L., Bower F.A. and Jesson J.P. (1977). 'The fluorocarbon-ozone theory -I. Production and release of CCl_3F and CCl_2F_2 through 1975. Atmos. Envir., 11, 491-497.

McClatchey R.A. (1966). 'Thesis: the effect of vibrational relaxation on atmospheric heating in the 4.3μ band'. Univ. of California, Los Angeles.

Merrill K.M. and Amme R.C. (1969). 'Deactivation of the CO_2 bending moment by collisions with N_2 and O_2 . J. Chem. Phys., 51, 844-846.

Mole R.H. (1980). 'Medical Aspects : u.v. and skin cancer'. Chlorofluorocarbons in the environment, ed. Sugden and West, Ellis Horwood, Chapter 7.

Molina M.J. and Rowland F.S. (1974). 'Stratospheric sinks for chlorofluoromethanes : chlorine atom-catalysed destruction of zone.' Nature, 249, 810-812.

Möller F. (1963). 'On the influence of changes in the CO_2 concentration in air on the radiation balance of the earth's surface'. J. Geophys. Res., 68, 3877-3886.

Murgatroyd R.J. (1969a). 'The structure and dynamics of the stratosphere '. The global circulation of the atmosphere, ed. Corby, Roy. Meteorol. Soc. London. 159-195.

Murgatroyd R.J. (1969b). 'A note on the contributions of mean and eddy terms to the momentum and heat balances of the troposphere and lower stratosphere.' Quart. J. Roy. Meteorol. Soc., 95, 194-202.

Murgatroyd R.J. and Goody R.M. (1958). 'Sources and sinks of energy from 30 to 90 km'. Quart. J. Roy. Meteorol. Soc., 84, 225-234.

Murgatroyd R.J. and Singleton F. (1961). 'Possible meridional circulations in the stratosphere and mesosphere'. Quart. J. Roy. Meteorol. Soc., 87, 125-135.

N.A.S. (1979). 'Stratospheric ozone depletion by halocarbons : chemistry and transport'. NAS Panel of stratospheric chemistry and transport, Washington D.C., 238 pp.

N.A.S.A. (1979). The Stratosphere : present and future. NASA reference publication 1049, ed Hudson and Reed, 432 pp.

Newell R.E. and Dopplick T.G. (1979). 'Questions concerning the possible influence of anthropogenic CO_2 on atmospheric temperature'. J. Appl. Meteorol., 18, 822-825.

Newell R.E., Vincent D.G., Dopplick T.G., Ferruzza D. amd Kidson J.W. (1969). 'The energy balance of the Global atmosphere'. The global circulation of the atmosphere, ed. Corby. Roy. Meteorol. Soc. London, 42-90.

Offermann D., Curtis P., Cisneros J.M., Lauche H., Petzoldt K., Rose G. and Satrustegui J. (1979). 'Atmospheric temperature structure during the Western European Winter Anomaly Campaign 1975/76'. J.Atmos.Terrest.Phys., 41, 1051-1062.

Plass G.N. (1956). 'The carbon dioxide theory of climatic change'. Tellus, 8, 140-154.

Pyle J.A. (1976). D. Phil. thesis, University of Oxford.

Pyle J.A. (1978). 'A simple calculation of ozone depletion by chlorofluoromethanes using a two-dimensional model'. Nature, 271, 42-43.

Pyle J.A. (1980). 'A calculation of the possible depletion of ozone by chlorofluorocarbons using a two-dimensional model'. Pure Appl. Geophys., 118, 355-377.

Pyle J.A. and Rogers C.F. (1980). 'Stratospheric transport by stationary planetary waves - the importance of chemical processes'. Quart. J. Roy. Meteorol. Soc., 106, 421-446.

Rasool S.I. and Schneider S,M, (1971). 'Atmospheric carbon dioxide and aerosols : effects of large increases on global climate'. Science, 173, 138-141.

Read A.W. (1965). 'Vibrational relaxation in gases'. Progress in Reaction Kinetics, 3, 205-235.

Reed R.J. and German K.E. (1965). 'A contribution to the problem of stratospheric diffusion by large-scale mixing.' Mon. Weath. Rev., 101 510-527.

Rodgers C.D. (1967). 'The radiative heat budget of the troposphere and lower, stratosphere'. M.I.T. planetary circulation project, Report A2, October 1967, 99 pp.

Rodgers C.D. and Walshaw C.D. (1966). 'The computation of infrared cooling rates in planetary atmospheres'. Quart. J. Roy. Meteorol. Soc., 92, 67-92.

Rodgers C.D. and Williams A.P. (1974). 'Integrated absorption of a spectral line with the Voigt profile'. J. Quart. Spectrosc. Radiat. Transfer, 14, 319-323.

Roper R.G. (1966). 'Dissipation of wind energy in the height range 80-140km'. J.Geophys. Res., 71, 4427-4428.

Roper R.G. and Elford W.G. (1963). 'Seasonal variation of turbulence in the upper atmosphere'. Nature, 197, 963-964.

Rottmann G.L. (1974). 'Disc values of the solar ultraviolet flux, 1150 A to 1850 A'. Trans. Am. Geophys. Union, 56, 1157.

Samain D. and Simon P.C. (1976). 'Solar flux determination in the spectral range 150-210 nm'. Solar Phys., 49, 33-41.

Scherhag R. (1952). 'Die explosionsartigen stratosphärener Warmungen des Spätwinters 1951-1952'. Ber. Deut. Wetterd., 6, 51-63.

Schoeberl M.R. and Strobel D.F. (1978). 'The zonally averaged circulation of the middle atmosphere'. J. Atmos. Sci., 35, 577-591.

Scholz T.G. and Offermann D. (1974). 'Measurements of neutral atmospheric composition at 85-15km by mass spectrometer with cryoion source'. J. Geophys. Res., 79, 307-310.

Schwartz R.N., Slawsky Z.I. and Herzfeld K.F. (1952). 'Calculation of vibrational relaxation times in gases'. J. Chem. Phys., 20, 1591-1599.

Shved G.M. (1965). 'Method of computing the deviation from Kirchhoff's law in the mesosphere for the transfer of radiation in the 15μ band of CO_2 Bull. Leningrad University, Series Phys. and Chem., Issue 1, 4, 67-79.

Simon P.C. (1975). 'Nouvelles mesures de l'ultraviolet solaire dans la stratosphere'. Bull. Acad. Roy. Belgique., Cl. Sci., 61, 399-

Simpson C.J.S.M., Gait P.D. and Simmie J.M. (1977). 'The vibrational deactivation of the bending mode of CO_2 by O_2 and by N_2'. Chem. Phys. Lett., 47, 133-136.

Stevens B. (1967). International encyclopeadia of physical chemistry and chemical physics. Topic 19 Gas kinetics, Volume 3 Collisional activation in gases. Pergamon Press.

Smil V. and Milton D. (1974). 'Carbon dioxide - alternative futures'. Atmos. Envir., 8, 1213-1223.

Stair A.T., Ulwick J.C., Baker K.D. and Baker D.J. (1975). 'Rocketborne observations of atmospheric infrared emissions in the auroral region'. Atmospheres of earth and the planets, ed McCormac, D.Reidel Publ. Co., Dordecht, 335-346.

Stair A.T., Ulwick J.C., Baker D.J., Wyatt C.L. and Baker K.D. (1974) 'Altitudes profiles of infrared radiance of O_3(9.6μm) and CO_2 (15μm)'. Geophys. Res. Lett., 1, 117-118.

Strobel D.F. (1978). 'Parameterisation of the atmospheric heating rate from 15 to 120 km due to O_2 and O_3 absorption of solar radiation'. J. Geophys, Res., 83, 6225-6230.

Stuiver M. (1978). 'Atmospheric carbon dioxide and carbon reservois changes'. Science, 199, 253-258.

Suess H.E. (1955). 'Radiocarbon concentration in modern wood'. Science, 122, 415-417.

Taylor R.L. and Bitterman S. (1969). 'Survey of vibrational relaxation data for processes important in the CO_2-N_2 laser system.' Rev. Mod. Phys. ,41, 26-47.

Thekaekara M.P. (1970). 'Proposed standard values of the solar constant and the solar spectrum'. J. Envir. Sci., 6-7.

Tousey R. (1963). 'The extreme ultraviolet spectrum of the sun'. Space Sci. Rev., 2, 3-69.

Trinks H. and Fricke K.H. (1978). 'Carbon dioxide concentrations in the lower thermosphere'. J. Geophys. Res., 83, 3883-3886.

Tuck A.F. (1977). 'Numerical model studies of the effect of injected nitrogen oxides on stratospheric ozone'. Proc. Roy. Soc. London, A355, 267-299.

Vidal-Madjar A.(1975). 'Evolution of the solar Lyman alpha flux during four consecutive years'. Solar Phys., 40, 69-86.

Vigroux E. (1953). 'Contributions à l'étude experimentale de l'absorption de l'ozone'. Annales de Physique, 8, 709-762.

Vincent D.G. (1968). 'Mean meridional circulation in the Northern Hemisphere lower stratosphere during 1964 and 1965'. Quart. J. Roy. Meteorol. Soc., 94, 333-349.

Volz A., Ehhalt D.H., Heidt L.E. and Pollack W. (1977). 'Vertical profiles of CH_4, CO and CO_2 in the stratosphere'. Proc. Joint Symp. on Atmos. Ozone, Dresden, 219-226.

Wallace L. (1962). 'The OH nightglow emission'. J. Atmos. Sci., 19, 1-16.

Walshaw C.D. and Rodgers C.D. (1963). 'The effect on the Curtis-Godson approximation on the accuracy of radiative heating rate calculations'. Quart. J. Roy, Meteorol. Soc., 89, 122-130.

Washington W.M. and Theile L.G. (1970). 'Digitised global monthly mean ocean surface temperatures'. N.C.A.R. technical note NCAR-TN-54, Dec. 1970.

Williams A.P. (1971a). D, Phil thesis, University of Oxford.

Williams A.P. (1971b). 'Relaxation of the 2.7μ and 4.3μ bands of carbon dioxide'. Mesospheric models and related experiments, ed. Fiocco, D.Reidel Publ. Co., Dordrecht, 177-187.

Williams A.P. and Rodgers C.D. (1972). 'Radiative transfer by the 15μ CO_2 band in the mesosphere'. Proc. Int. Rad. Symp., Sendai, Japan, 252-260.

Wilson A.T. (1978). 'Pioneer agriculture explosion and CO_2 levels in the atmosphere'. Nature, 273, 40-41.

Woodwell G.M.,Whittaker R.H.,Reiners W.A.,Likens G.E., Delwiche C.C. and Botkin D.B. (1978).'The biota and the world carbon budget.' Science,199,141-146.

Zimmerman S.P. and Rosenberg N.W. (1962). 'Wind energy deposition in the upper atmosphere'. Space Research, 12, 623-628.